FACULTAD DE CIENCIAS

DEPARTAMENTO DE QUÍMICA ORGÁNICA

Crosswise functionalized phthalocyanines as central cores in novel donor–π–acceptor arrays and metalloorganic ensembles

Doctoral Thesis presented by

ETTORE FAZIO

to opt for the grade of

DOCTOR IN ORGANIC CHEMISTRY

Madrid, 2018

Resumen

Las ftalocianinas (Pcs) (Figura 1) presentan un gran interés científico y tecnológico en las áreas de Ciencia de Materiales y Nanotecnología, con aplicaciones concretas como células fotovoltaicas, dispositivos electrocrómicos, en almacenamiento óptico de datos, sensores químicos, etc. Las ftalocianinas poseen un sistema electrónico bidimensional de carácter aromático de 18 electrones π, sobre el cual pueden llevarse a cabo múltiples modificaciones, incluyendo hasta 70 átomos diferentes en la cavidad central, o introduciendo una gran variedad de grupos funcionales en la periferia. Estos cambios permiten modular el comportamiento eléctrico y óptico de estos compuestos. Por otro lado, las ftalocianinas pueden organizarse en arquitecturas supramoleculares, lo que permite un control de la morfología a escala nanométrica que es de gran importancia para la fabricación de dispositivos eficientes basados en estas moléculas. Las ftalocianinas pueden, asimismo, formar nanoestructuras con geometrías particulares, o películas nanométricas altamente estructuradas sobre superficies para su uso, por ejemplo, en nanoelectrónica.

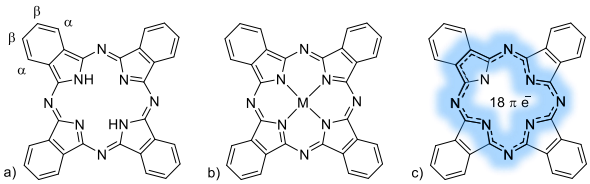

Figura 1. Estructura de: a) ftalocianina en forma de base libre, b) ftalocianinato metálico y c) principal modo de deslocalización electrónica del dianión ftalocianinato.

Las ftalocianinas han tenido un papel muy importante en el desarrollo de las células solares, debido a su carácter semiconductor y a su gran capacidad de absorción de la luz visible. Las ftalocianinas presentan altos coeficientes de extinción en torno a 700 nm, coincidiendo con el flujo de fotones máximo de la radiación visible. Además, las ftalocianinas muestran la capacidad dual de ceder o aceptar electrones a otro componente cuando han sido fotoexcitadas, en función de las características electrónicas de los sustituyentes periféricos. Ello da lugar a estados de separación de carga, electrones y huecos, que pueden moverse hacia los electrodos.

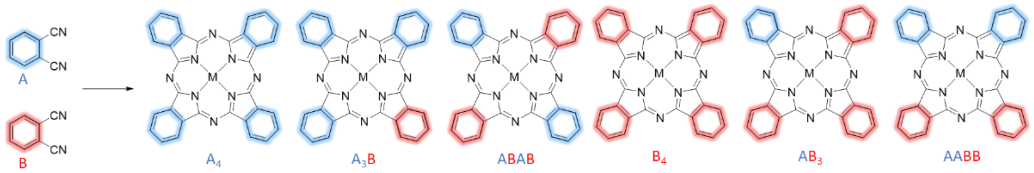

Figura 2. Productos obtenidos en la síntesis de ftalocianinas por condensación estadística de dos precursores diferentemente sustituidos, que conducen a isoindoles de tipo **A** y **B**.

Para la unión de las ftalocianinas a materiales semiconductores, así como para su unión covalente a otras moléculas electroactivas, se hace imprescindible la preparación de Pcs asimétricamante funcionalizadas, donde al menos uno de los isoindoles (**B** en la Figura 2) contenga un grupo de anclaje que permita la unión covalente buscada (Figura 2, Pc de tipo **AAAB**) y los otros isoindoles (**A** en la Figura 2) se encuentren funcionalizados con grupos alquilo alcoxi, fenoxi o tioeter que aumenten la solubilidad de la molécula. La aproximación sintética para preparar estas moléculas consiste simplemente en la condensación estadística de dos precursores, habitualmente ftalonitrilos, en las proporciones adecuadas, y la separación cromatográfica del producto buscado.

El objetivo general de la tesis es la preparación de ftalocianinas con un patrón de sustitución **ABAB** (Figura 2*)*, que permitan la incorporación de grupos dadores de electrones y grupos aceptores de electrones con una disposición lineal entre ellos para distintas aplicaciones. En primer lugar para obtener nuevos fotosensibilizadores de celulas solares con un patrón de sustitución "*push-pull"*, que den lugar al proceso de fotoinyección de forma más favorable. Además, este patrón de sustitución **ABAB** permitirá la preparación de estructuras covalentes y supramoleculares multicomponente con arquitecturas muy interesantes.

En el primer capitulo se ha descrito el desarollo de una estrategia general para la sintesis de Pcs **ABAB**. Para llevar a cabo la síntesis de Pcs de Zn(II) con ese patrón de sustitución, se han realizado en primer lugar ftalonitrilos con distintos sustituyentes voluminosos en las posiciones 3,6. Estos derivados se han sometido a condiciones de condensación estadística con ftalonitrilos oportunamente sostituidos para llevar a cabo subsequentes funcionalizaciones (por ejemplo el 4-iodoftalonitrilo). Solo utilizando el ftalonitrilo con grupos trifluorometilfenil se ha llevado a cabo de la separación con buen rendimiento de la ftalocianina con patrón de sustitución deseado (Esquema 1).

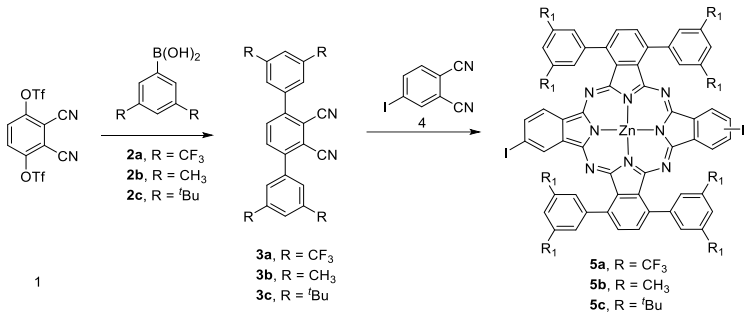

Esquema 1. Síntesis de Pcs ABAB.

En el segundo capitulo de la tesis, sobre la ftalocianina de Zn(II) con un patrón de sustitución ABAB, portadora de dos grupos iodo, se ha llevado a cabo reacciones de funcionalización asimétrica para introducir, en una misma molécula, grupos dadores de electrones y grupos aceptores de anclaje para una distribución electrónica de tipo push-pull. Para ello se han utilizado en una primera etapa reacciones de acoplamiento cruzado de tipo Buchwald o de Sonogashira, para introducir grupos amino dadores de electrones, y en una segunda etapa, carboxilaciones directas o reacciones de Sonogashira para introducir grupos COOH con espaciadores de tipo etinil o benzotiadiazol, entre otros (Esquema 2). Esas Pcs se han estudiado en celulas solares de tipo Grätzel en los laboratorios del Prof. Grätzel en el marco de nuestra colaboracion.

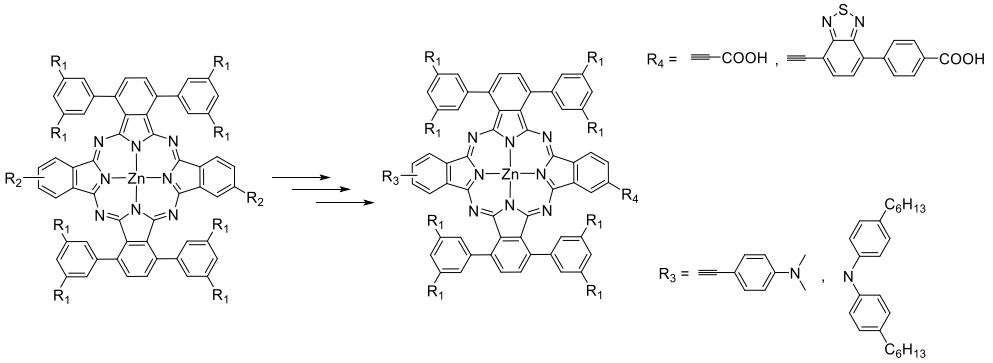

Esquema 2. Síntesis de ftalocianinas push-pull.

En la segunda parte del segundo capitulo se ha descrito la sintesis y los estudios de sistemas multicomponentes basados en Pcs. En primer lugar, se han llevado a cabo reacciones de funcionalización asimétrica para introducir, en una misma molécula, otros cromóforos como porfirinas y subftalocianinas. Para ello se han utilizado en unas primeras etapas reacciones de acoplamiento cruzado de tipo Sonogashira, para introducir una funcionalización fenólica en uno de los isoindoles, y una porfirina en el isoindol enfrentado. La última etapa es la introducción de la subftalocianina mediante coordinación axial. Los estudios fotofísicos de procesos de transferencia de energía intramolecular en sistemas multicomponente, de manera especifica una triada porfirina-ftalocianina-subftalocianina, se han llevado a cabo en el laboratorio del Prof. Guldi, en la Universidad de Erlangen, en el marco de nuestra colaboración en sistemas dador-aceptor como modelos fotosintéticos. Tras la excitación del anillo de ftalocianina por irradiación con una longitud de 676 nm se obtiene el estado de separacion de carga biradicalico ZnPor•+-ZnPc•−-SubPc. A su vez la ZnPc anion radical transfiere un electron al aceptor principal, la SubPc, obténiendose el estado con separación de carga espacial ZnPor•+-ZnPc-SubPc•− con un tiempo de vida de 1.8 ns (Figura 3).

En la ultima parte del segundo capitulo se ha descrito la preparación de hybridos multicomponente Por-Pc-grafeno, que se ha llevado a cabo mediante reacciones consecutivas de acoplamiento cruzado de tipo Suzuki para introducir una funcionalización 4-hidroximetilfenil en uno de los isoindoles, y una porfirina en el isoindol enfrentado mediante reacción de tipo Sonogashira. La reacción de esterificación con el ácido 4-(1-pirenil)-butanoico ha permitido preparar la diada Pc-pireno y la triada porpfirina – Pc – pireno (Figura 3). Los estudios de esfoliacion de grafito y de transferencia de energía intramolecular en esos hybridos se han llevado a cabo en el laboratorio del Prof. Guldi.

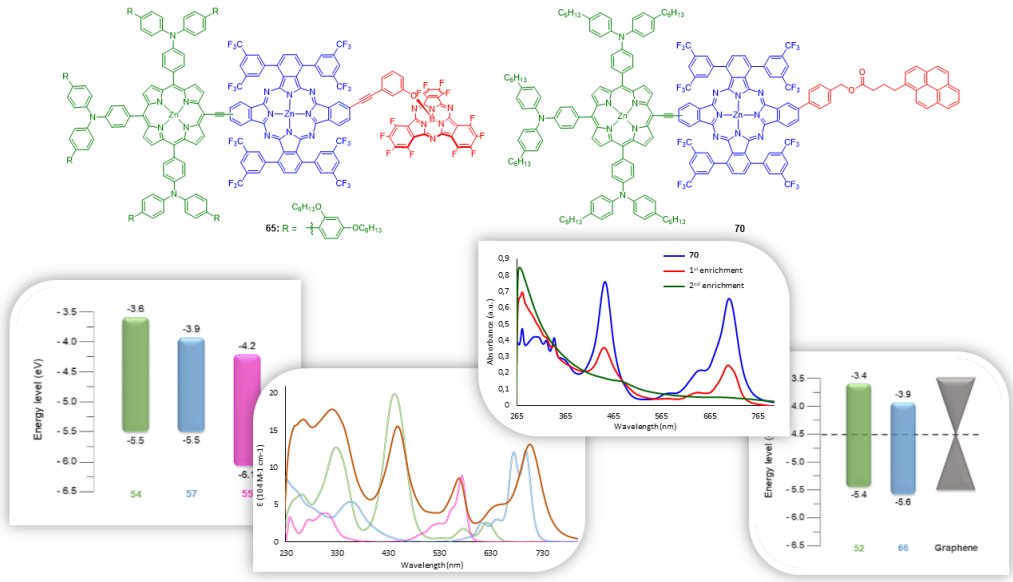

Figura 3. Resumen grafico de los resultados obtenido en la section *2.3.3* de la tesis.

En el tercer capitulo de la tesis se ha descrito la preparacion de helicatos de tipo organometalicos M_2L_3 basados en Pcs. Esas arquitecturas han sido realizadas utilizando

una ftalocianina **ABAB** funcionalizada con anilinas en dos unidades isoindolicas. Esa Pc en presencia de 2-formilpiridina y $Fe(OTf)_2$ da lugar a un helicato de tipo M_2L_3 donde tres Pcs con doble funcionalización imino-piridínica están unidas entre ellas a través de enlaces de coordinación con dos iones Fe(II), que representan los dos vértices del helicato. Por último se ha estudiado por ^{1}H-NMR y UV-vis las capacidades de esta arquitectura a comportarse como anfitrión en disolución de distintas moléculas neutras, así como de distintos aniones voluminosos. De esta manera, se ha observado la formación de complejos huésped-anfitrión 1:1 con fullerenos (C_{60}, C_{70} y $PC_{61}BM$). Al mismo tiempo se ha utilizado una unidad de tipo naftalenodiimida (NDI) funcionalizada con dos imidazoles para aprovechar la capacidad del Zn(II) presente en la cavidad central de las Pcs de formar un enlace de coordinación axial. De esta manera, se ha formado un complejo huésped-anfitrión muy estable, que puede dar origen a interaccione electrónicas entre las unidads electroactivas que lo componen (i.e. Pcs y NDI).

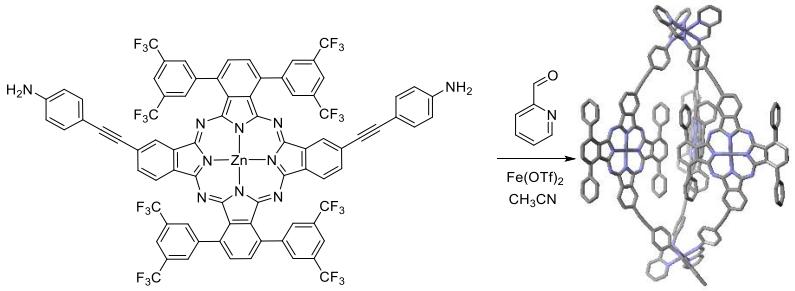

Esquema 3. Síntesis de helicatos de tipo organometalicos M_2L_3 basados en Pcs.

The present work has been developed at the Organic Chemistry Department of Universidad Autónoma de Madrid, under the supervision of Dr. Gema de la Torre Ponce and Prof. Tomás Torres Cebada.

Nullum Magnum Ingenium Sine Insania

(218 K)

Agradecimientos

Escribir una tesis es una tarea complicada y dificil, superada solo por la escritura de los agradecimientos.

In primis me gustaria agradecer **Tomas** por la oportunidad de trabajar en su grupo y por haberme animado en estos años a dar y hacer todo lo posible para la investigacion. Es el jefe que todo el mundo necesitaria y que poca gente se merece.

Un gracias especial es para **Gema** que ha sido jefa, tutora, cosejera y “mama cientifica”. Gracias por haber guiado mi curiosidad, por haberme ayudado a elegir el camino correcto cada vez que se me iba la olla entre los muchos, demasiados artículos leidos, por haber visto el mundo con ojos cercanos a los mios y por todos los refranes en castellano.

Quiero agradecer todos los *senior* del grupo de invistigacion: **Marivì**, **Puri**, **Salomé**, **Esmeralda**, **Andres**, **Gianni**, **Gunther**, **Miguel, Max**, **Ismael** y **David**; sois los espejos de diferentes culturas y historias, cada uno especial a su manera y todos necesarios para el perfecto funcionamiento de este grupo.

Ahora la parte mas complicada: intentar agradecer todos los compañeros de trabajo diarios. Siguiendo un orden cronológico, el primer agradecimiento es para aquellos con quienes comencé este viaje: **Vanesa**, **David**, **Joana** e **Eveline**. Gracias por haber compartido piso y aventuras al rededor de Madrid.

Un gracias para **Carol**, **Francesca**, **Olga**, **Maria**, **Javi, Julia**, **Ana** y **Anita** que con mucha calma me han enseñado mucho en el laboratorio de Madrid y fuera. Otro gracias especial es para el equipo de italianos que ha pasado por el grupo y por el departamento: **Nunzio**, **Giulia**, **Beatrice**, **Elisa**, **Ernesto** e **Marcello**.

No me puedo olvidar de **Melchor** y **Baltasar**, **Nico** y **MiguelAngel** (o al reves no me acuerdo), compañeros de desayunos y conspiraciónes.

Otro gracias especial es para todos los *juniors* del grupo de hoy y de ayer: **Lara**, **Luis**, **Vero**, **Diana Paola**, **Elena**, **Alvaro**, **Jose**, que son la verdadera alma de este grupo de investigacion.

Gracias a todos vosotros por haber compartido estos años conmigo!!

Acordar todos los nombres es una tarea ingrata y por eso me disculpo si olvidé mencionar a alguien.

Vorrei ora rivolgere la seconda parte dei ringraziamenti a tutta la mia famiglia.

A mio **nonno** e mio **zio**, per essere quei pilastri portanti ed esempi da cui posso apprendere tutti i giorni. A mia **nonna** per le cure affettuose e i “pensieri” che mi hanno accompagnato anche stando distante. A mia **zia** e **Antonino** per avermi regalato una risata ogni qualvolta ne ho avuto di bisogno.

Un grazie speciale va a mia **madre**, i cui sacrifici non potrò mai ripagare in modo appropriato ed egregio, e per i quali non potrò mai smettere di ringraziarla. Un grazie a **Loris**, per la grande serenità e l’aiuto che ha portato.

Un grazie altrettanto speciale va a **Serena**, la sorella che non merito ma di cui ho tanto bisogno, per la sua inestimabile onestà e sincerità, per i consigli e l’appoggio. So di poter contare sempre su di te e per questo ti ringrazio!

Dulcis in fundo dicevano i latini, e pertanto l’ultimo grazie, il più speciale e grande va a **Simona**. Per la tua pazienza e complicità quotidiana, per il sostegno e l’incoraggiamento necessario che ho sempre trovato nelle tue parole, e per non aver mai smesso di credere in noi, ti dico *grazie*!!

To date, the results reported in the present work have led to the following publications:

(i) "Efficient Synthesis of ABAB Functionalized Phthalocyanines", E. Fazio, J. Jaramillo-García, G. de la Torre and T. Torres, *Org. Lett.*, **2014**, *16*, 4706–4709.

(ii) "ABAB Phthalocyanines: Scaffolds for Building Unprecedented Donor–π–Acceptor Chromophores", E. Fazio, J. Jaramillo-García, M. Medel, M. Urbani, M. Grätzel, M. K. Nazeerudin, G. de la Torre and T. Torres, *ChemistryOpen*, **2017**, *6*, 121 –127.

(iii) "Giant M_2L_3 metallo-organic helicate based on phthalocyanines as a host for electroactive molecules", E. Fazio, C. Haynes, G. de la Torre, J. R. Nitschke and T. Torres, *Chem. Commun.*, **2018**, *accepted manuscript*.

(iv) "Unidirectional Charge Transfer Cascade Process in a Panchromatic Multiporphyrinoid Ensemble", E. Fazio, K. Winterfeld, G. de la Torre, D. M. Guldi and T. Torres, **2018**. *Submitted.*

During the development of the present work, pre-doctoral stays have been conducted in the following research centres:

1. Prof. Nitschke's Laboratory, Department of Chemistry, University of Cambridge, Cambridge, United Kingdom.

   Supervision: Prof. Jonathan Nitschke

   Date: March 28th to June 26th, 2016

2. Prof. Guldi's Laboratory, Department of Chemistry and Pharmacy of Friedrich-Alexander-Universität of Erlangen-Nürnberg, Germany,

   Supervision: Prof. Dirk Guldi

   Date: June 12nd to 30th, 2017

Table of contents

Abbreviations and acronyms

We have used standard Organic Chemistry abbreviations and acronyms following the recommendation of the “guidelines for authors”, *J. Org. Chem.* **2016**, which can be found in the journal webpage:

http://pubs.acs.org/paragonplus/submission/joceah/joceah_authguide.pdf

2FP	2-Formylpyridine
β-CD	β -Cyclodextrin
Boc	*tert*-Butoxycarbonyl
BHJ	Bulk heterojunction
BTA	Benzene-1,3,5-tricarboxamide
BTD	Benzothiadiazole
CB	Conduction band
CCD	Charge coupled device
CDL	Constitutional dynamic library
CIGS	Copper allium Indium Selenide
CHENO	Chenodeoxycholic acid
CNT	Carbon Nanotube
CSS	Charge separated state
D-A	Donor – Acceptor
dba	Dibenzylideneacetone
DBU	1,8-Diazabicyclo[5.4.0]undec-7-ene
DDQ	2,3-Dichloro-5,6-dicyano-1,4-benzoquinone
DFT	Density functional theory

DIPEA	N,N-Diisopropylethylamine
DMAE	Dimethylaminoethanol
DME	1,2-Dimethoxyethane
DMF	Dimethylformamide
DMSO	Dimethyl sulfoxide
DSSC	Dye-sensitized solar cell
ε	Molar extinction coefficient
Es	Taft's steric constant
Fc	Ferrocene
FF	Fill factor
FRET	Förster resonance energy transfer
Fs-TAS	Femtosecond transient absorption spectroscopy
FTO	Fluorine-doped tin oxide
G	Guest
H	Host
HS	High spin
IBX	2-Iodoxybenzoic acid
IPCE	Incident photon-to-current efficiency
I_{SC}	Short-circuit current
ITO	Indium Tin Oxide
J_{SC}	Short-circuit current density
L	Linker

LMCT	Ligand-to-metal charge transfer
LS	Low spin
MLCT	Metal-to-ligand charge transfer
MW	Microwave
NHE	Normal hydrogen electrode
o-DCB	o-Dichlorobenzene
OPV	Organic photovoltaics
Φ	Quantum yield
Pc	Phthalocyanine
PCBM	Phenyl-C_{61}-butyric acid methyl ester
PCE	Power conversion efficiency
PDI	Perylenediimide
PET	Photoinduced electron transfer
PHJ	Planar bilayer heterojunction solar cell
Por	Porphyrin
PTIO	2-Phenyl-4,4,5,5-tetra-methylimidazolineyloxyl-3-oxide
PTZ	Phenothiazine
PV	Photovoltaics
Py	Pyridine
r_W	van der Waals radius
SCO	Spin crossover

SubPc	Subphthalocyanine
SWNT	Single-walled nanotube
TCO	Transparent conductive oxide
TBAF	Tetrabutylammonium fluoride
TBAP	Tetrabutylammonium hexafluorophosphate
TDDFT	Time-dependent density functional theory
TEMPO	2,2,6,6-Tetramethylpiperidin-1-yl)oxyl
TPA	Triphenylamine
V_{OC}	Open-circuit voltage
VT	Variable temperature
X-Phos	2-Dicyclohexylphosphino-2′,4′,6′-triisopropylbiphenyl

Introduction and Objectives

Phthalocyanines

I once read a silly fairy tale, called "The Three Princes of Serendip": as their Highnesses travelled, they were always making discoveries, by accident and sagacity, of things which they were not in quest of; for instance, one of them discovered that a mule blind of the right eye had travelled the same road lately, because the grass was eaten only on the left side, where it was worse than on the right — now do you understand serendipity?[1]

In this letter wrote to a friend, Horace Walpole coined for the first time the word "serendipity" in 1754, suggested by a Persian fairy tale in which the heroes were always making discoveries by accident but also thanks to their sagacity. According the Oxford dictionary, the modern definition of serendipity is "the occurrence and development of events by chance in a happy or beneficial way".

The notion of serendipity is a common occurrence throughout the history of scientific innovation such as Alexander Fleming's accidental discovery of *penicillin* in 1928,[2] the detection of the *saccharine* by Constantin Fahlberg in 1879,[3] and the invention of the *mauveine*, also known as *aniline purple* by the eighteen year old William Henry Perkin in 1856.[4]

In the same way, by serendipity, phthalocyanines (Pcs) were discovered more than a century ago. In 1907, A.V. Braun and J. Tcherniac isolated a blue compound as a by-product of the preparation of *ortho*-cyanobenzamide, later identified as the metal-free Pc,[5] and in 1927, the first Cu(II)Pc was prepared by H. de Diesbach and E. von der Weid.[6] The investigators were attempting to prepare phthalonitrile by heating *ortho*-dibromobenzene, cuprous cyanide and pyridine in a sealed tube but, instead, the metal Pc was formed. In 1928, scientists at Scottish Dyes Ltd (later ICI) observed a greenish compound in phthalimide prepared from molten phthalic anhydride and ammonia. The reaction had been carried out in an enamelled cast-iron crucible that was chipped, and the resulting greenish impurity was Fe(II)Pc. After experiments for replacing iron by other metals, and, realizing the commercial value of the synthesis, Scottish Dye Works patented the Cu(II)Pc in 1929.[7]

Since their first synthesis, Pcs have established themselves as blue and green dyestuff par excellence. They are an important industrial commodity, used primarily in inks (especially ballpoint pens), coloring for plastics and metal surfaces, and dyes for jeans and other clothing. More recently, the unique properties of Pcs such as high optical stability, semiconductivity and excellent photophysical properties have widen their possible applications, and therefore, their commercial utility. Potential uses of Pcs include sensing elements in

chemical sensors, electrochromic display devices,[8] solar cells,[9,10] photodynamic reagents for cancer therapy,[11] catalysis and electrocatalysis,[12] electrophotography,[13] molecular electronics and photonics,[14] nonlinear optics,[15] and liquid crystal color display applications.[16,17]

Structure of phthalocyanines

Pcs [18–21] are planar macrocycles constituted by four isoindole units linked through nitrogen bridges, presenting an 18-π-electron aromatic internal cloud. In Figure 1 the structures of both metal-free and metallophthalocyanines are shown. The internal and external positions of the fused benzene rings are also commonly known as α- and β-positions, respectively (Figure 1a). The hydrogen atoms of the central cavity can be replaced by more than 70 different elements, generating the metallophthalocyanines (MPcs; Figure 1b).[22,23] The 42 π-electrons of Pcs are distributed over 32 carbon and 8 nitrogen atoms, but the electronic delocalization mainly takes place at the inner ring, which is constituted by 16 atoms and 18 π-electrons (Figure 1c), the outer benzene rings maintaining their electronic structure.[24]

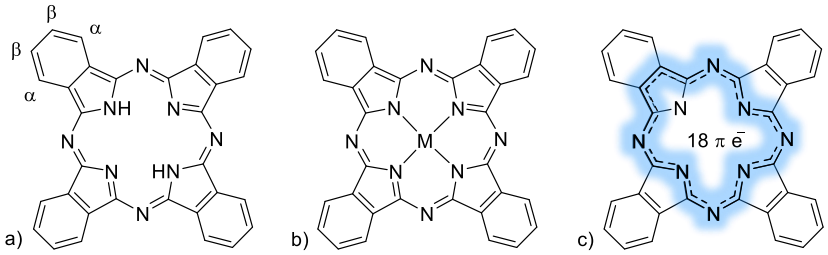

Figure 1. Structure: a) metal-free Pc, b) metallic Pc c) main electron delocalization mode of the Pc dianion.

The heteroaromatic and highly delocalized π–electron system defines the spectroscopic characteristics of Pcs, which absorb radiation corresponding to visible light and have a high optical stability.

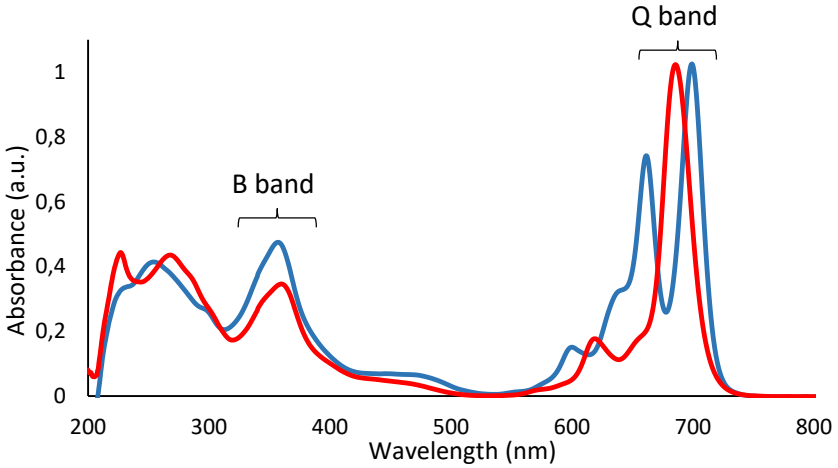

Figure 2. UV/Vis spectra of a metal-free Pc (blue line) and a Zn(II)Pc (red line).

The electronic absorption spectrum of these compounds (Figure 2) presents two main bands, the Q band and the Soret or B band. The first one is a quite intense absorption band in the visible region, near 700 nm, with molar absorption coefficients ε in the order of 10^5 M^{-1} cm^{-1}, and it derives from the transition from the ground state of a_{1g} symmetry to the first excited state of e_u symmetry. The Soret band is situated near 350 nm, with typical molar absorption coefficients ε in the order of 10^4 M^{-1} cm^{-1}, and it is related to π–π* transitions from lower-energy molecular orbitals. At higher energies, additional π–π^* transitions can be observed in UV transparent solvents.

One of the most important attributes of Pcs is their high thermal, chemical and electromagnetic stability, which is a common requirement for most technological applications. Nevertheless, the most remarkable feature that makes these molecules play an exceptional role in the area of material science is their chemical versatility, which in turn can be used as a tool to modify the electronic, and therefore the optical properties of Pcs. In fact, the shape and position of the absorption bands of Pcs, (particularly the Q band) are affected to varying degrees by the central metal, axial ligation, solvents, peripheral and non-peripheral substitution, and by extension of the conjugation.

Focusing on the role of the central metal in the optical properties, it is worth mentioning that while metal-free Pcs have a D_{2h} symmetry with a Q band split into two main absorptions, metallation imposes a D_{4h} symmetry, and, therefore, MPcs show a unique Q band in their absorption spectrum. In general, the introduction of metal ions inside the Pc cavity generates a slight blue shift of the Q band, since the metal ions reduce the electron density of the Pc. It has been demonstrated that the more electronegative the metal ion is, the more the Q band is blue-shifted.[25] In addition, the d orbitals of transition metals may lie between the HOMO and the LUMO of the Pc ligand; this may result in metal to ligand (MLCT) or ligand to metal (LMCT) charge transfer transitions (Figure 3). The charge-transfer absorption bands occur in general between the B and Q bands or in the near IR region.

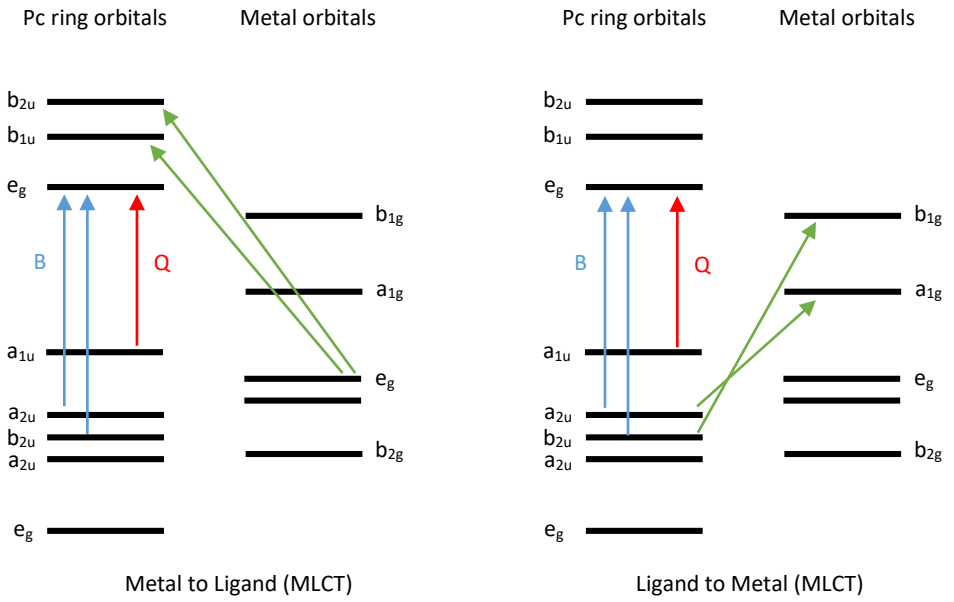

Figure 3. Schematic representation of the energetic levels and transitions in a metallophthalocyanine.

The redox properties of Pcs can also be tuned by the structural modifications of the Pc core. It is well known that the position of the Q band can be related to the energetic difference between the first ring oxidation and the first ring reduction, for MPcs containing non-redox active central metals. Generally, metal-free and MPcs exist as a dianionic (Pc^{-2}) species that can be oxidized or reduced in successive steps. The Pc ring redox activity is directly related to the frontier orbitals in the molecule. Therefore, the oxidation is related to the removal of electron(s) from the HOMO (a_{1u}), while reduction is the addition of electron(s) to the LUMO (e_g). Up to four electrons can be successively added to the doubly degenerate e_g orbitals of the LUMO to form Pc^{-3}, Pc^{-4}, Pc^{-5}, and Pc^{-6}, and two electrons can be removed from the HOMO to form Pc^{-1} and Pc^{0} (Figure 4). Oxidation or reduction of MPcs with redox active metals (i.e., those with vacant or partially occupied d orbitals) may occur both at the metal and at the ring, depending on the relative energies and proximity of metal d and Pc ring orbitals. The nature of the central metal, axial ligands and substituents on the ring periphery determines the redox properties of a given complex. For instance, electron-donating substituents such as alkylthio groups, increase the electron density of the ring and the central metal atom, thereby making it easier to oxidize and harder to reduce.[13]

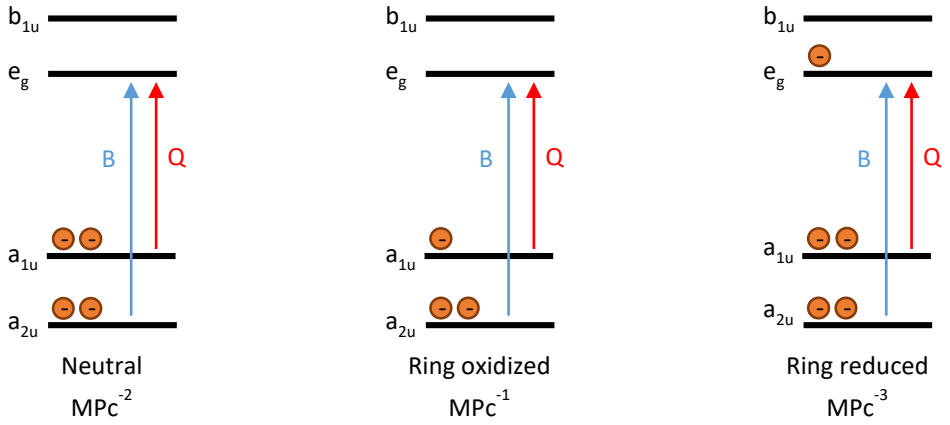

Figure 4. Energy level diagrams of neutral, one-electron ring oxidized, and one-electron ring reduced MPc complex (● = electron).

Either axial or peripheral attachment of different functional groups has a deep influence on both the electronic and chemical (for instance, solubility) properties of Pcs. The reported synthetic strategies devoted to the preparation of Pcs holding similar o different peripheral substituents at the different isoindole moieties are described in the next section. Regarding axial functionalization, the presence of certain metal atoms in the central cavity of the Pcs provides a site for the incorporation of functional groups. Examples of Pcs that can be axially functionalized are ruthenium (Ru(II)Pc),[26–28] zinc (Zn(II)Pc),[28–31] aluminium (Al(III)Pc) and silicon (Si(IV)Pc) derivatives,[32,33] among others. For Si(IV)Pcs and Al(III)Pcs (Figure 5a and b), the axial substituents are covalently linked to the central atom, while for Ru(II)Pcs and Zn(II)Pcs (Figure 5c and d) the bond has a supramolecular nature, yet the Ru(II)Pcs bind to axial ligands (generally N-containing) with much larger association constants than the Zn(II)Pcs.

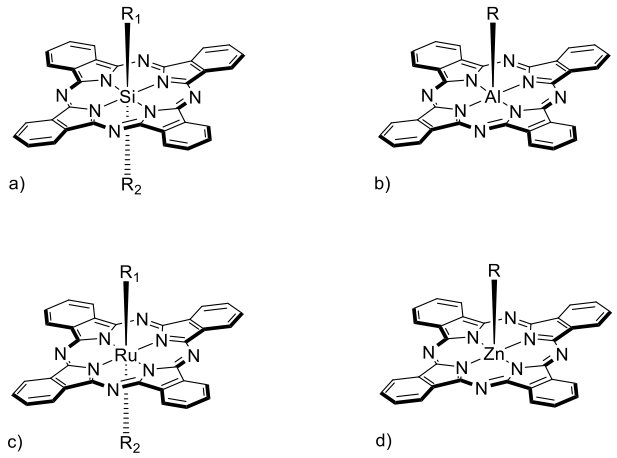

Figure 5. General structure of axially substituted Pcs: a) Si(IV)Pc (where R_1 and R_2 = alkoxy, phenoxy, silyloxy); b) Al(III)Pc (where R = alkoxy, phenoxy, silyloxy); c) Ru(II)Pc (where R_1 and R_2 =N-containing ligands able to coordinate to the central metal or CO), d) Zn(II)Pc (where R = N-containing ligands able to coordinate to the central metal).

The basic structure of the macrocyle can also be rationally modified, giving rise to Pc analogues (Figure 6)[34–39] via the following strategies: a) atom substitution;[8] b) extension of the aromatic system;[36,40] c) variation in the number of isoindole units;[38,41] and d) formation of dimers or oligomers;[37,42,43] All these modifications have a strong impact on the electronic features of the macrocycles.

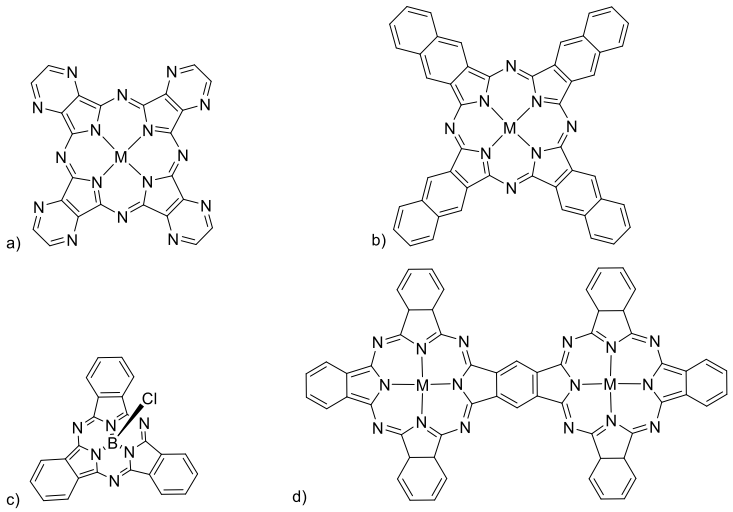

Figure 6. Phthalocyanine analogues: a) tetrapyrazinoporphyrazine; b) 2,3-naphthalocyanine; c) subphthalocyanine; d) fused ring Pc dimer.

Synthesis of phthalocyanines

Symmetrically substituted phthalocyanines

The synthesis of symmetrically substituted Pcs (**A_4**), that is, bearing identical substituents in each of the four isoindole units (**A**), is traditionally based on cyclotetramerization reactions of appropriately substituted precursors,[44] primarily phthalonitriles (1,2 – dicyanobenzenes), but also a wide variety of derivatives of *ortho*-phthalic acid, such as anhydrides, imides and amides can be also employed as precursors. The two most important synthetic pathways for the preparation of substituted phthalonitriles are: i) the phthalic acid transformation (i.e., the so-called 'acidic' route involving the acid – anhydride – imide – amide – nitrile sequence); and ii) the transformation of *ortho*-dihalide benzenes into dinitriles catalyzed by copper or palladium (e.g. Rosenmund-von Braun reaction).[45]

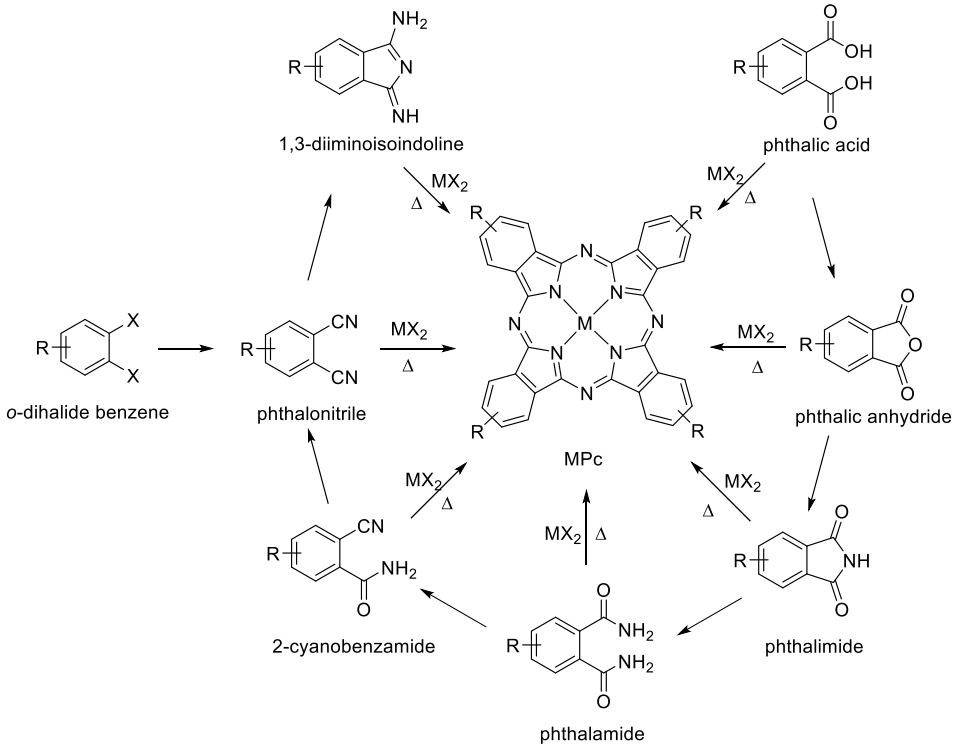

Scheme 1. General schematic representation of the synthesis of phthalonitrile derivatives and symmetrically substituted MPcs.

Classically, metallophthalocyanines have been prepared by the metal-templated reaction, which consist in heating a mixture of the corresponding phthalonitrile

and metal salt in a solvent with high boiling point (DMAE, DMF, *o*-DCB). When phthalonitriles are used as precursors, a basic catalyst – usually 1,8-diazabicyclo[5.4.0]undec-7-ene (DBU),[46] – is used in the presence of an alcohol, such as DMAE or 1-pentanol, thus generating an alkoxide which triggers the macrocyclization. On the other hand, the synthesis of metal-free Pcs is usually carried out employing 1,3 – diiminoisoindolines in the same reaction conditions. Lithium alkoxides are also used with phthalonitriles, giving rise to lithium Pcs that can be easily converted into the free base by treatment with a mineral acid.[47] In turn, metallic Pcs can be obtained by a later metallation of the metal-free Pc at refluxing temperature of a high-boiling point solvent, in the presence of the corresponding metal salt.

The mechanism of the formation of Pcs is still not completely understood, yet there exist various mechanistic hypotheses, all bearing some common features, which are generally accepted.[48–51] In general, when the reaction takes place in the presence of sodium or lithium alkoxides, the macrocyclization starts with the formation of the corresponding salt of 1-imido-3-alkoxyindoline (Scheme 2 – step 1),[52] followed by the nucleophilic attack of this intermediate to the cyano group of another phthalonitrile molecule (step 2). The resulting dimer can either react with a third phthalonitrile molecule in the same way, to form a trimer (step 3a), or undergo self-condensation with another dimer (step 3b), both mediated by the metallic cation as a template.

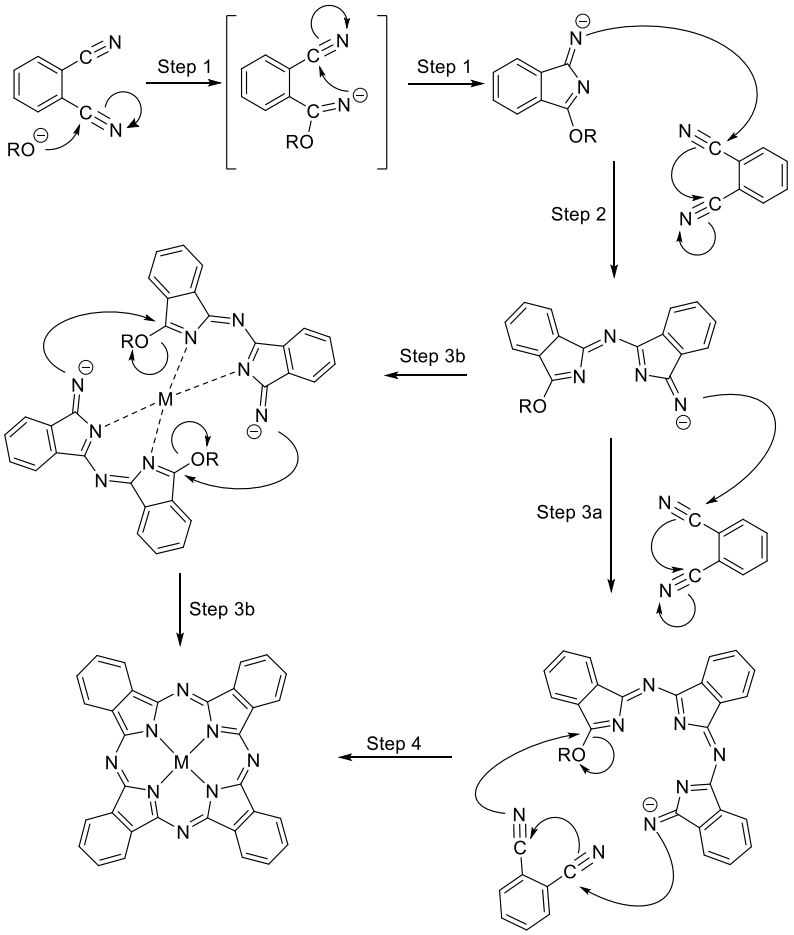

Scheme 2. Proposed mechanism for the synthesis of metallophthalocyanines by cyclotetramerization of phthalonitriles in the presence of a metal salt.

Another possibility consists in the metal-mediated formation of the Pc ring,[48,49] that is, a transition metal cation acting as a template to which the reacting phthalonitriles coordinate during the macrocyclization.

Apart from the well-established methods for the preparation of Pcs, other more recent approaches have been described, which allow to prepare Pcs with higher efficiencies and rather mild conditions. Treatment of phthalimides, phthalic anhydrides and phthalonitriles with metal salts and hexamethyldisilazane in DMF,[53,54] a double-addition of oximes to phthalonitriles,[55] or the use of microwave radiations[56] can be highlighted.

Depending on the desired properties and the final application, different custom-made Pcs can be prepared. In this regard, Pc precursors can be mono, di-, tri-

or tetrafunctionalized, depending on the necessary number of functional groups in the target Pc. One of the identified issues in the case of using 3- or 4-substituted phthalonitriles as starting materials is that the resulting tetrasubstituted Pcs are obtained as mixtures of four structural isomers with C_{4h}, D_{2h}, C_{2v} and C_s symmetries (Figure 7).[21] These regioisomers can be separated sometimes by chromatographic techniques[57,58] or obtained separately employing a regioselective approach.[59–61]

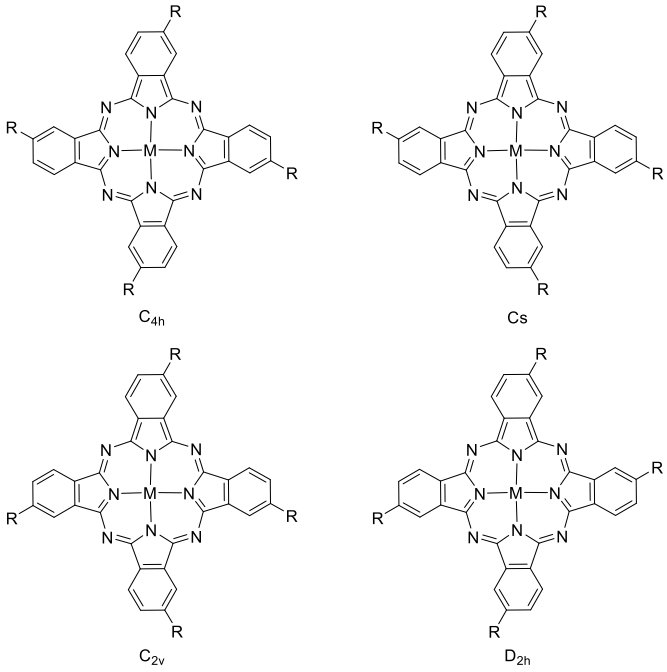

Figure 7. Four constitutional isomers of 2,9(10),16(17), 23(24)-tetrasubstituted phthalocyanines.

Unsymmetrically substituted phthalocyanines

The preparation of Pcs with two different substituents in the isoindole units (commonly notated as isoindoles **A** and **B**) is fundamental for many different applications (energy conversion, catalysis, etc…). Although the preparation of unsymmetrically substituted Pcs is more difficult than the synthesis of their symmetric analogues, different methodologies can be employed to undertake this task. The most utilized and simple strategy is the statistical condensation of two differently functionalized phthalonitriles or diiminoisoindolines (also called **A** and **B**) to produce a library of Pcs (Figure 8)[62,63] that, in a second step, are separated by column chromatography.

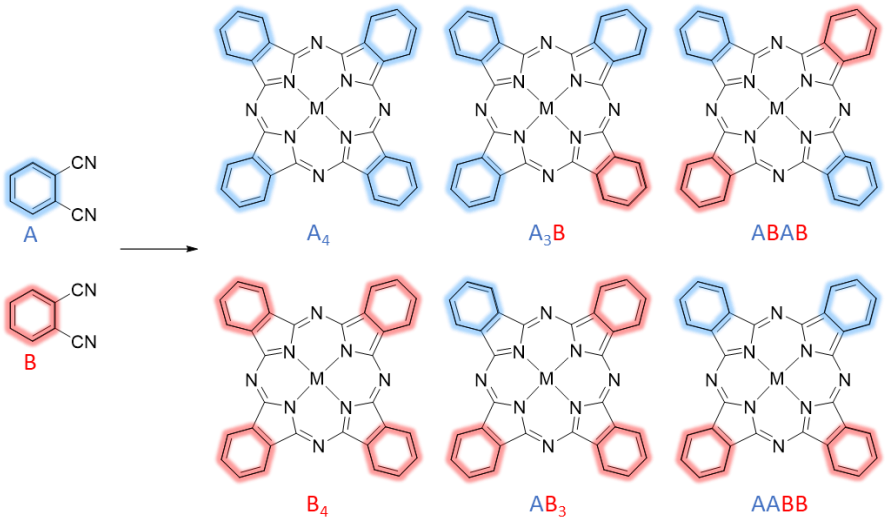

Figure 8. Mixture of Pcs obtained *via* statistical cyclotetramerization of two differently functionalized phthalonitriles or diiminoisoindolines, **A** and **B**.

Usually, the statistical route is the most popular approach to prepare **A_3B** compounds, since the reaction can be "directed" towards the target compound by using a relatively large excess of one of the phthalonitriles (from 3:1 to 9:1 relative ratios are the most common). Controlling the ratio of the reagents leads in many cases to the nearly exclusive formation of both the symmetric Pc from the most abundant precursor (**A_4**), and the **A_3B** derivative. Some factors, such as the steric effect of the substituents (employing bulky groups to supress aggregation and facilitate chromatographic separation) and the relative reactivity of the different precursors, have to be taken into account in order to increase the yield of the desired **A_3B** Pc and facilitate its isolation. On the other hand, statistical means are rarely used to prepare **A_2B_2** compounds, since the two constituting isomers (**AABB** and **ABAB**) are quite difficult to separate by chromatographic techniques, although still possible in some sporadic cases.[64,65]

To date, several chemoselective techniques for asymmetric **A_3B** Pc synthesis have been described in the literature including the ring expansion route and solid-phase synthesis:

- *Ring expansion.* This method for the selective synthesis of **A_3B** Pcs involves ring expansion of a subphthalocyanine (SubPc) by treating it with a succinimide or diiminoisoindoline derivative (Scheme 3).[66] SubPcs are lower Pc homologues consisting of three isoindole subunits linked together through aza bridges. In their central cavity they always bear a boron atom, which is coordinated by three nitrogen atoms of the macrocycle and one axial substituent.[67,68]
  The geometrically constrained SubPc core can readily cleave in the presence of a diiminoisoindoline unit, which is then incorporated into its framework to form a Pc derivative of type **A_3B**. This reaction has proved very selective and efficient in some cases, allowing to prepare previously unattainable Pcs.[69,70]

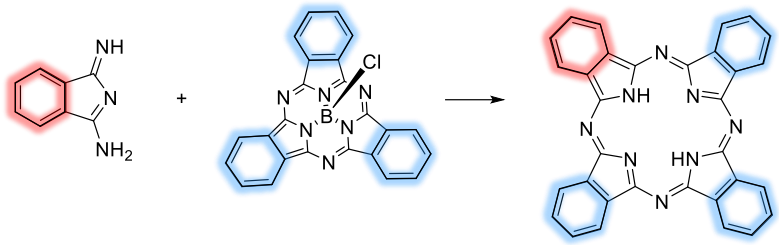

Scheme 3. General schematic representation of ring expansion reaction.

  Unfortunately, this method is only applicable to certain phthalonitrile precursors. For example, the condensation of a diiminoisoindoline having electron-donating groups and a SubPc either unsubstituted or holding electron-withdrawing groups, promotes the selective synthesis of **A_3B**-type Pcs. In contrast, the presence of electron-donating substitutents on the SubPc leads to a mixture of Pcs through a scrambling process that results from disassembly of the SubPc under the reaction conditions to form the Pc.[69,71]

- *Polymeric Support Method*. This is another approach for the selective preparation of **A_3B** Pcs mainly developed by Leznoff.[72,73] Solid-phase synthesis of Pcs starts with one of the phthalonitrile precursors **A** (Scheme 4) attached to the support via a cleavable linker. Reaction of the solid-supported phthalonitrile **A** with an excess of phthalonitrile **B** in solution produces the **AB_3**-type, asymmetrically substituted Pc on the solid support while the **B_4**-type symmetrical Pc forms in solution. Symmetrical Pc is removed by washing and subsequent cleavage of the linkage of "**A**" from the resin yields the pure **AB_3**-type Pc (Scheme 4).[72]
  The only restriction of this method is the necessity of an appropriate

functionalization on the phthalonitriles that can be bound to the polymer and subsequently cleaved from it.

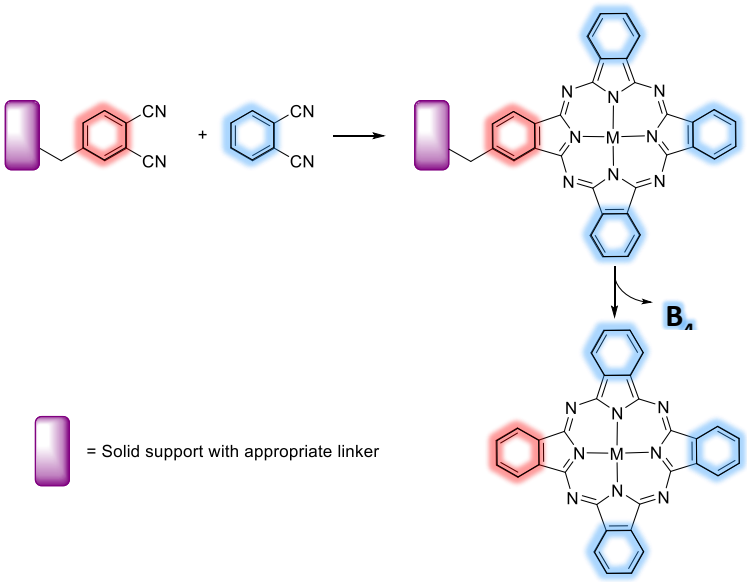

Scheme 4. General schematic representation of solid-phase synthesis of **A_3B** Pcs.

Specific methodologies can be employed also to obtain selectively the Pcs with **AABB** or **ABAB** relative distributions of substituents; some of them will be widely explored in *Chapter 1*.

Background in our group

During the last years, our group has focused on the preparation of Pcs and structural analogues, as well as on the study of their plausible application as molecular materials in different fields. Much effort has been concentrated on the preparation and study of molecular systems for energy conversion schemes, developing a large variety of covalent and non-covalent systems based on Pc chromophores and other electroactive species. Most of these systems have been studied by different spectroscopical techniques to analyze their photophysical properties, both in solution and in the solid state. The motivation of these studies is to identify and rationalize the photoinduced electron and/or energy transfer processes taking place in these artificial systems, which mimic the natural photosynthesis process.

Pcs usually perform as light-induced donors (and occasionally acceptors) of electrons in their donor-acceptor assemblies. Regarding the different acceptor counterparts, perylenediimides (PDIs) are good examples of effective oxidizing components in Pc based D-A hybrids.[74,75] Very recently, tetra- and octa – ferrocenyl Zn(II)Pcs and Ru(II)Pcs have been integrated into a series of orthogonal, supramolecular, cart-wheel-shaped Pc-PDI electron D-A systems (Figure 9).[28] In these arrays, coordination of ditopic PDI ligands containing two pyridyl substituents at its imido positions, enables selective interactions with the metal centers of Pcs. The presence of the strongly-donating ferrocene units in the Ru(II)Pc-PDI conjugates produces a slight acceleration of the charge separation upon photoexcitation of the PDI chromophore.

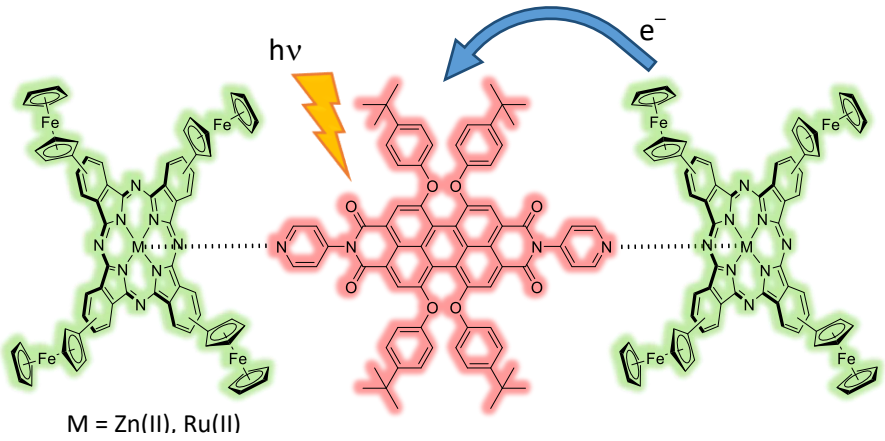

Figure 9. Structures of supramolecular cart-wheel-shaped Pc-PDI systems.

Among the acceptor units employed for the preparation of covalent and supramolecular systems, carbon nanostructures like fullerenes, carbon nanotubes (CNTs) and graphene deserve a special mention due to their excellent electron acceptor ability, which render them perfect molecular partners for photo- and electroactive systems.[76–81] Pc−C_{60} ensembles have been for a long time the main actors in this field, due to the commercial availability of C_{60} and the well-established synthetic methods for its functionalization. As a result, many Pc−C_{60} architectures have been prepared, featuring different connectivity (covalent or supramolecular), intermolecular interactions (self-organized or molecularly dispersed species), and Pc HOMO/LUMO levels.[80] In this context, Figure 10 shows an interesting D-A system, in which a *N*-pyridyl-substituted $Sc_3N@I_h$–C_{80} fulleropyrrolidines are axially coordinated to electron-rich or electron-deficient Zn(II)Pcs through zinc-pyridyl metal–ligand coordination, in order to activate oxidative and/or reductive electron transfer reactions.[79]

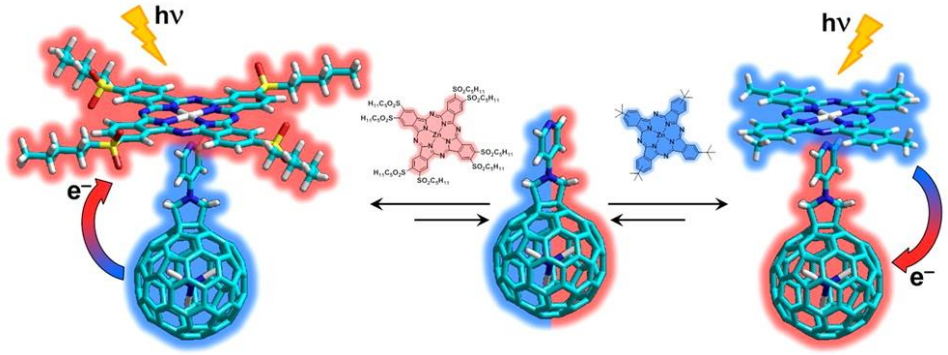

Figure 10. Self-assembly of photoresponsive, donor-acceptor supramolecular dyads.[79]

A breakthrough in the Pc−nanocarbon field was the appearance of CNTs and graphene, which opened a new avenue for the preparation of intriguing photoresponsive hybrid ensembles showing light-stimulated charge separation. The scarce solubility of these 1-D and 2-D nanocarbons, together with their lower reactivity with respect to C_{60} stemming from their less strained sp^2 carbon networks, has not meant an unsurmountable limitation for the preparation of variety of Pc-based hybrids.[80]

In this regard, our group extensively investigated the functionalization of single-walled carbon nanotubes (SWNTs) with Pcs, reporting several Pc-SWNT arrays achieved *via* covalent or supramolecular approaches. Figure 11 shows some of the strategies used so far: a) the Prato protocol, *via* 1,3-dipolar cycloaddition of appropriate formyl derivatives with *N*-octylglycine;[82] b) functionalization of SWNT with 4-ethynylbenzene derivative and the subsequent attachment of Pc

molecules using the Huisgen 1,3-dipolar cycloaddition;[83] c) *via* supramolecular approach using Pc-pyrene conjugates, taking advantage of the strong ability of pyrene to adhere to SWNT sidewalls by means of π-π interactions.[84] These systems, which show improved solubility and dispersibility features, bring together the unique electronic transport properties of CNTs with the excellent light-harvesting and tunable redox properties of Pcs.

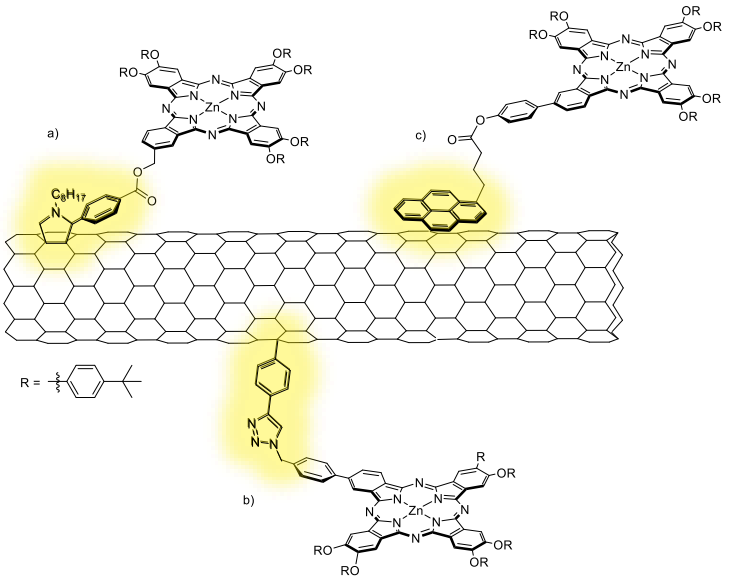

Figure 11. Molecular structure of Pc-SWNT ensembles obtained by: a) Prato protocol; b) click reaction; c) supramolecular strategy.

Graphene[85] enjoys a privileged position in the carbon nanoform family thanks to its unique optoelectronic features, namely, the extraordinarily high mobility of charges along its atomically flat structure, and its large surface area, which is suitable for the preparation of tailored hybrid materials by interaction with other optoelectronically active organic components. These properties make graphene a good candidate to explore its potential in solar energy conversion applications.

The liquid-phase exfoliation of graphite[86] recently evolved as a method to obtain stable dispersions of few defect, single-to-few-layer graphenes, which can be further covalently modified by means of chemical protocols such as cycloaddition or insertion reactions. The first approach pursued by the group to prepare these materials was the graphene supramolecular functionalization, using PPV oligomers bearing pendant Zn(II)Pcs.[87] These oligomers were able to assist the exfoliation of graphite in THF to form stable nanohybrids, since they feature strong adhesion capabilities towards graphene through π− π stacking interactions. Similarly, the group also prepared and studied covalently-linked Pc-

graphene hybrids with a relatively low functionalization degree of the graphene surface, that is beneficial to preserve the graphene electronic properties.[88,89] All these hybrid systems exhibit photoinduced electron transfer from the Pc component to the graphene layer.

On the other hand, our group has reported the first cases of covalent[90] and supramolecular[91] Pc−graphene ensembles showing an “inverted” graphene-to-Pc photoinduced charge transfer dynamics, taking advantage of the band-like electronic structure of these carbon nanoforms and the adjustable electronic levels of Pcs. In particular, peripheral functionalization of Pcs with strong electron-withdrawing substituents leads to a significant reduction of the HOMO and LUMO energies, thus making feasible an electron transfer process from the graphene sheets to the photoexcited Pc in Pc−graphene hybrids. Therefore, a covalently linked Pc−graphene ensemble was prepared by a “click” reaction between an azido-containing electron-accepting Zn(II)Pc and phenylethynyl-derivatized graphene (Figure 12).[90] On the other hand, linking pyrene to a alkylsulfonyl-functionalized Pc facilitates exfoliation of graphite leading to stable Pc−graphene supramolecular materials (Figure 12).[91]

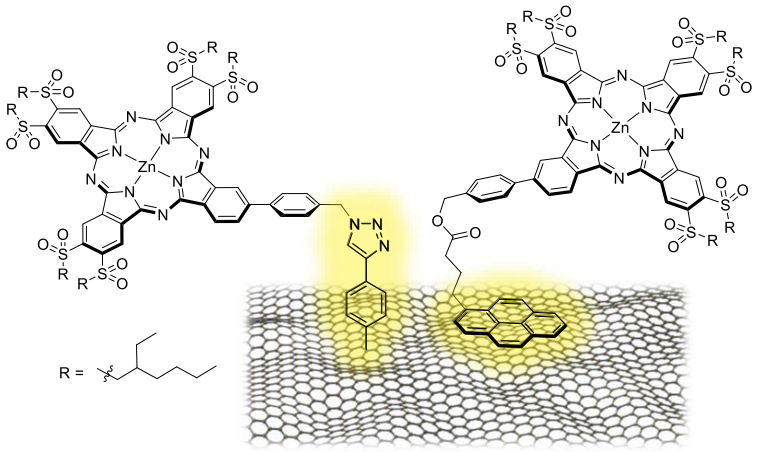

Figure 12. Molecular structure of covalent (left) and supramolecular (right) Zn(II)Pc−graphene ensembles.

Importantly, some of the Pc-CNT/graphene systems have been tested in photoelectrochemical cells to determine their potential application in solar conversion schemes.[82,87] Specifically, in the case of a H_2Pc-pyrene/SWCNT nanohybrid,[82] incident-photon-to-current (IPCE) efficiencies as large as 23% at a given wavelength were obtained, a value ranking among the highest reported for D–A SWCNT-based hybrids.

Closer to the real application is the work performed in the group in the field of organic photovoltaic devices (OPVs).[92–97] Also, the incorporation of Pcs and analogues as photosensitizers in organic-inorganic dye-sensitized solar cells (DSSCs) is another relevant field in which our group stood out in the last years. Briefly, DSSCs are devices consisting of a semiconductor layer, usually TiO_2, which is coated with a chromophore containing an anchoring moiety (i.e., a COOH group) that is able to inject electrons into the semiconductor after photoexcitation, thus creating an external current. Pcs are promising candidates for incorporation in DSSCs thanks to their physical and optical properties, namely photostability and absorption in the red/near IR region where the solar flux of photons is maximum. Promising results have been achieved using unsymmetrical **A_3B** Pcs showing a donor/acceptor pattern, in which three isoindolic units are functionalized with electron-donating groups, and the fourth isoindole is endowed with an anchoring/electron withdrawing carboxylic group.[9,10] The most relevant results in the photovoltaic field from us and others will be presented in detail in *Chapter 2*.

General Objectives

The main goal of this Doctoral Thesis is the synthesis of unprecedented unsymmetrically substituted Pcs with a linear, face-to-face arrangement of the functional groups anchored to the aromatic core, and their use as building blocks in the construction of novel and functional multicomponent systems.

The preparation of **ABAB** Pcs with appropriate crosswise functionalization, operational as ditopic units in multicomponent systems, has always been an intriguing but also an evanescent subject, as widely discussed in *Chapter 1*. Owing to the lack of synthetic methodologies leading to **ABAB** Pcs in reasonable amounts, the research related to the incorporation of this type of units in more complex molecular or supramolecular ensembles remains underdeveloped. This thesis poses the challenge of opening a new avenue for the preparation of face-to-face functionalized Pcs and, therefore, new intriguing systems based on them.

More in detail, the objectives of this work are defined as follows:

Chapter 1 is devoted to the development of a general strategy for the controlled synthesis of **ABAB** Pcs (Figure 13). For this purpose, a series of bulky phthalonitriles with appropriate functionalization in the α-positions to hamper their self-condensation will be designed and prepared. This approach should prevent the formation of the undesired **AABB** isomer and allow us to direct the synthesis towards the formation of the target **ABAB** Pcs. These bulky phthalonitriles will be reacted under statistical conditions with other phthalonitriles carrying functional groups that allow further functionalization of the crosswise **ABAB** Pcs obtained.

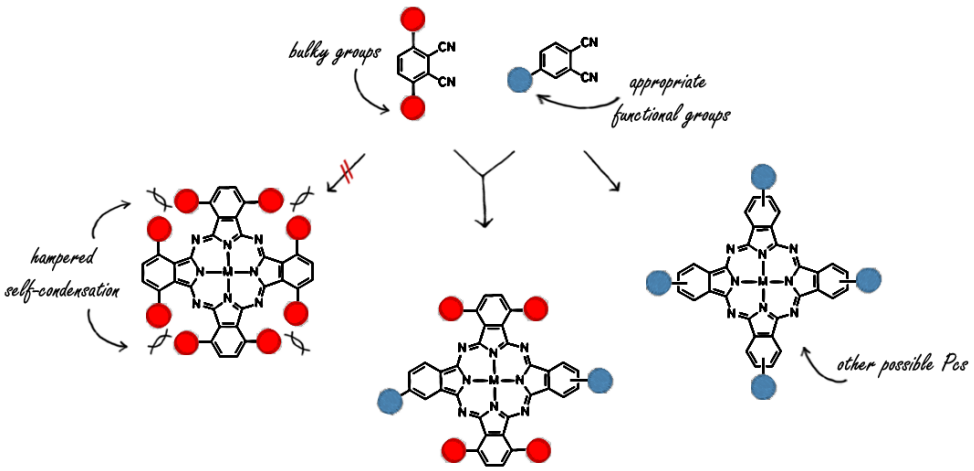

Figure 13. Schematic representation of the general strategy for the synthesis of **ABAB** Pcs that will be tackled in Chapter 1.

The aim of **Chapter 2** is the synthesis and characterization of novel, linear donor–π–acceptor systems based on Pcs.

First, a battery of linear push-pull Pcs will be prepared, which will be explored as photosensitizers in DSSCs. For this purpose, a starting **ABAB** Pc carrying appropriate functional groups (like iodine) will be asymmetrically functionalized with electron-donating and electron- withdrawing groups, the latter operating also as anchoring units for their implementation in the device. This functionalization pattern follows the donor–π–acceptor architecture of porphyrins (Pors) that have reached the highest photon-to-electron conversion efficiencies reported to date for this type of cells. It is our goal to optimize the efficiency as photosensitizers of the donor–π–acceptor Pcs through the variation in the nature of the linker between either the electron – donor or the electron – acceptor moieties and the Pc core.

In the same chapter, a family of new donor–π–acceptor multicomponent triads will be prepared as artificial photosynthetic models to study the fundamental energy/electron transfer process that can take place after photoexcitation of the absorbing units (Figure 14). In these systems, the Pc component will act as electron/energy funnel between the donor and the acceptor components, which must exhibit complementary features to the central Pc, namely suitable HOMO and LUMO energy levels and adequate absorption of solar light, in order to achieve a cascade – like photoinduced electron/energy transfer event.

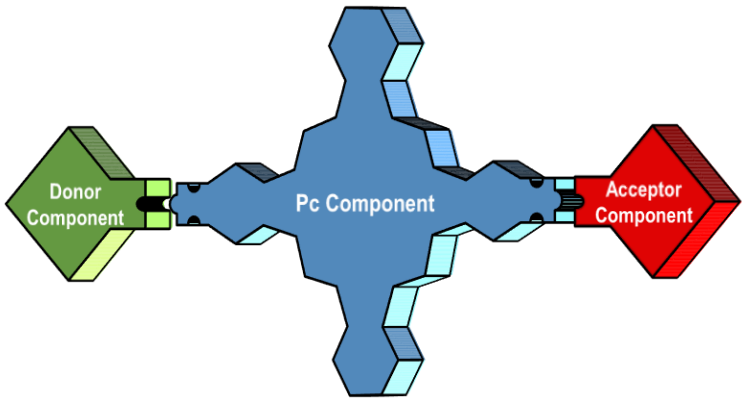

Figure 14. Schematic representation of the target D–π–A multicomponent systems based on crosswise functionalized Pcs that will be studied in Chapter 2.

Chapter 3 is focused on the synthesis and characterization of novel supramolecular architectures based on Pcs. The use of Pcs as subcomponents for the self-assembly of supramolecular hosts relies on the preparation of unsymmetrically functionalized **ABAB** derivatives holding two opposite bridging units. Until now, this fact has limited the use of Pcs for the preparation of polyhedral ensembles via supramolecular interactions. Making use of the **ABAB** Pcs prepared in this Thesis, the objective of this part of the work is the construction of unprecedented metallo-supramolecular assemblies based on Pc ligands (Figure 15). To this end, we plan to use well-established *metallo-organic subcomponent self-assembly strategies*. Furthermore, the Pc-based, supramolecular capsules will be explored as hosts for different organic guests with a good size-shape match.

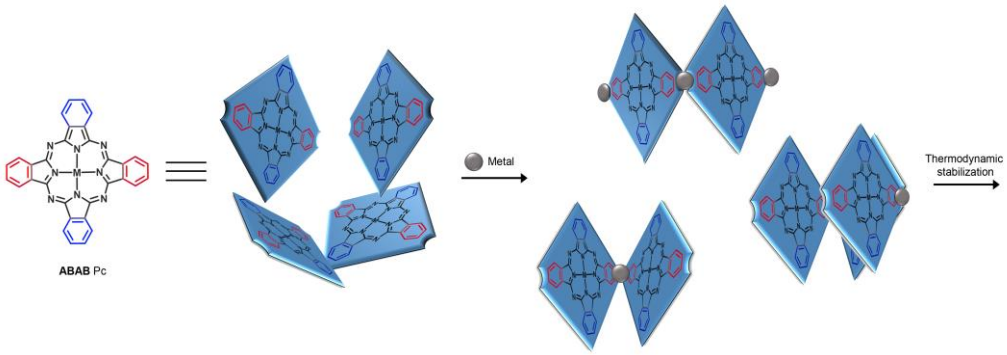

Figure 15. Schematic representation of the preparation of metallo-supramolecular assemblies based on Pc ligands that will be studied in Chapter 3.

References

(1) Lewis, W. S. Horace Walpole's Correspondence; University of Oklahoma Press, 1965.

(2) Lax, E. *The Mold in Dr. Florey's Coat: The Story of the Penicillin Miracle*; Holt Paperbacks, 2004.

(3) Myers, R. L.; Myers, R. L. *The 100 Most Important Chemical Compounds*; Westport, Conn: Greenwood Press, 2007.

(4) Travis, A. S. Perkin's Mauve: Ancestor of the Organic Chemical Industry. *Technol. Cult.* **1990**, *31*, 51–82.

(5) Braun, A.; Tcherniac, J. Über Die Produkte Der Einwirkung von Acetanhydrid Auf Phthalamid. *Berichte der Dtsch. Chem. Gesellschaft* **1907**, *40*, 2709–2714.

(6) de Diesbach, H.; von der Weid, E. Quelques Sels Complexes Des O-Dinitriles Avec Le Cuivre et La Pyridine. *Helv. Chim. Acta* **1927**, *10*, 886–888.

(7) Dahlen, M. A. The Phthalocyanines A New Class of Synthetic Pigments and Dyes. *Ind. Eng. Chem.* **1939**, *31*, 839–847.

(8) Leznoff, C. C.; Lever, A. B. P. *Phthalocyanines: Properties and Applications*; Phthalocyanines: Properties and Applications; VCH, 1989.

(9) Ikeuchi, T.; Nomoto, H.; Masaki, N.; Griffith, M. J.; Mori, S.; Kimura, M. Molecular Engineering of Zinc Phthalocyanine Sensitizers for Efficient Dye-Sensitized Solar Cells. *Chem. Commun.* **2014**, *50*, 1941–1943.

(10) Ragoussi, M.-E.; Cid, J.-J.; Yum, J.-H.; de la Torre, G.; Di Censo, D.; Grätzel, M.; Nazeeruddin, M. K.; Torres, T. Carboxyethynyl Anchoring Ligands: A Means to Improving the Efficiency of Phthalocyanine-Sensitized Solar Cells. *Angew. Chemie Int. Ed.* **2012**, *51*, 4375–4378.

(11) Ben-Hur, E.; Chan, W.-S. 117 - Phthalocyanines in Photobiology and Their Medical Applications A2 - Kadish, Karl M.; Smith, K. M., Guilard, R. B. T.-T. P. H., Eds.; Academic Press: Amsterdam, 2003; pp 1–35.

(12) Wöhrle, D. Phthalocyanines: Properties and Applications, Volume 3. Edited by C. C. Leznoff and A. B. P. Lever, VCH, Weinheim 1993, 303 Pp., Hardcover, DM 198, ISBN3-527-89638-4. *Adv. Mater.* **1993**, *5*, 943–944.

(13) Law, K. Y. Organic Photoconductive Materials: Recent Trends and Developments. *Chem. Rev.* **1993**, *93*, 449–486.

(14) Chen, Y.; Su, W.; Bai, M.; Jiang, J.; Li, X.; Liu, Y.; Wang, L.; Wang, S. High Performance Organic Field-Effect Transistors Based on Amphiphilic Tris(phthalocyaninato) Rare Earth Triple-Decker Complexes. *J. Am. Chem. Soc.* **2005**, *127*, 15700–15701.

(15) de la Torre, G.; Vázquez, P.; Agulló-López, F.; Torres, T. Role of Structural Factors in the Nonlinear Optical Properties of Phthalocyanines and Related Compounds. *Chem. Rev.* **2004**, *104*, 3723–3750.

(16) Kimura, M.; Ueki, H.; Ohta, K.; Shirai, H.; Kobayashi, N. Self-Organization of Low-Symmetry Adjacent-Type Metallophthalocyanines Having Branched Alkyl Chains. *Langmuir* **2006**, *22*, 5051–5056.

(17) Cammidge, A. N.; Gopee, H. Macrodiscotic Triphenylenophthalocyanines. *Chem. Commun.* **2002**, *0*, 966–967.
(18) de la Torre, G.; Bottari, G.; Hahn, U.; Torres, T. Functional Phthalocyanines: Synthesis, Nanostructuration, and Electro-Optical Applications. In *Functional Phthalocyanine Molecular Materials*; Jiang, J., Ed.; Structure and Bonding; Springer Berlin Heidelberg, 2010; Vol. 135, pp 1–44.
(19) Claessens, C. G.; Hahn, U.; Torres, T. Phthalocyanines: From Outstanding Electronic Properties to Emerging Applications. *Chem. Rec.* **2008**, *8*, 75–97.
(20) de la Torre, G.; Claessens, C. G.; Torres, T. Phthalocyanines: Old Dyes, New Materials. Putting Color in Nanotechnology. *Chem. Commun.* **2007**, 2000–2015.
(21) Mack, J.; Kobayashi, N. Low Symmetry Phthalocyanines and Their Analogues. *Chem. Rev.* **2011**, *111*, 281–321.
(22) Leznoff, C. C.; Lever, A. B. P. Phthalocyanines: Properties and Applications, Vols. 1–4VCH Publishers. *New York* **1989**.
(23) McKeown, N. B. *Phthalocyanine Materials Synthesis, Structure and Function*; Cambridge University Press, Cambridge, 1998.
(24) Ortí, E.; Brédas, J. L. Electronic Structure of Metal-free Phthalocyanine: A Valence Effective Hamiltonian Theoretical Study. *J. Chem. Phys.* **1988**, *89*, 1009–1016.
(25) Mack, J.; Stillman, M. J. Assignment of the Optical Spectra of Metal Phthalocyanines through Spectral Band Deconvolution Analysis and Zindo Calculations. *Coord. Chem. Rev.* **2001**, *219*, 993–1032.
(26) Rawling, T.; Austin, C.; Buchholz, F.; Colbran, S. B.; McDonagh, A. M. Ruthenium Phthalocyanine-Bipyridyl Dyads as Sensitizers for Dye-Sensitized Solar Cells: Dye Coverage versus Molecular Efficiency. *Inorg. Chem.* **2009**, *48*, 3215–3227.
(27) Rodríguez-Morgade, M. S.; Plonska-Brzezinska, M. E.; Athans, A. J.; Carbonell, E.; de Miguel, G.; Guldi, D. M.; Echegoyen, L.; Torres, T. Synthesis, Characterization, and Photoinduced Electron Transfer Processes of Orthogonal Ruthenium Phthalocyanine−Fullerene Assemblies. *J. Am. Chem. Soc.* **2009**, *131*, 10484–10496.
(28) Fernández-Ariza, J.; Krick Calderón, R. M.; Rodríguez-Morgade, M. S.; Guldi, D. M.; Torres, T. Phthalocyanine–Perylenediimide Cart Wheels. *J. Am. Chem. Soc.* **2016**, *138*, 12963–12974.
(29) Li, X.; Ng, D. K. P. Self-Assembly of Meso-Pyridylporphyrins and Zinc Phthalocyanines Through Axial Coordination. *Eur. J. Inorg. Chem.* **2000**, *2000*, 1845–1848.
(30) Guldi, D. M.; Ramey, J.; Martinez-Diaz, M. V.; Escosura, A. de la; Torres, T.; Da Ros, T.; Prato, M. Reversible Zinc Phthalocyanine Fullerene Ensembles. *Chem. Commun.* **2002**, *0*, 2774–2775.
(31) Kameyama, K.; Morisue, M.; Satake, A.; Kobuke, Y. Highly Fluorescent Self-Coordinated Phthalocyanine Dimers. *Angew. Chemie Int. Ed.* **2005**,

44, 4763–4766.
(32) Leng, X.; Choi, C.-F.; Lo, P.-C.; Ng, D. K. P. Assembling a Mixed Phthalocyanine−Porphyrin Array in Aqueous Media through Host−Guest Interactions. *Org. Lett.* **2007**, *9*, 231–234.
(33) van de Winckel, E.; Schneider, R. J.; de la Escosura, A.; Torres, T. Multifunctional Logic in a Photosensitizer with Triple-Mode Fluorescent and Photodynamic Activity. *Chem. – A Eur. J.* **2015**, *21*, 18551–18556.
(34) Kudrevich, S. V; van Lier, J. E. Azaanalogs of Phthalocyanine: Syntheses and Properties. *Coord. Chem. Rev.* **1996**, *156*, 163–182.
(35) Nicolau, M.; Cabezón, B.; Torres, T. Triazolephthalocyanines: Synthesis, Supramolecular Organization and Physical Properties. *Coord. Chem. Rev.* **1999**, *190–192*, 231–243.
(36) Kobayashi, N.; Miwa, H.; Nemykin, V. N. Adjacent versus Opposite Type Di-Aromatic Ring-Fused Phthalocyanine Derivatives: Synthesis, Spectroscopy, Electrochemistry, and Molecular Orbital Calculations. *J. Am. Chem. Soc.* **2002**, *124*, 8007–8020.
(37) Claessens, C. G.; Torres, T. Synthesis, Separation, and Characterization of the Topoisomers of Fused Bicyclic Subphthalocyanine Dimers. *Angew. Chemie Int. Ed.* **2002**, *41*, 2561–2565.
(38) Torres, T. From Subphthalocyanines to Subporphyrins. *Angew. Chemie Int. Ed.* **2006**, *45*, 2834–2837.
(39) Muranaka, A.; Yonehara, M.; Uchiyama, M. Azulenocyanine: A New Family of Phthalocyanines with Intense Near-IR Absorption. *J. Am. Chem. Soc.* **2010**, *132*, 7844–7845.
(40) Kobayashi, N.; Nakajima, S.; Ogata, H.; Fukuda, T. Synthesis, Spectroscopy, and Electrochemistry of Tetra-Tert-Butylated Tetraazaporphyrins, Phthalocyanines, Naphthalocyanines, and Anthracocyanines, Together with Molecular Orbital Calculations. *Chem. – A Eur. J.* **2004**, *10*, 6294–6312.
(41) Alexander, V. Design and Synthesis of Macrocyclic Ligands and Their Complexes of Lanthanides and Actinides. *Chem. Rev.* **1995**, *95*, 273–342.
(42) de la Torre, G.; Martínez-Díaz, M. V.; Ashton, P. R.; Torres, T. Novel Homo- and Heterodimetallic Heterobinuclear Phthalocyaninato-Triazolehemiporphyrazinate Complexes. *J. Org. Chem.* **1998**, *63*, 8888–8893.
(43) Dubinina, T. V; Ivanov, A. V; Borisova, N. E.; Trashin, S. A.; Gurskiy, S. I.; Tomilova, L. G.; Zefirov, N. S. Synthesis and Investigation of Spectral and Electrochemical Properties of Alkyl-Substituted Planar Binuclear Phthalocyanine Complexes Sharing a Common Naphthalene Ring. *Inorganica Chim. Acta* **2010**, *363*, 1869–1878.
(44) Kadish, K. M.; Smith, K. M.; Guilard, R. *The Porphyrin Handbook: Phthalocyanines : Synthesis*; The Porphyrin Handbook; Academic Press, 2003.
(45) Anbarasan, P.; Schareina, T.; Beller, M. Recent Developments and Perspectives in Palladium-Catalyzed Cyanation of Aryl Halides: Synthesis

of Benzonitriles. *Chem. Soc. Rev.* **2011**, *40*, 5049–5067.
(46) Tomoda, H.; Saito, S.; Ogawa, S.; Shiraishi, S. Synthesis of Phthalocyanines from Phthalonitrile with Organic Strong Bases. *Chem. Lett.* **1980**, *9*, 1277–1280.
(47) Leznoff, C. C.; Hu, M.; Nolan, K. J. M. The Synthesis of Phthalocyanines at Room Temperature. *Chem. Commun.* **1996**, *0*, 1245–1246.
(48) Day, V. W.; Marks, T. J.; Wachter, W. A. Large Metal Ion-Centered Template Reactions. Uranyl Complex of cyclopentakis(2-Iminoisoindoline). *J. Am. Chem. Soc.* **1975**, *97*, 4519–4527.
(49) Busch, D. H.; Stephenson, N. A. Molecular Organization, Portal to Supramolecular Chemistry. *Coord. Chem. Rev.* **1990**, *100*, 119–154.
(50) Rager, C.; Schmid, G.; Hanack, M. Influence of Substituents, Reaction Conditions and Central Metals on the Isomer Distributions of 1(4)-Tetrasubstituted Phthalocyanines. *Chem. – A Eur. J.* **1999**, *5*, 280–288.
(51) Leznoff, C. C.; D'Ascanio, A. M.; Yildiz, S. Z. Phthalocyanine Formation Using Metals in Primary Alcohols at Room Temperature. *J. Porphyr. Phthalocyanines* **2000**, *4*, 103–111.
(52) Oliver, S. W.; Smith, T. D. Oligomeric Cyclization of Dinitriles in the Synthesis of Phthalocyanines and Related Compounds: The Role of the Alkoxide Anion. *J. Chem. Soc. Perkin Trans. 2* **1987**, *0*, 1579–1582.
(53) Uchida, H.; Tanaka, H.; Yoshiyama, H.; Reddy, P. Y.; Nakamura, S.; Toru, T. Novel Synthesis of Phthalocyanines from Phthalonitriles under Mild Conditions. *Synlett* **2002**, *2002*, 1649–1652.
(54) Uchida, H.; Yoshiyama, H.; Reddy, P. Y.; Nakamura, S.; Toru, T. Novel Synthesis of Metal-Free Phthalocyanines from Phthalimides and Phthalic Anhydrides with Hexamethyldisilazane. *Synlett* **2003**, *2003*, 2083–2085.
(55) Kopylovich, M. N.; Kukushkin, V. Y.; Haukka, M.; Luzyanin, K. V; Pombeiro, A. J. L. An Efficient Synthesis of Phthalocyanines Based on an Unprecedented Double-Addition of Oximes to Phthalonitriles. *J. Am. Chem. Soc.* **2004**, *126*, 15040–15041.
(56) Nas, A.; Kaya, E. Ç.; Kantekin, H.; Sökmen, A.; Çakır, V. Microwave-Assisted Synthesis and Characterization of Novel Symmetrical Substituted 19-Membered Tetrathiadiaza Metal-Free and Metallophthalocyanines and Investigation of Their Biological Activities. *J. Organomet. Chem.* **2011**, *696*, 1659–1663.
(57) Rodríguez-Morgade, S.; Hanack, M. Synthesis, Separation and Characterization of the Structural Isomers of Octa-Tert-Butylphthalocyanines and Dienophilic Phthalocyanine Derivatives. *Chem. – A Eur. J.* **1997**, *3*, 1042–1051.
(58) Hanack, M.; Schmid, G.; Sommerauer, M. Chromatographic Separation of the Four Possible Structural Isomers of a Tetrasubstituted Phthalocyanine: Tetrakis(2-ethylhexyloxy)phthalocyaninatonickel(II). *Angew. Chemie Int. Ed. English* **1993**, *32*, 1422–1424.
(59) Kimura, M.; Sugihara, Y.; Muto, T.; Hanabusa, K.; Shirai, H.; Kobayashi, N. Dendritic Metallophthalocyanines—Synthesis, Electrochemical

Properties, and Catalytic Activities. *Chem. – A Eur. J.* **1999**, *5*, 3495–3500.
(60) Kobayashi, N.; Kobayashi, Y.; Osa, T. Optically Active Phthalocyanines and Their Circular Dichroism. *J. Am. Chem. Soc.* **1993**, *115*, 10994–10995.
(61) Iida, N.; Tanaka, K.; Tokunaga, E.; Mori, S.; Saito, N.; Shibata, N. Synthesis of Phthalocyanines with a Pentafluorosulfanyl Substituent at Peripheral Positions. *ChemistryOpen* **2015**, *4*, 698–702.
(62) Torres, T. Perspectives in the Selective Synthesis of Phthalocyanines and Related Compounds. *J. Porphyr. Phthalocyanines* **2000**, *4*, 325–330.
(63) de la Torre, G.; Claessens, C. G.; Torres, T. Phthalocyanines: The Need for Selective Synthetic Approaches. *European J. Org. Chem.* **2000**, *2000*, 2821–2830.
(64) El-Nahass, M. M.; Youssef, T. E. Thin Films of Asymmetrically Substituted "ABAB-Type" Indium Phthalocyanine Chloride: Preparation, Structural Characterization and Optical Properties. *J. Lumin.* **2011**, *131*, 1419–1427.
(65) Youssef, T. E.; O'Flaherty, S.; Blau, W.; Hanack, M. Phthalocyaninatoindium(III) Acetylacetonates for Nonlinear Optics. *European J. Org. Chem.* **2004**, *2004*, 101–108.
(66) Kobayashi, N.; Kondo, R.; Nakajima, S.; Osa, T. New Route to Unsymmetrical Phthalocyanine Analogs by the Use of Structurally Distorted Subphthalocyanines. *J. Am. Chem. Soc.* **1990**, *112*, 9640–9641.
(67) Claessens, C. G.; González-Rodríguez, D.; Torres, T. Subphthalocyanines: Singular Nonplanar Aromatic CompoundsSynthesis, Reactivity, and Physical Properties. *Chem. Rev.* **2002**, *102*, 835–854.
(68) Claessens, C. G.; González-Rodríguez, D.; Rodríguez-Morgade, M. S.; Medina, A.; Torres, T. Subphthalocyanines, Subporphyrazines, and Subporphyrins: Singular Nonplanar Aromatic Systems. *Chem. Rev.* **2014**, *114*, 2192–2277.
(69) Sastre, A.; Torres, T.; Hanack, M. Synthesis of Novel Unsymmetrical Monoaminated Phthalocyanines. *Tetrahedron Lett.* **1995**, *36*, 8501–8504.
(70) Kudrevich, S. V; Gilbert, S.; van Lier, J. E. Syntheses of Trisulfonated Phthalocyanines and Their Derivatives Using Boron(III) Subphthalocyanines as Intermediates. *J. Org. Chem.* **1996**, *61*, 5706–5707.
(71) Sastre, Á.; del Rey, B.; Torres, T. Synthesis of Novel Unsymmetrically Substituted Push-Pull Phthalocyanines. *J. Org. Chem.* **1996**, *61*, 8591–8597.
(72) Erdem, S. S.; Nesterova, I. V; Soper, S. A.; Hammer, R. P. Solid-Phase Synthesis of Asymmetrically Substituted "AB3-Type" Phthalocyanines. *J. Org. Chem.* **2008**, *73*, 5003–5007.
(73) Leznoff, C. C.; Hall, T. W. The Synthesis of a Soluble, Unsymmetrical Phthalocyanine on a Polymer Support. *Tetrahedron Lett.* **1982**, *23*, 3023–3026.

(74) Sekita, M.; Jiménez, Á. J.; Marcos, M. L.; Caballero, E.; Rodríguez-Morgade, M. S.; Guldi, D. M.; Torres, T. Tuning the Electron Acceptor in Phthalocyanine-Based Electron Donor–Acceptor Conjugates. *Chem. – A Eur. J.* **2015**, *21*, 19028–19040.

(75) Jimenez, A. J.; Calderon, R. M. K.; Rodriguez-Morgade, M. S.; Guldi, D. M.; Torres, T. Synthesis, Characterization and Photophysical Properties of a Melamine-Mediated Hydrogen-Bound Phthalocyanine-Perylenediimide Assembly. *Chem. Sci.* **2013**, *4*, 1064–1074.

(76) Hahn, U.; Engmann, S.; Oelsner, C.; Ehli, C.; Guldi, D. M.; Torres, T. Immobilizing Water-Soluble Dendritic Electron Donors and Electron Acceptors—Phthalocyanines and Perylenediimides—onto Single Wall Carbon Nanotubes. *J. Am. Chem. Soc.* **2010**, *132*, 6392–6401.

(77) Bottari, G.; de la Torre, G.; Guldi, D. M.; Torres, T. Covalent and Noncovalent Phthalocyanine−Carbon Nanostructure Systems: Synthesis, Photoinduced Electron Transfer, and Application to Molecular Photovoltaics. *Chem. Rev.* **2010**, *110*, 6768–6816.

(78) de la Torre, G.; Bottari, G.; Sekita, M.; Hausmann, A.; Guldi, D. M.; Torres, T. A Voyage into the Synthesis and Photophysics of Homo- and Heterobinuclear Ensembles of Phthalocyanines and Porphyrins. *Chem. Soc. Rev.* **2013**, *42*, 8049–8105.

(79) Trukhina, O.; Rudolf, M.; Bottari, G.; Akasaka, T.; Echegoyen, L.; Torres, T.; Guldi, D. M. Bidirectional Electron Transfer Capability in Phthalocyanine–Sc3N@Ih–C80 Complexes. *J. Am. Chem. Soc.* **2015**, *137*, 12914–12922.

(80) Bottari, G.; de la Torre, G.; Torres, T. Phthalocyanine–Nanocarbon Ensembles: From Discrete Molecular and Supramolecular Systems to Hybrid Nanomaterials. *Acc. Chem. Res.* **2015**, *48*, 900–910.

(81) Wolf, M.; Villegas, C.; Trukhina, O.; Delgado, J. L.; Torres, T.; Martín, N.; Clark, T.; Guldi, D. M. Mediating Reductive Charge Shift Reactions in Electron Transport Chains. *J. Am. Chem. Soc.* **2017**, *139*, 17474–17483.

(82) Ballesteros, B.; de la Torre, G.; Ehli, C.; Aminur Rahman, G. M.; Agulló-Rueda, F.; Guldi, D. M.; Torres, T. Single-Wall Carbon Nanotubes Bearing Covalently Linked Phthalocyanines − Photoinduced Electron Transfer. *J. Am. Chem. Soc.* **2007**, *129*, 5061–5068.

(83) Campidelli, S.; Ballesteros, B.; Filoramo, A.; Díaz, D. D.; de la Torre, G.; Torres, T.; Rahman, G. M. A.; Ehli, C.; Kiessling, D.; Werner, F.; et al. Facile Decoration of Functionalized Single-Wall Carbon Nanotubes with Phthalocyanines via “Click Chemistry.” *J. Am. Chem. Soc.* **2008**, *130*, 11503–11509.

(84) Bartelmess, J.; Ballesteros, B.; de la Torre, G.; Kiessling, D.; Campidelli, S.; Prato, M.; Torres, T.; Guldi, D. M. Phthalocyanine−Pyrene Conjugates: A Powerful Approach toward Carbon Nanotube Solar Cells. *J. Am. Chem. Soc.* **2010**, *132*, 16202–16211.

(85) Novoselov, K. S.; Geim, A. K.; Morozov, S. V; Jiang, D.; Zhang, Y.; Dubonos, S. V; Grigorieva, I. V; Firsov, A. A. Electric Field Effect in Atomically Thin Carbon Films. *Science (80-.).* **2004**, *306*, 666 LP-669.

(86) Hernandez, Y.; Nicolosi, V.; Lotya, M.; Blighe, F. M.; Sun, Z.; De, S.; T., M.; Holland, B.; Byrne, M.; Gun'Ko, Y. K.; et al. High-Yield Production of Graphene by Liquid-Phase Exfoliation of Graphite. *Nat Nano* **2008**, *3*, 563–568.

(87) Malig, J.; Jux, N.; Kiessling, D.; Cid, J.-J.; Vázquez, P.; Torres, T.; Guldi, D. M. Towards Tunable Graphene/Phthalocyanine–PPV Hybrid Systems. *Angew. Chemie Int. Ed.* **2011**, *50*, 3561–3565.

(88) Ragoussi, M.-E.; Malig, J.; Katsukis, G.; Butz, B.; Spiecker, E.; de la Torre, G.; Torres, T.; Guldi, D. M. Linking Photo- and Redoxactive Phthalocyanines Covalently to Graphene. *Angew. Chemie Int. Ed.* **2012**, *51*, 6421–6425.

(89) Malig, J.; Jux, N.; Guldi, D. M. Toward Multifunctional Wet Chemically Functionalized Graphene—Integration of Oligomeric, Molecular, and Particulate Building Blocks That Reveal Photoactivity and Redox Activity. *Acc. Chem. Res.* **2013**, *46*, 53–64.

(90) Ragoussi, M.-E.; Katsukis, G.; Roth, A.; Malig, J.; de la Torre, G.; Guldi, D. M.; Torres, T. Electron-Donating Behavior of Few-Layer Graphene in Covalent Ensembles with Electron-Accepting Phthalocyanines. *J. Am. Chem. Soc.* **2014**, *136*, 4593–4598.

(91) Roth, A.; Ragoussi, M.-E.; Wibmer, L.; Katsukis, G.; Torre, G. de la; Torres, T.; Guldi, D. M. Electron-Accepting Phthalocyanine-Pyrene Conjugates: Towards Liquid Phase Exfoliation of Graphite and Photoactive Nanohybrid Formation with Graphene. *Chem. Sci.* **2014**, *5*, 3432–3438.

(92) Ryan, J. W.; Anaya-Plaza, E.; Escosura, A. de la; Torres, T.; Palomares, E. Small Molecule Solar Cells Based on a Series of Water-Soluble Zinc Phthalocyanine Donors. *Chem. Commun.* **2012**, *48*, 6094–6096.

(93) Gommans, H.; Aernouts, T.; Verreet, B.; Heremans, P.; Medina, A.; Claessens, C. G.; Torres, T. Perfluorinated Subphthalocyanine as a New Acceptor Material in a Small-Molecule Bilayer Organic Solar Cell. *Adv. Funct. Mater.* **2009**, *19*, 3435–3439.

(94) Verreet, B.; Rand, B. P.; Cheyns, D.; Hadipour, A.; Aernouts, T.; Heremans, P.; Medina, A.; Claessens, C. G.; Torres, T. A 4% Efficient Organic Solar Cell Using a Fluorinated Fused Subphthalocyanine Dimer as an Electron Acceptor. *Adv. Energy Mater.* **2011**, *1*, 565–568.

(95) Cnops, K.; Zango, G.; Genoe, J.; Heremans, P.; Martinez-Diaz, M. V.; Torres, T.; Cheyns, D. Energy Level Tuning of Non-Fullerene Acceptors in Organic Solar Cells. *J. Am. Chem. Soc.* **2015**, *137*, 8991–8997.

(96) de la Torre, G.; Bottari, G.; Torres, T. Phthalocyanines and Subphthalocyanines: Perfect Partners for Fullerenes and Carbon Nanotubes in Molecular Photovoltaics. *Adv. Energy Mater.* **2016**, 1601700.

(97) Duan, C.; Zango, G.; García Iglesias, M.; Colberts, F. J. M.; Wienk, M. M.; Martínez-Díaz, M. V.; Janssen, R. A. J.; Torres, T. The Role of the Axial Substituent in Subphthalocyanine Acceptors for Bulk-Heterojunction Solar Cells. *Angew. Chemie Int. Ed.* **2017**, *56* (1), 148–152.

Chapter 1 – Synthesis of ABAB phthalocyanines

1.1 State of the art

As stated in the Introduction Chapter, statistical cyclotetramerization of two different phthalonitriles leads to the formation of a mixture of Pcs that, in a second step, has to be separated by chromatography. Using this methodology, the synthesis of $\mathbf{A_2B_2}$ compounds has proven more challenging than that of their $\mathbf{A_3B}$ counterparts, due to the difficult separation of the two isomers, namely **ABAB** and **AABB**, by chromatographic techniques. To overcome this issue, several research groups have used the so-called *directed approach* to synthesize selectively a single constitutional isomer of the $\mathbf{A_2B_2}$ type. This strategy involves the rational design of phthalonitrile precursors which are *"forced"* to lead to only one isomer.

Kobayashi and co-workers paved the way for this approach, describing the exclusive formation of a D_{2h} symmetrically tetrasubstituted Pc by simply linking two phthalonitrile units at their 4-positions with appropriate spacers. In particular, they obtained a chiral D_{2h} isomer using an optically active 2,29-dihydroxy-1,19-binaphthyl bridge (Figure 1.1a).[1] One year later, Leznoff and co-workers followed a similar strategy to generate solely the D_{2h} isomer of a tetrasubstituted Pc, using a dimer composed of two phthalonitrile units linked through their 3-positions with a 2,2-disubstituted propan-1,3-diol spacer (Figure 1.1b).[2]

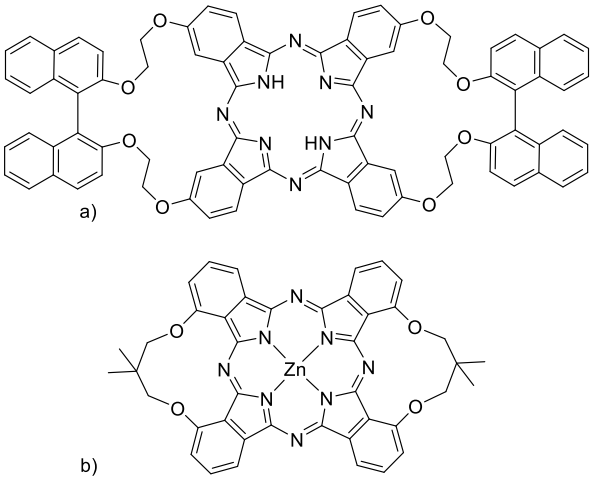

Figure 1.1. Structures of D_{2h} isomers of symmetrically substituted Pcs.

Following the same concept, Kobayashi undertook the synthesis of **AABB** derivatives using bis(phthalonitriles) linked by appropriately constrained bridging groups, such as the above mentioned 2,29-dihydroxy-1,19-binaphthyl. Such precursors react with other differently substituted phthalonitriles to furnish the adjacent-type Pcs in 20-25% yield (Scheme 1.1).[3,4]

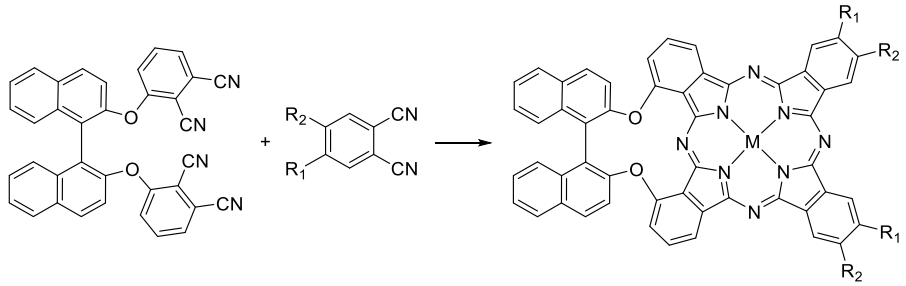

Scheme 1.1. Example of directed synthesis of **AABB**-type asymmetric Pcs.

A second approach, developed by Leznoff and co-workers, can be used to obtain selectively **AABB** Pcs, which is sometimes referred to as the *lithium method*. This methodology involves the use of a *half-Pc* intermediate, which can be isolated and subsequently treated with another phthalonitrile under very mild conditions (Scheme 1.2).[5] The preparation of half intermediates had been reported previously,[6] but it was proposed that only phthalonitriles bearing strong electron-withdrawing groups could give rise to such stable intermediates. In Leznoff's work, treatment of 4,5-bis(3,3-dimethyl-1-butynyl)phthalonitrile with lithium alkoxide in refluxing methanol gave the corresponding intermediate, which was then treated with phthalonitrile in a second step (Scheme 1.2) to furnish the **AABB** Pc in 20% yield, along with some amounts of other possible Pcs.

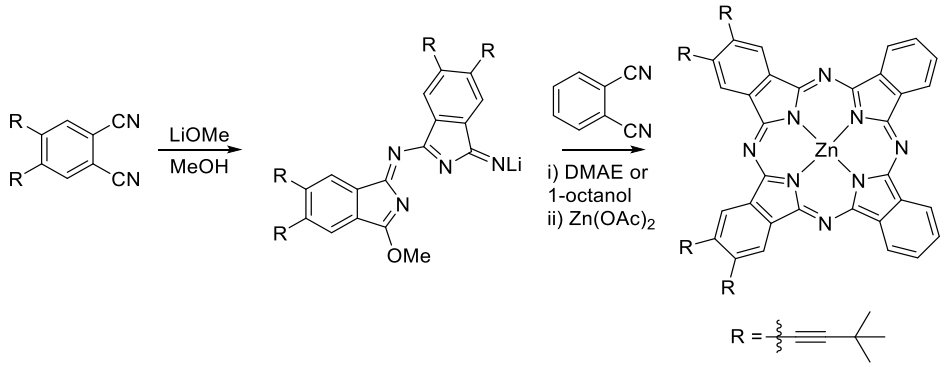

Scheme 1.2. Leznoff's approach to selectively form **AABB** Pcs.

Subsequently, Kobayashi refined this method using 3,6-diphenylphthalonitrile. This bulky phthalonitrile reacted to form a stable *half-Pc* in the presence of lithium hexyl oxide at *ca*. 150 °C, which did not evolve to the Pc because tetramerization is disfavored by the steric hindrance between neighboring peripheral substituents. Subsequent reaction with a second type of precursor resulted in the selective formation of the **AABB** compound (Scheme 1.3).[7,8] However, it should be mentioned that the corresponding octakis[*α*-aryl]Pcs can be obtained using harsher conditions, and in the absence of a second phthalonitrile.[9]

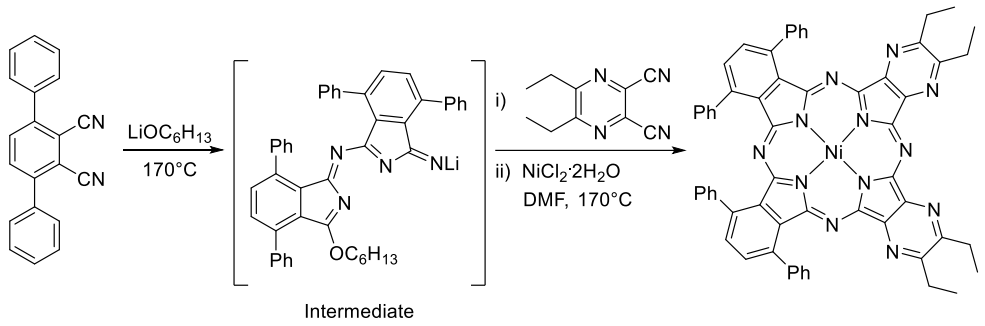

Scheme 1.3. Kobayashi's work to selectively form **AABB** Pcs.

The key factor of the *lithium method* is, indeed, the use of lithium at the first stage, which stabilizes the anionic *half-Pc* intermediate. After that, the addition of a transition metal salt to the reaction mixture, together with a second phthalonitrile, yields the adjacent substituted Pc. However, when transition metals are used from the beginning, this stepwise method does not work out, and **AABB** type Pcs cannot be obtained selectively.[10,11]

Alternatively, phthalonitriles functionalized with bulky substituents at the α-positions have been used to form **ABAB** rather than **AABB** compounds in the presence of transition metal salts. Some examples of this methodology are shown in Scheme 1.4. The reaction of phthalonitriles substituted at the 3,6-positions with phenyl,[4] decyl[12] or isopropoxy[13] with equimolar amounts of other non-hindered phthalonitrile derivatives led to the respective **ABAB** isomer in good yields. Key factors for these results are, on one hand, the hindered self-condensation of the bulky phthalonitriles and, on the other hand, the impeded aggregation capabilities of the macrocycles that facilitates chromatographic separation. However, this approach is not always successful. For example, a significant yield of the **AABB** isomer was obtained during a mixed condensation of tetraphenylphthalonitrile and 4-phenylthiophthalonitrile in the presence of $CuCl_2$ at 260 °C, probably because of the use of a strongly coordinating metal and high temperature.[14]

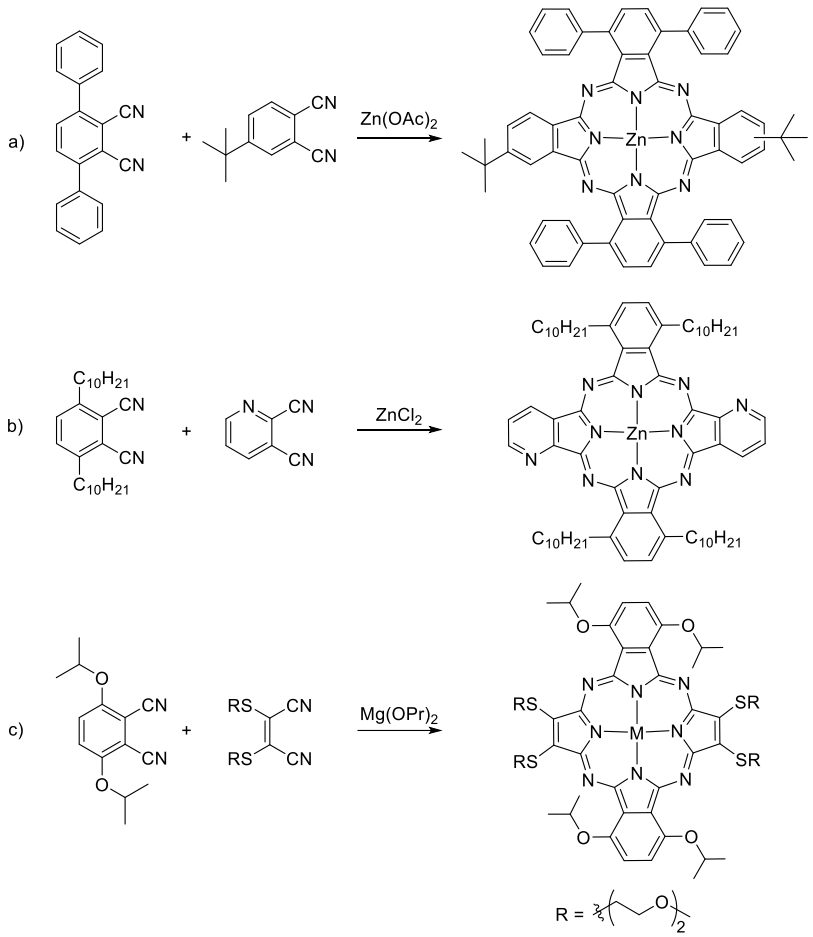

Scheme 1.4. Examples of directed synthesis of **ABAB**-type asymmetric Pcs and analogues.

One of the most interesting approaches used to form **ABAB** structures is the cross-condensation between two types of precursors in which six of the eight nitrogens at the inner perimeter of the product can only be provided by one type of precursor. This methodology was originally reported as a patent in 1978 by Idelson on behalf of the Polaroid Corporation.[15] A reaction between aminoimino- and trihalosubstituted-pyrrolines in the presence of an acid acceptor and a hydrogen donor was reported to result in the preferential formation of **ABAB** porphyrazine structures. Lever and Leznoff[16] on one hand, and Shirai and co-workers[17] on the other, were the first to use this type of reaction in an academic setting (Scheme 1.5). They envisioned that a completely new approach was required to obtain selectively **ABAB** – type Pcs. For this purpose, they performed a cross – condensation reaction of precursors in which one of the substrates is

unable to self-condense, and, lowering the temperature of the Pc formation reaction, the crossed condensation would be favoured over self – condensation of the other substrate. For this reason, they chose as precursors 1,3-diiminoisoindoline and thiophthalimides. It is well known, in fact, that 1,3-diiminoisoindoline and its derivatives readily form Pcs at 150°C but only slowly below 100°C unless special catalytic bases are used. On the other hand, the self-condensation of thiophthalimides is not allowed, but in cross – condensation reactions, the nucleophilic addition of the 1,3-diiminoisoindoline to a dithiophthalimide is much faster than its self-condensation, thanks to the high reactivity of the thiocarbonyl group.[18]

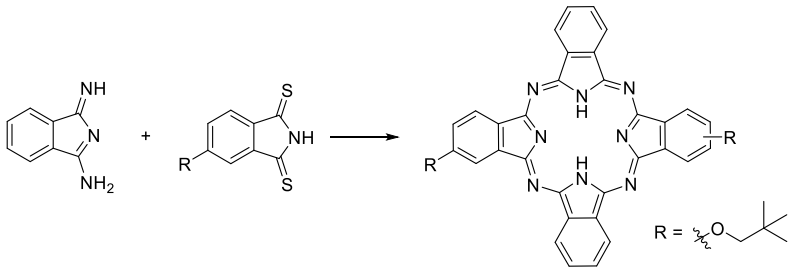

Scheme 1.5. Selective formation of an **ABAB** Pc from a cross-condensation reaction of a thiophthalimides and a 1,3-isoindolediimine.

In 1990, Young and Onyebuagu reported a cross-condensation reaction involving 1,3-diiminoisoindoles and 1,3,3-trichloro-6-nitroisoindolenine as precursors, in the presence of a base and a reducing agent. The yields obtained by this reductive coupling process were significantly high (*ca*. 50%) and the authors claimed that only the **ABAB** derivative was formed under these conditions (Scheme 1.6).[19] Stihler *et al*. subsequently pointed out, however, that while the **ABAB** structure is the predominant product, a trace of the **AAAB** product is also found, which has to be separated by chromatography.[20]

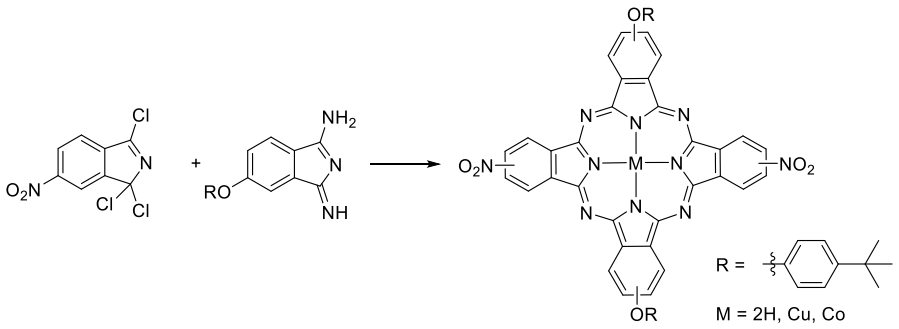

Scheme 1.6. Selective formation of an **ABAB** Pc from 1,3,3-trichloro-6-nitroisoindolenine and a 1,3-isoindolediimine.

Despite the unquestionable selectivity of this method, Idelson's approach has only rarely been utilized by Pc researchers due to the unfriendly synthetic routes to prepare the precursors and the low tolerance to many functional goups.[21,22] The most recent example of the application of these conditions is the work of Bretonnière and co-workers.[23,24] They synthesized a series of octupolar nonlinear optical chromophores based on double-decker lanthanide (III) complexes of crosswise **ABAB** Pc ligands bearing thioether electron donor groups in opposite isoindoles (Scheme 1.7). The alternation of subunits with different electron density in the Pc structure is the key factor to obtain the desired octupolar symmetry of the final double-decker complexes, which is important for the engineering of second-order nonlinear optical materials.

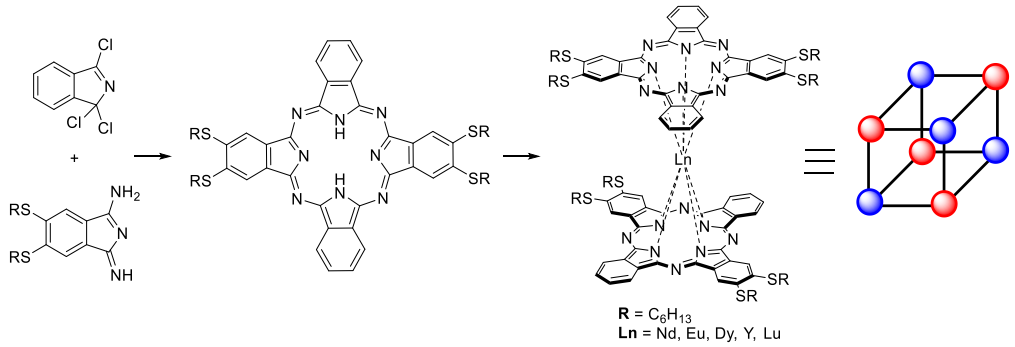

Scheme 1.7. Selective formation of an **ABAB** Pc bearing alternate electron-rich and non-functionalized isoindoles and the subsequent synthesis of double-decker lanthanide (III) complexes.

Pc with more than two different isoindole units remain extremely rare, despite the obvious interest they could present towards the preparation of multicomponent systems. Obtaining such type of Pcs is, of course, not plausible by statistically mixing three different phthalonitriles or other precursors of the same type, as the number of potential products preclude the isolation of the target compound in an acceptable yield (Figure 1.2).

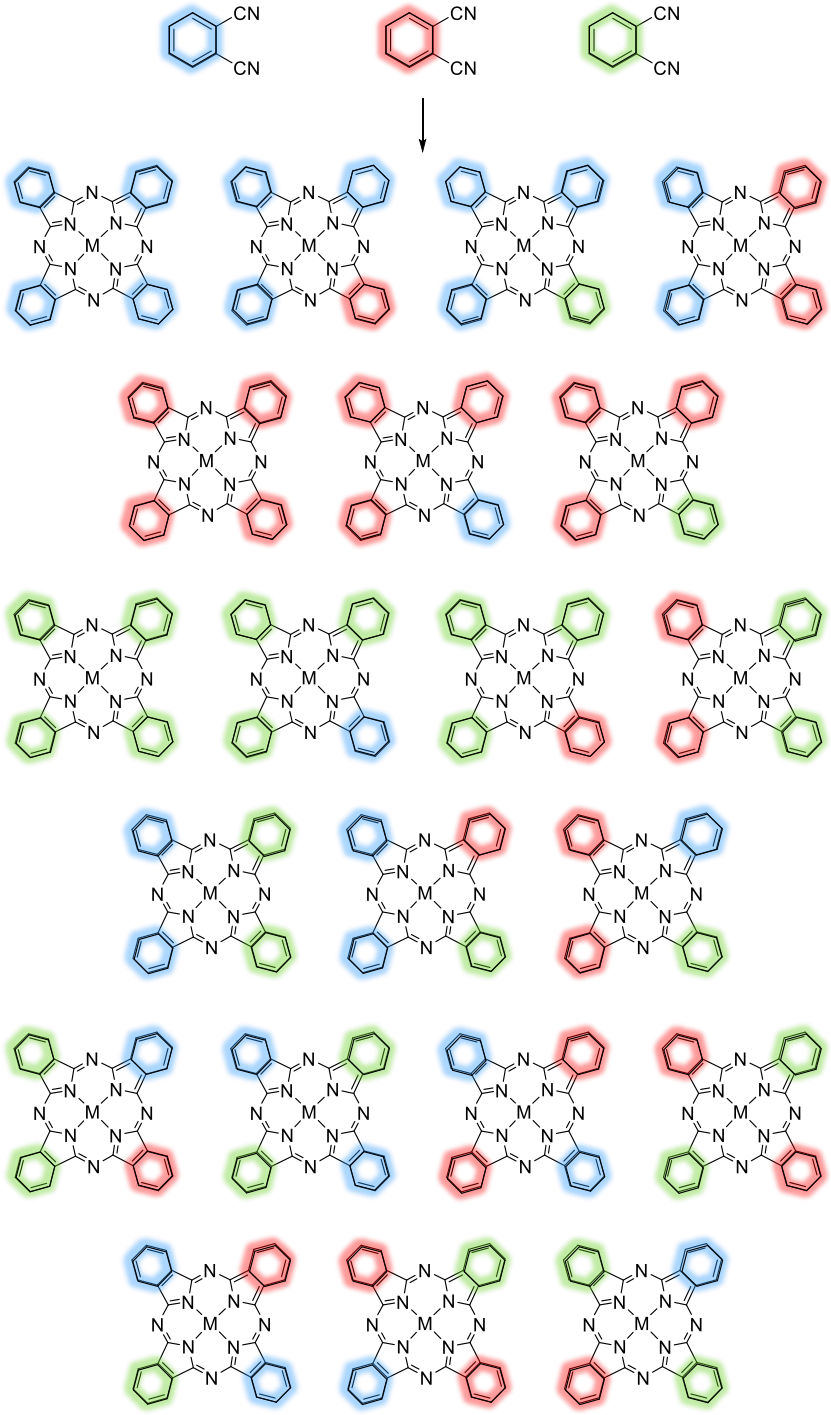

Figure 1.2. Possible Pcs obtained in a hypothetical statistical cyclotetramerization of three differently functionalized phthalonitriles or diiminoisoindolines, **A**, **B** and **C**

In this regard, in 2008 Dumoulin and Ahsen reported the synthesis of an **ABAC** Pc on the basis of Idelson's approach.[25] The key point of their strategy is the use of a statistical mixture of two different diiminoisoindolines (bearing the **B** and **C** functionalization respectively) to be condensed with a trichloroisoindolenine bearing the **A** substituent (Scheme 1.8). The number of possible products in this reaction is, in principle, quite large, namely the three possible crosswise Pcs (the desired **ABAC** and the two "symmetric" ones **ABAB** and **ACAC**), the Pcs resulting from the condensation of three diiminoisoindoline units and one trichloroisoindolenine (**ABBB**, **ACCC**, **ABCC**, **ABBC**, **ABCB** and **ACBC**), and the six Pcs resulting from the condensation of four diiminoisoindoline units (**BBBB**, **BCCC**, **BBCC**, **BCBC**, **BBBC** and **CCCC**). To reduce the number of products and increase the yield of the **ABAC** target compound, Dumoulin *et al*. used two equivalents of trichloroisoindolenine **A**, relative to the total molar amount of diiminoisoindolines (**B**+**C**), which facilitated the formation of the crosswise Pcs and limited the formation of the other Pcs.

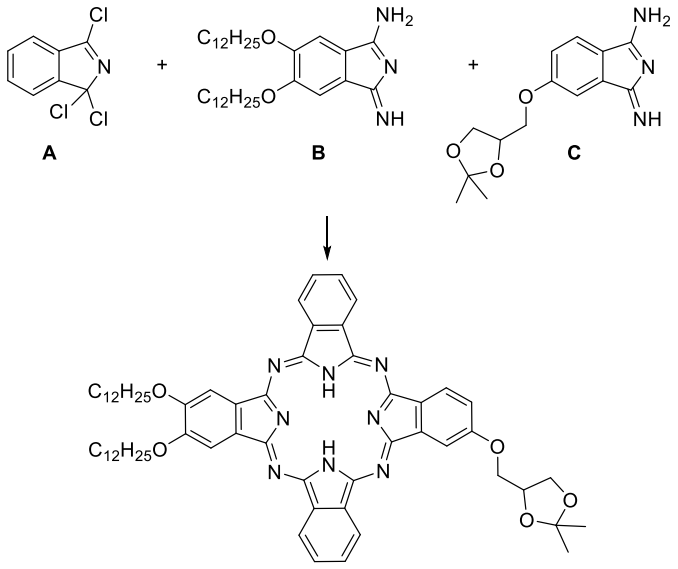

Scheme 1.8. Synthesis of an **ABAC** Pc by Dumoulin *et al.*

More recently, a new approach towards the selective synthesis of Pcs has been reported by Chow and Ng.[26] They programmed a general synthetic strategy for low-symmetry Pcs, which involves a preselection and conjugation of four phthalonitrile precursors, followed by a base-promoted intramolecular cyclization in the presence of a metal template. This controlled pathway allows to prepare low-symmetry analogues that cannot be synthesized readily by conventional methods, including the **ABCD**-type Pcs (Scheme 1.9).

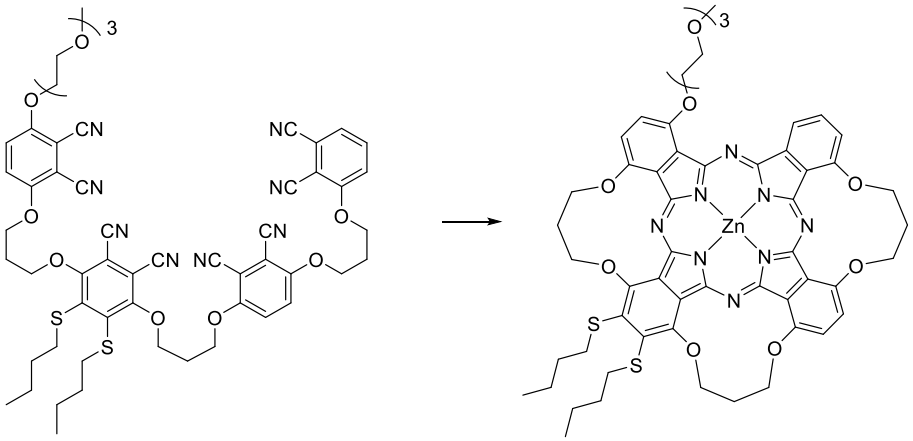

Scheme 1.9. Selective formation of an **ABCD** Pc.

According to this synthetic pathway, the disposition of the four isoindoles in the final Pc depends on the sequence of the four phthalonitrile units in the tetrakisphthalonitrile derivative. Although isomerically pure products are obtained following this methodology, the main disadvantage of this route is that several steps are required to obtain the tetrakisphthalonitrile precursor.

1.2 Specific objectives of *Chapter 1*

The main goal of the present chapter is the development of a general strategy for the controlled synthesis of functional **ABAB** Pcs. For this purpose, a series of bulky phthalonitriles functionalized in the α-positions, with hampered self-condensation capabilities, will be formerly designed and prepared. In particular, we will include bulky substituents of different sizes to explore their capabilities to give crossed-condensation reaction in a selective and efficient manner. In a second step, the prepared phthalonitriles will be tested in cross-condensation reactions with other phthalonitriles bearing functional groups. We expect from this experiments to find an efficient and general approach that will allow us to prepare **ABAB** Pcs adequately functionalized for their further implementation into unprecedented multicomponent systems.

Most of the examples shown in the previous section afford unsymmetric Pcs, which preparation is in itself the final target of the work. However, a subject that is still pending is the further incorporation of this type of asymmetric Pc units in multicomponent systems, taking advantage of their particular distribution of substituents, as otherwise well developed in the case of **A_3B** Pcs. In this regard, the present chapter is devoted to develop a general approach that can be applied for the preparation of different **ABAB** Pcs. In particular, we are interested in the synthesis of **ABAB** Pcs holding reactive groups in opposite isoindoles, which enable both the preparation of donor-Pc-acceptor systems and the incorporation of these Pcs in linear multicomponent arrays, as described in the following two chapters.

Taking into account that octakis[α-aryl]phthalocyanines have been prepared starting from 3,6-diphenylphthalonitrile under certain conditions,[9] the functionalization with bare phenyl rings at the α-positions of the phthalonitrile precursor seems to not be enough to avoid the formation of Pcs with adjacent phenyl-substituted isoindoles. In this regard, the objective of this work is to synthesize new 3,6-arylphthalonitriles, in which the α-phenyl substituents will be functionalized with bulky, alkyl, or trifluoroalkyl moieties in order to hamper their self-condensation. Using these new bulky precursors, we aim to direct more efficiently the statistical condensation towards the formation of **ABAB** Pcs. The ciclotetramerization reactions will be carried out with phthalonitriles carrying iodine atoms or other appropriate functional groups that allow further functionalization of the crosswise **ABAB** macrocycle (Scheme 1.10).

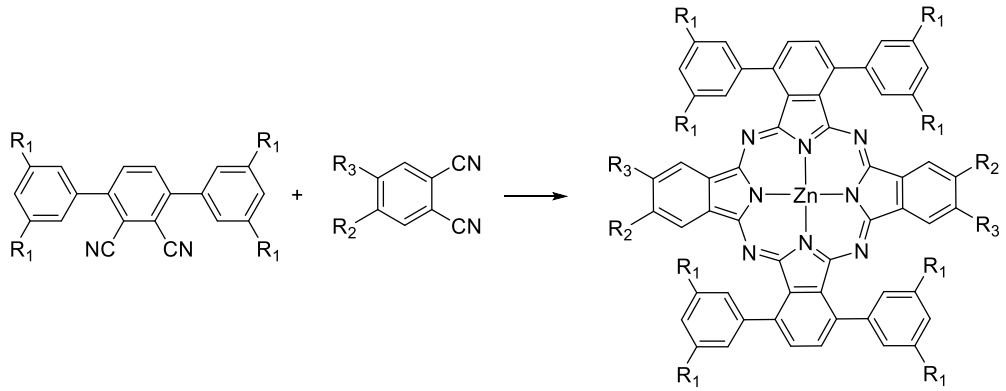

R_1 = alkyl or trifluoroalkyl groups
R_2 and/or R_3 = Halide or other appropriate functional groups

Scheme 1.10. Statistical synthesis of **ABAB** Pcs.

1.3 Results and discussion

1.3.1 Synthesis of phthalonitriles

To direct the cyclotetramerization reaction to the **ABAB** isomer, a series of bulky 3,6-diarylphthalonitriles with hampered self-condensation abilities have been prepared. As the synthesis of 3,6-diarylphthalonitriles had been previously described in the literature using phenylboronic reagents and 3,6-bis(trifluoromethanesulfonyloxy) phthalonitrile **1**, we decided to follow this route for the preparation of our target phthalonitriles. Therefore, the synthesis of **1** was carried out according to a reported procedure (Scheme 1.11).[27,28] Moreover, 3,6-bis(tosyloxy)phthalonitrile (**2**) was also prepared,[29] since this sulfonic ester can also react with phenylboronic derivatives under Suzuki−Miyaura conditions to obtain the desired 3,6-diarylphthalonitriles (Scheme 1.11).

Then, the Suzuki−Miyaura coupling to obtain 3,6-diphenyl-substituted phthalonitriles was first attempted and optimized using **1** or **2** and 3,6-bis(trifluoromethyl)boronic acid (Scheme 1.11). A subset of our experiments towards the preparation of **3** are summarized in Table 1.1. In a first attempt, we tried to use the conditions reported in literature, with $Pd(PPh_3)_4$ as the catalyst and Na_2CO_3 as the base in toluene/water,[27] but in our case (i.e., use of 3,5-bis(trifluoromethyl)phenylboronic acid) the reaction proceeded with a very low yield (entry 1). In the last decade, nickel-catalyzed Suzuki−Miyaura conditions[30] have been successfully applied to many substrates. Using $NiCl_2(PCy_3)_2$ as the catalyst and $PCy_3{\cdot}HBF_4$ as the ligand,[31,32] compound **3** was isolated in 25% yield (entry 3). Better conversions were achieved when using a Ni(II) catalyst and the bistosylate **2** as starting material (entry 4). However, a strong experimental drawback was that the reaction could not be scaled up above 150 mg. Considering that the yield was still low and that other species were formed during the process, we checked the thermal stability of the sulfonic esters **1**, **2**. Evidence of degradation appeared when heating both compounds over 100 °C, driving us to reduce the temperature of the coupling reaction. Therefore, an improved 42% yield was obtained when using **1**, $NiCl_2(PCy_3)_2$ as a catalyst, and K_3PO_4 as a base in 1,4-dioxane at 90 °C under MW irradiation (entry 5). Revisiting the applied Pd(II)-catalyzed Suzuki−Miyaura conditions of entry 1, but keeping the temperature below 100 °C (entries 7−8), did not afford appreciable conversions to the target phthalonitrile **3**. Eventually, optimal yields were obtained by changing the base to K_2CO_3, in DMF as the solvent, and at 90 °C under MW irradiation (entry 9).

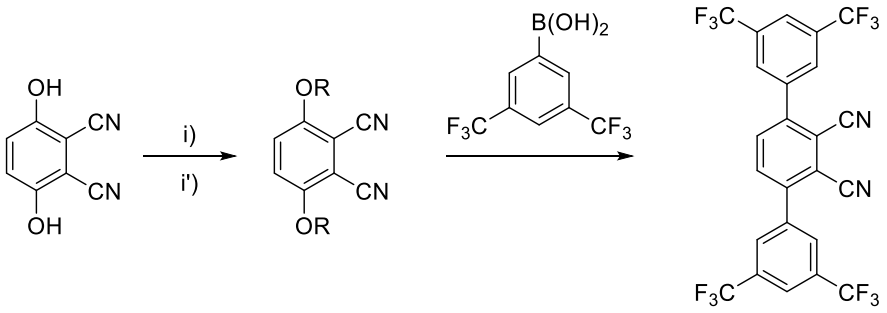

1: R = Tf
2: R = Ts

3

Scheme 1.11. Synthesis of phthalonitrile **3**. Conditions: i) → **1**: trifluoromethanesulfonic anhydride, NEt_3, CH_2Cl_2, -70°C, 70%; i') → **2**: tosyl chloride, K_2CO_3, acetone, reflux, 70%.

Table 1.1. Comparison of the different Suzuki−Miyaura conditions tested for the synthesis of **3**.

Entry	Catalist	Base	Solvent	Ester	Yield
1	$Pd(PPh_3)_4$ [a]	Na_2CO_3	Toluene/H_2O [c]	1	9%
2	$NiCl_2$(dppp)	K_3PO_4	1,4-dioxane	2	15%
3	$NiCl_2(PCy_3)_2/PCy_3{\cdot}HBF_4$ [a]	K_3PO_4	1,4-dioxane [c]	1	25%
4	$NiCl_2(PCy_3)_2/PCy_3{\cdot}HBF_4$ [a]	K_3PO_4	1,4-dioxane [c]	2	30%
5	$NiCl_2(PCy_3)_2/PCy_3{\cdot}HBF_4$ [a]	K_3PO_4	1,4-dioxane [d, e]	2	42%
6	$NiCl_2(PCy_3)_2/PCy_3{\cdot}HBF_4$ [a]	K_3PO_4	1,4-dioxane [d, e]	1	35%
7	$Pd(PPh_3)_4$ [a]	Na_2CO_3	Toluene/H_2O [d, e]	1	-
8	$Pd(PPh_3)_4$ [b]	Na_2CO_3	DME [c]	1	8%
9	$Pd(PPh_3)_4$ [b]	K_2CO_3	DMF [d, e]	1	70%

[a] 10% mol. [b] 5% mol. [c] Reaction at reflux temperature. [d] Reaction at 90 °C. [e] Reaction under MW irradiation

With the optimized Suzuki–Miyaura conditions in hand, the preparation of phthalonitriles **4** and **5** functionalized with 3,5-dimethyl- and 3,5-di-*tert*-butylphenyl moieties, respectively, was carried out starting from the corresponding boronic acids (Scheme 1.12).

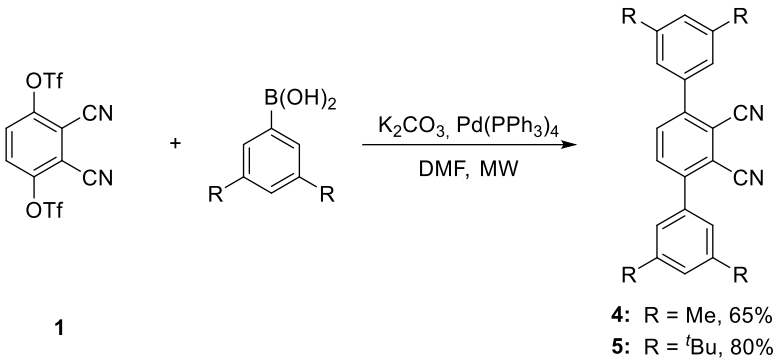

Scheme 1.12. Synthesis of phthalonitriles **4** and **5**.

While the 3,5-dimethylphenylboronic acid is commercially available, the 3,5-di-*tert*-butylphenyl boronic acid **6** was synthesized from the commercial bromophenyl derivative as shown in Scheme 1.13, following the reported conditions.[33]

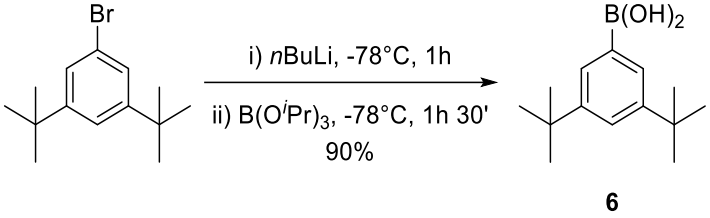

Scheme 1.13. Synthesis of 3,5- di-*tert*-butylphenyl boronic acid (**6**).

On the other hand, 4-iodophthalonitrile and 4,5-diiodophthalonitrile were chosen as precursors for the crossed condensation, since the presence of the iodine atoms in the final **ABAB** Pc will make possible to perform a wide variety of transformations by means of cross-coupling reactions (e.g. Suzuki–Miyaura coupling, Buchwald–Hartwig amination, and Sonogashira reaction). The synthesis of 4-iodophthalonitrile (**8**) was carried out according to literature procedures,[34,35] as shown in Scheme 1.14.

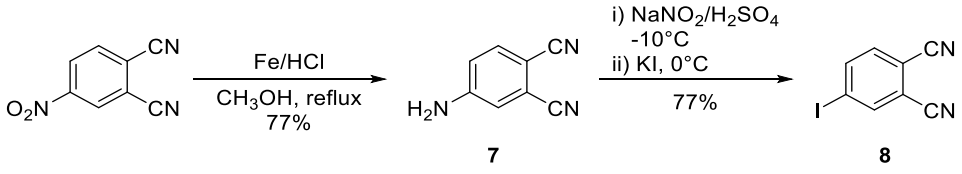

Scheme 1.14. Synthesis of 4-iodophthalonitrile (**8**).

The chemoselective reduction of 4-nitrophthalonitrile with iron in a mixture of concentrated hydrochloric acid and methanol gave 4-aminophthalonitrile (**7**),[34] which was transformed to 4-iodophthalonitrile (**8**) in 77% yield via diazotization and subsequent nucleophilic aromatic substitution reaction in the presence of potassium iodide.[35]

The preparation of 4,5-diiodophthalonitrile (**11**) was also carried out according to a literature procedure (Scheme 1.15).[36]

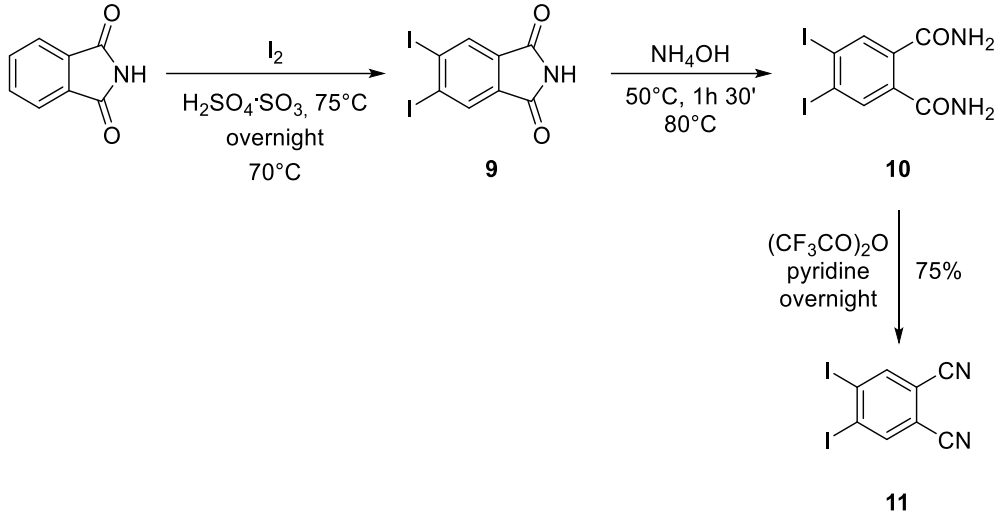

Scheme 1.15. Synthesis of 4,5-diiodophthtalonitrile (**11**).

Phthalimide was directly iodinated with iodine in 30% fuming sulfuric acid at 75 °C to give 4,5-diiodophthalimide (**9**), which was isolated in 70% yield. Treatment with concentrated ammonia, gave pure 4,5-diiodophthalamide (**10**), which was successfully converted to 4,5-diiodophthalonitrile (**11**) in 75% yield by using trifluoroacetic anhydride in pyridine.

1.3.2 Synthesis of ABAB Pcs

With the phthalonitrile precursors in hand, we proceeded to perform the cross-condensation reaction to obtain the target **ABAB** Pcs. First, optimization of the statistical condensation was performed with the bulky phthalonitrile **3** and 4-iodophthalonitrile (**8**) in the preparation of Zn(II)Pc **12** (Scheme 1.16).

Usual conditions were first applied, namely, heating a 1:1 ratio of the precursors in the presence of $Zn(OAc)_2$ and DBU in pentanol for 12 h. Under these conditions only three of the six possible Pcs were formed, which were satisfactorily separated by column chromatography, since the presence of bis(trifluoromethyl)phenyl substituents strongly diminished the aggregation trend of Pcs and, therefore, facilitated the isolation. The first compound to elute was the target **ABAB** Pc **12**, isolated in 4% yield, sequentially followed by the **AB_3** Pc **13** (18%) and the **B_4** Pc **14** (25%) (Scheme 1.16). It is important to mention that none of the possible compounds with adjacent bis(trifluoromethyl)phenyl-substituted isoindoles were formed.

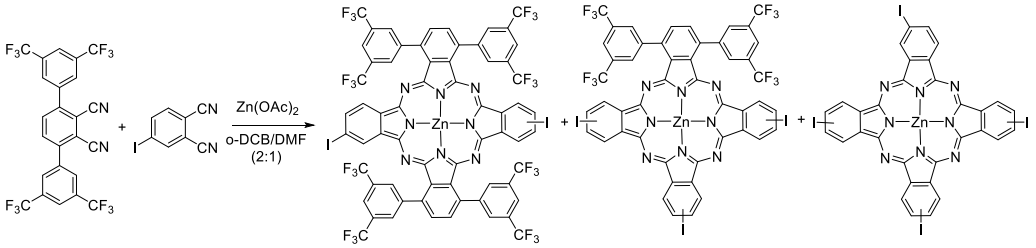

3 **8** **12** **13** **14**

Scheme 1.16. Statistical synthesis of Pc **12** under optimized conditions.

Therefore, the approach proved fruitful in terms of selectivity, but rather inefficient in terms of yield. Considering that phthalonitrile **3** is not consumed in self-condensation processes, relative yield in **12** should be higher. Thus, 3,6-disubstituted phthalonitrile **3** seems much less reactive than 4-iodophthalonitrile **8**, and the crossed condensation processes between them is not favoured either. Aiming at increasing the yield in **12**, the proportion of sterically hindered phthalonitrile **3** was increased, but it did not afford a significant improvement and complicated the purification process, due to the presence of a huge amount of unreacted phthalonitrile **3**. Further attempts were done in order to improve the yield in **12**, while maintaining the selectivity towards the formation of the less sterically hindered compounds. First, microwave irradiation in similar conditions brought about an increase in the yield from 4% to 10%. Major improvements were achieved by changing the solvent to DMF/*o*-DCB mixtures and increasing the

reaction temperature to 150 °C, which led to a 16% yield of isolated product (i.e., **12**) for a 1:1 ratio of the starting phthalonitriles (Scheme 1.16). Changing to a 2:1 ratio of **3** and **8**, respectively, did not afford a worthwhile increase of the yield in **12**.

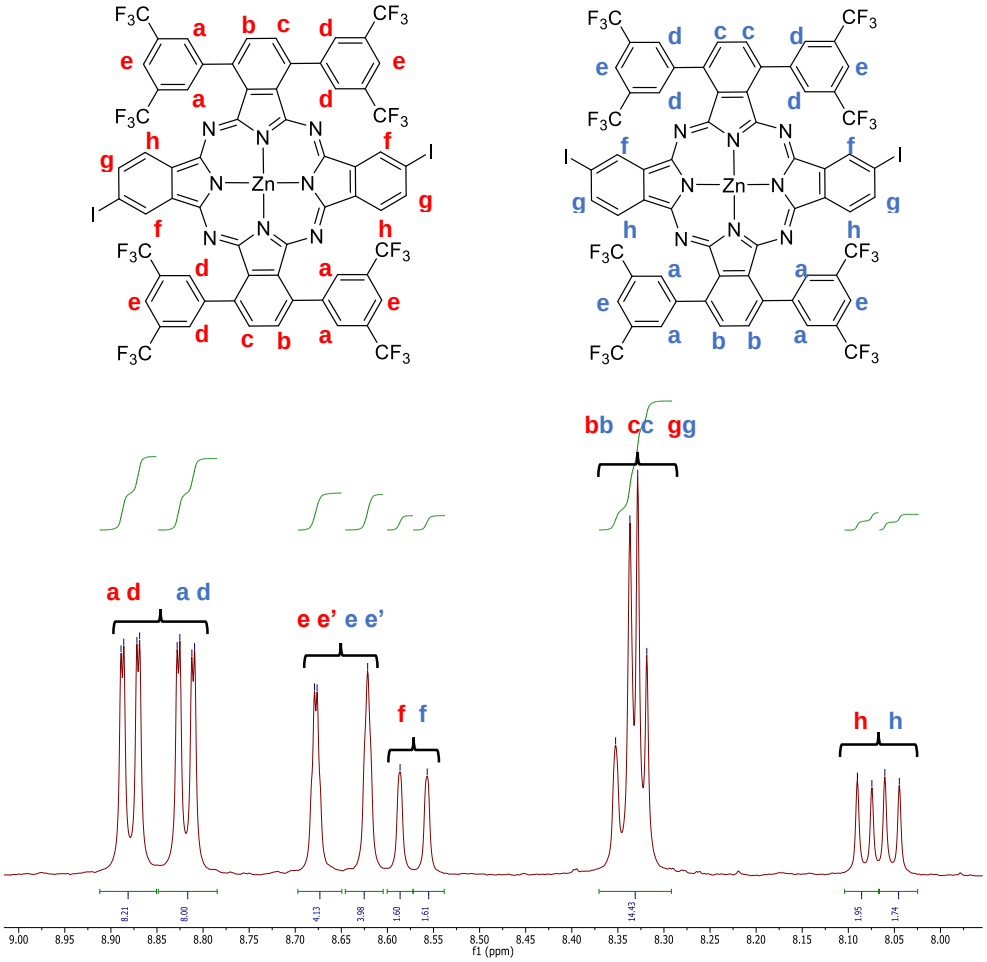

Figure 1.3. Magnification of the aromatic region of the ^{1}H NMR spectra in THF-d_8 of **12**.

The structure of Pc **12** was unequivocally confirmed by MALDI-TOF mass spectrometry, UV−vis, and NMR. Strong evidence of the successful preparation and isolation of the **ABAB** compound **12** arises from the highly symmetric ^{1}H NMR. In Figure 1.3, magnification of the aromatic part shows six split signals for the protons of the bis(trifluoromethyl)phenyl rings, and also for the α-protons of the iodine-substituted isoindole. This is due to the fact that **12** is comprised of a

mixture of two regioisomers, which differ in the relative position of the two iodine atoms (i.e., *syn* and *anti*). As shown in Figure 1.3, for each type of protons, two sets of signals of similar intensity are discernible, which are consistent with the different chemical environments for related protons of the two component regioisomers present in a nearly equimolar mixture. This assignment is supported by the COSY spectrum (Figure 1.4), which shows correlations between signals arising from the same isomer. Also, the ^{19}F NMR spectrum of **12** features four close singlets, owing to the presence of CF_3 groups with two different environments for each of the regioisomers (Figure 1.5). It is worth mentioning that all the signals in the ^{1}H-NMR spectra of **12** are perfectly resolved, as expected for a Pc with hampered aggregation capabilities.

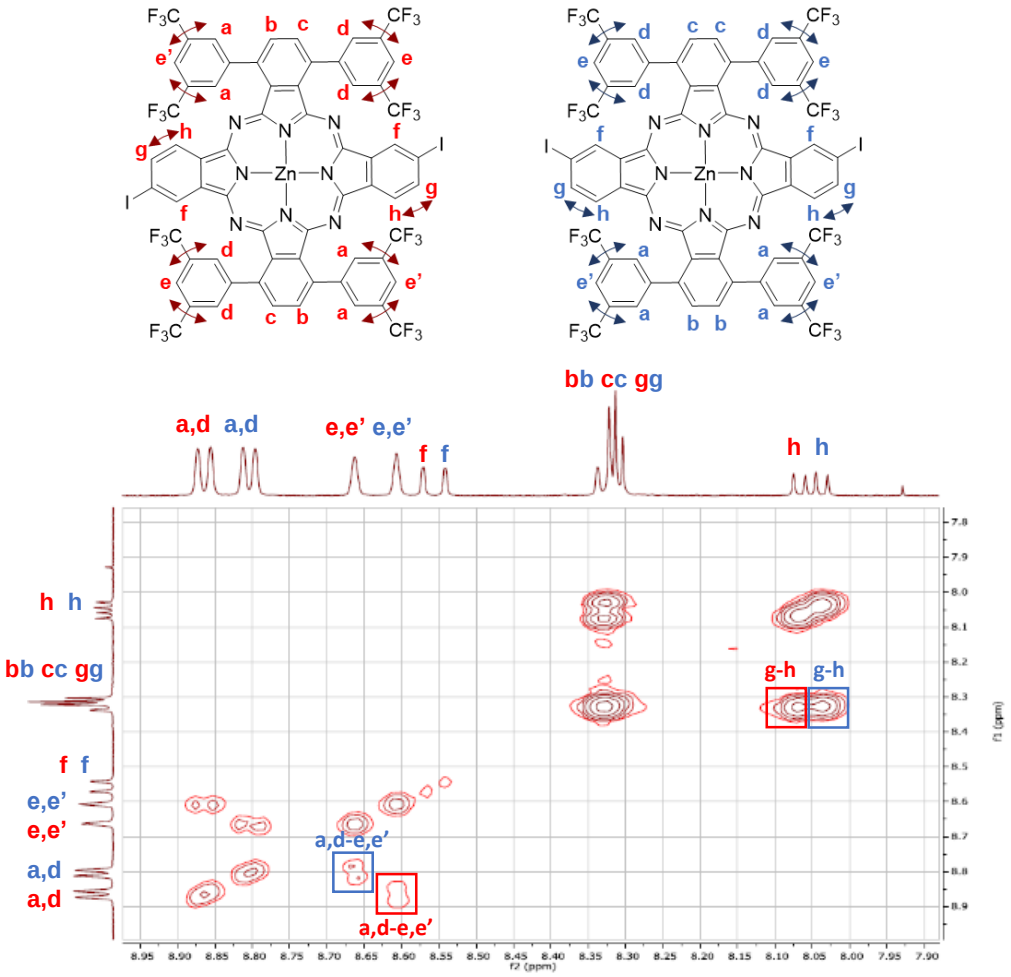

Figure 1.4. COSY spectrum of **12** in THF-d_8.

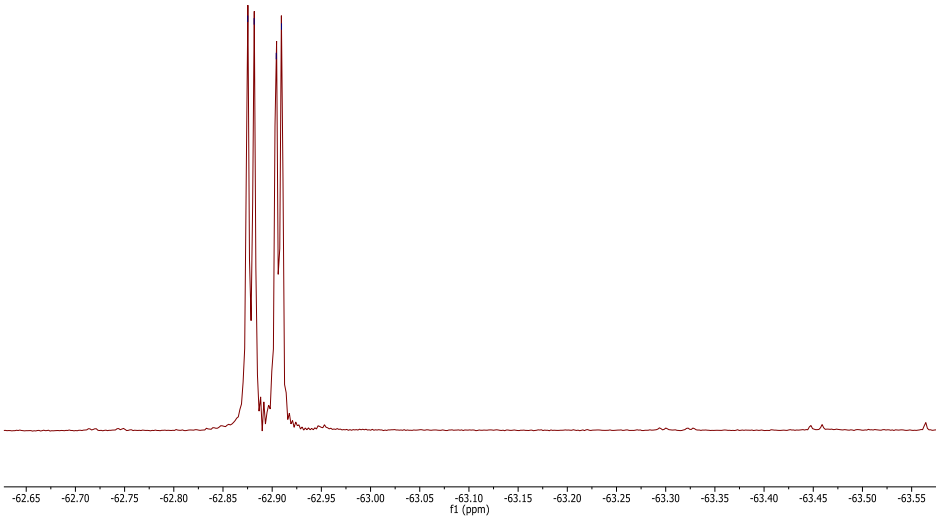

Figure 1.5. ^{19}F-NMR spectrum of **12** in THF-d_8.

In order to check the scope of the method, we carried out the reaction under optimized conditions found for **12** between the bulky phthalonitrile **6** and other phthalonitriles containing functional groups that are able to give straightforward chemical transformations. Therefore, we proceeded to do the reaction, between **6** and the commercially available 4-nitrophthalonitrile (Scheme 1.17), as the nitro moiety can give rise to either *ipso* substitution reactions or reduction and further diazotization/substitution processes. This reaction yielded, as expected, the corresponding **ABAB** (**15**), **AB$_3$** (**16**) and **B$_4$** (**17**) Pc derivatives, from which the target **ABAB** Pc **15** was isolated as a mixture of positional isomers in 12% yield. Finally, in order to circumvent the regioisomer issue, we also undertook the synthesis of Pc **18**, by reacting 4,5-diiodophthalonitrile **11** and phthalonitrile **3** as starting materials under the same optimized conditions (Scheme 1.17). As in the previous case, only three of the six possible Pcs were formed, which were easily separated by column chromatography. Also in this case, the first compound to elute was the target **ABAB** Pc **18** (isolated in a 10% yield), followed by the **AB$_3$** Pc **19** and the **B$_4$** Pc **20**. An in depth structural characterization of Pcs **15** and **18** was performed by MALDI-TOF mass spectrometry, UV−vis, and NMR spectroscopies.

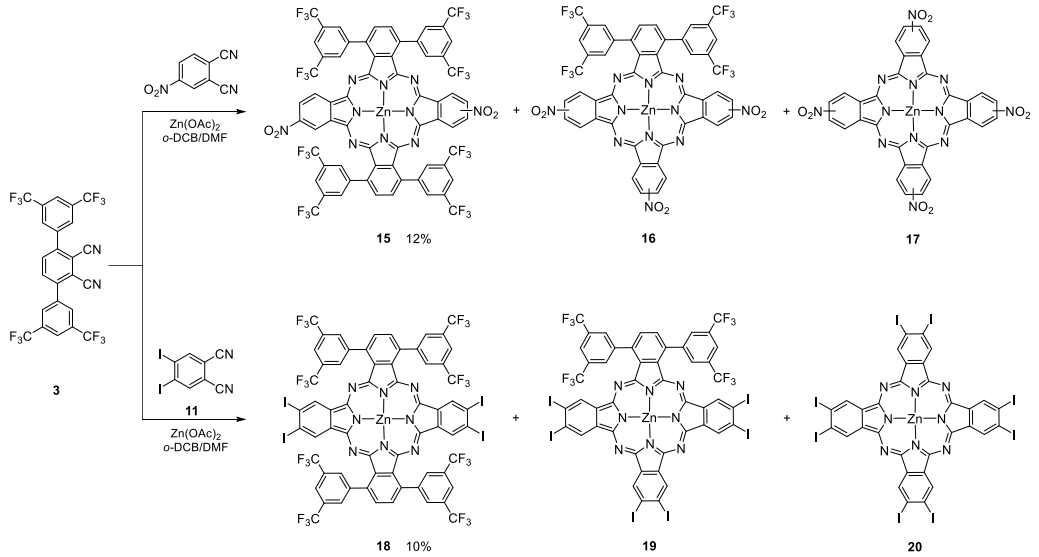

Scheme 1.17. Statistical synthesis of Pc **15** and **18** under optimized conditions.

Unquestionable confirmation of the D_{2h}-symmetry and lack of isomers of Pc **18** come from the ^{1}H-NMR spectrum (Figure 1.6). As expected, it appears significantly simpler than the spectrum of the related monoiodinated Pc **12**. In fact, only four singlets can be observed in this case, two for the protons of the bis(trifluoromethyl)phenyl rings, and other two singlets for the two different types of aromatic Pc centered nuclei.

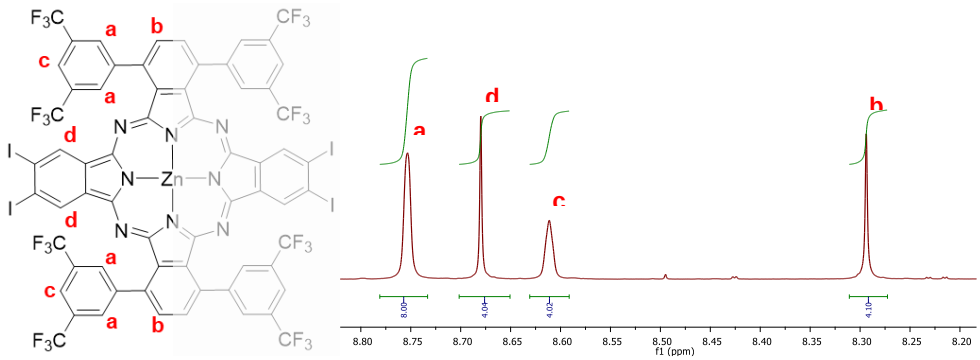

Figure 1.6. Magnification of the aromatic region of the ^{1}H NMR spectra in THF-d_8 of **18**.

The UV−vis spectrum of **12** and **15** (Figure 1.7) showed symmetric, split Q bands (i.e., at 675 and 691 nm for **12**, 680 and 700 nm for **15** in THF), as it is generally observed in Pcs with D_{2h}-symmetry, and in face-to-face substituted derivatives in particular.[4] However, D_{2h} Pc **18** exhibits only one Q-band in its absorption spectrum (Figure 1.7). This observation can be rationalized considering not only the symmetry of the Pc derivative but also the effect that the substituents exert on the electronic levels of the aromatic core. Therefore, in the case of **18**, the electronic effect imparted by this particular substitution counterbalances the splitting of the electronic levels produced by the symmetry.

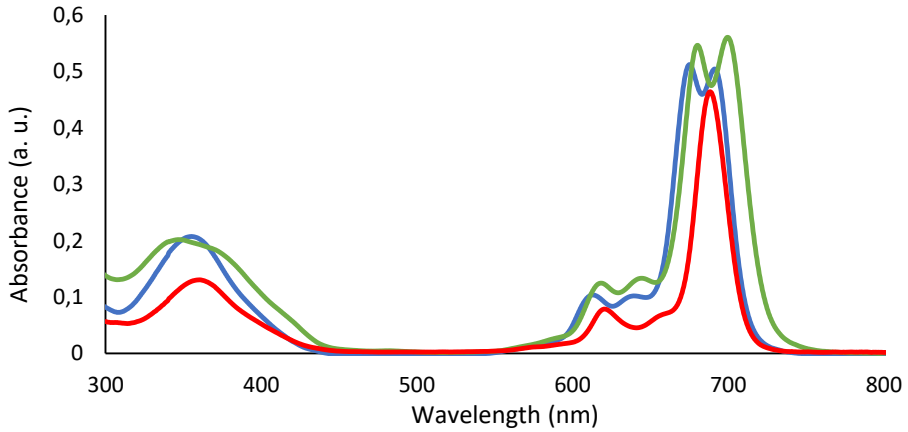

Figure 1.7. UV-vis spectra of **12** (— 4.4 μM), **15** (— 10 μM)and **18** (— 2 μM) in THF.

Next, we tested the preparation of other **ABAB** Pcs (i.e., **21** and **22**) using other type of bulky phthalonitriles, namely 3,6-bis(dimethyl)phenyl- and 3,6-bis(di-*tert*-butyl)phenyl-functionalized phthalonitriles (**4** and **5** respectively), in crossed condensation reactions with 4-iodophthalonitrile (**8**), as it proved the most reactive in previous experiments. Using the optimized conditions found for **12**, no traces of the desired products were observed (Scheme 1.18). In fact, using these conditions, only the **AB_3** Pcs **23**, **24** and the **B_4** Pc **14** were obtained, while most of the corresponding bulky phthalonitriles **4** and **5** remain unreacted in each case.

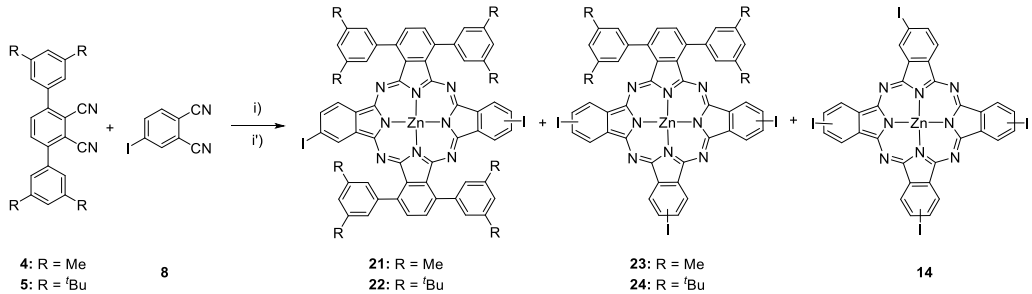

Scheme 1.18. Statistical synthesis of Pcs **21** and **23**. Conditions: i) → Pcs **23**, **24** and **14**: $Zn(OAc)_2$, *o*-DCB/DMF (2:1), at 135°C; i') → Pcs **21**, **22**, **23**, **24** and **14**: $Zn(OAc)_2$, DMAE / DBU, at 135°C.

In view of the previous results, other conditions were checked for the preparation of Pcs **21** and **22**. Table 1.2 summarizes a set of our experiments towards the preparation of different **ABAB** Pcs starting from **4** or **5** and **8**.

Table 1.2. Investigated conditions for the reaction of bulky phthalonitriles **4** and **5** with 4-iodophthalonitrile **8**.

Entry	Bulky Phthalonitrile	Conditions	Yield
1	**4**	*o*-DCB/DMF[a]	-
2	**4**	1-pentanol / DBU[a]	-
3	**4**	DMAE/DBU[a]	8% [c]
4	**4**	Li / 1-pentanol[b]	19% [c]
5	**4**	Li / 1-hexanol[b]	18% [c]
6	**5**	*o*-DCB/DMF[a]	-
7	**5**	DMAE / DBU[a]	2.5%
8	**5**	Li / 1-pentanol[b]	< 2%

[a] Reaction with $Zn(OAc)_2$ and at 135°C. [b] Reaction at 150°C affording the corresponding free base Pcs. [c]Mixture of **ABAB** and **AABB** isomers.

In the case of 3,6-bis(dimethyl)phenyl-substituted phthalonitrile **4**, a first improvement was achieved changing the solvent to DMAE and using DBU as base in catalytic amounts. Under these conditions, a new compound was obtained in low yield, after separation by column chromatography from the Pcs **20** and **14** (entry 3). The new compound was identified by MS analysis as the desired **ABAB** Pc. Aiming at increasing the yield, further conditions were tested. The use of Li/1-pentanol or 1-hexanol had been applied in the literature with 3,6-diphenylphthalonitriles. In our case, these conditions led to a mixture of metal – free Pcs, which chromatographic separation proved quite difficult. For that reason, the crude mixture of free bases obtained by the reaction of **4** with **8** was further reacted with $Zn(OAc)_2$ in DMF at reflux, since the metallated Zn(II)Pcs are, in general, easier to separate by chromatography (entry 4 and 5). Using these conditions, we separated from the mixture the Zn(II)Pc compound identified by MS spectrometry as the **ABAB** Pc. However, the ^{1}H-NMR spectrum of the Pcs obtained in entries 3-5 showed, as compared with the spectrum of **ABAB** Pc **12**, a large splitting of the aromatic signals. The loss of symmetry observed in the spectra can be rationalized considering that the product resulting from these reactions is, actually, a mixture of the **ABAB** Pc **21** and the corresponding **AABB** regioisomer (Pc **25**) (Figures 1.8 and 1.9). The lack of symmetry is equally appreciable in the signals corresponding to the methyl groups (Figure 1.9). In fact, two signals are expected in the case of the **ABAB** Pc **21**, since it comprises a mixture of *syn* and *anti* isomers, but in this case, additional singlets appear, probably coming from the methyl groups in two adjacent aryl rings in **25** (Figure 1.9). At the same time, a minor fraction eluted from the reaction mixture was identified by MS as the $\mathbf{A_3B}$ Pc **26**, having three

adjacent dimethylphenyl-substituted isoindoles, which also supported the NMR evidence of the formation of the adjacent **AABB** isomer **25** (Figure 1.8). Unfortunately, the chromatographic separation of **21** and **25** was not possible.

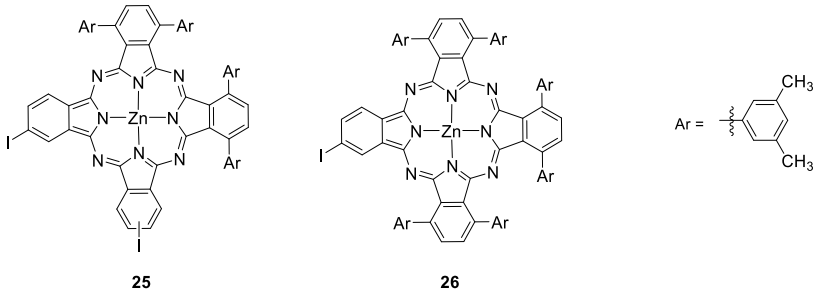

25 **26**

Figure 1.8. Structure of the additional Pcs obtained when using conditions 3-5 of Table 1.2.

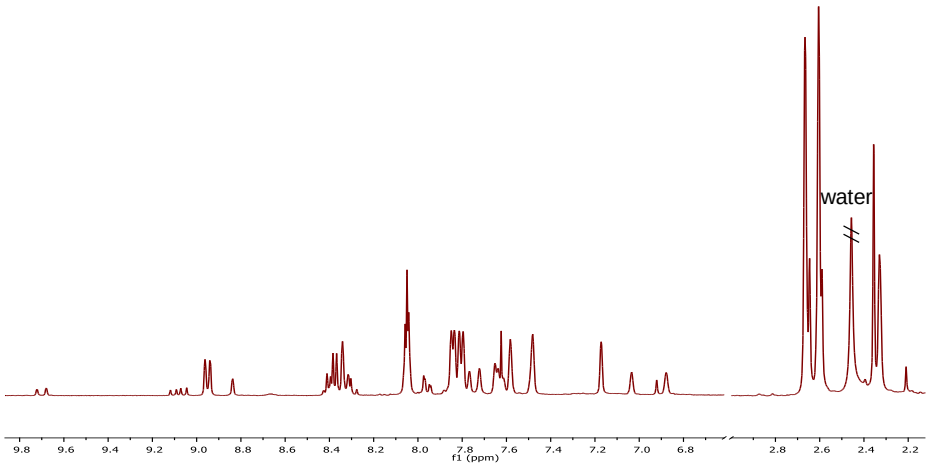

Figure 1.9. Magnification of the aromatic region and methyl signals of the ^{1}H NMR spectra in THF-d_8 of mixture of **21** and **25**.

In order to obtain Pc **22** functionalized with bis(di-*tert*-butyl)phenyl rings, we applied the conditions used with either bulky phthalonitrile **3** or **4** that successfully gave cross-condensation with **8** (Table 1.2, entries 7 and 8). As in the case of phthalonitrile **4**, only the reaction in alcoholic solvents (DMAE/DBU and Li/1-pentanol) resulted in the formation of a mixture of Pcs, namely **22**, **24** and **14** (Scheme 1.18). In this case, we characterized these compounds only by MS analysis because of the very low conversion achieved (i.e., the yield in **22** was 2.5 % under the best conditions, entry 7). In conclusion, di-*tert*-butylphenyl-functionalized phthalonitrile **5** showed much less reactive than its methyl-homologue **3**.

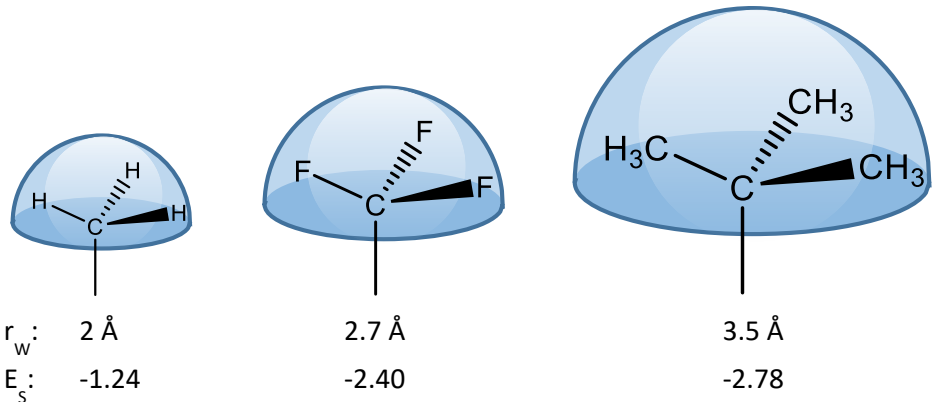

Figure 1.10. van der Waals radii (r_W) and Taft's Steric constant values (E_S) for methyl, trifluromethyl and t-butyl groups.

The reactivity of phthalonitriles **3**, **4** and **5** in competing self- and cross-condensation steps follow a logical trend in line with the size of the different bulky groups. As shown in Figure 1.10, the methyl groups possess the smallest van der Waals radius, which leads to an inadequate steric volume to afford selectivity towards the formation of the opposite **ABAB** isomer *versus* the adjacent one. On the other hand, the more bulky ^{t}Bu groups direct the reaction towards the **ABAB** Pc, but the reactivity of *tert*-butyl substituted phthalonitrile **5** is so low that make us discard these compounds for further characterization and derivatization.

On the other hand, the size of CF_3 is relatively large: in fact, it has a van der Waals radius between that of methyl and *tert*-butyl groups, and a steric volume in the order of Me < ^{i}Pr < CF_3 < ^{t}Bu according the Taft's Steric constant values (E_S).[37,38] This feature favors the process towards the selective formation of the crosswise Pc **12**. Furthermore, the electron withdrawing effect of CF_3 activates the phthalonitrile **3**, thus leading to good yields in the crossed condensation with **8** to give **12**.

1.4 Summary and conclusions

In the present chapter, the synthesis and characterization of different crosswise funtionalized **ABAB** Pcs has been explored.

Initially, with the aim of obtaining **ABAB** Pcs by statistical means, the synthesis of appropriate bulky phthalonitriles (**A**) that can direct the cyclotetramerization reaction to the crosswise Pc isomer, avoiding the self-condensation and the formation of the adjacent **AABB** Pc was carried out. Thus, the synthesis of the bulky 3,6-diphenyl substituted phthalonitriles was realized using Suzuki-Miyaura cross-coupling reactions between a phthalonitrile containing triflate leaving groups at the 3,6-positions and phenyl boronic acids. The use of microwave irradiation was essential to increase the yield of the final compounds. Optimization of this procedure has allowed the preparation of a series of 3,6-diarylphthalonitriles **3**-**5** in good yield, in which the α-phenyl substituents are functionalized with bulky CF_3 (**3**), CH_3 (**4**) or ^{t}Bu (**5**) moieties.

Using these bulky precursors, we carried out the crossed condensation with phthalonitriles endowed with other functional groups (**B**), aiming at preparing **ABAB** Pcs able to render chemical transformations that will allow us to obtain more complex, cutting-edge derivatives. Optimization of the reaction conditions was firstly carried out in the reaction between bis-3,6-(3,5-trifluoromethyl)phenylphthalonitrile (**3**) and 4-iodophthalonitrile (**8**), which yielded Pc **12** in a rather good yield 16%, considering the statistical nature of the reaction. Then, we found that applying the same conditions for the reaction between **3** and 4-nitrophthalonitrile or 4,5-diiodophthalonitrile (**11**) we successfully obtained the corresponding **ABAB** Pcs **15** and **18**, in 12% and 10% yields, respectively.

However, the replacement of the trifluoromethy groups by alkyl-type groups, either methyl or *tert*-butyl substituents, did not afford the target **ABAB** Pc derivatives in their crossed condensation reactions with 4-iodophthalonitrile. In the case of bis-3,6-(3,5-dimethylphenyl)phthalonitrile **4**, the reaction was not selective and the target crosswise Pc was obtained, but contaminated with the corresponding **AABB** regioisomer. On the other hand, for the reaction with bis-3,6-(3,5-di-*tert*-butylpheny)phthalonitrile **5**, the corresponding **ABAB** Pc was obtained without traces of the adjacent isomer, but in a very low yield in all the conditions tested. These results follow a logical trend in line with the van der Waals radius of the different bulky groups. In fact, the methyl groups do not possess the steric volume necessary to afford selectivity towards the formation of the opposite **ABAB** isomer *versus* the adjacent one. On the other hand, the more bulky ^{t}Bu groups direct the reaction towards the **ABAB** Pc, but the reactivity of the *tert*-butyl substituted phthalonitrile **5** is so low that the reaction proves quite inefficient. Lastly, CF_3 is a rather bulky substituent, with a van der Waals radius

between that of ^{i}Pr and ^{t}Bu groups, thus favoring the process towards the formation of the crosswise Pc **12**. Furthermore, the electron withdrawing effect of CF_3 activates the phthalonitrile **3**, thus leading to good yields in the corresponding Pc **12**, and its related analogues **15** and **18**.

In conclusion, the use of bis-3,6-(3,5-trifluoromethyl)phenylphthalonitrile **3** (**A**) in statistical cross-condensation reactions with other phthalonitriles (**B**) has proved a general method to efficiently obtain **ABAB** Pcs. The **ABAB** Pcs **12**, **15** and **18** are outstanding building blocks for the construction of more complex structures, as discussed in the next two following chapters.

1.5 Experimental section

In this *Experimental section*, the preparation and characterization of the compounds has been organized following the order as they appear in the text.

1.5.1 Materials and general methods

Chemical reagents were purchased from Aldrich Chemical Co., Alfa Aesar, Acros Organics or Fluka Chemie and were used without further purification. “Synthetic grade” solvents were used for chemical reactions and column chromatography purifications, and “anhydrous grade” for reactions under dry conditions. Additionally, some solvents were further dried by distillation with Na/benzophenone (THF and Toluene), or with previously activated molecular sieves (3 or 4 Å), or with a solvent purifying system by Innovative Technology Inc. MD-4-PS.

Microwave irradiation technique: microwave reactions were carried out in a Biotage Initiator+ system. All reactions were performed in capped glass vials under argon atmosphere.

Chromatography: the monitoring of the reactions was carried out by thin layer chromatography (TLC), employing aluminium sheets coated with silica gel type 60 F254 (0.2 mm thick, E. Merck). The analysis of the TLCs was carried out with an UV lamp of 254 and 365 nm. Purification and separation of the synthesized products was performed by column chromatography, using silica gel (230-400 mesh, 0.040-0.063 mm, Merck). Eluents and relative proportions of the solvents are indicated for each particular case. Size exclusion chromatography was performed using Bio-Beads S-X1 (200-400 mesh, Bio-Rad).

Melting point (Mp): melting points were measured in open-end capillary tubes by using a Büchi 504392-S apparatus, and are uncorrected.

Nuclear Magnetic Resonance (NMR): monodimensional and/or bidimensional NMR spectra (^{1}H-NMR, ^{13}C-NMR and ^{19}F-NMR) were recorded on a Bruker AC-300 (300 MHz) or a Bruker XRD-500 (500 MHz) instruments either in the Organic Chemistry Department or in SIdI (Servicio Interdepartamental de Investigación). In each case, the deuterated solvent employed is indicated between brackets. Chemical shifts (δ) are reported in ppm and calibrated relative to residual solvent signals using literature reference values,[39] and coupling constants (J) are reported in hertz (Hz). The following abbreviations are used to indicate the multiplicity in ^{1}H-NMR spectra: s, singlet; d, doublet; t, triplet; q, quartet; quint, quintet; m, multiplet; bs, broad signal.

Mass Spectrometry (MS) and High Resolution Mass Spectrometry (HRMS): mass spectra were recorded in SIdI, employing Electronic Impact (EI), Fast Atom Bombardment (FAB-MS) or Matrix Assisted Laser Desorption/Ionization-Time of Flight (MALDI-TOF), using a VG-AutoSpec spectrometer for EI and FAB-MS and a Bruker Reflex III spectrometer, with a nitrogen laser operating at 337 nm, for MALDI-TOF. The different matrixes employed are indicated for each spectrum. Mass spectrometry data are expressed in *m/z* units.

Ultraviolet–visible spectroscopy (UV-Vis) and Fluorescence Spectroscopy: spectroscopic grade solvents were used for spectroscopic measurements. UV-Vis spectra were recorded in the Organic Chemistry Department of UAM, employing a JASCO-V660 UV-Vis spectrophotometer. Fluorescence studies were carried out with a JASCO-V8600 fluorometer.

Infrared Spectroscopy (FT-IR): infrared spectra were recorded in the Organic Chemistry Department on a Bruker Vector 22 spectrophotometer, employing in all cases solid samples (KBr pressed disks).

1.5.2 Synthesis of precursor phthalonitriles

1.5.2.1 Synthesis of bulky phthalonitriles

*2,3-Dicyano-1,4-phenylenebis(trifluoromethanesulfonate (**1**)*[27,28]

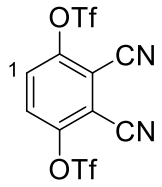

Triethylamine (5.0 mL, 36 mmol), CH_2Cl_2 (25 mL), and dimethylaminopyridine (0.20 g, 1.6 mmol) were added to 2,3-dicyanohydroquinone (2.4 g, 15 mmol) under Ar while maintaining the temperature of the reaction mixture below -70ºC, and the mixture was stirred for 24h at rt. Trifluoromethanesulfonic anhydride (6.0 mL, 37 mmol) was added dropwise at -70ºC, and the mixture stirred for 24h at rt. The reaction mixture was poured into CH_2Cl_2 (200 mL), washed with aqueous HCl 0.5M (5 mL), and the organic layer separated and evaporated under reduced pressure to obtain an orange solid. Yield: 68%

^{1}H-NMR (300 MHz, $CDCl_3$), δ (ppm): 7.9 (s, 2H; H-1).

*2,3-dicyano-1,4-phenylene bis(4-methylbenzenesulfonate) (**2**)*[29]

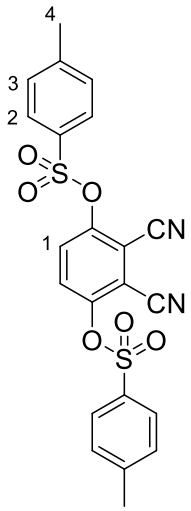

To a flask, 2,3-dicyanohydroquinone (1.0 g, 6.0 mmol), K_2CO_3 (3.5 g, 25 mmol), and tosyl chloride (2.6 g, 14 mmol) were dissolved in 8 mL of acetone and the mixture was stirred under reflux for 2 h. Then the mixture was poured into water and stirred for 1 h. The residue was corrected with filtration, washed with water and dried under vacuum at 60°C. The title compound was obtained as a pale brown powder (2.59 g, 92%).

^{1}H-NMR ($CDCl_3$) δ (ppm): 7.81 (d, J = 6.0 Hz, 4H; H-2), 7.78 (s, 2H; H-1), 7.39 (d, J = 6.0 Hz, 4H; H-3), 2.48 (s, 6H; H-4).

*General procedure for the synthesis of bulky phthalonitriles **3** – **5***

1 (0.473 mmol, 200 mg), boronic acid (1.88 mmol), K_2CO_3 (2.82 mmol, 390 mg), $Pd(PPh_3)_4$ (0.048 mmol, 55 mg) were dissolved in dry DMF (2.4 mL) and the mixture heated in the microwave for an hour at 90 ºC with a power of 100 W (10 bar of limit pressure). Then the mixture was diluted with dichloromethane, washed with aqueous sodium hydroxide 2 M (2 x 20 mL) and brine (20 mL). After that, the organic phase was dried with $MgSO_4$, filtered and the solvent removed under vacuum.

*3,6-(3,5-difluoromethyl)phenylphthalonitrile (**3**)*

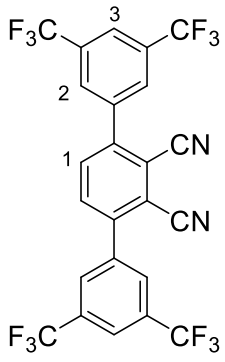

The resulting crude was dissolved in toluene and filtered over silica, then the solvent was evaporated under vacuum and the solid was washed with heptane to obtain the resulting 3,6-biarylphthalonitrile **3** (180 mg, 69% yield).

^{1}H-NMR (300MHz, $CDCl_3$) δ (ppm): 8.09 (s, 1H; H-3), 8.06 (s, 2H; H-2), 7.93 (s, 1H; H-1).

^{19}F-NMR (282 MHz, $CDCl_3$), δ (ppm): -62.97 (s).

^{13}C-NMR (75.5 MHz, $CDCl_3$), δ (ppm): 143.8, 137.7, 134.3, 133.0 (q, J = 34.1 Hz), 129.0, 124.6, 121.0, 116.7, 114.2.

HR-MS (TOF EI+) m/z Calcd for $[C_{24}H_8F_{12}N_2]$: 552.0496; Found: 552.0480.

*3,6-(3,5-Dimethyl)phenylphthalonitrile (**4**)*

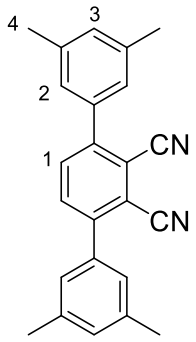

The resulting crude was washed with heptane to obtain the resulting 3,6-biarylphthalonitrile **4** (103 mg, 65% yield).

^{1}H-NMR (300MHz, $CDCl_3$) δ (ppm): 7.7 (s, 1H; H-1), 7.1 (s, 2H; H-2), 7.0 (s, 1H; H-3), 2.3 (s, 6H; H-4).

^{13}C-NMR (75MHz, $CDCl_3$) δ (ppm): 146.0, 138.8, 136.5, 134.0, 131.3, 126.6, 115.9, 115.6, 21.5.

HR-MS (TOF EI+) m/z Calcd for $[C_{24}H_{20}N_2]$: 336.1626; Found: 336.1621.

*3,6-(3,5-Di-tert-butyl)phenylphthalonitrile (**5**)*

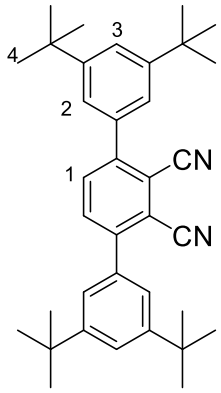

The resulting crude was dissolved in toluene and filtered over silica, then the solvent was evaporated under vacuum and the solid was washed with heptane to obtain the resulting 3,6-biarylphthalonitrile **5** (191 mg, 80% yield).

^{1}H-NMR (300MHz, $CDCl_3$) δ (ppm): 7.7 (s, 1H; H-1), 7.5 (t, J = 1.8Hz, 1H; H-3), 7.4 (d, J = 1.5Hz, 2H; H-2), 1.3 (s, 18H; H-4).

^{13}C-NMR (75MHz, $CDCl_3$) δ (ppm): 151.7, 145.7, 135.8, 134.0, 123.4, 116.2, 115.9, 35.3, 31.6.

HR-MS (TOF EI+) m/z Calcd for [$C_{36}H_{44}N_2$]: 504.3504; Found: 504.3499.

*3,5-Di-tert-butylphenyl boronic acid (**6**)*[33]

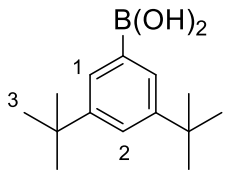

1-bromo-3,5- di-*terz*-butyl benzene (25 g, 9.3 mmol) was dissolved in dry THF (40 mL) and the mixture was cooled at -78ºC. Then ^{n}BuLi (9.4 mmol, 5.9 mL of 1.6 M solution in hexane) was added dropwise and the mixture was stirred for 1h at this temperature and after that triisopropyl borate (5.5 mL, 23.25 mmol) was added. The solution was brought to room temperature and left stirring for 1h and 30 minutes. Then the mixture was washed with aqueous HCl 10%, the organic phase was dried with $MgSO_4$, filtered and the solvent removed under vacuum. The resulting crude was further purified by column chromatography on silica gel using heptane/ethyl acetate (3:1) as eluent to obtain the desired product as a white solid. Yield: 61%, 1.3 g.

^{1}H-NMR (300 MHz, $CDCl_3$), δ (ppm): 8.2 (d, J = 2.0 Hz, 2H; H-1), 7.7 (t, J = 2.0 Hz, 1H; H-2), 4.8 (s, 2H; OH), 1.5 (s, 18H; H-3).

^{13}C-NMR (75.5 MHz, $CDCl_3$), δ (ppm): 150.3, 129.6, 127.5, 127.1, 35.0, 31.6.

1.5.2.2 Synthesis of 4-iodophthalonitrile

*4-Aminophthalonitrile (**7**)*[34]

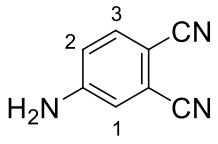

To a mixture of MeOH (450 mL) and concentrated HCl (96 mL), 4-nitrophthalonitrile (115 mmol, 20 g) was added. Upon heating to reflux, the total dissolution of the solid was observed and, at that moment, iron powder (329 mmol, 22 g) was added in small portions over 1h. The brown solution was stirred at reflux for another 1 h and allowed to warm up to rt. Cold water (600 mL) was poured over the mixture, resulting in the precipitation of a yellow-green solid which was filtered, washed with water and vacuum-dried. Recrystallization from toluene led the product as other crystalline needles. Yield: 76%.

^{1}H-NMR (300 MHz, DMSO-d_6), δ (ppm): 7.6 (d, J = 8.7 Hz, 1H; H-3), 7.0 (d, J = 2.5 Hz, 1H; H-1), 6.8 (dd, J = 8.7 Hz, J = 2.5 Hz, 1H; H-2), 6.7 (s, br, 2H; NH_2).

MS (EI) m/z: 143.0 [M^+].

*4-Iodophthalonitrile (**8**)*[35]

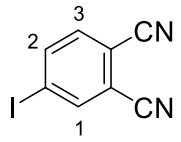

A suspension of **7** (35 mmol, 5 g) in H_2SO_4 2.5M (70 mL) was cooled to -10ºC and a solution of $NaNO_2$ (39 mmol, 2.8 g) in water (10 mL) was added dropwise under constant stirring. After total addition, the mixture was further stirred for 30 min at 0ºC and then a solution of KI (39 mmol, 6.5g) in cold water (40 mL) was added dropwise. The resulting mixture was stirred for 45 min at rt, and then the brown solid was filtered, washed with water and dissolved in $CHCl_3$ (200 mL). The organic solution was consecutively washed with a saturated solution of $Na_2S_2O_3$ (30 mL), and water (30 mL), and dried over Na_2SO_4. After filtration of the drying agent, the solvent was vacuum-evaporated and the yellow solid obtained was purified by chromatography column on silica gel using CH_2Cl_2 as eluent. In this way, the product was obtained as a white solid. Yield: 69%

^{1}H-NMR (300 MHz, $CDCl_3$), δ (ppm): 8.2 (d, J = 1.6 Hz, 1H; H-1), 8.1 (dd, J = 8.2 Hz, J = 1.6 Hz, 1H; H-2), 7.5 (d, J = 8.6 Hz, 1H; H-3).

MS (EI) m/z: 253.9 [M^+].

1.5.2.3 Synthesis of 4,5-Diiodophthalonitrile

*4,5-Diiodophthalimide (**9**)*[36]

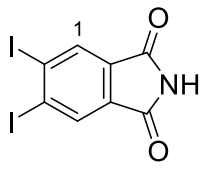

To a suspension of phthalimide (14.7 g, 100 mmol) in 60 mL of 30% fuming sulfuric acid was added iodine (50.8 g, 200 mmol). The reaction mixture was heated to 70 °C for 24 h. After cooling to room temperature, the mixture was poured onto 400 g of ice. The precipitated brown solid was filtered and washed with water (2 x 100 mL), a 2% solution of K_2CO_3 (100 mL), a saturated solution of $Na_2S_2O_3$ (100 mL) and water (100 mL) again. The solid was extracted with acetone (1 L) in a Soxhlet extractor for 48 h. The precipitate formed in the solvent vessel was filtered from the acetone and 100 mL of water was added. This solution was concentrated to 500 mL and the solid obtained was filtered off and vacuum-dried, yielding 32.3 g (81.0 mmol) of 4,5- diiodophthalimide as a white solid. Yield: 81%.

^{1}H-NMR (300 MHz, Acetone-d_6): δ (ppm) = 8.26 (s, 2H; H-1).

*4,5-Diiodophthalamide (**10**)*[36]

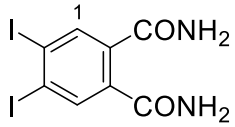

A suspension of 4,5-diiodophthalimide (12.0 g, 30.0 mmol) in 33% aqueous ammonia (100 mL) was heated to 60 °C for 1 h. The white solid obtained was filtered, washed with water (3 x 25 mL) and MeOH (2 x 25 mL) and vacuum-dried over P_2O_5. In so doing, 9.4 g (22.6 mmol) of 4,5- diiodophthalamide were isolated as a white solid. Yield: 75%.

^{1}H-NMR (300 MHz, DMSO-d_6): δ (ppm) = 7.92 (s, 2H; H-1), 7.8, 7.4 (2xs br, 4H, NH_2).

*4,5-Diiodophthalonitrile (**11**)*[36]

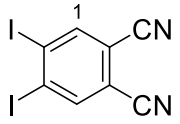

To an ice-cooled stirred suspension of 4,5-diiodophthalamide (8.3 g, 20 mmol) in 80 mL of dry dioxane and 18 mL of dry pyridine was added 16 mL of trifluoroacetic anhydride at 0-5 °C. After the addition was complete, the reaction mixture was warmed to room temperature, stirred for 16 h, and poured onto ice. The product was extracted with AcOEt (3 x 50 mL). The organic layer was washed with water (100 mL), 1 M HCl (2 x 100 mL), a dilute solution of Na_2CO_3 (2 x 200 mL) and water (50 mL) again and dried over $MgSO_4$. After filtration of the drying agent, the solvent was vacuum-evaporated and the yellow solid obtained was subjected to column chromatography on silica gel using toluene/$CHCl_3$ 3:2 as eluent. In this

way, 4.1 g (10.8 mmol) of 4,5-diiodophthalonitrile were obtained as a white solid. Yield: 54%.

^{1}H-NMR (300 MHz, $CDCl_3$): δ (ppm) = 8.19 (s, 2H; H-1).

1.5.3 Synthesis of ABAB Pcs

*General procedure for the synthesis of **ABAB** Pcs **12**, **15** and **18***

3 (0.597 mmol, 330 mg), phthalonitrile **8**, **11** or 4-nitrophthalonitrile (0.597 mmol) and anhydrous $Zn(AcO)_2$ (0.597 mmol, 110 mg) were placed in a 25 mL flask equipped with a magnetic stirrer and then 6 mL of o-diclorobenzene/DMF (2:1) was added.

*1,4,15,18-Tetrakis(3,5-bis(trifluoromethyl)phenyl)-9[10],23[24]-diiodo- zinc (II) phthalocyanine (**12**)*

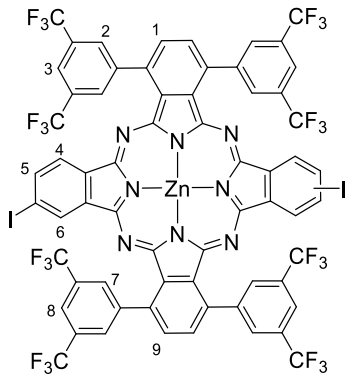

The crude was purified by silica-gel column chromatography (hexane/THF 4:1), the first fraction to elute containing the desired product, followed by compounds **13** and **14**. Compound **12** was further purified by an additional column chromatography on silica gel using toluene as eluent. A blue solid was obtained, which was washed with methanol/water (5:1). Yield: 85 mg, 16%

^{1}H-NMR (500 MHz, THF-d_8), δ (ppm): 8.85 (s, 4H; H-2, H-7), 8.83 (s, 4H; H-2, H-7), 8.78 (s, 4H; H-2, H-7), 8.77 (s, 4H; H-2, H-7), 8.64 (s, 4H; H-3, H-8), 8.58 (s, 4H; H-3, H-8), 8.56 (s, 2H; H-6), 8.53 (s, 2H; H-6), 8.31 (m, 12H; H-1, H-9, H-5), 8.06 (d, J = 7.8 Hz, 2H; H-4), 8.03 (d, J = 7.8 Hz, 2H; H-4).

^{13}C-NMR (125 MHz, THF-d_8), δ (ppm): 153.1 (C=N), 153.1 (C=N), 152.8 (C=N), 152.8 (C=N), 152.7 (C=N), 152.7 (C=N), 152.0 (C=N), 152.0 (C=N), 143.2, 143.1, 143.0, 142.9, 138.9, 138.7, 137.9, 137.2, 135.5, 135.4, 135.4, 135.3, 131.9 (q, C-CF_3, J = 6.25 Hz), 131.7, 131.5, 131.4, 131.3, 131.0, 124.0 (q, CF_3, J = 270 Hz), 123.6, 121.9, 95.5 (C-I).

^{19}F-NMR (471 MHz, THF-d8), δ (ppm): -62.88 (2 x s), -62.91 (2 x s).

HR-MS (MALDI) m/z Calcd for [$C_{64}H_{22}F_{24}I_2N_8Zn$]: 1675.8965; Found: 1675.8961.

UV-Vis (THF) λmax (log ε): 691 (5.17), 675 (5.18), 354 (4.90) nm.

IR (KBr) ν^{-1} (cm^{-1}): 3641, 3385, 2953, 2926, 2858, 1649, 1380, 1272, 1137, 894, 840, 745, 705.

Mp > 250°C

*1,4,15,18-Tetrakis(3,5-di-tert-butylphenyl)-9[10],23[24]-dinitro zinc (II) phthalocyanine (**15**)*

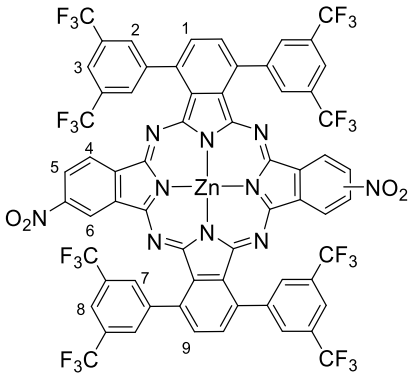

The crude was purified by silica-gel column chromatography (heptane/THF 3:2), the first fraction to elute containing the desired product **15**, followed by compounds **16** and **17**. A blue solid was obtained, which was washed with methanol/water (5:1). Yield: 53 mg, 12%.

^{1}H-NMR (300 MHz, THF-d_8), δ (ppm): 8.99 (d, J = 1.8 Hz, 2H; H-5), 8.96 (d, J = 1.8 Hz, 2H; H-5), 8.85 (m, 12;H; H-2, H-7, H-6), 8.77 (2 x s, 8H; H-2, H-7), 8.73 (s, 4H; H3, H-8), 8.64 (s, 4H; H3, H-8), 8.43 (s, 2H; H-4), 8.40 (s, 2H; H-4), 8.38 – 8.32 (m, 8H; H-1, H-9).

HR-MS (MALDI) m/z Calcd for [$C_{64}H_{22}F_{24}N_{10}O_4Zn$]: 1514.0728; Found: 1514.0779.

UV-Vis (THF) λmax (log ε): 700 (4.74), 680 (4.73), 345 (4.29), 256 (4.52) nm.

Mp > 250°C

*1,4,15,18-Tetrakis(3,5-bis(trifluoromethyl)phenyl)-9,10,23,24-tetraiodo- zinc (II) phthalocyanine (**18**)*

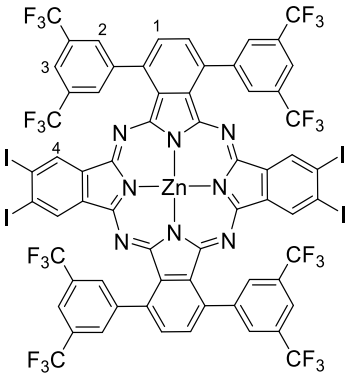

The mixture was heated to 150ºC for 12h under Ar atmosphere and, after cooling, the solvent was removed under vacuum. The crude was purified by silica-gel column chromatography (hexane/THF 4:1), the first fraction to elute containing the desired product, followed by compounds **19** and **20**. Compound **18** was further purified by an additional column chromatography on silica gel using CH_2Cl_2/heptane (6:1). A blue solid was obtained, which was washed with methanol/water (5:1). Yield: 57 mg, 10%.

^{1}H-NMR (500 MHz, THF-d_8), δ (ppm): 8.75 (s, 8H; H-2), 8.68 (s, 4H; H-4), 8.61 (s, 4H; H-2), 8.29 (s, 4H; H-1).

^{13}C-NMR (125 MHz, THF-d_8), δ (ppm): 151.1 (C=N), 149.8 (C=N), 141.1, 136.6, 135.3, 133.6, 130.8, 129.6 (q, C-CF_3, J = 33 Hz), 129.5, 129.1, 122.1 (q, CF_3, J = 271.25 Hz), 120, 107 (C-I).

HR-MS (MALDI) m/z Calcd for [$C_{64}H_{20}F_{24}I_4N_8Zn$]: 1927.6898; Found: 1927.6917.

UV-Vis (THF), λmax (log ε): 688 (5.27), 350 (4.69) nm.

IR (KBr) ν^{-1} (cm^{-1}): 2924, 2854, 1963, 1605, 1443, 1281, 1142

Mp > 250°C

*1,4,15,18-Tetrakis(3,5-dimethylphenyl)-9[10],23[24]-diiodo zinc (II) phthalocyanine (**21**)*

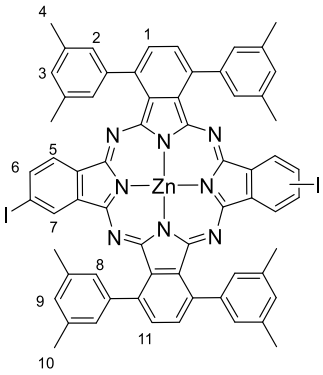

Lithium (2.4 mmol, 17 mg) placed in a 25 mL two-neck flask equipped with a magnetic stirrer and then was dissolved in 1 – pentanol (5.4 mL) at reflux in an hour. After that, phthalonitriles **4** (0.812 mmol, 273 mg) and **8** (0.812 mmol, 206 mg) were added and the mixture was heated at reflux for 3h under Ar atmosphere. After cooling, acetic acid (2 mL) was added and the mixture was stirred for other 15 minutes. Then the mixture was diluted with dichloromethane, washed with water (2 x 20 mL). After that, the organic phase was dried with $MgSO_4$, filtered and the solvent removed under vacuum. Then the mixture of phthalocyanines was dissolved in dry DMF (5 mL) and placed in a 25 mL flask equipped with a magnetic stirred. Anhydrous $Zn(AcO)_2$ (0.9 mmol, 165 mg) was added and the mixture was stirred at 110ºC for 1h. After that, the solvent was removed under vacuum and the crude was purified by silica-gel column chromatography (heptane / THF 4:1); the second fraction to elute contained a mixture of the desired product **21** and the adjacent isomer **25**, preceded by compound **26** and followed by compounds **23** and **14**. A blue solid was obtained, which was washed with methanol / water (5:1). Yield: 97 mg, 19% (mixture of two isomers).

^{1}H-NMR (300 MHz, THF-d_8), δ (ppm): 9.70 (d, J = 12.6 Hz, 1H), 9.10 (d, J = 7.8 Hz, 1H), 9.06 (d, J = 8.1 Hz, 1H), 8.95 (d, J = 6.6 Hz, 4H), 8.84 (s, 1H), 8.43 – 8.27 (m, 13H), 8.06 – 8.04 (m, 12H), 7.96 (dd, J = 7.8 Hz, J = 1.8 Hz, 2H), 7.82 (dd, J = 11.2 Hz, J = 4.2 Hz, 20H), 7.77 (s, 2H), 7.72 (s, 2H), 7.65 – 7.51 (m, 8H), 7.58 (s, 5H), 7.48 (s, 6H), 7.17 (s, 4H), 7.03 (s, 2H), 6.92 (s, 1H), 6.88 (s, 2H), 2.67 (s, 24H; H-4, H-10), 2.65 (s, 6H; H-4, H-10), 2.61 (s, 24H; H-4, H-10), 2.59 (s, 6H; H-4, H-10).*

HR-MS (MALDI) m/z Calcd for [$C_{64}H_{46}I_2N_8Zn$]: 1244.1226; Found: 1244.1213.

Mp > 250°C.

* The interpretation of ^{1}H-NMR spectrum of this compound could not be fully performed due to the complexity of the system resulting from the mixture of **21** and **25**.

*1,4,15,18-Tetrakis(3,5-di-tert-butylphenyl)-9[10],23[24]-diiodo zinc (II) phthalocyanine (**22**)*

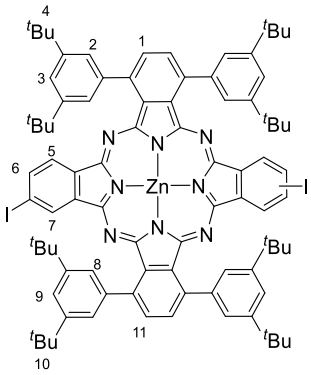

8 (0.26 mmol, 67 mg), phthalonitrile **5** (0.26 mmol, 131 mg) and anhydrous $Zn(AcO)_2$ (0.26 mmol, 48 mg) were placed in a 25 mL flask equipped with a magnetic stirrer and then 2.8 mL of DMAE was added. The mixture was heated to 140 ºC for 24 h under Ar atmosphere and, after cooling, the solvent was removed under vacuum. The crude was purified by silica-gel column chromatography (heptane / dioxane 4:1), the first fraction to elute containing the desired product **22**, followed by compounds **24** and **14**. A blue solid was obtained, which was washed with methanol/water (5:1). Yield: 5 mg, 2.5%*.

HR-MS (MALDI) m/z Calcd for [$C_{88}H_{94}I_2N_8Zn$]: 1580.4982; Found: 1580.4986.

* The characterization of this compound could not be fully performed due to the low amount of compound available, which was not enough to obtain well-defined ^{1}H-NMR spectra.

1.6 References

(1) Kobayashi, N.; Kobayashi, Y.; Osa, T. Optically Active Phthalocyanines and Their Circular Dichroism. *J. Am. Chem. Soc.* **1993**, *115*, 10994–10995.

(2) Drew, D. M.; Leznoff, C. C. The Synthesis of Pure 1,11,15,25-Tetrasubstitutedphthalocyanines as Single Isomers Using Bisphthalonitriles. *Synlett* **1994**, *1994*, 623–624.

(3) Miwa, H.; Kobayashi, N. A Novel Naphthalocyanine Isomer: A Dinaphthophthalocyanine with C2v Symmetry. *Chem. Lett.* **1999**, *28*, 1303–1304.

(4) Kobayashi, N.; Miwa, H.; Nemykin, V. N. Adjacent versus Opposite Type Di-Aromatic Ring-Fused Phthalocyanine Derivatives: Synthesis, Spectroscopy, Electrochemistry, and Molecular Orbital Calculations. *J. Am. Chem. Soc.* **2002**, *124*, 8007–8020.

(5) Nolan, K. J. M.; Hu, M.; Leznoff, C. C. “Adjacent” Substituted Phthalocyanines. *Synlett* **1997**, *1997*, 593–594.

(6) Oliver, S. W.; Smith, T. D. Oligomeric Cyclization of Dinitriles in the Synthesis of Phthalocyanines and Related Compounds: The Role of the Alkoxide Anion. *J. Chem. Soc. Perkin Trans. 2* **1987**, *0*, 1579–1582.

(7) Fukuda, T.; Kobayashi, N. Efficient Synthesis of a Donor-Acceptor Phthalocyanine Having Adjacently-Fused Pyrazine Rings. *Chem. Lett.* **2002**, *31*, 866–867.

(8) Kobayashi, N.; Fukuda, T. Mono-Aromatic Ring-Fused versus Adjacently Di-Aromatic Ring-Fused Tetraazaporphyrins: Regioselective Synthesis and Their Spectroscopic and Electrochemical Properties. *J. Am. Chem. Soc.* **2002**, *124*, 8021–8034.

(9) Kobayashi, N.; Fukuda, T.; Ueno, K.; Ogino, H. Extremely Non-Planar Phthalocyanines with Saddle or Helical Conformation: Synthesis and Structural Characterizations. *J. Am. Chem. Soc.* **2001**, *123*, 10740–10741.

(10) Kobayashi, N.; Ashida, T.; Osa, T.; Konami, H. Phthalocyanines of a Novel Structure: Dinaphthotetraazaporphyrins with D2h Symmetry. *Inorg. Chem.* **1994**, *33*, 1735–1740.

(11) Kobayashi, N.; Togashi, M.; Osa, T.; Ishii, K.; Yamauchi, S.; Hino, H. Low Symmetrical Phthalocyanine Analogues Substituted with Three Crown Ether Voids and Their Cation-Induced Supermolecules. *J. Am. Chem. Soc.* **1996**, *118*, 1073–1085.

(12) Sakamoto, K.; Ohno-Okumura, E.; Kato, T.; Watanabe, M.; Cook, M. J. Investigation of Zinc bis(1,4-Didecylbenzo)-bis(2,3-Pyrido) Porphyrazine as an Efficient Photosensitizer by Cyclic Voltammetry. *Dye. Pigment.* **2008**, *78*, 213–218.

(13) Sholto, A.; Lee, S.; Hoffman, B. M.; Barrett, A. G. M.; Ehrenberg, B. Spectroscopy, Binding to Liposomes and Production of Singlet Oxygen by Porphyrazines with Modularly Variable Water Solubility. *Photochem. Photobiol.* **2008**, *84*, 764–773.

(14) Nemykin, V. N.; Kobayashi, N.; Nonomura, T.; Luk’yanets, E. A. Low Symmetrical Phthalocyanines Having Spectroscopic and Electrochemical Properties Characteristic of Unexpected Accidental S1 State Degeneracy

and Non-Planar Distortions. *Chem. Lett.* **2000**, *29*, 184–185.
(15) Idelson, E. M. U.S. Patent. 4.061.654, 1977.
(16) Leznoff, C. C.; Greenberg, S.; Khouw, B.; Lever, A. B. P.; Leve, A. B. P. The Syntheses of Mono- and Disubstituted Phthalocyanines Using a Dithioimide. *Can. J. Chem.* **1987**, *65*, 1705–1713.
(17) Shirai, H.; Hanabusa, K.; Kitamura, M.; Masuda, E.; Hirabaru, O.; Hojo, N. Functional Metal Porphyrazine Derivatives and Their Polymers, 14. Synthesis and Properties of [Bis- or Tetrakis(decyloxycarbonyl)phthalocyaninanto]metal Complexes. *Die Makromol. Chemie* **1984**, *185*, 2537–2542.
(18) Reid, E. E. Organic Chemistry of Bivalent Sulfur. 1958, p ii.
(19) Young, J. G.; Onyebuagu, W. Synthesis and Characterization of Di-Disubstituted Phthalocyanines. *J. Org. Chem.* **1990**, *55*, 2155–2159.
(20) Stihler, P.; Hauschel, B.; Hanack, M. Synthesis of a Bisdienophilic Phthalocyanine and of Precursors for Repetitive Diels-Alder Reactions Based on Hemiporphyrazines and Phthalocyanines. *Chem. Ber.* **1997**, *130*, 801–806.
(21) Youngblood, W. J. Synthesis of a New Trans-A2B2 Phthalocyanine Motif as a Building Block for Rodlike Phthalocyanine Polymers. *J. Org. Chem.* **2006**, *71*, 3345–3356.
(22) Wang, J.-D.; Lin, M.-J.; Wu, S.-F.; Lin, Y. 1,15-Bis-(2′,2′,4′-Trimethyl-3′-Pentoxy)phthalocyanine, a Trans-Form Nonperipheral Di-Substituted Phthalocyanine Synthesized by the “cross Condensation” Method. *J. Organomet. Chem.* **2006**, *691*, 5074–5076.
(23) Ayhan, M. M.; Singh, A.; Hirel, C.; Gürek, A. G.; Ahsen, V.; Jeanneau, E.; Ledoux-Rak, I.; Zyss, J.; Andraud, C.; Bretonnière, Y. ABAB Homoleptic Bis(phthalocyaninato)lutetium(III) Complex: Toward the Real Octupolar Cube and Giant Quadratic Hyperpolarizability. *J. Am. Chem. Soc.* **2012**, *134*, 3655–3658.
(24) Ayhan, M. M.; Singh, A.; Jeanneau, E.; Ahsen, V.; Zyss, J.; Ledoux-Rak, I.; Gürek, A. G.; Hirel, C.; Bretonnière, Y.; Andraud, C. ABAB Homoleptic Bis(phthalocyaninato)lanthanide(III) Complexes: Original Octupolar Design Leading to Giant Quadratic Hyperpolarizability. *Inorg. Chem.* **2014**, *53*, 4359–4370.
(25) Dumoulin, F.; Zorlu, Y.; Menaf Ayhan, M.; Hirel, C.; Isci, Ü.; Ahsen, V. A First ABAC Phthalocyanine. *J. Porphyr. Phthalocyanines* **2009**, *13*, 161–165.
(26) Chow, S. Y. S.; Ng, D. K. P. Synthesis of an ABCD-Type Phthalocyanine by Intramolecular Cyclization Reaction. *Org. Lett.* **2016**, *18*, 3234–3237.
(27) Heeney, M. J.; Al-Raqa, S. A.; Auger, A.; Burnham, P. M.; Cammidge, A. N.; Chambrier, I.; Cook, M. J. Routes to Some 3,6-Disubstituted Phthalonitriles and Examples of Phthalocyanines Derived Therefrom: An Overview. *J. Porphyr. Phthalocyanines* **2013**, *17*, 649–664.
(28) Kobayashi, N.; Ogata, H.; Nonaka, N.; Luk’yanets, E. A. Effect of Peripheral Substitution on the Electronic Absorption and Fluorescence Spectra of Metal-Free and Zinc Phthalocyanines. *Chem. – A Eur. J.* **2003**, *9*, 5123–5134.
(29) Kobayashi, N.; Furuyama, T.; Satoh, K. Rationally Designed

Phthalocyanines Having Their Main Absorption Band beyond 1000 Nm. *J. Am. Chem. Soc.* **2011**, *133*, 19642–19645.

(30) Tang, Z.-Y.; Hu, Q.-S. Room-Temperature Ni(0)-Catalyzed Cross-Coupling Reactions of Aryl Arenesulfonates with Arylboronic Acids. *J. Am. Chem. Soc.* **2004**, *126*, 3058–3059.

(31) Zim, D.; Lando, V. R.; Dupont, J.; Monteiro, A. L. NiCl2(PCy3)2: A Simple and Efficient Catalyst Precursor for the Suzuki Cross-Coupling of Aryl Tosylates and Arylboronic Acids. *Org. Lett.* **2001**, *3*, 3049–3051.

(32) Ramgren, S. D.; Hie, L.; Ye, Y.; Garg, N. K. Nickel-Catalyzed Suzuki–Miyaura Couplings in Green Solvents. *Org. Lett.* **2013**, *15*, 3950–3953.

(33) Heller, D. P.; Goldberg, D. R.; Wu, H.; Wulff, W. D. An Examination of VANOL, VAPOL, and VAPOL Derivatives as Ligands for Asymmetric Catalytic Diels–Alder Reactions. *Can. J. Chem.* **2006**, *84*, 1487–1503.

(34) Griffiths, J.; Roozpeikar, B. Synthesis and Electronic Absorption Spectra of Dicyano-Derivatives of 4-Diethylaminoazobenzene. *J. Chem. Soc. Perkin Trans. 1* **1976**, 42–45.

(35) Marcuccio, S. M.; Svirskaya, P. I.; Greenberg, S.; Lever, A. B. P.; Leznoff, C. C.; Tomer, K. B. Binuclear Phthalocyanines Covalently Linked through Two- and Four-Atom Bridges. *Can. J. Chem.* **1985**, *63*, 3057–3069.

(36) Terekhov, D. S.; Nolan, K. J. M.; McArthur, C. R.; Leznoff, C. C. Synthesis of 2,3,9,10,16,17,23,24-Octaalkynylphthalocyanines and the Effects of Concentration and Temperature on Their ^{1}H NMR Spectra. *J. Org. Chem.* **1996**, *61*, 3034–3040.

(37) Mikami, K.; Itoh, Y.; Yamanaka, M. Fluorinated Carbonyl and Olefinic Compounds: Basic Character and Asymmetric Catalytic Reactions. *Chem. Rev.* **2004**, *104*, 1–16.

(38) Seebach, D. Organic Synthesis—Where Now? *Angew. Chemie Int. Ed. English* **1990**, *29*, 1320–1367.

(39) Fulmer, G. R.; Miller, A. J. M.; Sherden, N. H.; Gottlieb, H. E.; Nudelman, A.; Stoltz, B. M.; Bercaw, J. E.; Goldberg, K. I. NMR Chemical Shifts of Trace Impurities: Common Laboratory Solvents, Organics, and Gases in Deuterated Solvents Relevant to the Organometallic Chemist. *Organometallics* **2010**, *29*, 2176–2179.

Chapter 2 – Linear Donor–π–Acceptor Systems Based on Phthalocyanines

2.1 State of the art

2.1.1 Overview of Current Energy Trends

In the last decade, the global primary energy consumption has grown at an average rate of 2.1% per year,[1] despite the greatest world economic crisis since World War II. During 2014 and 2015 it grew only by 0.9% and 1% respectivly[1]—the weakest increase since 2009 and a possible clue of a tendency to moderation in the years to come—reaching a value of almost 13 billion tons of oil equivalents (btoe),[1] which corresponds to an average rate of consumption of 17.2 TW. As shown in Figure 2.1, fossil fuels still provide 86% of the global primary supply, but renewables are about 10% overall share. Nuclear has slightly increased in the last couple of years, but this will hardly affect a general trend to a reduced relevance of this source, as the decommissioning of many reactors in the US and Europe approaches.[2]

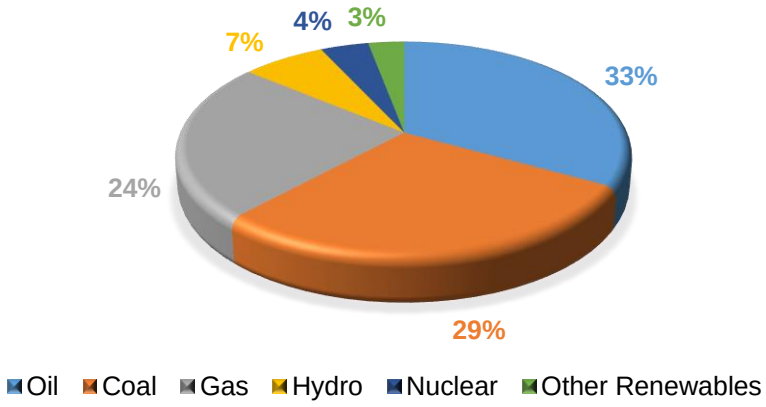

Figure 2.1. Global supply of commercially traded primary energy, from BP 2016.[1]

The world's demand for fossil energy amounts to 1066 barrels of oil, 108,000 cubic meters of natural gas and 250 tonnes of coal per second.[1] Oil continues to represent the first energy source, the largest majority of which (*ca.* 80%) is used to power the world transportation system, the remainder being used for heat and electricity, petrochemicals, asphalt, and lubricants, in order of decreasing importance.[3,4] Recently, the predominance of oil products in transportation has started to be slightly undermined by biomass-derived combustibles, natural gas, and electricity, which, for instance, in the US now globally represent 8.5% of the transportation fuels, the largest nonpetroleum share since 1954.[5]

Natural gas is the most geographically concentrated energy resource. By far, Iran, Qatar and Russia host nearly 50% of the world's estimated reserves, but in the last decade, the US natural gas production has increased by over 40%, reinstating the country as the world's largest producer, well ahead of Russia.[1]

The estimated reserves of coal are by far the largest among fossil fuels, as they might cover the present world demand for over 110 years, to be compared to 52.5 and 54.1 years for oil and natural gas, respectively.[1] The main use of coal remains electricity generation, followed by the production of metallurgical coke, cement manufacturing, and a variety of minor uses.[6]

Alas, the disadvantages of fossil fuels are well known: the scientific consensus on global warming and climate change is that it is caused by anthropogenic greenhouse gas emissions, two thirds of which comes from industrially burning fossil fuels.[7,8] Specific examples of environmental and public health concerns, that are now under intense scrutiny,[9,10] include groundwater contamination,[11] methane release in the atmosphere,[12] induced seismicity upon reinjection of fracking wastewater,[13,14] and rapidly declining rates of well production, which leads to highly intensive drilling.[15]

Fortunately, over the last decade, the most relevant change in the world energy landscape is the relentless rise of renewable energies, primarily in the electricity sector. In 2014, for the first time, global carbon emissions associated with energy production remained stable despite continued economic growth. This is primarily attributable to the increasing penetration of renewables and enhanced energy efficiency, particularly in the affluent world.[16] The key player in this changing scenario is China, which now produces as much electricity from water, wind, and sunlight, as all France and Germany's power plants combined, covering 20% of its demand.[17] Between 2008 and 2012 its investments in non-fossil power plants increased by 40%, whilst those in fossil-fuelled facilities were substantially reduced. The almost 7-fold drop of the photovoltaic (PV) module price in the last decade has been primarily the consequence of the 10-fold increase of the Chinese production; this has made PV a truly game changer in the global energy market. The number of locations where PV electricity is competitive with conventional technologies (e.g., coal or nuclear) is constantly increasing and its portion of electricity production in some industrialized countries has become remarkable.[17]

All the renewable energy sectors (i.e., solar, geothermal, ocean, wind, hydropower and biomass) continue to grow. The estimated renewable share of final energy consumption is about 19%, modern technologies and traditional

biomass being at 10 and 9% respectively.[16] By far, the most important renewable sector is electricity production, with 22.8% of the overall world's generation. At the end of 2015, hydroelectric global capacity exceeded 1 TW, wind was 430 GW, and PV almost 230 GW; they covered 16.6, 3.1 and 0.9 %, respectively, of the world electricity demand.[16] The two last shares appear to be small, but it has to be highlighted that hydroelectricity has been an established technology for over 120 years, whereas wind and PV were virtually non-existing just two decades ago.

The above selected data suggest that the energy transition from fossil fuels to renewables is already ongoing. However, since the energy system is a gigantic and complex machine spread all over the planet, it will be a long, complicated, and difficult process, [6,18] but it will offer big challenges along with great opportunities and is poised to radically change our way of living.[19]

2.1.2 Solar Energy

As a matter of fact, solar energy alone possesses the potential of becoming the successor of fossil fuels, which will cover the world's current energetic needs.[20] Sunlight strikes the Earth's surface with enough energy every hour to supply world consumption per annum. This is by far the biggest source of energy available to us, and a great candidate for a transition to a more sustainable production of energy. Furthermore, this energy source is ubiquitous, and it is expected that the deployment of solar energy will give political stability to many areas of the planet because of the more balanced distribution of a primary source of energy.

In the last five years, the world PV system has undergone substantial developments in terms of manufacturing distribution (largely shifted from Europe to Asia), global deployment, and even new photoactive materials that are very promising but, at present, remain at the research laboratory stage. PV technology exhibits a series of remarkable merits such as:

1. Possibility to be scaled from the KW to the GW scale without affecting efficiency and economic performance (conventional fossil fuel and nuclear plants have an optimal operational size; below that or above that, they under-perform).
2. An up-front investment followed by decades of electricity produced by a 100% guaranteed free primary source.
3. No moving parts, implying negligible wear and very low maintenance cost.
4. Installation possible on existing platforms (e.g., roofs) with no land consumption.
5. Decentralization of the electricity production system, as needed to enhance energy security.
6. Possibility of providing electricity to communities in off grid rural or isolated areas, improving the quality of life in underdeveloped regions.[21]

Solar energy[22] can be transformed into electricity either thermodynamically or electronically. In the first method, the solar thermal energy,[23] is usually focused in the design of optical collectors to generate electricity by heating a fluid to drive a turbine connected to an electrical generator. The second method, instead, converts directly the solar energy into electricity by opto-electronic devices, called solar cells. Light shining on the solar cell produces both a current and a voltage to generate electric power. This process requires firstly, a material in which the absorption of light raises an electron to a higher energy state, and

secondly, the movement of this higher energy electron from the solar cell into an external circuit. The electron then dissipates its energy in the external circuit and returns to the solar cell. A variety of materials and processes can potentially satisfy the requirements for photovoltaic energy conversion, but in practice nearly all photovoltaic energy conversion uses semiconductor materials in the form of a p-n junction.

The efficient production of electricity by means of solar cells is nowadays available and PV is one of the fastest growing renewable energy technology.

2.1.2.1 Characteristic parameters of solar cells

The properties of photovoltaic devices can be characterized by plotting the measured current output *J* of the cell versus the voltage output *V* of the cell (*J*-*V* graph). In the dark, this *J*-*V* curve passes through the origin, since at that moment no current is flowing through the device and no potential is present. By exposing the photovoltaic device to light, the *J*-*V* curve shifts downwards, as can be seen in Figure 2.2. The most important characteristic parameters of photovoltaic devices can be found on this *J*-*V* curve.

- Open-circuit voltage (*Voc*): It is the maximum voltage available from a solar cell, and this occurs at zero current.
- Short-circuit current (*Isc*): It is the current through the solar cell when the voltage across it is zero (i.e., when the solar cell is short circuited). The short-circuit current is the largest current which may be drawn from the solar cell. It depends on a number of factors, such as the area of the solar cell. To remove the dependence of the solar cell area, it is more common to list the short-circuit current density (J_{SC} in mA/cm^2), rather than the short circuit current (I_{SC} in mA).
- Maximum power point (M_{pp}): It is the point (V_m, J_m) on the *J*-*V* curve at which the maximum power is produced. Power is the product of current *J* and voltage *V*. This is represented in Figure 2.2 as the area of the rectangle formed between a point on the *J*-*V* curve and the axes *J* and *V*. The maximum power point is that point on the *J*-*V* curve at which the area of the resulting rectangle, *J* x *V*, is largest.
- Fill Factor (FF): It is defined as the ratio of the maximum power output from the solar cell to the product of *Voc* and *Jsc*. Graphically, the FF is a measure of the “squareness" of the solar cell and is also the area of the largest rectangle which will fit in the *J*-*V* curve. This is a very important property used to measure photovoltaic device performance. FF can be written down as follows (Equation 2.1).

$$FF = \frac{J_m \times V_m}{J_{sc} \times V_{oc}} \qquad (2.1)$$

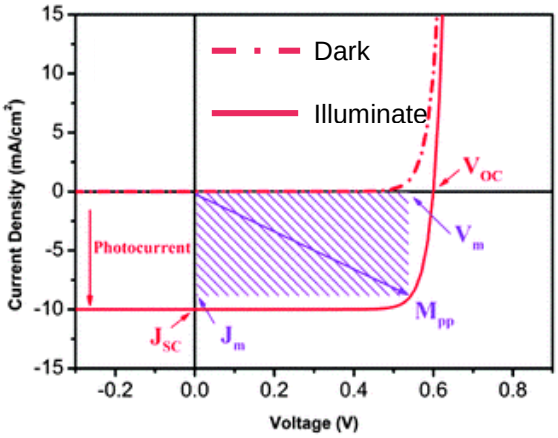

Figure 2.2. Typical *J-V* curve for any type of solar cell in the dark and under illumination (the most important photovoltaic parameters are indicated).

- Power Conversion Efficiency (*PCE* or *η*): It is defined as the ratio of power output, P_{out}, to power input, P_{in}. *PCE* measures the amount of power produced by a photovoltaic device relative to the power available in the incident solar radiation. P_{in} is the sum over all wavelengths, which usually has a value of 100 mW/cm^2 when solar simulators are used. This is the most general way to define the efficiency of a photovoltaic device. *PCE* can be written down as follows (Equation 2.2).

$$PCE\ (\eta) = \frac{P_{out}}{P_{in}} \times 100 = \frac{J_m \times V_m}{P_{in}} \times 100 = \frac{J_{sc} \times V_{oc} \times FF}{P_{in}} \times 100 \qquad (2.2)$$

PCE is the most commonly used parameter to compare the performance of one solar cell to another. It depends on the spectrum and intensity of the incident sunlight and the temperature of the solar cell. To determine their PCE, the cells are typically illuminated at a constant density of roughly 100 mW/cm^2, which is defined as the standard "1 Sun" value, with a spectrum consistent to an air-mass global value of 1.5 (*AM 1.5G*), at a temperature of 25 ºC. Air mass describes the spectrum of radiation and can be defined as the amount of atmosphere though which sunlight has to travel to reach the Earth's surface. This is abbreviated as *AMx*, in which *x* is the inverse of the cosine of the zenith angle of the sun θ. The above mentioned *AM 1.5G* conditions correspond to the spectrum and irradiance

of sunlight incident when $\theta = 48.2^{o}$; solar cells intended for space use are measured under *AM0* conditions (Figure 2.3).

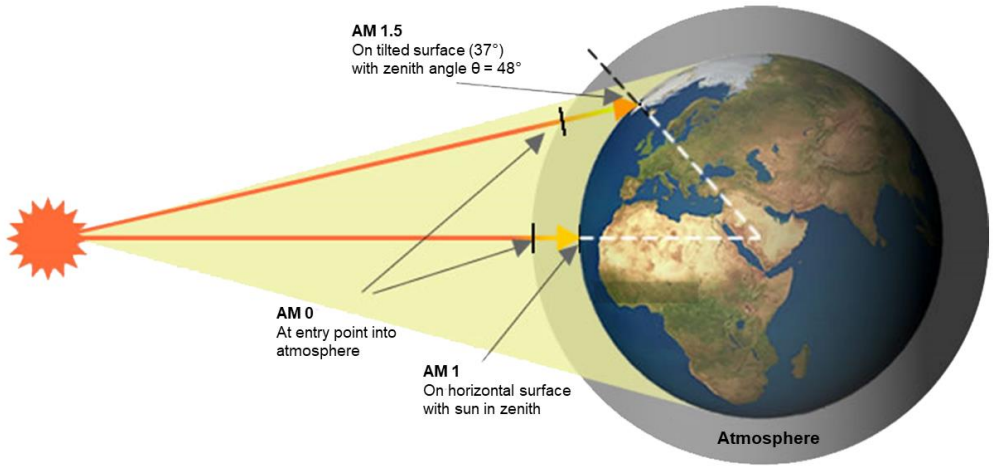

Figure 2.3. The air-mass value *AM 0* equates to insolation just outside the earth's atmosphere. *AM 1.0* represents sunlight with the sun at zenith above the Earth's atmosphere. *AM 1.5* is the same, but with the Sun at an oblique angle of 48.2º, which simulates a longer optical path through the Earth's atmosphere.

2.1.2.2 Silicon and inorganic thin film technologies

Over 90% of today's commercial solar cells are still based on the same material and basic concepts developed at the Bell Laboratories in the early 1950s:[24] light-induced charge separation at p–n junction between two slices (wafers) of doped silicon in either single-crystal or polycrystalline form (sc-Si and poly-Si, respectively). These crystalline solar cells, both mono- and polycrystalline, are known as 1st generation solar cells. Their maximum efficiencies, 25.0% and 20.4%, respectively, are close to the Shockley–Queisser theoretical limit, i.e., 33%.[25]

In the early 60s, the 2nd generation of PV cells appeared: *thin film inorganic solar cells*,[26] based primarily on chemical vapour deposited amorphous silicon (a-Si, maximum efficiency of 13.4%), as well as polycrystalline indium or cadmium telluride (InSe or CdTe, maximum efficiency of 21.5%) or copper gallium indium selenide ($CuInGaSe_2$, known as CIGS with maximum efficiency of 21.7%).

The global share of Si PV has increased from about 80% in 2009 to over 90% in 2014, while thin film technologies have also grown, but at a much lower rate.[27] The success of crystalline silicon (c-Si) technologies is based on a series of peculiar advantages that, even in the future, will be hardly rivalled by new PV concepts. The technology is over 60-years old and deeply established; the lifetime of modules is in the decades time scale; efficiency of energy conversion (light-to-electricity, 15–22%) is comparable or even higher than that of successful devices which have pervaded the world; cost reduction trajectories recall those of past disruptive technologies;[28] key materials (e.g., copper, silver, aluminum, plastics, silicon) are abundant and non-toxic; recycling at end-life is easy and amenable to further improvements within the first massive wave of replacements, not expected for another 20 years.[29,30] Last but not least, silicon PV cumulative production will reach a TW scale within a decade, a landmark goal for future dominance not only in the PV, but also in the entire electricity market.

When compared to 1st generation solar cells, thin film technologies are, in general, less efficient, but also less expensive. Thin film solar cells are designed in such a way that they use less material, resulting in lower cost, manufacturing processes.

Some drawbacks, like resource scarcity, toxicity of the active materials and limiting shape and rigidity of Si PV cells, triggered research on 3rd generation solar cells during the last two decades. In the latter generation, highly efficient solar cells are based on environmentally friendly materials that allow inexpensive solvent-based fabrication techniques.[31]

2.1.2.3 Organic Photovoltaics (OPV)

All-organic photovoltaics, as well as *hybrid solar cells*, are considered also as a type of 3rd generation devices, and have the merits of low cost, stability, simple fabrication and flexibility.[32] By means of these cells, the Shockley-Queisser limit as defined for 1st generation solar cells is expected to be bypassed.

In the late 50s and 60s, it was discovered that many common dyes, such as methylene blue, many important biological molecules like carotenes and chlorophylls, and other porphyrins (Pors) and related synthetic analogues such as Pcs, had semiconducting properties. These dyes were among the first organic materials exhibiting the photovoltaic effect. As early as 1958, Kearns et al. reported the photovoltaic effect of a cell based on a single layer of magnesium Pc, which had a photovoltage of 200 mV.[33] From then on, organic materials have

gained broader interest and several new concepts associated to the configuration of the device have been presented. A milestone came in 1986 when Tang used a two component, donor/acceptor active layer (planar bilayer heterojunction, PHJ, or p-n solar cell, Figure 2.4a).[34] This structural modification benefits from the facile formation of the charge carriers (electrons and holes) by electron transfer from the photoexcited donor to the acceptor component. Also, the separated charge transport layers ensure connectivity with the correct electrode and give the separated charge carriers only a small chance to recombine with their counterparts. The drawback is that only excitons (i.e., electron-hole pairs formed by light excitation) formed very close to the interface between donor and acceptor layers are able to dissociate. To overcome this structural problem, the concept of bulk-heterojunction (BHJ, Figure 2.4b) was introduced by Yu et al,[35] in which a blend of a donor and an acceptor with a bi-continual phase separation is formed.[36–38] The advantage of this type of cell is the large interface area, if molecular mixing occurs on a scale that allows for a good contact between materials, and that enables most of the excitons to reach the p-n interface. Ultimately, another type of architectures called tandem solar cells (Figure 2.4c), have gained a lot of attention. They consist in a combination of two or more single junction cells (one on top of the other) that absorb in different wavelength ranges. Their advantage is that a combination of absorbing molecules can allow for a large spectral coverage with efficient absorption, which would be difficult to obtain with a single heterojunction.[39–42]

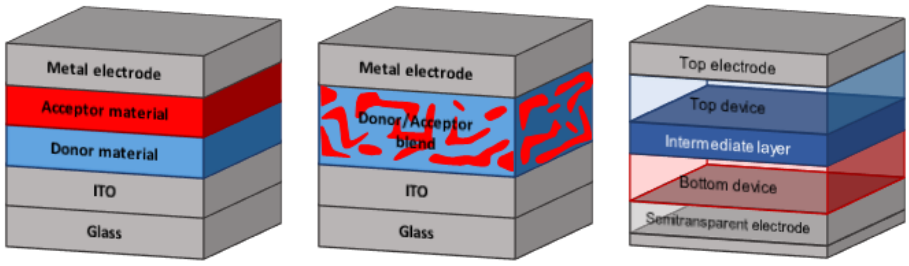

Figure 2.4. Schematic representation of a) planar bilayer, b) bulk heterojunction and c) tandem solar cell.

From a different point of view, another classification of the organic solar cells based on the active material can be established: *polymer-based photovoltaic cells*, also known as *plastic solar cells*,[43–45] which are constituted by conjugated polymers; and *small molecule-based photovoltaic devices*, in which discrete chromophores form the active layer.[38,46,47]

Regarding efficiencies, while polymeric tandem solar cells have reached a conversion efficiency of 12%,[48] it is worth noting that the record in multi-junction architectures is held by Heliatek,[49] that reported a tandem oligomer-based device with a certified power conversion efficiency of 13.2%. The best conversion efficiency for a single junction device has been achieved by Toshiba Corporation, reaching a 11.2% value.[50,51]

2.1.2.4 Dye-Sensitized Solar Cells (DSSCs)

Apart from the fully organic solar cells, combinations of organic-inorganic materials have been of great relevance in recent years. In this sense, the development of DSSCs in the 90s opened up new horizons in the area of photovoltaics, and entered dynamically the race for cost-efficient devices functioning at the molecular and nanoscale levels.[52,53] The seminal paper by O'Regan and Grätzel in 1991[54] introduced a pioneering architecture, an n-type DSSC, in which an organic light-absorbing dye is anchored to a mesoporous inorganic n-type semiconductor film (this semiconductor operates as photoanode) and filled in with a redox-active electrolyte. This type of DSSCs has shown a good potential and, in the future, it could turn out to be a good alternative to the standard silicon photovoltaics,[55] thanks to the already obtained efficiencies. Actually, the PCEs have grown from 7% in the seminal report,[54] using ruthenium complexes as the dye, to the current 13.0% employing Pors as sensitizers, which leave out the need for rare and costly, ruthenium-based sensitizers as a requirement for high efficiencies.[56] Alternatively, p-type DSSCs (an active photocathode) have been also explored but they have not exhibited yet energy conversion values as high as conventional DSSCs. This has been ascribed to drawbacks associated with the electrolytes and the p-type semiconductors,[57] and to date, there is just one example of "comparable" efficiency, i.e., 2.51%.[58] Other important point is the growing tendency nowadays to develop all-solid state devices versus the liquid-based DSSCs, which represents a step forward into the future commercialization.[59,60]

The working principle of a n-type DSSC is depicted in Figure 2.5. A sensitizing dye is chemically anchored to a nanocrystalline semiconductor,[61] such as TiO_2, ZnO or SnO_2, deposited onto an adequate conducting glass substrate. The semiconducting material is mesoporous, in order to produce a high surface area for dye coverage, thus increasing the light harvesting capabilities of the cell. After photoexcitation, the organic dye is able to inject electrons from its LUMO into the conduction band (CB) of the semiconductor. Electrons pass through the

nanocrystalline structure and arrive at the conductive substrate; after that the circuit is closed in the counter electrode where an electrolyte (usually I^-/I_3^- or cobalt complexes)[62] is reduced and regenerates the chromophore (Figure 2.5).

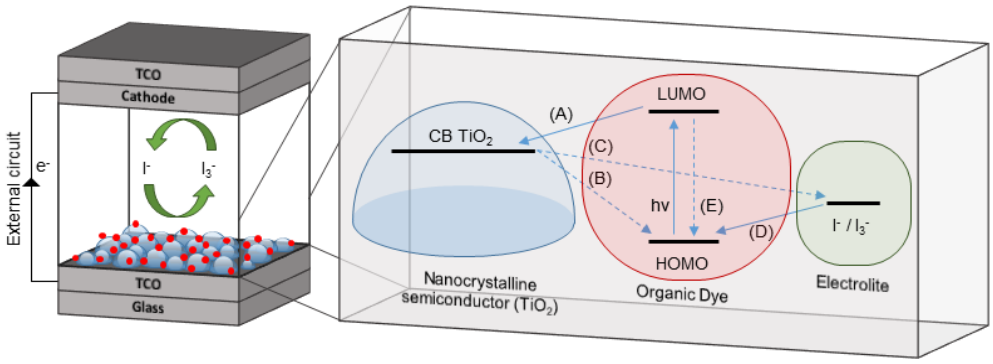

Figure 2.5. Left: Schematic illustration of a typical n-type DSSC; right: Schematic representation of the energy levels of a DSSC indicating competing photophysical pathways, including (A) electron injection, (B) electron recombination with dye cations and (C) with the electrolyte, (D) regeneration of dye cations by the electrolyte, (E) non-radiative relaxation of dye.

The solar-to-electric power conversion efficiencies of DSSCs depend on a delicate balance of the kinetics for injection, dye regeneration and recombination reactions.[63] In fact, in addition to the basic processes, other unwanted and competitive processes can take place in the cell, such as the recombination of injected electrons in the CB of TiO_2 with the oxidized form of the dye, or with the electrolyte (the so called “dark current”). Furthermore, the chromophore can return to its ground state by a non-radiative relaxation (Figure 2.5).

This plethora of photophysical processes are dependent on the three main components of the cell: the light-absorber dye, the nanocrystalline semiconductor, and the redox couple in the electrolyte. In order for a device to be successful, all three components require fine-tuning.[64] In terms of the dye in particular, until ten years ago, the best performance had been achieved by polypyridyl complexes of ruthenium as the molecular sensitizer, with overall PCEs of 11.5% being reached.[65,66] In an effort to produce Ru-free sensitizers, in view not only of their high cost, economic as well as environmental, but also of their insufficient light-harvesting properties (their absorption spectra are rather broad but the NIR absorption is restricted and the molar extinction coefficients are low), much research has focused on the use of organic sensitizers,[67,68] and particularly Pors.[69,70]

More recently, many research groups achieved excellent results using perovskites as Ru-free sensitizers in DSSCs.[71–75] A wide class of compounds that have the general formula ABX_3 are termed perovskites (A and B are two cations of different size and X is an anion that binds to both – Figure 2.6). These materials display a multitude of chemical formulations that can lead to a variety of technologically relevant physical properties, such as thermoelectricity and superconductivity. Perovskites utilized in PV devices are synthetic hybrid organic–inorganic methylammonium lead halide materials of general formula $CH_3NH_3PbX_3$ (in which X=I, Br, Cl), first utilized for solar applications in a seminal paper by Miyasaka and co-workers in 2009[76] and then by Park and co-workers two years later.[77] In these works, the hybrid perovskite $CH_3NH_3PbI_3$ was implemented in a classical DSSC architecture and deposited over a mesoporous TiO_2 photoanode to serve as light absorber, in the presence of a traditional liquid electrolyte (iodide/triiodide). The reported cell efficiency was 3.5% in 2009[76] and 6.5% in 2011;[77] in the latter case, $CH_3NH_3PbI_3$ was used in a nanocrystal form.

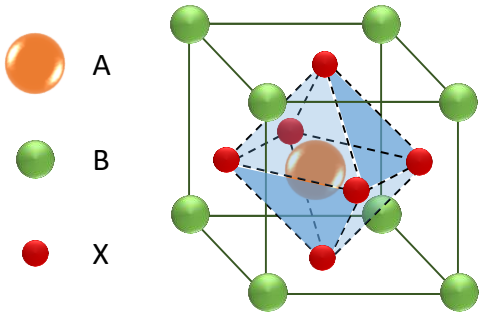

Figure 2.6. ABX_3 crystal structure of perovskites.

At present, the record certified efficiency for a perovskite cell is 22.1%,[78] a truly impressive value if one considers that these devices were non-existent ten years ago. The by far dominant material in the PV perovskite field remains $CH_3NH_3PbI_3$, the best performer described in the seminal paper of Miyasaka and co-workers. Unfortunately, this is a material with significant problems.[79–81] Its solubility makes it excellent for facile device fabrication, but, on the other hand, the device needs to be rigorously kept away from moisture, substantially enhancing sealing requirements. Moreover, its perfect crystallinity can be lost at temperatures typically experienced inside solar panels under intensive irradiation and, upon dissolution, it generates PbI_2, a carcinogen banned in many countries. It has been recently demonstrated that environmental contamination would not be disastrous even in the case of catastrophic failure of perovskite modules and

exposition to rain.[82] However, should the stability issues be overcome, robustness under any circumstances must be strictly guaranteed for market distribution. The routes attempted to overcome the $CH_3NH_3PbI_3$ impasse have been recently reviewed.[80] The most obvious one, namely replacing Pb with less toxic Sn, has been relatively disappointing, as tin tends to oxidize and the perovskite tends to lose crystallinity over time.[80]

Porphyrins and Phthalocyanines in DSSCs

Since the negative aspects of perovskites, a promising alternative is represented by organic dyes as Pors. On account of their intense absorption in the visible region of the solar spectrum and their appropriate redox properties for sensitization of TiO_2 films, numerous Por dyes have been tested as light-harvesting components for DSSCs. The success of these dyes lies in their physicochemical properties, which can be tuned through appropriate molecular design, as well as in their high extinction coefficients in the visible part of the solar spectrum.

To be useful for a DSSC device, a Por sensitizer must possess at least one anchoring group in its molecular structure to allow the attachment of the dye to the TiO_2 metal oxide.[83] Inevitably, the anchoring moiety is also an inherent acceptor, and simultaneously acts as an electron-withdrawing group. Historically, the first use of porphyrinoid sensitizers in TiO_2-DSSCs was reported in 1993 for β-substituted chlorophyll derivatives and related natural Pors, reaching a maximum PCE of 2.6%.[84] Since 2009 and until now, unsymmetrical *meso*-Pors have been the most efficient class of Por sensitizers reported in DSSCs.[69,85,86]

The main advantage of the **A_3B** design is the possibility to incorporate easily a wide range of solubilizing and/or bulky groups at the periphery of the Por, which is of high importance to reduce dye aggregation and, therefore recombination processes, at the TiO_2 interface. At the same time, **A_3B** symmetry disturbs the π-delocalized electrons system of the macrocycle creating a dipole moment that affects notably the photophysical and electrochemical properties of the Por. In DSSCs, this permanent and intrinsic dipole moment would favor the electron injection of the excited dye into the TiO_2 CB.

A breakthrough in this field was the incorporation of linear, push-pull Por derivatives in DSSCs, which has led to remarkable progress in this family of sensitizers, reaching record PCE values. These Pors show a push-pull substitution pattern, that is a linear arrangement between an electron–donor group (i.e., diphenylamino) and an electron–acceptor group (i.e., 4-carboxyphenylethynyl). Figure 2.7 shows three compounds that can be

considered milestones in the field, because they constituted a significant advance in Por-sensitized solar cells: YD2 dye attained a PCE of 11%,[87] followed by the striking 12.3% and 13% obtained with its analogues YD2-oC8[88] and SM315,[56] respectively (Figure 2.7). The key point in these compounds is the introduction of a strong donor group at the opposite *meso* position of the acceptor/anchoring group, which allows the access to donor–(π-bridged chromophore)–acceptor (D- π-A) structures, with enhanced permanent dipole moments.

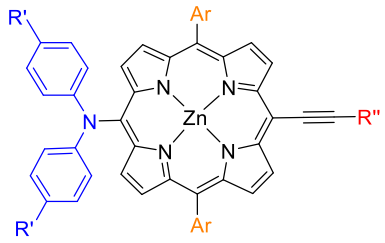

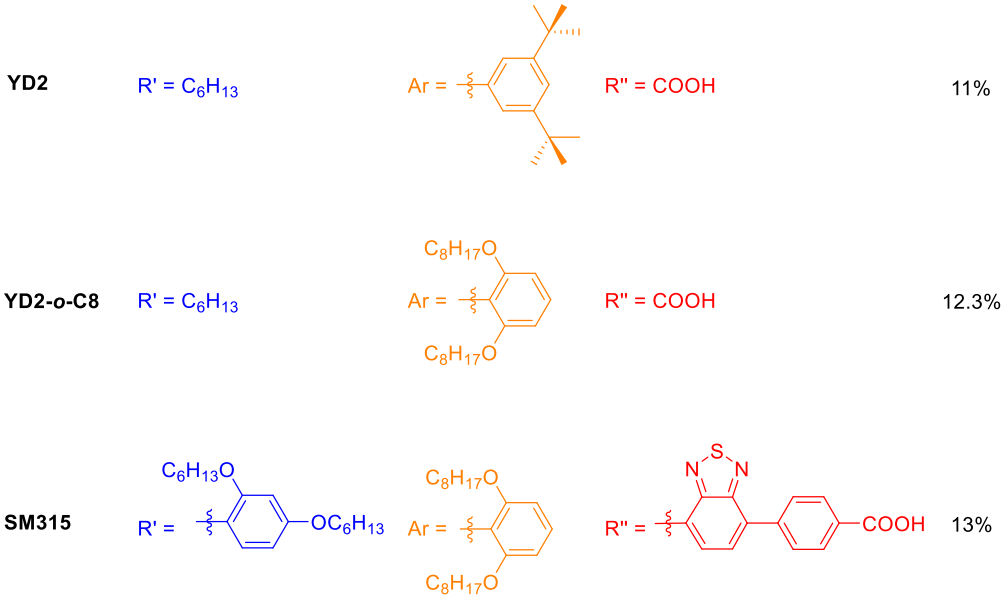

Figure 2.7. Structures of the most efficient Por dyes for DSSCs.

Although the high efficiencies reached by these dyes, the main disadvantages of Pors are their low photostability and their weak absorption in the red/near IR region, where the solar flux of photons is maximum.

It is in this context that Pcs emerged on the scene, showing remarkable thermal and chemical robustness, together with high extinction coefficients in the far

red/near-IR spectral region. In addition, their redox properties are suitable both for sensitization of TiO_2 films and for dye regeneration by the electrolyte. All these key points render Pcs promising candidates for incorporation in DSSCs, representing ideal light harvesting systems for light-to-energy conversion devices.[89,90]

However, despite the adequate characteristics of these macrocycles, the PCEs attained by Pc-sensitized solar cells have not yet been able to match the values obtained by Por-based devices, even though there has been a remarkable progress in recent years.[91,92] The development of Pcs has been hindered by a strong tendency towards aggregation on the metal oxide semiconductor surface, more pronounced in Pcs than in Pors due to their more π-extended system, which can led to non-radiative deactivation of the dye in the excited state.

In an effort to overcome this major drawback, the first breakthrough came with the Zn(II)Pc sensitizers PCH001,[93] by Reddy et al., and TT1,[94] by our group, both employing three bulky *tert*-butyl groups in the periphery of the macrocycle to suppress the stacking of the dye on the TiO_2 surface (Figure 2.8). The two dyes differed in the number of carboxylic acid anchoring groups, and the resulting efficiencies were 3.05% for PCH001 and 3.5% for TT1. This great PCE values were attributed not only to the aggregation issue being partially sorted out, but also – in the case of TT1, in which the carboxylic acid is conjugated to the aromatic ring – to the directionality in the linkage of the dye to TiO_2.

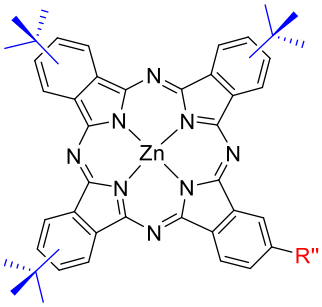

PCH001	R" = 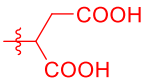	PCE = 3.05%
TT1	R" = COOH	PCE = 3.5%

Figure 2.8. Structures and PCEs of PCH001 and TT1.

Nevertheless, the use of CHENO (chenodeoxycholic acid, 3α,7α-dihydroxy-5β-cholic acid) as a co-adsorbent was still necessary to prevent aggregation of TT1 at the TiO_2 surface, since the bulky *tert*-butyl groups were not sufficient to

suppress it completely. CHENO is known to bind strongly to the surface of nanostructured TiO_2, thus displacing dye molecules and hindering the formation of dye aggregates.[95] Furthermore, it was demonstrated from PCE and absorption spectra that the load of the Pc sensitizers is strongly dependent on the molar concentration of CHENO. In addition, the Voc of the DSSC was increased, due to the enhanced electron lifetime in TiO_2 together with the band edge shift of the nanocrystalline semiconductor to negative potentials.[96]

In 2010, Mori, Kimura *et al*. reported on the use of the even bulkier 2,6-diphenylphenoxy groups at the periphery of a Zn(II)Pc, succeeding in completely supressing stacking of the dyes without the need for a co-adsorbent.[97] The 2,6-diphenylphenoxy groups lie perpendicular to the planar Pc macrocycle, introducing severe steric hindrance. An excellent 4.6% efficiency, with an IPCE of 78% at the maximum of the Q-band, was achieved with the dye PcS6 (Figure 2.9). In this case, the bulky groups not only avoid macrocycle aggregation, but also seem to block the interactions between the Pc aromatic surface and the I_3^- electrolyte, reducing the so-called catalysis of recombination and unwanted dark currents.[98] The same group later prepared PcS15 (Figure 2.9), an analogue of PcS6 bearing electron-donating methoxy groups in the 2,6-diphenylphenoxy substituents to strengthen the push-pull character of the dye.[99] Indeed, a higher efficiency of 5.3% was consequently reported.

However, the best performances were achieved with PcS20,[100] reported by Mori's research group, and TT40,[101] prepared in our research group, with PCEs of 6.4% and 6.1%, respectively (Figure 2.9). Both dyes have three isoindole units functionalized with very bulky phenoxy substituents (i.e., 2,6-dibutoxyphenoxy for PcS20 and 2,6-diphenylphenoxy for TT40), and differ in the spacer between the anchoring group and the Pc core. While PcS20 shows a direct attachment of a carboxylic acid to the Pc, the innovation of TT40 is the carboxyethynyl group used as anchoring moiety. The ethynyl spacer was selected in view of its very successful implementation in Por dyes, inducing very high efficiencies.[87,88] This non-flexible spacer allows to induce directionality and a perpendicular arrangement of the dyes on the TiO_2 surface, as well as an adequate electronic communication between the chromophore and the semiconductor.

Noteworthy, these dyes show a donor/acceptor (phenoxy/carboxylic acid) pattern, but in a non-linear arrangement. In view of the excellent results obtained with face–to–face D-π-A Pors, the preparation of linear D-π-A Pcs for DSSCs is a challenge.

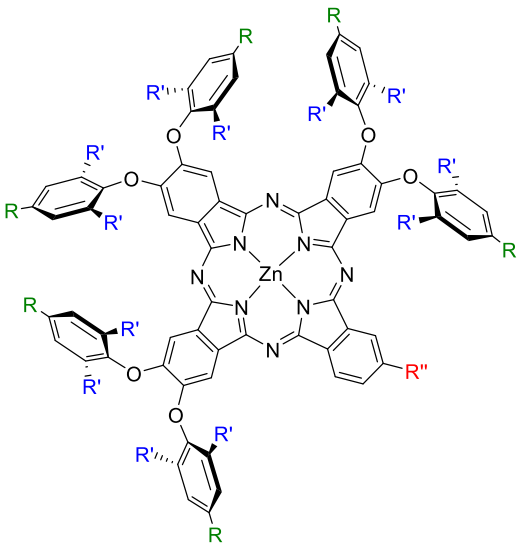

Pc S6	R = H	R' = Ph	R'' = 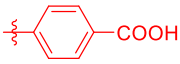	PCE = 4.6%
Pc S15	R = OMe	R' = Ph	R'' = 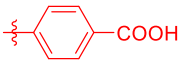	PCE = 5.3%
Pc S20	R = H	R' = $O(CH_2)_3CH_3$	R'' = COOH	PCE = 6.4%
TT40	R = H	R' = Ph	R'' = 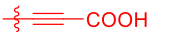	PCE = 6.1%

Figure 2.9. Structures of the best efficient Pc dyes reported in DSSCs.

2.1.3 Electron transfer as inspiration from Nature

Nature has solved many engineering problems such as self-healing abilities, environmental exposure tolerance and resistance, hydrophobicity, self-assembly, and specially harnessing solar energy. In fact, the photosynthetic system found in nature is the photoactive device par excellence that has served as inspiration to many scientists. Photosynthesis[102] is the process employed by plants, algae and cyanobacteria to convert the radiant energy from the sun into chemical energy to fuel the activities of these organisms. The success of this conversion relies upon the efficient absorption and conversion of sunlight. Much effort has been devoted to the understanding of the mechanism of light conversion in the photosynthetic system, with the aim of designing artificial ensembles that can behave similarly in human's profit.

The main players in the photosynthetic process are chlorophylls and carotenoids with characteristic absorption features. While the latter play mainly a photoprotective role, chlorophylls are involved in light harvesting and charge separation processes.[102] Photosynthetic systems present two basic components: an antenna complex for light harvesting, and a reaction center for charge separation The first step in photosynthesis is light absorption by the antenna complex. Photoinduced energy transfer is a process of great importance in the light harvesting complex. Energy transfer is a photophysical process where the excitation of a chromophore is transferred to a radiation-less relaxation. Spectral overlap between the emission of the donor and the absorption of the acceptor is required for energy transfer to occur. The aim of this event in the photosynthetic system is to progressively direct the energy from sunlight to the reaction centre and trigger the charge separation process.

In the case of photosynthesis, energy transfer takes place through the dipolar coupling mechanism described by Theodore Förster in 1914. Förster resonance energy transfer (FRET) takes place when non-radiative excitation transfer occurs between two molecular entities separated by distances that exceed the sum of their Van der Waals radii.[103] This energy exchange happens *via* the electromagnetic field associated to the electron in the LUMO of the donor, which causes a perturbation on the electrons in the HOMO of the acceptor. The effectiveness of the energy transfer depends on the distance between the chromophores and the relative orientation of the chromophores. In this regard, organization of the chromophores is very important for an efficient photosynthetic process. A common feature of photosynthetic systems is a ring-like organization of the antenna (Figure 2.10) complex around the reaction center. Such degree of organization of the photosynthetic pigments, addressed to ensure formation of

efficient antennas and reaction centers, is based on supramolecular interactions involving not only the pigments but also proteins and protein dimers.

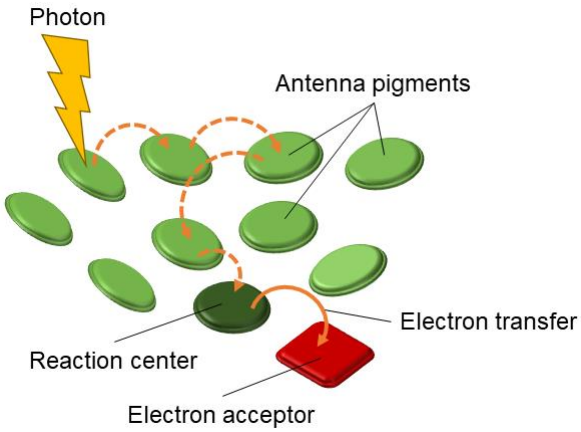

Figure 2.10. Schematic representation of photosystem.

Eventually, conversion of sunlight energy into chemical energy takes place through a cascade of unidirectional electron transfer reactions that ultimately lead to the synthesis of carbohydrates. The success of this process relies on the effectiveness of these electron transfers and the lack of recombination reactions that would interrupt the process and cause a waste of the absorbed energy. In terms of charge separation, the characteristics of the individual electron acceptors and electron donors are decisive to determine the overall efficiency.

Resuming, in natural photosynthetic systems, cascades of energy– and electron–transfer reactions are triggered either directly by photoexcitation or indirectly by energy transfer from light–harvesting antenna systems. Therefore, designing, synthesizing, and probing efficient energy capacitors and chromophores featuring unique panchromatic absorptive, redox, and electrical properties is of a crucial importance for the preparation of artificial photosynthetic models. Considering the structural complexity presented by the natural photosynthetic systems, much of the scientific effort has been devoted towards the preparation and study of structurally simpler systems, with the aim of reproducing some of the fundamental steps occurring in natural photosynthesis, one of the most important being the photoinduced charge separation.[104–106]

2.1.3.1 Photoinduced electron transfer in artificial systems

In their most simple version, artificial photosystems are constituted by an electron donor unit (D) connected to an electron acceptor moiety (A) through a linker (L). This linker can connect both units either by covalent or supramolecular interactions (Figure 2.11).

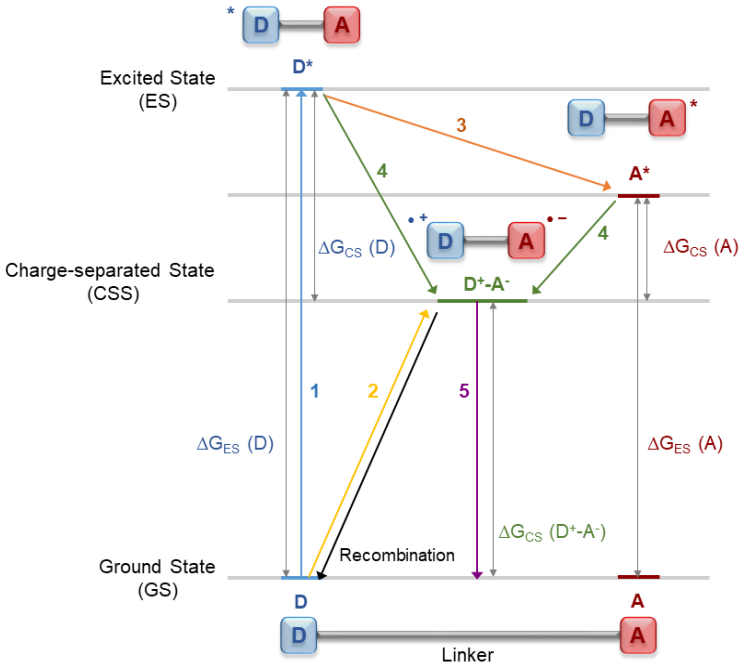

Figure 2.11. Schematic representation of PET between a donor and an acceptor connected through a linker, indicating photophysical pathways: **1** – Absorption; **2** – Optical electron transfer; **3** – Energy transfer; **4** – Photoinduced electron transfer; **5** – Charge-separated state emission.

Photoinduced electron transfer (PET) is a process by which an excited electron is transferred from a donor to an acceptor, and in can take place in two different ways.[107–109] If the electron donor is photoexcited, an electron will be promoted from its HOMO to its LUMO and then, it will be transferred to the energetically lower-lying LUMO of the electron acceptor (Figure 2-12a). On the other hand, if the electron acceptor is the part of the molecule being photoexcited, a hole will appear in its HOMO, which is filled with an electron originating from the higher-lying HOMO of the electron donor (Figure 2.12b). Both possibilities lead to the formation of an ion-pair or charged separated state (CSS) which will subsequently recombine to the electronic ground state.

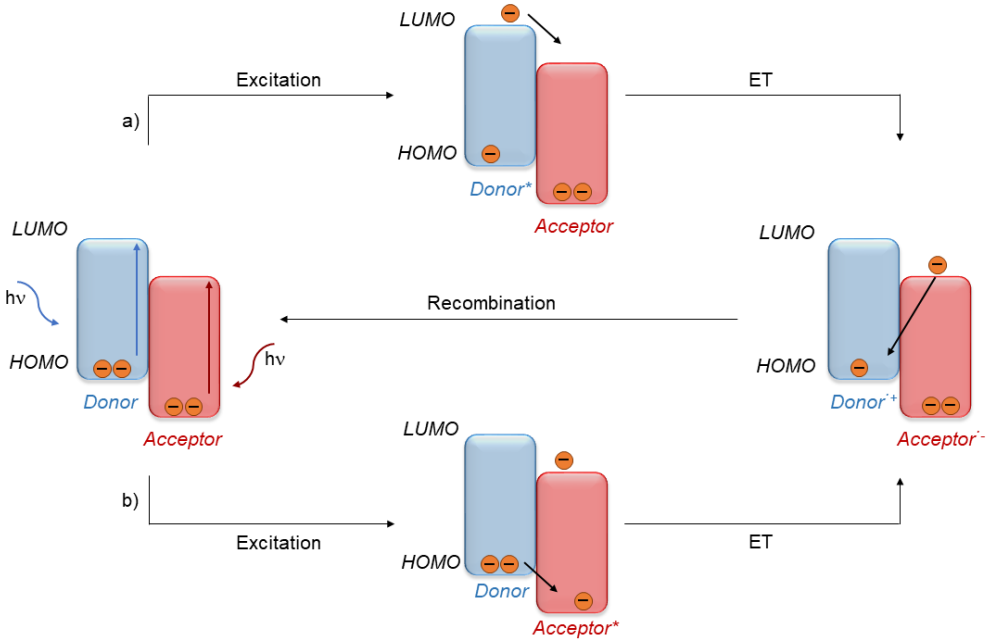

Figure 2.12. Possible pathways for PET reactions: a) photoexcitation of the donor; b) photoexcitation of the acceptor.

Within this context, the molecular or supramolecular systems must fulfil several requirements regarding PET:

- High extinction coefficients in the visible range of the spectrum.
- The charge separation processes quantum yield must be close to 1, so there are no losses of the excitation energy.
- The energetic level of the CSS must be high and close to the energy level of the initial excited state, to minimize de energy loss.
- Recombination kinetics must be as slow as possible so the CSS lifetime is as high as possible.

2.1.4 Multicomponent systems for electron transfer

Among the chromophores that have been used as molecular components in artificial photosynthetic systems, porphyrinoids, the ubiquitous molecular building blocks employed by Nature in natural photosynthesis, have been the preferred and obvious choice, due to their intense optical absorption and rich redox chemistry.[110–113]

Pors are important components of the porphyrinoid family due to their photophysical properties. Pors are fully conjugated aromatic macrocycles composed of four modified pyrrole subunits interconnected at their α carbon atoms *via* methine bridges, leading to a macrocycle with 22 conjugated π electrons.[114] However, the aromatic system of Pors is ascribed to a delocalized cloud of 18 π electrons, as shown in Figure 2.13a and b.[115,116] Typical Por absorption spectra consist of an intense Soret band centered at 400-450 nm with ε in the order of 10^5 M^{-1} cm^{-1}, and a series of moderately absorbing Q bands at 500-650 nm with ε in the order of 10^4 M^{-1} cm^{-1} (Figure 2.14).

On the other hand, within the large family of synthetic porphyrinoid systems, Pcs enjoy a privileged position as constituting chromophores of photoactive, multicomponent systems, thanks to their formidable optical and photophysical properties, as already discussed in the Introduction chapter of this thesis. Not only Pcs, but other related aza-bridged synthetic porphyrinoids such as SubPcs are outstanding chromophores to study photoactivated processes. SubPcs are 14 π-electron aromatic compounds that comprise three N-fused, diiminoisoindole units in a cone-shaped geometry, and a central boron atom axially substituted with a halogen atom or other type of ligands. (Figure 2.13c and d). Owing to their intense absorption in the visible region of the solar spectrum (i.e., ε as high as 6 x 10^4 M^{-1} cm^{-1}) (Figure 2.14) and high optical and thermal stabilities, they have evolved as perfect light-harvesting building blocks. Moreover, they possess a rich redox chemistry that can be tuned, even easier than in the case of Pcs, by the introduction of different peripheral functional groups.

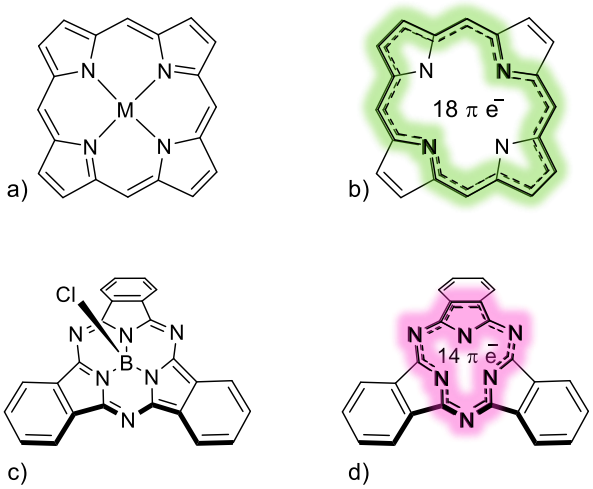

Figure 2.13. Molecular structure and electron delocalization of Pors (top) versus SubPcs (bottom).

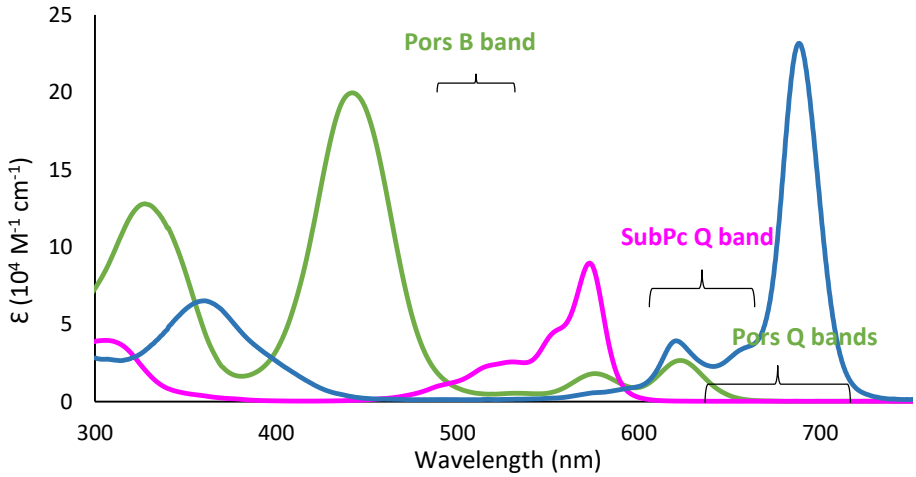

Figure 2.14. UV/Vis spectra of a metallic Por (green line), a SubPc (pink line) and a Zn(II)Pc (blue line).

The synthetic versatility of these three chromophores, namely Pors, Pcs and SubPcs has allowed many scientist, including our research group, to synthesize and study a wide range of covalent and non-covalent, multicomponent D-A systems, in combination with other electroactive units of diverse nature and redox character, for instance carbon nanostructures like fullerenes, CNTs and

graphene.[117] Also, these chromophores have been combined with each other through covalent or supramolecular means to form multichromophoric heteroarrays.[118–121] In particular, Pc-Por ensembles have been targets of choice since the two macrocycles present unique physicochemical properties as individual chromophores and intense and complementary optical absorption, which cover a large portion of the UV-vis-near infrared component of the solar spectrum. Moreover, the easy modulation of the electronic character of these macrocycles through the introduction of substituents of different chemical nature permits to adapt the electron donor/acceptor abilities of each unit to that of its counterpart. Covalent and supramolecular Pc–Por systems have been prepared using different synthetic strategies, namely, metal-catalyzed coupling reactions or metal–ligand interactions between appropriately substituted Pc and Por macrocycles, leading to covalent or supramolecular assemblies, respectively. Many of these systems have been case of study to determine their ability to generate photoinduced, charge-separated states. On the other hand, SubPc–Pc conjugates are also perfectly suited for the study of intramolecular energy/electron-transfer processes since the energy level of their excited states and, therefore, of their optical transitions are very well suited for the efficient absorption and directional funnelling, *via* energy/electron transfer processes, of photoexcitation energy.[121]

The control gained in the last years in the chemistry of Pors, Pcs and SubPcs has made it possible to extend research to increasingly complex targets that include more than two different chromophores alone or in combination with other redox-active units. In some of these systems, a cascade of energy– and electron–transfer reactions from the primary electron donor to the next components until the final electron acceptor entity allows to achieve radical–ion pairs ($D^{\bullet+}$–L–$A^{\bullet-}$) with relatively high CSS lifetimes. This stepwise charge/energy transfer through the different components of the systems is the key point to slow down the undesired recombination reactions and to achieve high efficient systems, which mimic as much as possible the natural photosynthetic process.

For instance, a triad system constituted of a Zn(II)Por unit, a H_2Pc unit and ferrocene as electron-acceptor unit has been prepared by Ambroise et al. (Figure 2.15).[122] Electrochemical studies on this system showed electrochemical potentials close to those of the individual molecular components, thus suggesting a relatively weak, ground-state coupling between these subunits in the array. Excitation of the ferrocene-Zn(II)Por-Pc triad in the Pc absorption band resulted in typical Pc emission. In this case, the location of the ferrocene quite distant from the Pc resulted in little if any quenching of the fluorescence output unit.

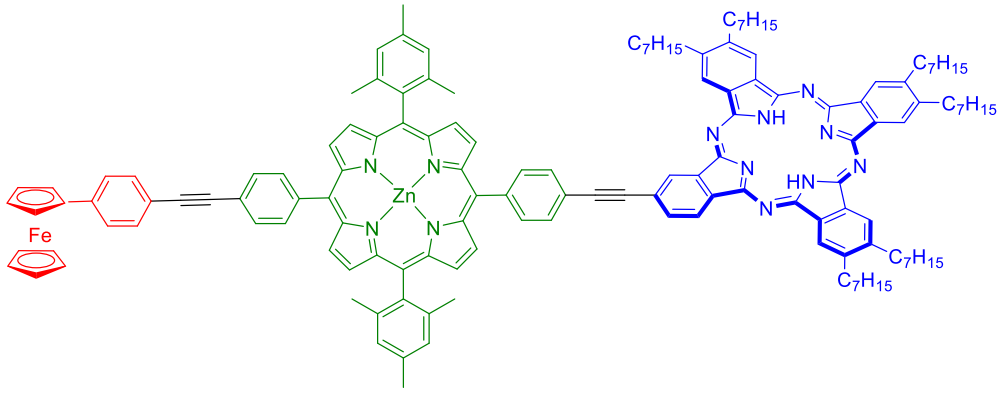

Figure 2.15. Molecular structure of ferrocene–Zn(II)Por–Pc triad reported by Ambroise et al.

In 2010, D'Souza's research group reported the synthesis, characterization, and photochemical events in a molecular triad constituted of a SubPc unit and a Zn(II)Por unit linked together by a triphenylamine (TPA) moiety, and, successively, they investigated the complexation of this triad by an imidazole-substituted C_{60} fullerene (Scheme 2.1).[123] The absorption spectrum of SubPc–TPA–Zn(II)Por triad presents common features of both the electron-donor Zn(II)Por–TPA and the electron-acceptor SubPc subunits, suggesting negligible electronic interactions between these chromophores in the ground state. The electron-transfer process from the electron-donating Zn(II)Por and TPA entities to the electron-accepting SubPc to form $SubPc^{\bullet-}$–TPA–$Zn(II)Por^{\bullet+}$ was confirmed by different photochemical techniques. By utilizing femtosecond laser photolysis, the electron transfer from the singlet Zn(II)Por, which is generated either by energy transfer from SubPc or through direct excitation, to the electron-accepting SubPc was observed, forming the radical-ion pair $SubPc^{\bullet-}$–TPA–$Zn(II)Por^{\bullet+}$ with lifetimes of 256 and 140 ps in benzonitrile and toluene, respectively. On the other hand, in the supramolecular tetrad obtained by axial coordination of an imidazole-substituted C_{60} to the Zn(II)Por metal center, photoexcitation led to the formation of the radical-ion pair SubPc–TPA–$Zn(II)Por^{\bullet+}$ – $ImC_{60}^{\bullet-}$ with a long lifetime of the charge-separated state in toluene in the order of microseconds. This long-lived charge-separated state is a consequence of the triplet multiplicity of the radical ion-pair, which is populated by electron transfer from the triplet Zn(II)Por to the attached imidazole-C_{60} ligand.

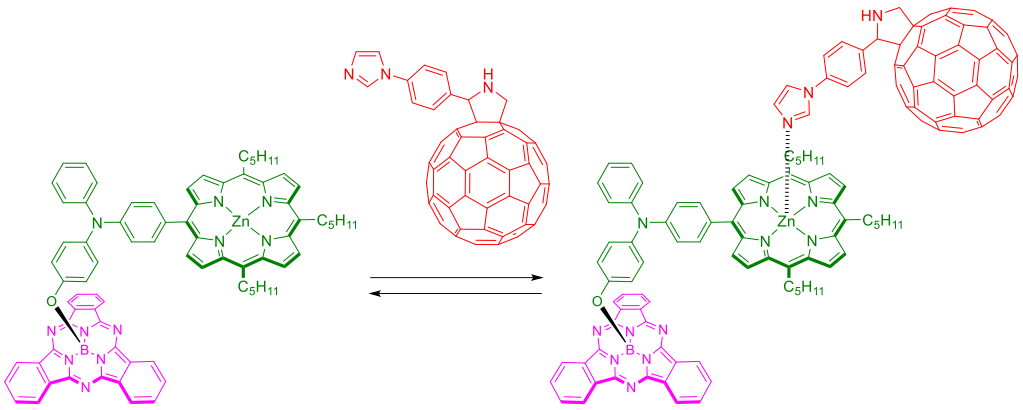

Scheme 2.1. Complexation of SubPc–TPA–Zn(II)Por triad by imidazole-substituted C_{60} ligand leading to a supramolecular tetrad.

Another interesting example of a multicomponent chromophoric heteroarray is depicted in Figure 2.16. In 2012 the groups of Ermilov and Ng used host – guest interactions between a tetrasulfonate Por, a Si(IV)Pc axially-substituted with two permethylated β-cyclodextrin (CD) units, and a β-CD substituted SubPc for the construction of a ternary supramolecular complex SubPc-Por-Si(IV)Pc.[124] The supramolecular triad was constructed using the affinity of β-CD to anionic sulfonate groups, by the simultaneous complexation of the tetrasulfonated Por with the SubPc and the Si(IV)Pc units, as shown in Figure 2.16. In this case photophysical (steady-state and time-resolved fluorescence and transient absorption) experiments were used in order to shed light onto the possible interactions between the three macrocycles in solution. Upon excitation of the SubPc part of this complex, the excitation energy is delivered to the Si(IV)Pc part *via* energy transfer, the Por component acting as an energy transfer funnel.

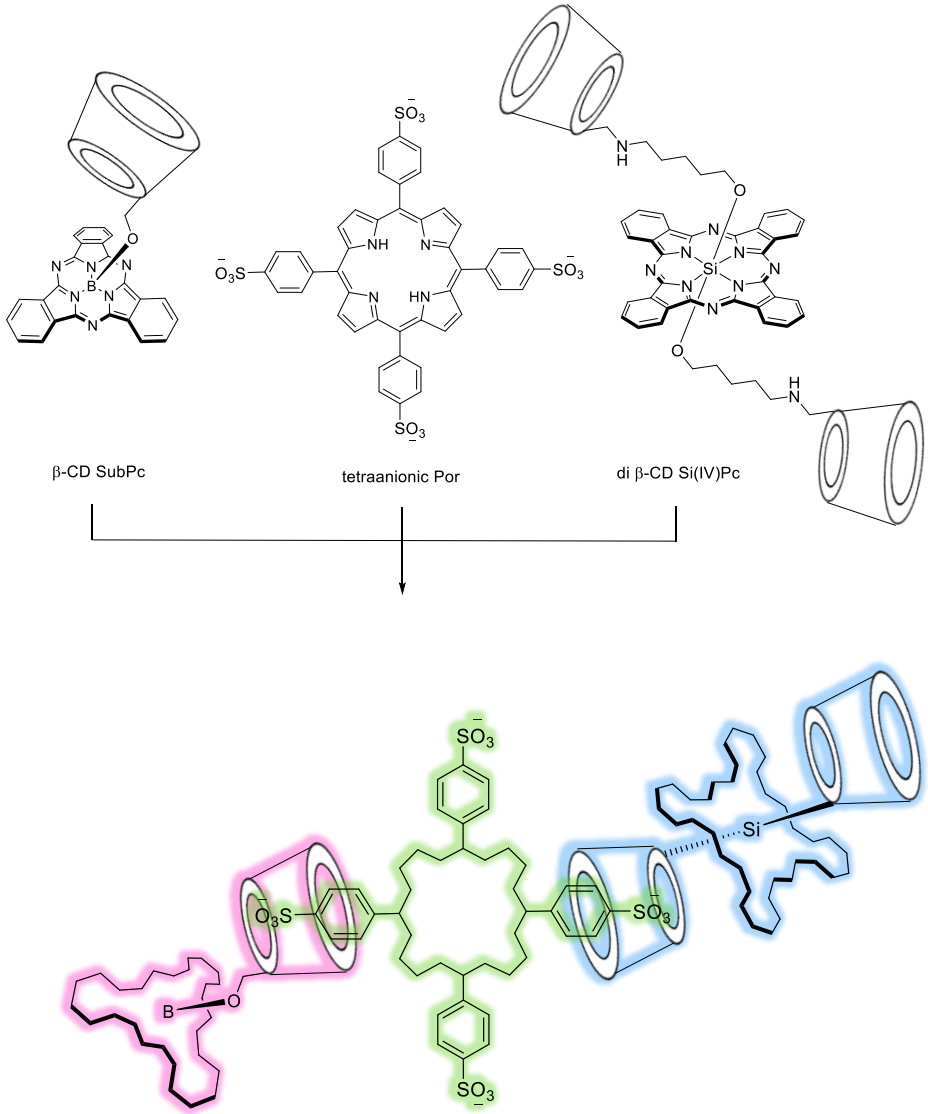

Figure 2.16. Molecular structures of β-CD-substituted SubPc, tetrasulfonated Por, β-CD-substituted Si(IV)Pc, and schematic representation of the supramolecular triad.

It is important to highlight that in these and many other examples of multicomponent systems, the Pc component is located at the outer part of the system. Works in which the Pc component is located at the center of the system, acting as an energy/electron transfer bridge, are rare, and nearly always achieved *via* axial bonds.

In 2012, our group described the synthesis and photophysical properties of some Por–C_{60}–Pc triads and Por_2–Zn(II)Pc–$(C_{60})_2$ pentads (Figure 2.17).[125] These structures represent one of the few examples of covalent multicomponent systems in which the Pc component acts as an energy funnel, although it is not located at the center of the systems.

Zn(II)Por–C_{60}–Zn(II)Pc triad (Figure 2.17a) gave rise, upon excitation of the Zn(II)Por component, to a sequence of energy and charge transfer reactions with fundamentally different outcomes. Exclusive photoexcitation of the Zn(II)Por at either 428 or 425 nm led to a fluorescence pattern that is reminiscent of that of the Pc, while a significant quenching of the Zn(II)Por centered fluorescence was seen. Such an observation implied an efficient transduction of singlet excited state energy from the Zn(II)Por to the Zn(II)Pc. Support for this notion was lent from excitation spectra as well as transient absorption measurements. In Zn(II)Por–C_{60}–Zn(II)Pc, an initial energy transfer (8.3×10^{11} s^{-1}) from the excited Zn(II)Por to the Zn(II)Pc, followed by a charge transfer (1.5×10^{11} s^{-1}) from this to the fullerene entity, powered the formation of Zn(II)Por– ($C_{60}^{\bullet-}$)–Zn(II)$Pc^{\bullet+}$. No appreciable evidence of the involvement of the one-electron oxidized Zn(II)Por radical cation was observed, due to the strong coupling between Zn(II)Por and Zn(II)Pc.

Similar to the previous system, Zn(II)Por_2–Zn(II)Pc–$(C_{60})_2$ and $(H_2Por)_2$–Zn(II)Pc–$(C_{60})_2$ pentads (Figure 2.17b) gave rise, upon excitation of their Zn(II)Por or H_2Por components, to a sequence of energy and charge transfer reactions with, however, fundamentally different outcomes. In Zn(II)Por_2–Zn(II)Pc–$(C_{60})_2$ the major pathway was a highly exothermic charge transfer to afford (Zn(II)Por)(Zn(II)$Por^{\bullet+}$)–Zn(II)Pc–($C_{60}^{\bullet-}$)(C_{60}). Spectroscopic evidence for $(Zn(II)Por)_2$–(Zn(II)$Pc^{\bullet+}$)–($C_{60}^{\bullet-}$)(C_{60}) was also gathered. In stark contrast, the lower singlet excited state energy of H_2Por (i.e., *ca*. 0.2 eV) renders the direct charge transfer from the Por units in $(H_2Por)_2$–Zn(II)Pc–$(C_{60})_2$ not competitive. Instead, a transduction of singlet excited state energy prevails to form the Zn(II)Pc singlet excited state. This triggers then an intramolecular charge transfer reaction from Zn(II)Pc to the fullerene entity to form exclusively $(H_2Por)_2$–(Zn(II)$Pc^{\bullet+}$)–($C_{60}^{\bullet-}$)(C_{60}).

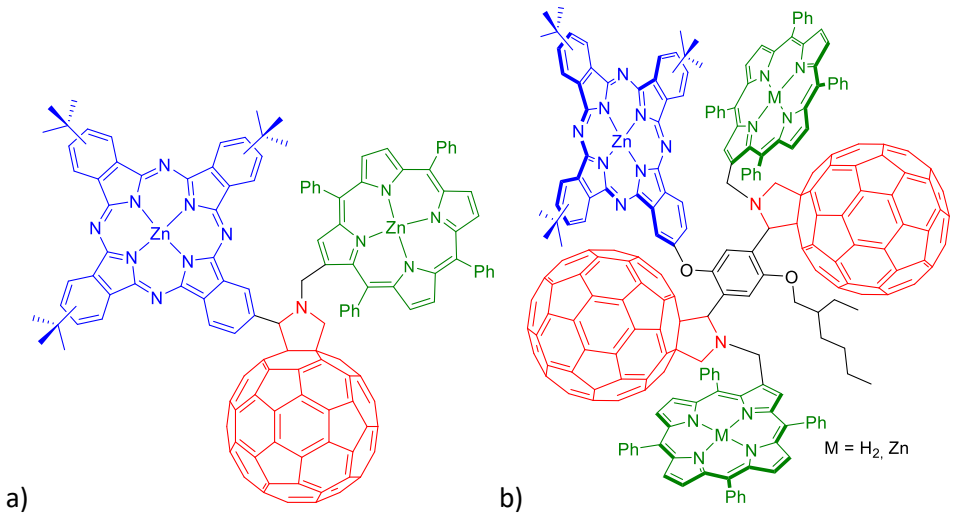

Figure 2.17. Molecular structure of: a) Zn(II)Por–C_{60}–Zn(II)Pc triad; b) and Por_2–Zn(II)Pc–$(C_{60})_2$ pentads.

Another interesting example is depicted in Figure 2.18, where the synergistic effect of hydrogen bonding and metal-ligand interactions occurring at two different sites of an amidine-functionalized Zn(II)Pc was used to trigger the dissociation of the spontaneously formed Pc dimer and the concomitant formation of three-component phenothiazine-Zn(II)Pc-C_{60} system.[126] Interestingly, laser stimulation of this supramolecular triad generated an electron transfer process from the photoexcited Zn(II)Pc to the electron-accepting C_{60} moiety, followed by a charge shift from the electroactive phenothiazine (PTZ) moiety to the oxidized Pc leading to a $PTZ^{\bullet+}$ − Pc −$C_{60}^{\bullet-}$ supramolecular species.

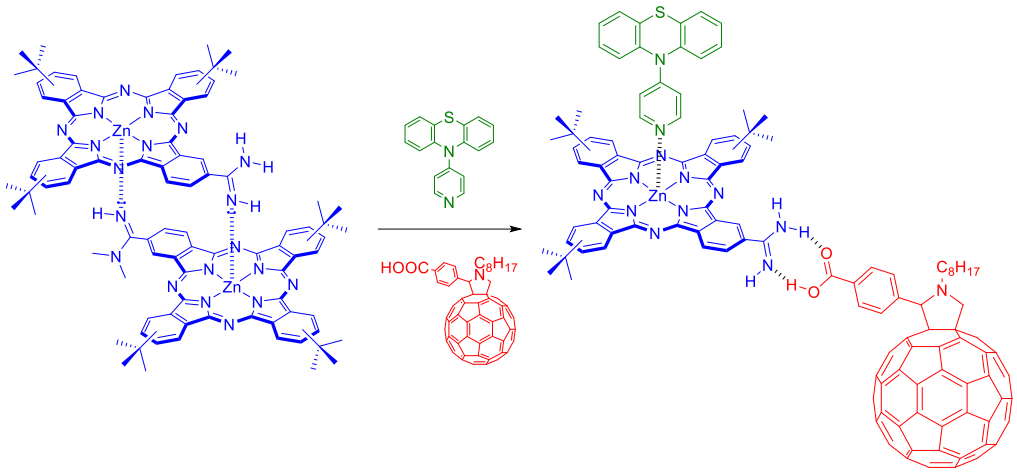

Figure 2.18. Self-assembly of photoresponsive, donor-acceptor supramolecular triad triggered by the disassembly of supramolecular Pc dimer in the presence of pyridine and benzoic acid derivatives functionalized with a phenothiazine donor and a C_{60} acceptor moiety, respectively.

Resuming, as illustrated in these last examples, the use of Pcs as π-bridged chromophore between electron – donor and electron – acceptor units in multicomponent systems has been achieved only in a few cases, either through the preparation of very complicated covalent ensembles or by the use of supramolecular axial interactions.

In this context, the preparation of linear D-π-A multicomponent systems in which the Pc unit is located in the central position transferring charge/electrons from the electron – donor to the electron – acceptor units is a stimulating challenge.

2.2 Specific objectives of *Chapter 2*

2.2.1 Novel donor-π-acceptor substituted Pcs for DSSCs

The first goal of the present chapter comprises the synthesis and characterization of unprecedented linear push-pull Pcs and their application as photosensitizers in DSSCs. As mentioned previously, the PCEs of linear push-pull Pors in DSSCs largely surpassed those obtained with other substitution patterns. However, in the case of Pcs, the problematic preparation of **ABAB** Pcs endowed with crosswise reactive groups for further unsymmetrical chemical transformations has precluded the preparation of Pcs with a linear push-pull pattern for DSSCs. In the framework of this Doctoral Thesis, and taking advantage of our developed methodology for the preparation of functional **ABAB** Pcs such as **12**, we aim to prepare novel donor-π-acceptor substituted Pcs for DSSCs, following functionalization patterns related to those of record Pors. Starting from iodo-containing Pc **12,** we will tackle its unsymmetric functionalization with electron donating groups and anchoring/electron withdrawing groups by Pd – catalyzed methodologies (Scheme 2.2). An additional important feature of the target compounds is that the presence of trifluoromethyl groups is expected to hinder the agggregation of the Pc photosensitizers at the TiO_2 surface, thus precluding undesired desactivation pathways.

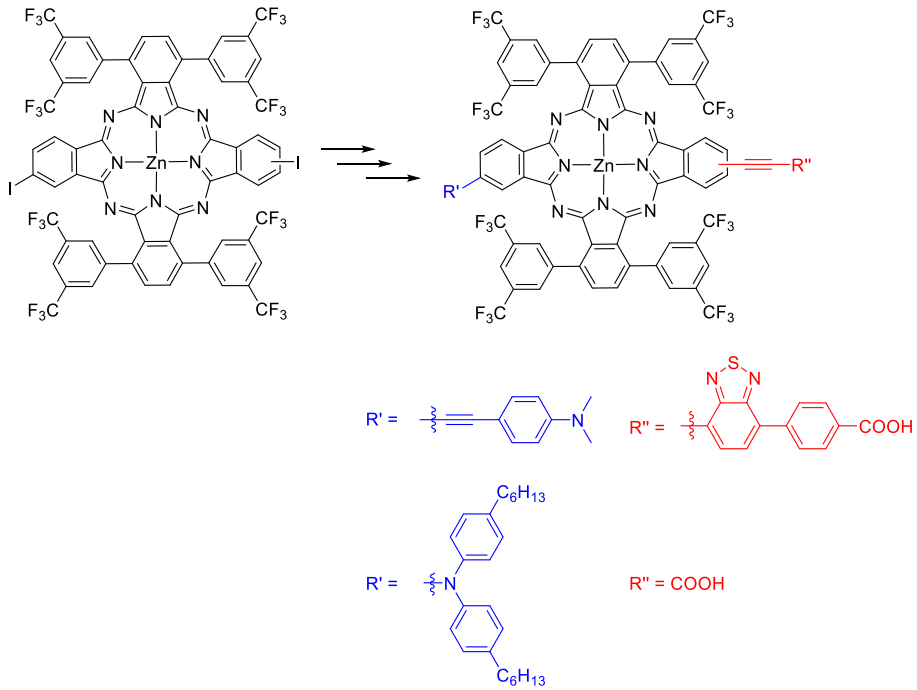

Scheme 2.2. Synthesis of linear push-pull Pcs.

We will use as donor groups bis(4-hexylphenyl)amine and 4-ethynyl-*N,N*-dimethylaniline, broadly incorporated as donor units in push-pull Por photosensitizers. On the other hand, the acceptor moiety of the designed Pcs will be the carboxyethynyl group,[101] as it has been recognized as an optimum TiO_2 linker for Pc-sensitized solar cells. Also, a benzo[c][1,2,5]thioadiazole (BDT) moiety will be tested as spacer between the alkynyl bride and the carboxylic acid, following the design rules of record Por sensitizers. The aim is to optimize the efficiency as photosensitizers by the variation in the nature of the linker between either the electron – donor or the electron – acceptor moieties and the Pc core.

The photovoltaic studies using these dyes as photosensitisers will be performed at EPFL in Lausanne (Switzerland) within the group of Prof. Michael Graetzel and Md. Nazeeruddin.

2.2.2 Novel donor-π-acceptor multicomponent systems based on Pcs

The second goal of the present chapter is the preparation of novel covalent D–π–A multicomponent systems as artificial photosynthetic models to study cascade charge/energy transfer processes. The novelty of these covalent systems relies on the position of the Pc component as central unit of the triad, which will act as an energy/electron transfer funnel between the electron – donor and the electron – acceptor components. For this purpose, we also plan to use as starting material the **ABAB** Pc **12**, which will be unsymmetrically functionalized with complementary electron-donating and electron withdrawing components by Pd – catalyzed Sonogashira couplings (Scheme 2.3).

The first designed system is a multichromophoric triad bearing a Zn(II)Por and a SubPc as donor and acceptor components, respectively, linked to the central Zn(II)Pc. The absorption and fluorescence spectra of Zn(II)Por and SubPc complement that of Zn(II)Pc, offering a broad-band coverage. In order to achieve an adequate energy level alignment for a cascade charge/energy transfer process, a perfluorinated SubPc will be used because of its well-known ability as acceptor material as a consequence of its low LUMO energy level.[127,128] Additionally, the *meso*-positions of the Zn(II)Por will be functionalized with three bulky TPA units both to increase the donor character of the Zn(II)Por and as additional antennas that would capture light from the 300 nm range and funnel it to the Zn(II)Por center. An additional advantage of the *meso*-triphenylamine-substituted Por is its well-known abilities to stabilize charge separated states in

donor-acceptor dyads.[129,130] Therefore, long-lived charge separation states are expected for these Zn(II)Por – Zn(II)Pc – SubPc triads.

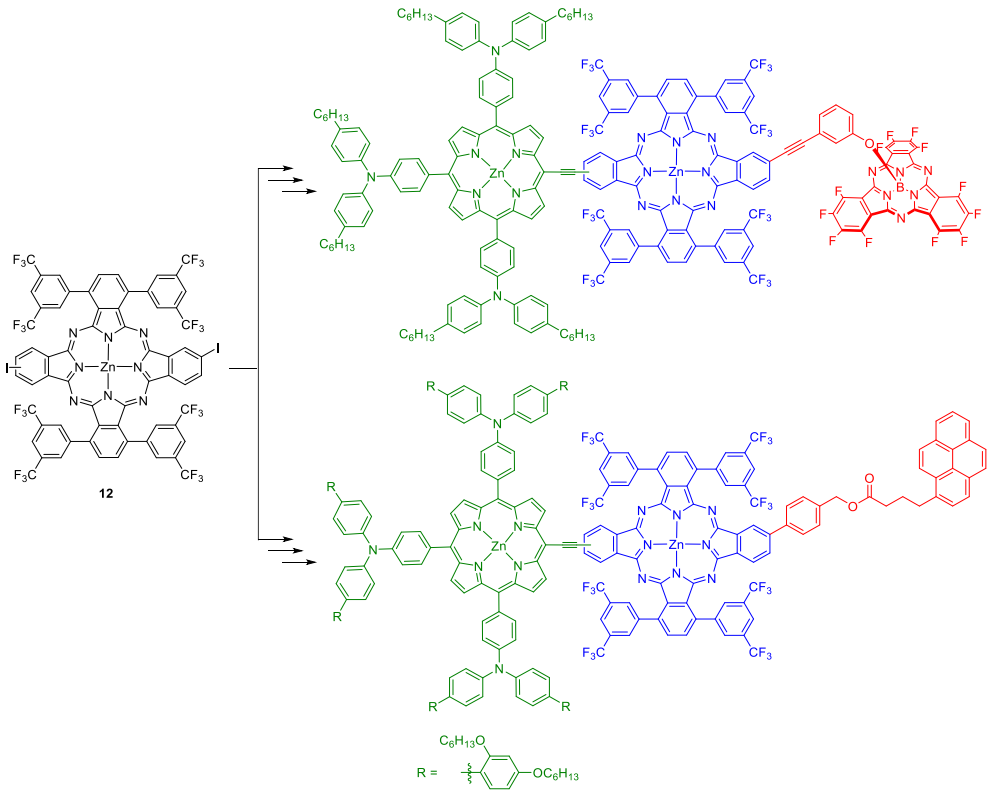

Scheme 2.3. Synthesis of linear donor-π-acceptor triads.

The second targeted system is a Zn(II)Pc-centered triad bearing the same tris(TPA)-Zn(II)Por as donor component, but a pyrene moiety linked to the opposite isoindole. This triad can be exploited for the exfoliation of graphite, taking advantage of the presence of the pyrene moiety that has proved very efficient to assist the exfoliation process due to its strong π–π interaction with the graphene surface. This approach is expected to lead to stable Por–Pc–graphene non-covalent ensembles, in which the graphene sheets may behave as the final acceptor component.

Photophysical and electrochemical studies of these systems will be carried out in order to retrieve information on the interactions between the different components. Fluorescence quenching experiments, fluorescence quantum yields and transient absorption spectroscopy will be carried out in the laboratories of Prof. Dirk M. Guldi (Friedrich-Alexander Univertität Erlangen-Nürnberg).

2.3 Results and discussion

2.3.1 Synthesis and characterization of novel donor-π-acceptor substituted Pcs for DSSCs

The preparation of novel push-pull Pcs was carried out by an unsymmetric functionalization of the diodo-functionalized Pc **12** with electron donating and anchoring/electron withdrawing groups.

We started with the synthesis of compound **30** (Scheme 2.4) that holds a carboxyethynyl group as electron-withdrawing group and a dimethylaminophenylethynyl moiety as electron-donor. It is worth mentioning that carboxyethynyl had been proved in our group as the optimal anchoring unit for Pc photosensitizers, since it provides directionality and fast electron transfer to the TIO_2 in the device.[101] On the other hand, the dimethylaminophenylethynyl group had been previously used in Pors[131,132] and can be easily linked to the Pc through a reliable Sonogashira coupling. Starting from **12**, **27** was obtained in good yield (83%) by a Sonogashira reaction with propargylic alcohol. Then, **28** was obtained through another Sonogashira coupling between **27** and 4-ethynyl-*N,N*-dimethylaniline also in good yield (88%). The oxidation of **28** to **30** was carried out following a two-step procedure widely used for the oxidation of primary alcohol to carboxylic acids.[101] The first step involved the treatment with IBX, leading to **29** in nearly quantitative yields, but, unfortunately, the last oxidation reaction with sulfamic acid and $NaClO_2$ afforded a mixture of compounds that were identified by MS-spectrometry as derivatives of **30** with different contents of chlorine atoms. This chlorination is probably occurring at the highly activated dimethylamino ring (Scheme 2.4).

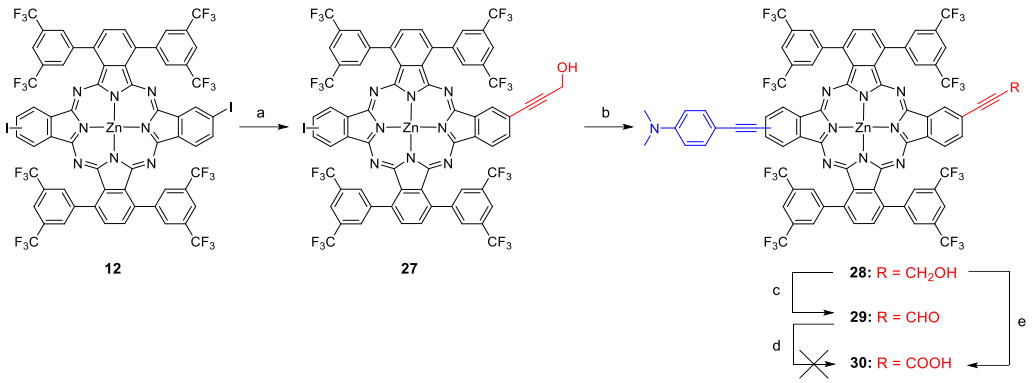

Scheme 2.4. Synthesis of **30**. Conditions: a) propargylic alcohol, $Pd(PPh_3)_4$, CuI, Et_3N, THF, 83%; b) 4-ethynyl-*N,N*-dimethylaniline, $Pd(PPh_3)_4$, CuI, Et_3N, THF, 88%; c) IBX, THF, DMSO; d) Sulfamic acid, $NaClO_2$, THF; e) IBX, THF, DMSO and then *N*-hydroxysuccinimide, THF, DMSO, 90%.

In view of this result, a one – step oxidation of the hydroxymethylethynyl derivate **18** to **30** was tried (Scheme 2.4), following the conditions described by Mazitsche *et al*,[133] which consist in the oxidation of a primary alcohol group to a carboxylic acid in the presence of IBX and certain O-nucleophiles at ambient temperature. In fact, the reaction of **28** with IBX afforded the aldehyde **29**, which in situ reacts with *N*-hydroxysuccinimide to give compound **30** in high yield. It is worth mentioning that changing the reaction sequence, that is, coupling first the 4-ethynyl-*N*,*N*-dimethylaniline to Pc **12**, followed by Sonogashira reaction with propargyl alcohol and subsequent oxidation, gave rise to lower overall yields.

Next we focused on the preparation of Pcs endowed with a N-linked diphenylamino unit, similarly to the case of record Por sensitizers.[56] The direct linkage of the N atom to the Pc core is expected to increase the electron donating effect of the amino group over the Pc. Amination reactions can be performed by either Buchwald – Hartwig amination protocols or by Ullmann conditions. As amination reactions over iodo derivatives usually takes place using high excess of the amine, we proceed first with the amination of Pc **27** (i.e., having only one iodine atom available for the coupling) with bis(4-hexylphenyl)amine (**31**), which was synthetized using a modified version of the procedure reported in literature.[134] Using conditions that had been previously described for the amination of Pcs,[135] namely $Pd_2(dba)_3$ as the catalyst, BINAP as ligand and Cs_2CO_3 as the base in dry toluene at 120°C (Scheme 2.5), did not afford the desired amination and, in fact, only deiodinated products were obtained. On the other hand, we decided to try an Ullmann coupling to carry out the linkage of the

diphenylamino derivative, since this procedure has been recently applied with success to introduce good electron-donating groups such as carbazoles, phenoxazines or phenothiazines in the *meso* positions of different Por substrates in good yield.[136] We performed this Cu(I) – catalyzed reaction on Pc **27** and Pc **32**, the latter holding a formyl – ethynyl group obtained by IBX oxidation of **27**. However, both reactions failed to give the desired coupling with amine **31** (Scheme 2.5). During the development of the experimental work, optimized conditions for the Buchwald – Hartwig coupling of diphenylamino derivatives and bromoporphyrins were found in the group. In our case, application of these conditions, namely $Pd_2(dba)_3$, $^tBu_3P$ and ^{t}BuONa in refluxing toluene, was the key to obtain Pc derivatives containing diphenylamino units. First, as the reaction is carried out with excess of the amine, we decided to prove the amination with Pc **27**. However, as in previous attempts, the reaction did not work. MS analysis confirmed that, under these conditions, losses of iodine and hydroxymethyl residues were taking place in the reaction (Scheme 2.5).

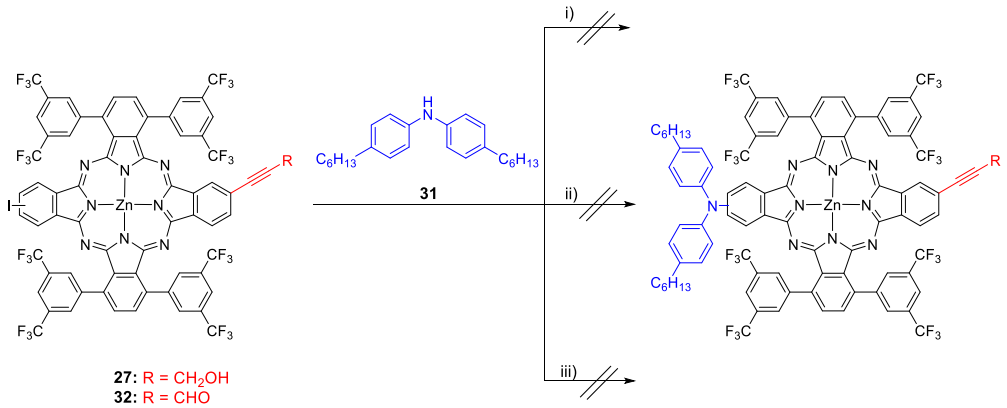

Scheme 2.5. Functionalization using Buchwald – Hartwig or Ullmann methodologies. Conditions: i) **27**, amine **31**, $Pd_2(dba)_3$, BINAP, Cs_2CO_3, dry toluene at 120°C; ii) **27** or **32**, amine **31**, CuI, *N*-phenyl benzohydrazide, Cs_2CO_3, dry DMSO at 120°C; iii) **27**, amine **31**, $Pd_2(dba)_3$, $^tBu_3P$, ^{t}BuONa, dry toluene at 120°C.

Finally, we decided to carry out the amination reaction over Pc **12** following the same reaction conditions, but with less excess of amine **31**. In this case, a mixture of products was obtained, from which, the di-coupled product **34**, the fully deiodinated Pc **36**, and the desired product **33** combined with the mono deiodinated derivative **35** were separated (Scheme 2.6). Unfortunately, a complete separation of **33** from **35** was not achieved. As previously mentioned, deiodinated Pc derivatives had been observed in previous Buchwald – Hartwig

amination reactions, and also as secondary products in other Pd – catalyzed conversions at high temperatures. In order to decrease the amount of deiodinated Pcs and facilitate the isolation of Pc **33**, we performed the amination of **12** at lower temperature, i.e., at 100ºC, but it did not yield the target compound. Hence, it was necessary to set the following reactions with a mixture of Pcs **33** and **35**, relying on the lack of reactivity of the deiodinated derivative **35** under the applied conditions.

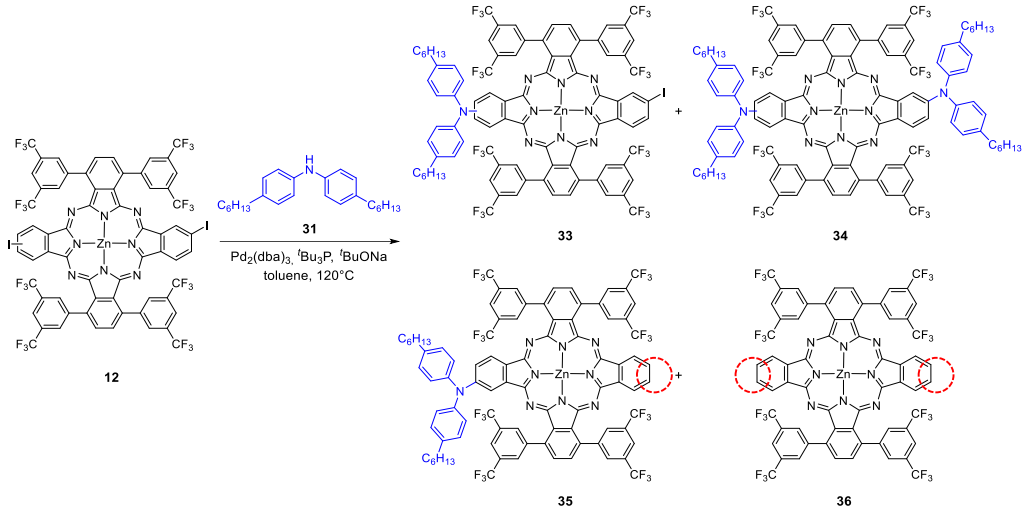

Scheme 2.6. Mixture of products obtained from the Buchwald coupling of **12**.

With Pc **30** in our hands, we proceeded to prepare two different push–pull Pcs holding different acceptor/anchoring groups (Scheme 2.7). The first one (Pc **39**) was obtained through a Sonogashira coupling between **33** and propargylic alcohol in the same conditions already mentioned for the synthesis of **27**. This reaction proceeded in good yield, and compound **37** could be easily separated from the deiodinated Pc **35**. The oxidation of **37** with IBX in order to obtain **38** proceeded in quasi-quantitative yield. Finally, the last oxidation of the formyl group to carboxylic acid by $NaClO_2$ in presence of sulfamic acid (Scheme 2.7) gave the target compound **39** in 58% yield. Interestingly, in this case, the formation of products that contain chlorine atoms was not observed, probably due to the lower activation of the diphenylamino rings for the electrophilic substitution with chlorine in comparison with the *N,N*-dimethylaminophenyl ring of product **30**.

Last, the second Pc synthetized starting from **33** was obtained by the incorporation of the benzothiadiazole (BTD) unit **43** as a π-conjugated linker in

between the anchoring group and the chromophore. The BTD unit had been already successfully used with Pors[137] to obtain high PCEs in DSSCs because of its high electron acceptor effect. Its synthesis is shown in Scheme 2.8. Starting from 4-iodo-methylbenzoate, the organotin aryl compound **40** was formed, which was subsequently reacted with commercial dibromobenzothiadiazole in order to obtain compound **41**. After that, a simple Sonogashira coupling was carried out to obtain the desired compound **42** having a trimethylsilylacetylene group. Further deprotection with TBAF afforded compound **43** (Scheme 2.8). This product was used to functionalize **33** by another Sonogashira reaction, followed by a rapid and quantitative hydrolysis of the ester group to afford the final push-pull Pc **45** (Scheme 2.7).

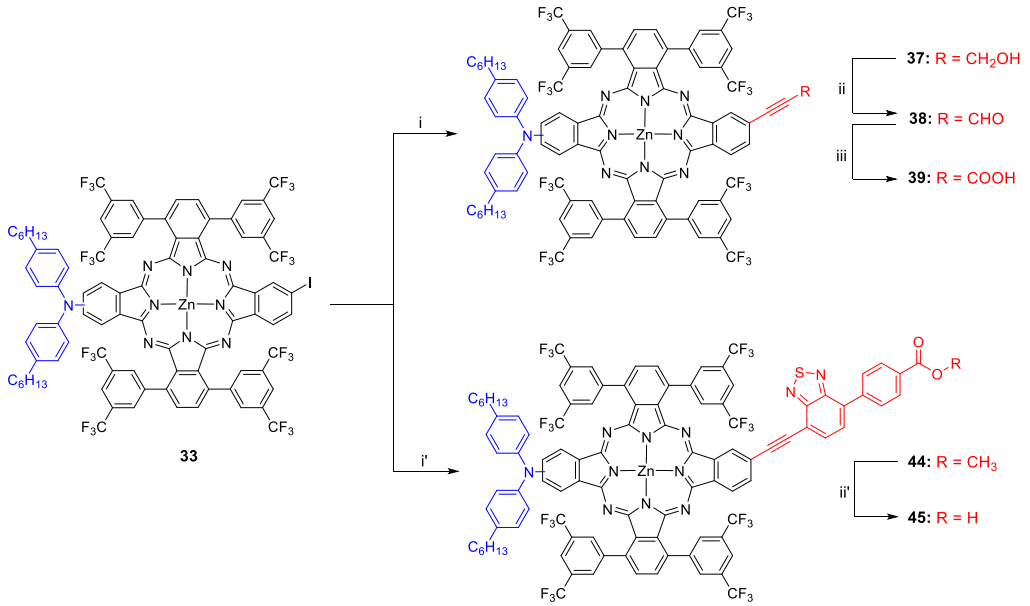

Scheme 2.7. Synthesis of Pcs **39** and **45**. Conditions: i) Propargylic alcohol, $Pd(PPh_3)_4$, CuI, Et_3N, THF to obtain **37**, 75%; ii) IBX, DMSO to obtain **38**, 77%; iii) Sulfamic acid, $NaClO_2$, THF to obtain **39**, 58%; i') Benzothiadiazole **43**, $Pd(PPh_3)_4$, CuI, Et_3N, THF to obtain **44**, 64%; ii') NaOH 20%, MeOH/THF to obtain **45**, 62%.

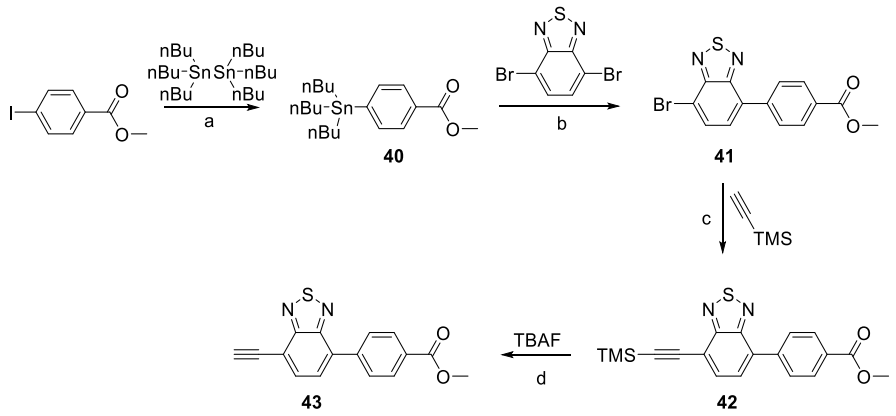

Scheme 2.8. Synthesis of benzothiadiazole **43**. Conditions: a) $Pd(PPh_3)_4$, toluene, reflux, 73%; b) CsF, $PdCl_2$, CuI, $^tBu_3P$, DMF, 45ºC, 17%; c) $PdCl_2(PPh_3)_2$, CuI, THF, Et_3N, 50ºC, 20%; d) TBAF, THF, r.t.

The structure of Pc **30**, **39** and **45** was unequivocally confirmed by MALDI-TOF mass spectrometry, UV−vis, IR and NMR. UV-vis spectra demonstrate the lack of aggregation of these products in THF solution (Figure 2.19). A bathochromic shift of the Q – band is observed from **30** (691 nm) to **39** (704 nm) and **45** (708 nm), due to an increase of the electron – releasing effect of the N – donor group, and also to an increase of the electron – withdrawing effect of the acceptor/anchoring group. The Q band of Pcs **39** and **45** is notably wider, yielding improved light-harvesting capabilities in the red region. The larger extinction coefficient of the Q band of Pc **45** *(*i.e., 4.94 *vs* 4.58 and 4.48 for **30** and **39**, respectively) is also remarkable, and similar to that previously observed in Pors containing the BTD unit.[56] In the 500 – 600 nm region of the spectra of Pcs **39** and **45**, a weak and constant absorption is observed, which is absent in the spectrum of **30** and is probably as a result of an electron-donating effect from the diphenylamino group to the Pc core. Noteworthy, a band at 448 nm is present also in the spectrum of **45** associated to the BTD unit.[56]

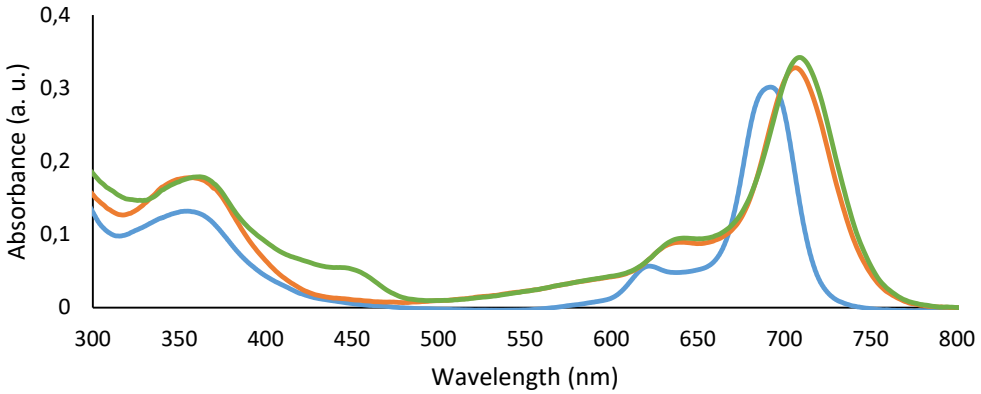

Figure 2.19. UV-vis spectra of **30** (— 8 μM), **39** (— 10 μM) and **45** (— 7 μM) in THF.

A complete assignment of all the signals in the ^{1}H-NMR spectra is not realizable because of the complexity of the systems, but characteristic peaks of the diphenylamino rings for Pcs **29** and **45**, and of the dimethylamino ring for Pc **30** are discernible. Figure 2.20 shows, as representative example, the ^{1}H-NMR of Pc **39** in THF-d_8, in which it is possible to discriminate the principal different groups of protons.

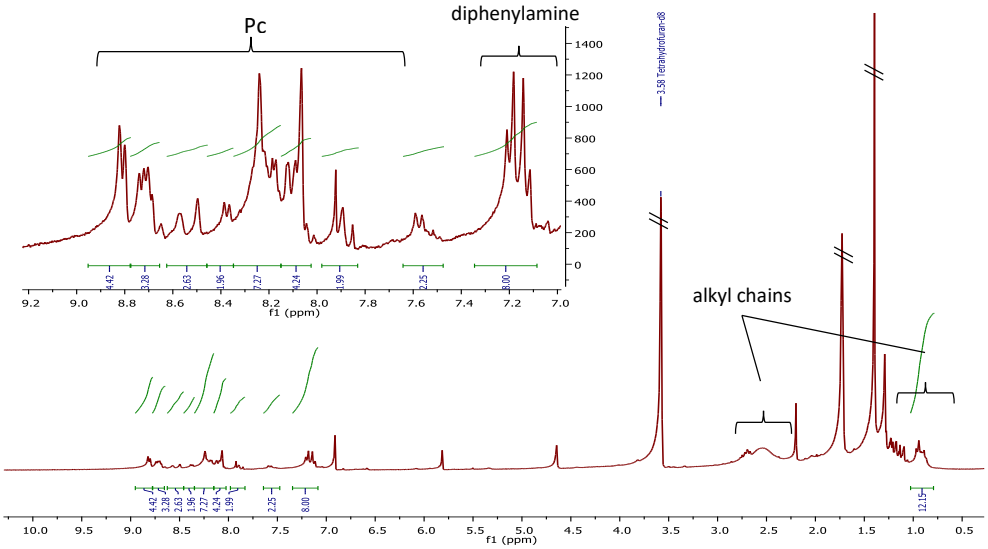

Figure 2.20. ^{1}H-NMR spectrum of **39** in THF-d_8.

Steady-state fluorescence spectra of compounds **30**, **39** and **45** were also recorded by exciting at the heights of the corresponding Q bands (Figure 2.21). Notably, the emissions of compounds **39** and **45** are notably quenched as a consequence of the strong electron donation from the directly linked dimethylamino group.

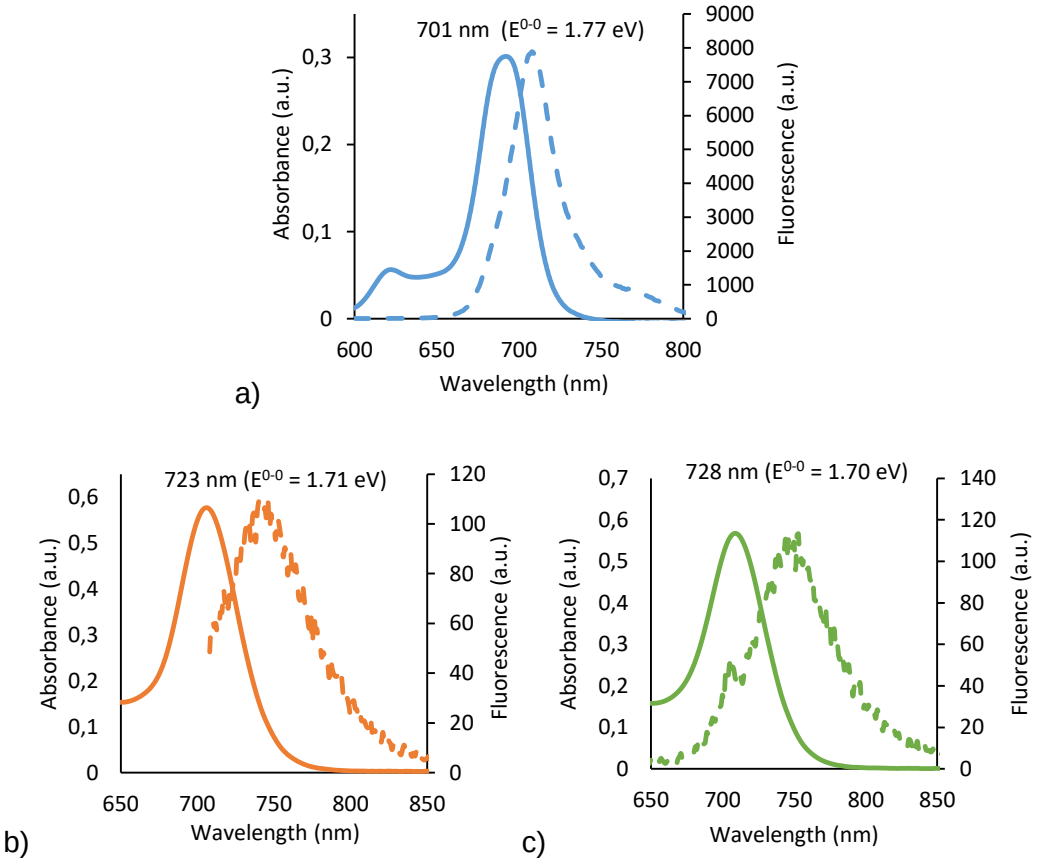

Figure 2.21. Absortion (solid lines) and fluorescence spectra (dashed line) of Pcs a) **30** (excitation wavelength, 685 nm), b) **39** (excitation wavelength, 700 nm), and c) **45** (excitation wavelength, 702 nm) in THF.

Electrochemical characterization of **30**, **39** and **45** was performed using cyclic voltammetry in 0.1M tetrabutylammonium phosphate (TBAP) CH_2Cl_2 solutions, using ferrocene as internal reference. Figure 2.22 shows the cyclic voltammograms, in which the redox processes do not appear as well defined waves. This may be due to the presence of the carboxylic acid group, which induces the aggregation of the molecule on the electrode surface, as already observed in other Pc-COOH.[138] The half – wave potentials ($E^{1/2}$) of the redox

processes were obtained by square wave measurements (Figure 2.22). The respective oxidation/reduction potentials, together with the HOMO/LUMO values vs the normal hydrogen electrode (NHE), are summarized in Table 2.1. HOMO and LUMO levels were estimated from peak potentials by setting the oxidative peak potential of Fc/Fc^{+} *vs* NHE to 0.642 V. [139,140]

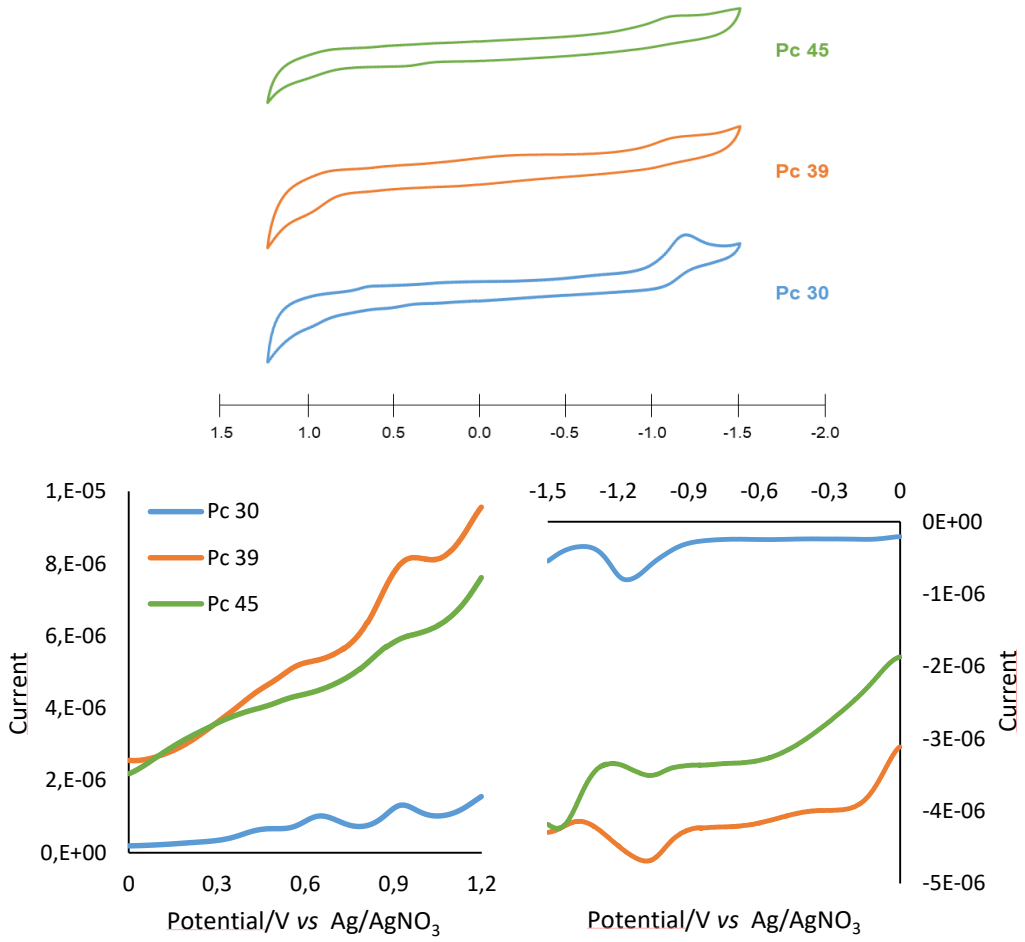

Figure 2.22. Cyclic voltammograms and square-wave voltammetry of Pcs **30**, **39** and **45**. Potential values are registered *vs* $Ag/AgNO_3$ reference electrode.

Table 2.1. First oxidation and reduction potentials and HOMO/LUMO levels for Pcs **30**, **39** and **45**.

Pc	$E_{ox}^{1/2}$ [V *vs* Fc/Fc$^+$]	$E_{red}^{1/2}$ [V *vs* Fc/Fc$^+$]	E^{0-0} [eV]	HOMO [eV *vs* NHE]	LUMO [eV *vs* NHE]	ΔG_{inj} [eV]	ΔG_{reg} [eV]
30	0.42 [a]	-1.40 [b]	1.77	1.06	-0.76	-0.26	-0.53
39	0.30 [c]	-1.37 [b]	1.71	0.94	-0.73	-0.23	-0.41
45	0.26 [c]	-1.35 [b]	1.70	0.90	-0.71	-0.21	-0.37

[a] Reversible. [b] Irreversible. [c] Quasi-reversible.

The first oxidation reactions of compounds **30**, **39** and **45** were reversible or quasi-reversible processes, with values in the range 0.42–0.26V versus Fc/Fc$^+$. The potential of compounds **39** and **45** are 120 and 160 mV lower than that of **30**, respectively, thus evidencing the strong impact that the direct linkage of the diphenylamino group has on the HOMO of the Pc macrocycle. On the other hand, the first reduction is irreversible for all compounds and occurs at very similar potentials, between -1.40 V (for **30**) and -1.45 V (for **45**) versus Fc/Fc$^+$. Incorporation of the BTD unit between the Pc core and the COOH group in **45** has limited influence on the electronic properties of the Pc, namely, a slight stabilization of the HOMO and LUMO levels with regard to Pc **39**. Notably, the electrochemical HOMO–LUMO bandgap is consistent with the optical (E^{0-0}) bandgap obtained from the interception between the absorption and emission spectra (Figure 2.21).

Figure 2.23 shows an energy-level diagram for the Pc dyes, comparing their HOMO–LUMO levels with the standard potential for the CB of TiO_2 *vs.* NHE (E_{CB} *= –0.5 V*), and for the iodide/triiodide (I^-/I_3^-) redox couple *vs.* NHE (*E = 0.53 V*).[141–144] The driving forces for electron injection from the Pc excited singlet state to the CB of TiO_2 (ΔG_{inj}) and for the regeneration of the Pc radical cation by the I^-/I_3^- redox couple (ΔG_{reg}) in a conventional DSSC have been determined (Table 2.1). Both processes are thermodynamically feasible and allow electron transfer in a solar cell.

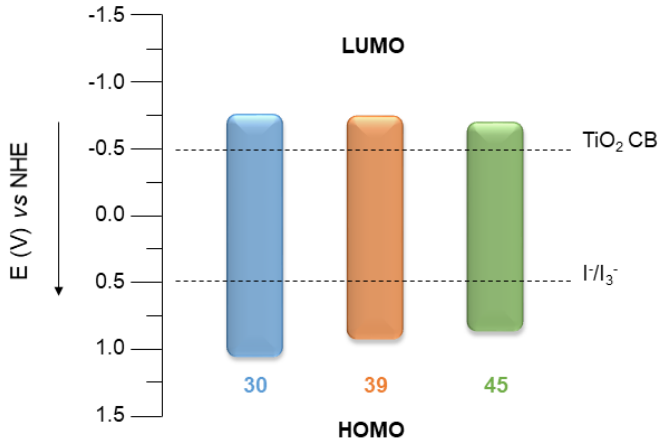

Figure 2.23. Schematic energy-levels diagram of Pcs **30**, **39** and **45**.

Additionally, DFT and TDDFT calculations have been performed to get insights into the electronic structure of the synthetized dyes, which can help in the understanding of the photovoltaic results of the corresponding cells. In all three dyes, the HOMO has extended delocalization toward the donor moiety (Figure 2.24). However, the LUMO has a slight delocalization onto the acceptor group for Pcs **30** and **39** and is rather centered in the Pc core for **44**, whereas the $LUMO^{+1}$ is completely centered in the Pc core for Pcs **30** and **45** and has a small delocalization toward the acceptor group in the case of **39** (Figure 2.24). The degree of delocalization of the LUMO and $LUMO^{+1}$ orbitals on the acceptor group is one of the factors considered to rationalize the photovoltaic behaviour of these molecules, as mentioned in the next section.

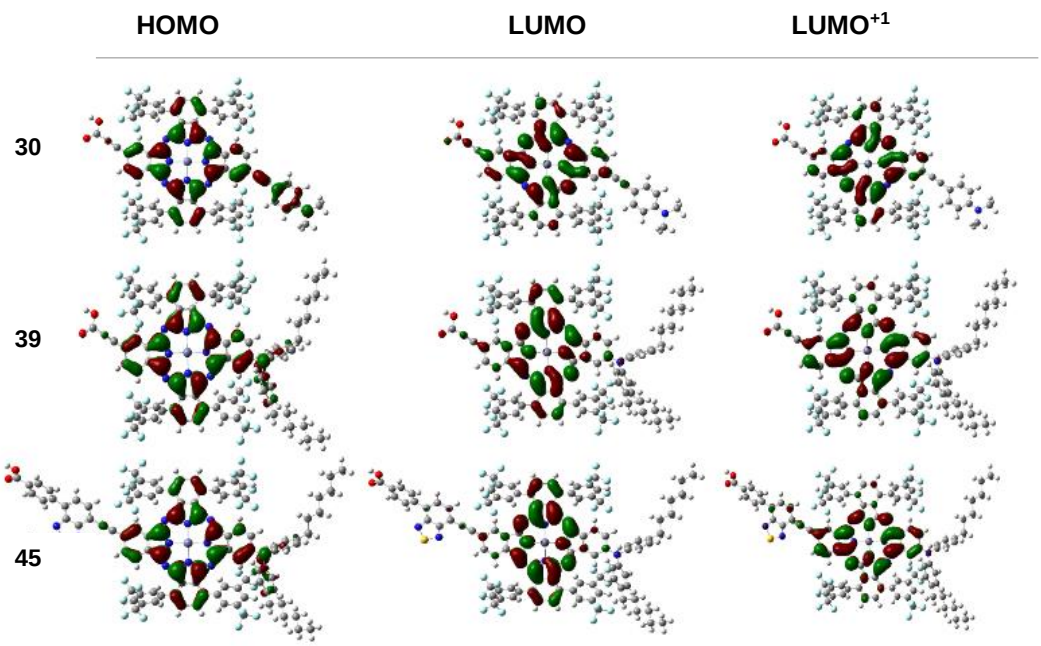

Figure 2.24. Contour plots for the HOMO (left), LUMO (center), and LUMO^{+1} (right) of Pcs **30** (top), **39** (middle), and **45** (bottom) computed by using wB97xD/6-31G(d)/CPCM(THF). Isovalue set to 0.02.

2.3.2 Photovoltaic studies of novel donor-π-acceptor substituted Pcs for DSSCs

The incorporation of Pcs **30**, **39** and **45** in DSSCs has been performed in the group of Prof. Grätzel, in École Polytechnique Fédérale de Lausanne (EPFL), Switzerland, following protocols well established in the group.

Pcs **30**, **39** and **45** were tested in DSSCs on [9+4] μm thick TiO_2 films, which consist of a 9 μm thick active layer and an additional 4 μm thick scattering layer. For the preparation of the devices, the TiO_2 photoanodes were immersed in a 0.1 mM solution of the corresponding Pc in THF for 16 h. Table 2.2 summarizes the dye-loading densities and photovoltaic data obtained for the Pc-based DSSC devices.

Table 2.2. Dye-loading (*DL*) densities and photovoltaic data of the devices [a] made with Pc dyes on [9+4] μm thick TiO_2 films under simulated one sun illumination (AM 1.5G) and active area of 0.159 cm^{-2}.[b]

Pc	DL [nmol cm^{-2}]	I_0 [mW cm^{-2}]	V_{oc} [mV]	J_{SC} [mA cm^{-2}]	FF	η [%]
30 [c, d]	-	97.53	401.41	0.30	0.75	0.09
30 [e]	87.1	100.35	386.22	8.16	0.61	**1.92**
30 [c, e]	-	100.61	338.52	0.99	0.63	0.21
39 [d]	-	102.56	400.95	0.39	0.69	0.11
39 [e]	26.1	100.81	426.75	9.88	0.58	**2.43**
45 [d]	-	101.13	427.20	0.28	0.74	0.09
45 [c, d]	-	100.29	415.29	0.30	0.75	0.09
45 [e]	14.1	100.81	410.55	4.46	0.60	**1.09**

[a] Four to five devices of equal quality were made for each dyes; the values obtained for the best cell are presented in each case. [b] The TiO_2 films have a total thickness of 13 μm consisting of a 9 μm thick TiO_2 active layer and an additional 4 μm of scattering layer. [c] CHENO 10mM; [d] electrolyte 1; [e] electrolyte 2.

Unfortunately, the photovoltaic parameters were lower than expected, with Pc **39** exhibiting the best efficiency of the series (i.e., 2.43 %), whereas the worst performing is Pc **45** (η = 1.09%). These values are lower than the PCEs obtained with the best performing Pc photosensitizers, namely, **TT40** and **S20**.

Although the final PCEs obtained are moderate, some useful information can be extracted from the different experiments. It can be observed that the key factors are the presence or absence of CHENO and the choice of the electrolyte. As said previously, CHENO is usually utilized as co-adsorbent in order to prevent dye aggregation.[92] In fact, CHENO is known to bind strongly to the surface of nanostructured TiO_2, displacing some dye molecules and thus hindering the formation of dye aggregates.[95] In our case the bistrifluoromethylphenyl groups are bulky enough to strongly prevent the Pc aggregation; so the use of a co-absorbent only limits the number of dye molecules adsorbed on the TiO_2 surface, decreasing the conversion efficiency.

Regarding the electrolyte, different concentrations and additives have been tested, but in table 2.2 only two electrolyte compositions are given as they are the most revealing about the behavior of the cells. Electrolyte 1 was composed by LiI 0.2M, 1,3-dimethylimidazolium iodide (DMII) 0.6M, 4-*tert*-butylpyridine (TBP) 0.28M, I_2 0.04M and guanidinium thiocyanate (GuNCS) 0.05M in acetonitrile; electrolyte 2 was composed only by LiI 0.5M, NaI 0.5M and I_2 0.05M in acetonitrile. One of the most convenient ways to enhance the photovoltaic efficiency of DSSCs is the addition of appropriate chemical species to the I^-/I_3 electrolyte to finely tune the semiconductor – electrolyte interface. For instance, nitrogen heterocyclic compounds such as TBP and *N*-methylbenzimidazole (NMBI) are added in the electrolyte to improve the *Voc*[145,146] while GuNCS was found to increase both *Voc* and *Jsc*.[147,148] The exact role the additives play is now well known; it seems that TBP and NMBI deprotonate the TiO_2 surface by adsorption and, thus, shift the CB toward negative potentials and passivate the surface active recombination sites.[149,150] Usually, these electrolytes increase the efficiencies of DSSCs. However, in this case, efficiencies found when using electrolyte 1 were negligible, mainly due to the very low J_{SC} values associated to the lack of injection. It therefore follows that using additives such as TBP and / or DMII cause an excessive displacement of the value of the CB toward negative potentials. This does not allow the electronic injection from the LUMO orbital of Pcs to the semiconductor CB. Aiming at increasing the J_{SC}, an electrolyte lacking TBP and DMII additives, namely electrolyte 2, was used. In this case, efficiencies of 1.92%, 2.43% and 1.09% are reached for Pcs **30**, **39** and **45**, respectively, owing to an increase in the J_{SC} even if a decrease of the *Voc* and FF is observed.

To rationalize the different sensitization capability of these compounds, the responses of Pc **30** and Pc **39** are firstly compared. Both dyes have the same anchoring group and Pc core and differ only in the corresponding donor group. Pc **30**, despite having both the most negative LUMO and positive HOMO (which,

in principle, should confer to this sensitizer the best electron-injection and dye-regeneration efficiencies, respectively), displays a lower J_{SC} (8.16 mAcm^{-2}) than Pc **39** (9.88 mAcm^{-2}), and the poorest *Voc* (386 mV) of the series. On the other hand, the dye-loading density of Pc **39** was estimated to be three times lower than that of Pc **30**, which can be explained by the strong steric repulsion induced by the bulky bis(hexyloxy)phenylamino groups of Pc **39**, which needs more space to accommodate on the TiO_2 surface than Pc **45**, functionalized with a smaller 4-ethynyl-*N,N*-dimethylaniline moiety. Considering this fact, a superior J_{SC} should be expected for Pc **30**. However, the opposite trend was observed, which is otherwise in agreement with the incident photon-to-current efficiency (IPCE) response observed for Pcs **30** and **39**. In accordance with their corresponding absorption spectra, the IPCE response of Pc **39** is red shifted by about 50 nm with regard to that of Pc **30** (Figure 2.25). In addition, Pc **30** displays a significant drop in the IPCE response between 475 and 550 nm, whereas Pc **39** fulfils this valley much better. This factor may, in part, contribute to the difference observed in their J_{SC} values. Also, the degree of delocalization of the LUMO and LUMO^{+1} orbitals onto the acceptor group is lower for Pc **30** (Figure 2.24), which is consistent with its poorer injection. On the other hand, the lower *Voc* obtained for Pc **30** can be ascribed to a faster electron recombination at the TiO_2/electrolyte interface $e^-/(TiO_2CB)\leftrightarrow I_3^-$ (dark current), which should also contribute to lower the J_{SC}. The presence of the bulky amino group tethered with hexyl chains in Pc **39** (and as well in Pc **45**) must better prevent the penetration of the oxidized species to the surface, thus reducing the dark current, a strategy commonly used and previously reported,[86,151] which is also coherent with the observed improved *Voc* for Pc **39**. Next, the photovoltaic performances of Pc **39** and Pc **45**, which differ only by the presence in the latter of an additional BTD bridge between the Pc and the acceptor group, are compared. Although the LUMO of Pc **45** is much less delocalized over the acceptor part (Figure 2.24) and slightly lower in energy than that of **39**, these two factors might not be sufficient to solely explain the huge difference observed in the J_{SC}, which is almost half for Pc **45** (4.46 mAcm^{-2}) than for Pc **39** (J_{SC} =9.88 mAcm^{-2}). An important contribution must arise from the difference in the amount of adsorbed dye molecule to the TiO_2 surface, which is twice as large for Pc **39** compared to Pc **45**. Another possible contribution should come from faster recombination between oxidized dyes and photoinjected electrons in the TiO_2 CB caused by the BTD bridge in Pc **45**, as previously reported.[56,137] Although it was recently reported[152] that the BTD unit facilitates the electron recapture by the charge carrier at the TiO_2/electrolyte interface (i.e., dark current), the dark current seems to be similar for Pc **39** and Pc **45**, as their *Voc* values are also similar (427 and 411 mV, respectively), and, thus, it does not rationalize the different J_{SC} values. Most importantly, the IPCE values in the

whole visible region are continually half for Pc **45** (ca. 10–15%) compared to that for **39** (ca. 20–35%) (Figure 2.25), matching well with the difference observed in the J_{SC} values.

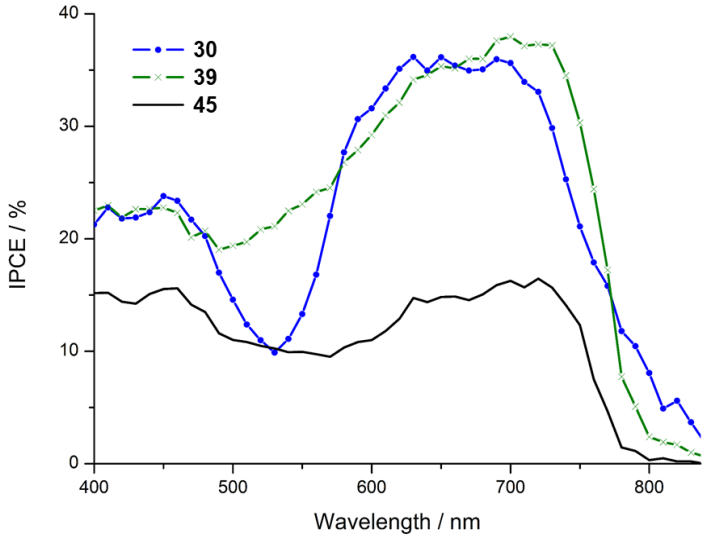

Figure 2.25. *IPCE* spectra of the DSSC devices made with Pcs **30**, **39** and **45**.

2.3.3 Novel donor-π-acceptor multicomponent systems based on Pcs

2.3.3.1 Zn(II)Por-Zn(II)Pc-SubPc triads

Synthesis and characterization

The preparation of novel donor-π-acceptor multicomponent systems based on Pcs was first carried out by an unsymmetric functionalization of the Pc **12** with a Zn(II)Por donor component and a SubPc acceptor chromophore. As these triads have been designed to achieve cascade-type, charge/energy transfer from the primary electron donor, namely the Por unit, to the final acceptor component, namely the SubPc component, these two macrocycles should incorporate appropriate electron-donor or electron-withdrawing substituents, respectively.

Therefore, the first goal undertaken for the preparation of the designed triads was the preparation of Zn(II)Pors funtionalized with TPA units capable to increase the energy of the HOMO level of the aromatic macrocycles. Functionalization of Pors with amino-containing substituents at the so-called *meso* positions of the ring (namely, at the methine bridges) exerts an strong impact on the electron density of the dyes. To obtain *meso*-functionalized Pors, it is necessary to prepare aldehydes which will give rise to crossed condensation reaction with pyrrole, affording the substituted derivatives. Schemes 2.9 and 2.10 show the preparation of two bulky TPA-containing aldehydes, **46** and **50** as precursors of the targeted Pors, which were designed to provide solubility and hindered aggregation to the the final Pors.[56,88]

Compound **46** was obtained by two consecutive Buchwald–Hartwig cross-coupling reactions, the first one between 1-bromo-4-hexylbenzene and 4-hexylaniline to afford bis(4-hexylphenyl)amine **31**,[134] and a second amination reaction with 4-bromobenzaldehyde.

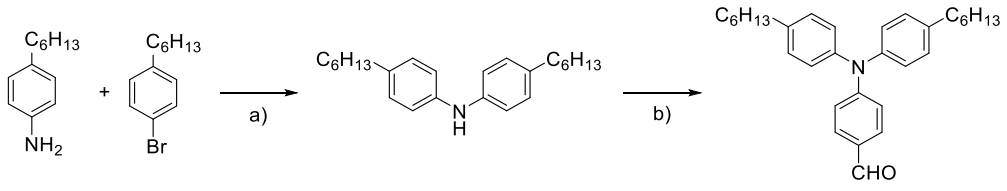

31 **46**

Scheme 2.9. Synthesis of TPA aldehyde **46**. Conditions: a) $Pd_2(dba)_3$, $^tBu_3P$, ^{t}BuONa, toluene, reflux, 86%; b) K_3PO_4, $Pd_2(dba)_3$, X-Phos, dioxane, 80ºC, 40%.

In the case of compound **50**, the synthetic pathway started from bromoresorcinol, which was O-alkylated under Williamson conditions. Then, the arylbromide undergoes a bromo-lithium exchange and a subsequent trans-metallation with isopropyl pinacol boronic ester to yield compound **48**. After that, compound **50** was prepared through initial Suzuki reactions between **48** and bis(4-bromophenyl)amine, and a successive Buchwald–Hartwig amination with 4-bromobenzaldehyde.

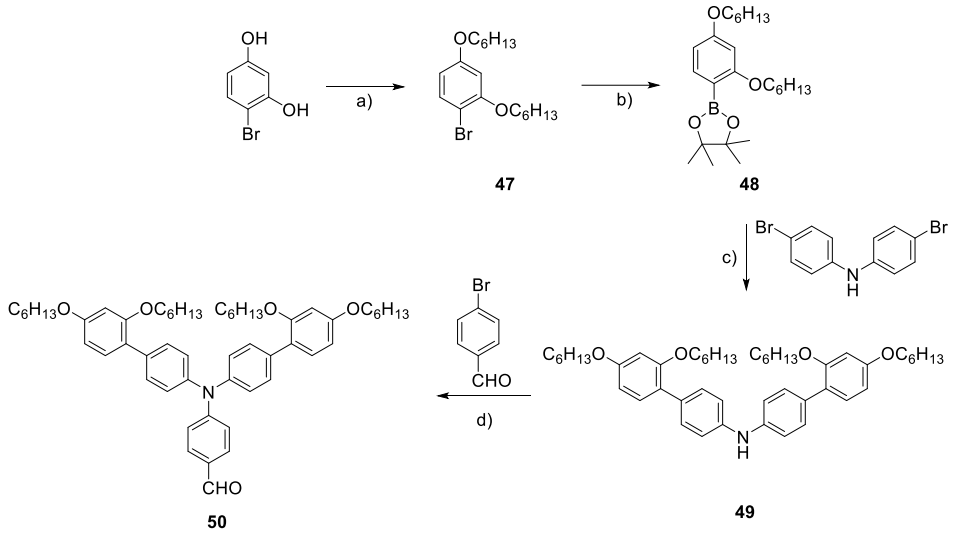

Scheme 2.10. Synthesis of TPA aldehyde **50**. Conditions: a) 1-bromohexane, K_2CO_3, DMF, 90°C, 74%; b) n-BuLi, isopropyl pinacol borate, THF, from -78°C to r.t., 43%; c) K_2CO_3, $Pd(PPh_3)_4$, toluene, reflux, 42%; d) K_3PO_4, $Pd_2(dba)_3$, X-Phos, dioxane, 80ºC, 72%.

With these TPA aldehydes in our hands, we proceeded to prepare two different donor Zn(II)Pors according to the Lindsey strategy, under high-dilution of the correponding aldehydes and pyrrole in the presence of an acid catalyst, and a subsequent treatment with an oxidant.[153] Considering that the Por unit has to be linked to the central Zn(II)Pc unit, we undertook the preparation of unsymmetrically functionalized **A_3B** Pors containing three TPA donor substituents and one TMS-protected ethynyl moiety that will be used as linking group through Shonogashira couplings. To direct as much as possible the reaction towards the **A_3B** Pors, a 3:1 ratio of the corresponding TPA aldehyde (**46** or **50**) (**A**) and 3-(trimethylsilyl)-2-propynal (**B**) was used, the mixture of aldehydes being in a 1:1 ratio with respect to the pyrrole (Scheme 2.11). In the corresponding reactions, all possible *meso*-substituted metal-free Pors (i.e., **A_4**, **A_3B** and **A_2B_2**) were obtained, the targeted tris(triphenylamine)Pors **51** and **53** being isolated from the mixture by column chromatography in low yields.

Finally, the treatment of each metal-free Por with $Zn(OAc)_2$ afforded the corresponding Zn(II)Pors **52** and **54** in quantitative yields.

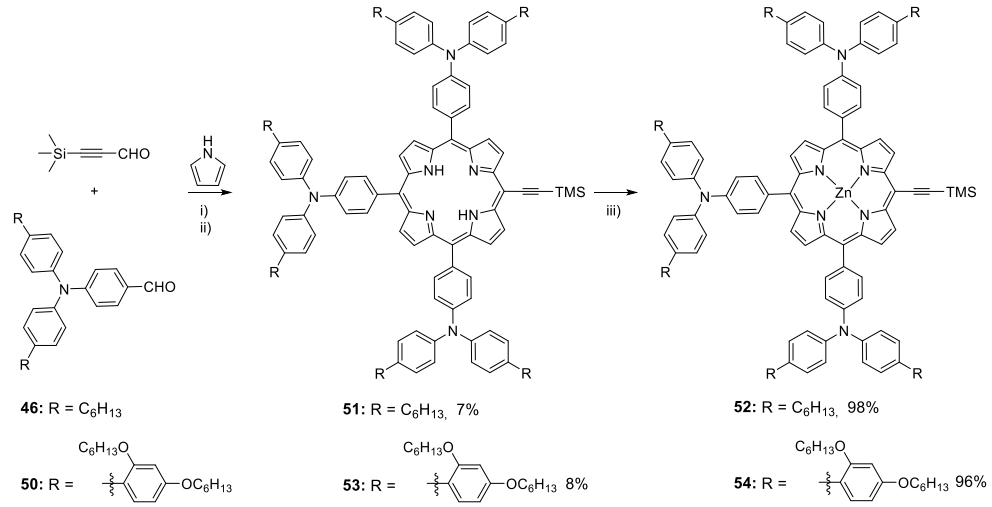

Scheme 2.11. Synthesis of Zn(II)Pors **52** and **54**. Conditions: i) BF_3OEt_2, EtOH, $CHCl_3$, r.t.; ii) DDQ, NEt_3, r.t; iii) $Zn(OAc)_2$, CH_2Cl_2/MeOH (3:1), r.t.

On the other hand, the perfluorinated SubPc **55** was chosen as acceptor component because it is synthesized in good yields, it is highly photostable and easy-to-handle (Scheme 2.12).[127,128,154]. More importantly, its HOMO-LUMO energy levels are appropriate to accept electrons from the Pc component of the triad.

The most widespread method for the preparation of SubPcs involves the cyclotrimerization of a phthalonitrile in the presence of boron trichloride (or other boron source) in a high-boiling point solvent. For the preparation of **55**, tetrafluorophthalonitrile was refluxed in the presence of boron trichloride in *p*-xylene. Taking advantage of the reactivity of B-Cl bond at the axial position of SubPcs, which is susceptible to substitution reactions with different nucleophiles, we performed a reaction between SubPc **55** and 3–ehynylphenol in toluene solution in the presence of DIPEA, yielding the SubPc **56** that possesses a free ethynyl amenable to give rise to further Sonogashira coupling (Scheme 2.12).

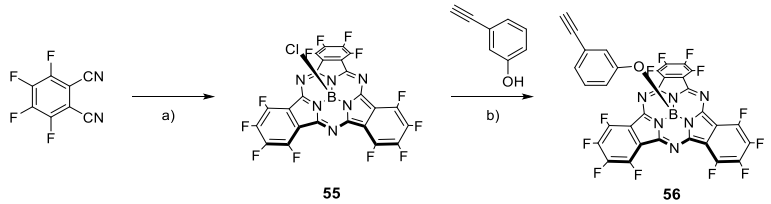

Scheme 2.12. Synthesis of F_{12}SubPc **55** and **56**. Conditions: a) BCl_3, *p*-xylene, reflux, 53%; b) DIPEA, toluene, reflux, 38%.

With both donor (i.e., Zn(II)Pors **52** and **54**) and acceptor (i.e., SubPc **56**) components and the **ABAB** Pc **12** in our hands, we proceeded to assemble them into the triad systems. Since the synthetic route for the SubPc **56** is more straightforward and high-yielding than that for the Zn(II)Pors, we decided to carry out first a Sonogashira coupling between Pc **12** and SubPc **56** (Scheme 2.13) following protocols that had been described previously in the literature for related SubPc derivatives with a terminal alkyne substituent in the axial position.[155] A new compound was obtained in this reaction, but, unfortunately, it was not identified as the expected dyad, but as Pc **57** bearing a phenolic residue. A reasonable explanation could be the low stability of SubPc **56** under these conditions. For this reason, different solvent mixtures were tested (namely, toluene/Et_3N, toluene/$^{i}Pr_2NH$, THF/Et_3N and THF/ $^{i}Pr_2NH$ in 20:1, 10:1 and 5:1 ratios for each), but, in all the cases, a dramatic change of colour from pink to black was observed, with the simultaneous formation of 3–ehynylphenol as monitored by TLC.

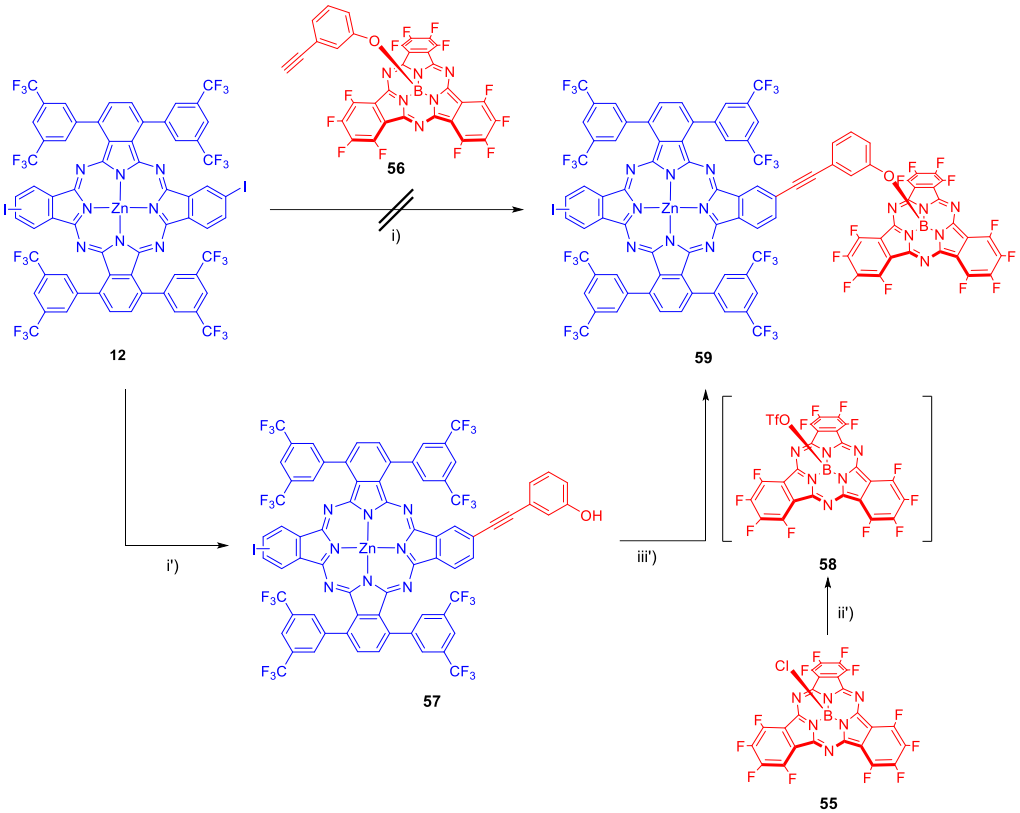

Scheme 2.13. Synthesis of Pc **57** and Pc-SubPc dyad **59**. Conditions: i) $Pd(PPh_3)_4$, CuI, toluene/NEt_3 (5:1), 50°C; i') 3–ehynylphenol, $Pd(PPh_3)_4$, CuI, THF/NEt_3 (3:1), 60°C, 30%; ii') AgOTf, toluene, r.t; iii') DIPEA, reflux, 15%.

In view of the lability of the axially-functionalized SubPc **56**, we decided to undertake an alternative synthetic route to achieve the Pc-SubPc dyad, as depicted in Scheme 2.13. The key-point of this method is the generation of triflate-SubPcs **58** as reaction intermediate by axial chlorine exchange of SubPc **55**, according to a well-establisced methodology developed in our research group.[156] This in-situ formed intermediate is capable of readily give rise to axial substitution reaction with nucleophiles, for instance, the phenol-containing Pc **57**, obtained as a secondary product in the previous route. Then, we prepared Pc **57** starting from Pc **12**, by a Sonogashira reaction with 3–ethynylphenol. Then, the preparation of the target dyad **59** involved a one-pot, two-step reaction, with the initial conversion of SubPc **55** into the triflate derivative **58** by addition of AgOTf and DIPEA (added to neutralize the triflic acid generated in this step), followed by the addition of Pc **57** (Scheme 2.13).

Due to the low stability of the axial bond that SubPc **56** showed under Sonogashira conditions, we were concerned about the stability of Pc-SubPc dyad **59** in further Sonogashira coupling with Zn(II)Por derivatives. For that reason, we put dyad **59** aside for further use as reference compound in photophysical studies, and decided to tackle the preparation of the target triads carrying out first the synthesis of Zn(II)Por-Zn(II)Pc dyads **61** and **63** (Scheme 2.14), leaving the axial substitution on the SubPc components as last step of the synthesis. For that purpose, an initial deprotection of the alkyne group of Zn(II)Pors **52** and **54** was carried out in the presence of TBAF. After that, dyads **61** and **63** were obtained in excellent yields by coupling Pc **57** with the corresponding deprotected Zn(II)Pors under Sonogashira conditions. For these transformations, a copper-free Sonogashira methodology was used in order to avoid the formation of Zn(II)Por-Zn(II)Por homocoupling products.[157,158]

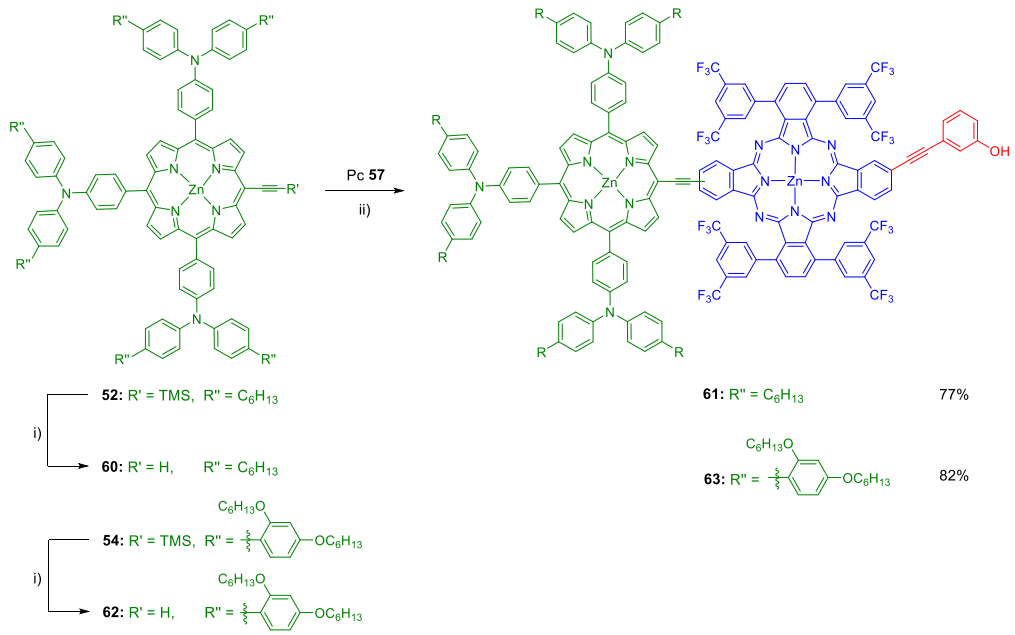

Scheme 2.14. Synthesis of Por-Pc dyads **61** and **63**. Conditions: i) TBAF, THF, 0°C; ii) Pc **57**, $Pd_2(dba)_3$, $AsPh_3$, THF/NEt_3 (2:1), 60°C.

Finally, the target triads **64** and **65** were obtained from SubPc **55** and the corresponding Zn(II)Por-Zn(II)Pc dyads, following the SubPc-triflate intermediate protocol described above for the synthesis of Pc-SubPc dyad **56**, and showed in Scheme 2.15.

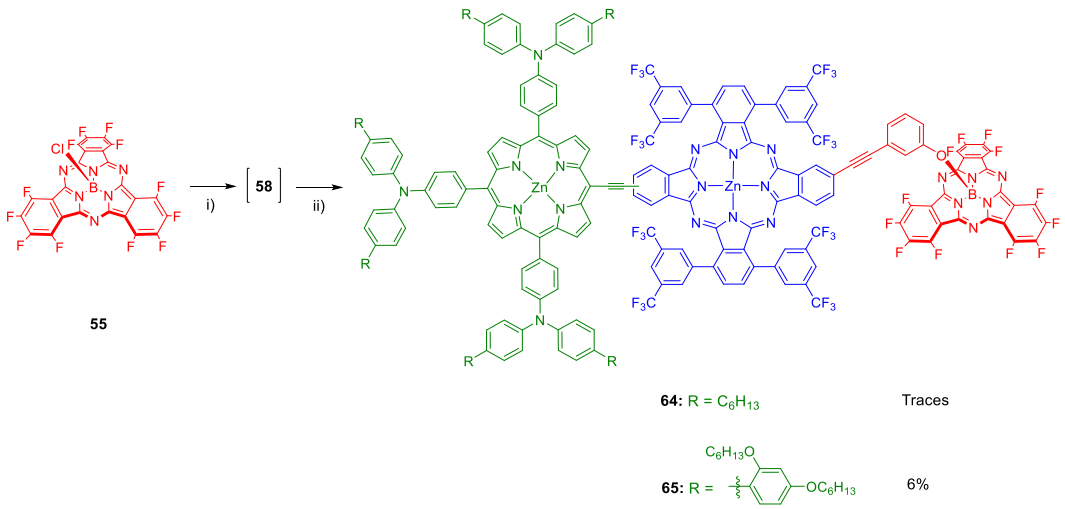

Scheme 2.15. Synthesis of Por-Pc-SubPc triads **64** and **65**. Conditions: i) AgOTf, toluene, r.t; ii) Dyad **61** or **63**, DIPEA, reflux.

The structure of triad **65** was unequivocally confirmed by HR-MALDI-TOF mass spectrometry, UV−vis, IR and NMR. In the case of **64**, its structure was confirmed by HR-MS, but, due to the low amount of compound obtained, a complete characterization could not be performed, which made us discard this triad for further studies.

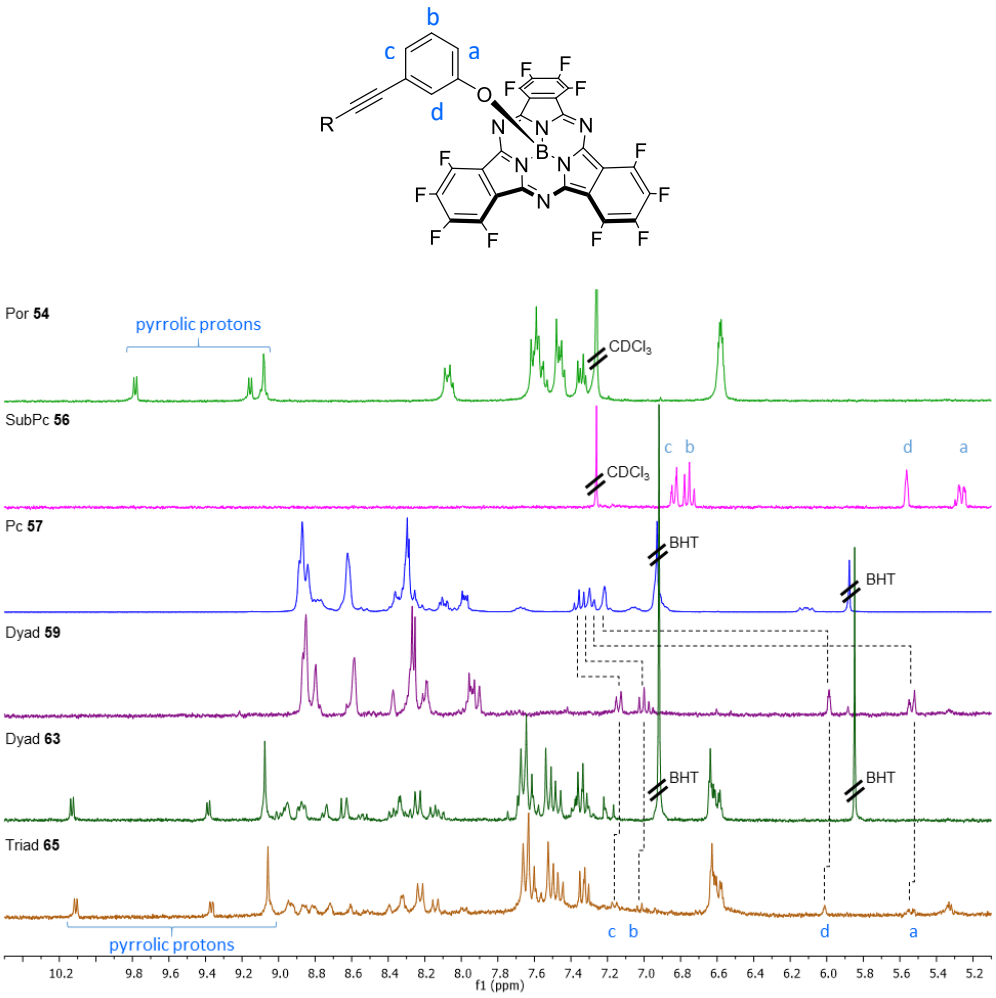

Figure 2.26. Comparison of ^{1}H-NMR spectra of **54** and **56** in $CDCl_3$, and **57**, **59**, **63** and **65** in THF-d_8. Dashed lines are drawn to guide the eye to the changes in chemical shifts of protons Ha, Hb, Hc and Hd.

Figure 2.26 compares the ^{1}H-NMR spectra of the individual Por, Pc and SubPc components, Por-Pc and Pc-SubPc dyads and triad **65**. Despite the complexity of these systems, it is possible to distinguish protons of the different components.

In particular, it is very informative to follow the changes in the chemical shift of the phenolic protons as if the phenol is bound or not to the boron atom of the SubPc (Figure 2.26).

Whatever the combination of chromophores in the synthesized dyads and triads, their UV-vis spectra show the presence of the corresponding bands of the individual components. (Figures 2.27, 2.28 and 2.29). For instance, the UV-vis spectrum of dyad **59** is a superimposition of the Q-band of SubPc **56** at 567 nm and the characteristic split Q-band of Pc **57** in the region between 650 and 730 nm (Figure 2.27). Likewise, Por-Pc dyad **63** exhibits three significant bands at around 330, 450 and 700 nm (Figure 2.28), the first two bands corresponding to the TPA moieties and B-band of Por **54**, respectively. Noteworthy, the Q band of the Pc component at 700 nm is affected by the linkage to the Por unit, showing broadening, red-shifting and no splitting with respect to the Q band of Pc **57**. This is a consequence of the electronic effect imparted by the donor TPA-Por, and the existing conjugation between the two components. As expected, the UV-vis spectrum of **65** shows four significant bands at around 330, 450, 570 and 700 nm. Three of these match perfectly with the bands described for Por-Pc dyad **63**, while the additional band arises from the SubPc component (Figure 2.29). Worth of mention is that triad **65** presents a panchromatic absorption in the UV and visible range.

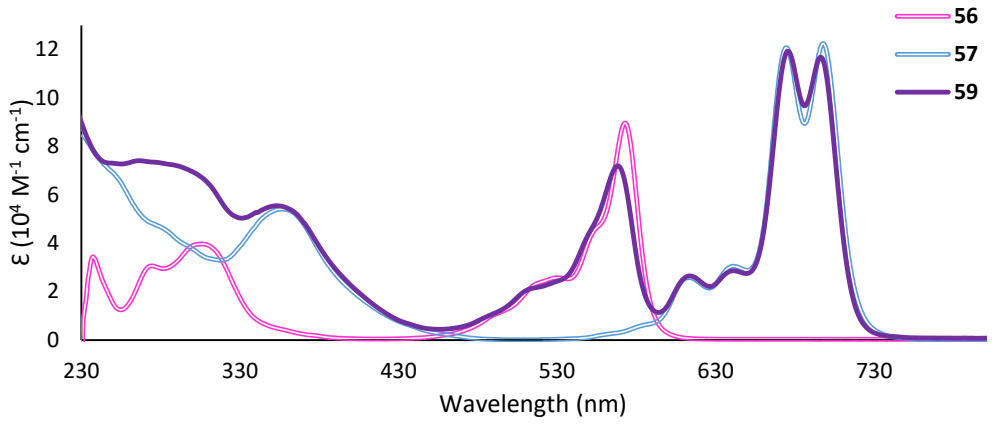

Figure 2.27. Comparison of UV-vis spectra of SubPc **56**, Pc **57** and Pc-SubPc dyad **59** in THF.

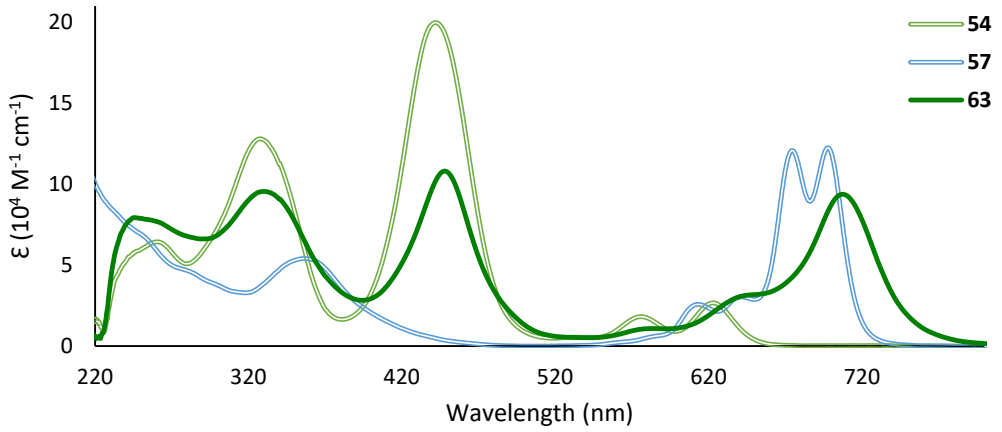

Figure 2.28. Comparison of UV-vis spectra of Por **54**, Pc **57** and Por-Pc dyad **63** in THF.

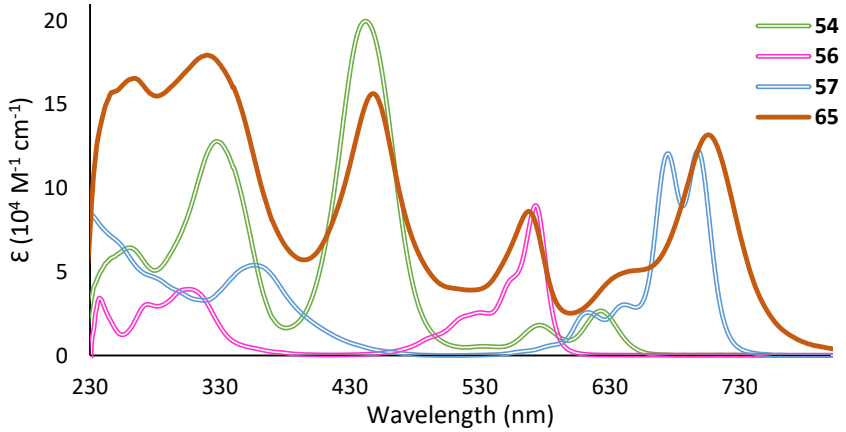

Figure 2.29. Comparison of UV-vis spectra of Por **54**, SubPc **56**, Pc **57** and triad **65** in THF.

Electrochemical studies

To determine the ability of triad **65** to generate photoinduced charge-separated states, we performed electrochemical studies over this triad, and the corresponding chromophore components, specifically Por **54** and Pc **57**, while the redox data for the SubPc **55** were obtained from the literature. Electrochemical characterization was performed using cyclic voltammetry in 0.1M TBAP CH_2Cl_2 solutions, using ferrocene as internal reference (Figure 2.30a). The half – wave potentials ($E^{1/2}$) of the redox processes were obtained by square wave measurements. As shown in Figure 2.30a, the first reduction

reactions of compounds **54** and **57** were quasi-reversible or reversible processes with values of -1.51 and -1.18 V versus Fc/Fc^+, respectively. The first oxidation reaction appears as a clear reversible process for **57** ($E_{ox}^{1/2}$ = 0.4 V vs Fc/Fc^+). On the other hand, compound **51** shows complicated oxidation processes in the range 0.2 – 0.9 V vs Fc/Fc^+, probably due to additional redox events taking place at the TPA substituents, as previously established for other arylamino-substituted derivatives.[144,159] Table 2.3 compiles the redox values registered for compounds **54** and **57**, and those for SubPc **55** collected from the literature. Regarding the CV of the triad **65**, the observed redox waves are reminiscent of to those of the individual components.

Together with the respective oxidation/reduction potentials, table 2.3 summarizes also the HOMO/LUMO values of the single components **54**, **55** and **57**. The energy levels of HOMO and LUMO orbitals *vs.* vacuum were obtained using the approximation depicted in Equation 2.3, based on the revised potential of the Fc/Fc^+ redox couple considering the influence of the different reference electrodes employed described by Cardona *et al.*[139] It is important to mention that, considering the difficulty to obtain an accurate value of $E_{ox}^{1/2}$ of **54**, the HOMO value was obtained using optical ($E_{0\text{-}0}$) bandgap obtained from the interception between the absorption and emission spectra (Figure 2.30b).

$$E_{HOMO/LUMO} = -5.1 - E_{ox/red}^{1/2}\,(vs\ Fc/Fc^+)(eV) \qquad (2.3)$$

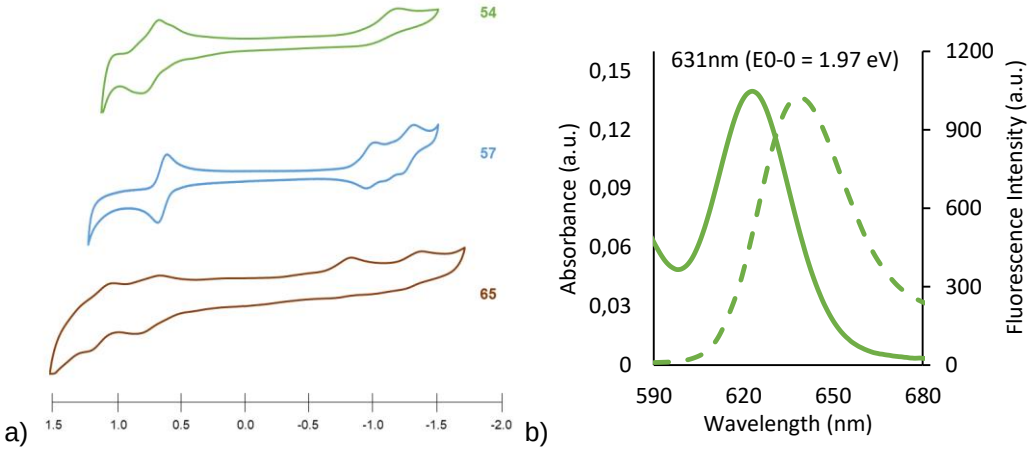

Figure 2.30. a) Cyclic voltammograms of **54**, **57** and **65**. Potential values are registered *vs* $Ag/AgNO_3$ reference electrode; b) Absorption (solid lines) and fluorescence spectra (dashed line) of **54** (excitation wavelength, 440 nm)

Table 2.3. First oxidation and reduction potentials, optical bandgap and HOMO/LUMO levels for **54**, **55** and **57**.

	$E_{ox}^{1/2}$ [V *vs* Fc/Fc$^+$]	$E_{red}^{1/2}$ [V *vs* Fc/Fc$^+$]	$E_{0\text{-}0}$ [eV]	HOMO [eV]	LUMO [eV]
54	-	-1.51 [b]	1.97	- 5.5 [e]	- 3.6 [d]
55	1.00 [a]	-0.92 [a]	-	- 6.1 [d]	- 4.2 [d]
57	0.40 [c]	-1.18 [c]	-	- 5.5 [d]	- 3.9 [d]
65	0.46 [c]	-1.10 [b]	-	-5.6 [d]	-4.0 [d]

[a] Literature data. [b] Quasi-reversible. [c] Reversible. [d] Calculated using Equation 2.3. [e] Calculated using $E_{0\text{-}0}$.

From the previous data, it could be assumed that the HOMO of the triad **65** is more centered in the Por component, while the LUMO is mostly located in the SubPc acceptor, as otherwise expected. A schematic representation of the HOMO/LUMO energy values of the single components is depicted in Figure 2.31. From this HOMO/LUMO distribution, it seems plausible that, after excitation of any of the components of the triad, cascade – like charge transfer processes could take place, originating charge separated states with the Por component in its radical cation form, and the SubPc as radical anion (i.e., Por$^+$–Pc–SubPc$^-$). The central Pc is capable to perform the anticipated dual role of accepting energy/electrons from the Por unit and transferring electrons to the SubPc.

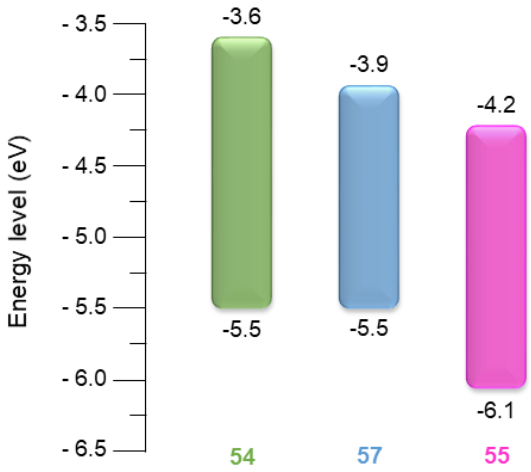

Figure 2.31. Schematic energy-levels diagram of **54**, **55** and **57**.

Photophysical studies

TechnIques. To shed light onto excited state interactions of the triad **65**, dyads and single components synthesized, transient absorption measurements were conducted.

Femtosecond transient absorption spectroscopy (fs-TAS) is a method that allows the generation and investigation of ultra-short-lived species (i.e., transients of a molecule) and the corresponding electron dynamics *via* kinetic studies.[160]

In fs-TAS, the excitation of the sample is induced by ultra-short laser pulses on the femtosecond time-scale (10^{-15} s), which provides the opportunity of observing the temporal evolution of excited states.[161]

In principle, an intense, quasi monochromatic laser pulse – the pump pulse – transfers the sample from the electronic ground state into an excited state. A white-light probe pulse simultaneously monitors the induced optical density changes *ΔOD* at time delays *Δt* after the excitation according to Equation 2.4:

$$\Delta OD = \log \frac{I(\lambda,\infty)}{I(\lambda,\Delta t)} \qquad (2.4)$$

where *I(λ, ∞)* and *I(λ, Δt)* are the spectral intensities of the probe pulse having passed through the sample, measured without any excitation and with a time delay *Δt* after excitation, respectively.[162] By recording *ΔOD* with different time delays *Δt* deactivation pathways of excited species with the corresponding kinetics can be resolved.

A typical transient absorption system, as depicted in Figure 2.32, consists of a pulsed Titanium:Sapphire laser with a pulse width of 150 fs and a wavelength of 775 nm. The pulsed beam from the laser light source is split up into a pump and a probe beam by a beam splitter. In order to obtain different wavelengths of the pump pulse, second harmonic (SHG) or third harmonic generation (THG) are utilized, leading to excitation wavelengths of 387 and 258 nm, respectively. Alternatively, with the help of a two stage non-collinear optical parametric amplifier (NOPA), the pump pulse can be tuned to excitation wavelengths between 470 and 1200 nm as well as to their second harmonics. The probe beam, on the other hand, runs through a mirror system of variable path length along a delay line, is focused on a sapphire crystal to generate a continuum of white light and finally passes the sample. Since the speed of light is constant, the different path lengths Δx result in different time delays *Δt* of the probe and the pump pulse, which allows variable time delays between 0 and 8 ns. The probe pulse is subsequently detected by a CCD camera (Charge Coupled Device). The

differential spectrum (*ΔOD*) is obtained by measuring the absorbance of the sample with and without excitation at given time delays, which is possible by means of a chopper wheel in the pump beam blocking every second excitation pulse. The excited state lifetime of a fluorophore is derived from the exponential decay of the intensity.

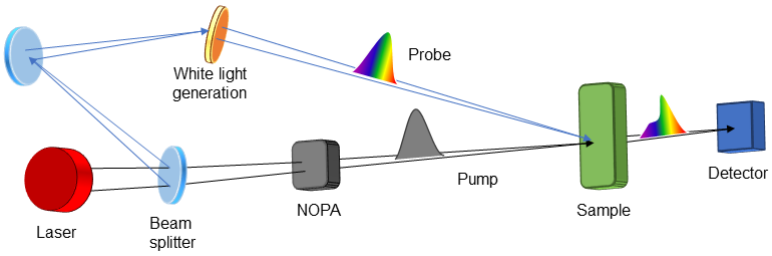

Figure 2.32. Schematic setup of a fs-TAS pump/probe system.

Studies on single component chromophores. We first turned our attention to the individual components. Based on a ground state absorption spectrum of Zn(II)Por **54** in toluene, in which Soret band transitions at 445 nm and Q-band transitions at 558 and 602 nm are discernible, 430 nm photoexcitation was selected for fs-TAS. The instantaneous population of the second singlet excited state with characteristic features at 486 and 782 nm is accompanied by ground state bleaching at 448 nm. A 0.5 ps lasting internal conversion is the predominate fate of the second singlet excited state and, in turn, leads to the formation of the first singlet excited state. Major singlet excited state features for Zn(II)Por are maxima at 487 and 580 nm and minima at 448, 560 and 617 nm. The fluorescence maximizes at 619 nm with an underlying fluorescence quantum yield of 0.086. The strongly fluorescent first singlet excited state transforms with 1.6 ns *via* intersystem crossing into to the poorly phosphorescent and long-lived triplet excited state. For Zn(II)Por **54**, the spectral characteristics of the triplet excited state include new maxima at 480 and 810 nm.

In F_{12}SubPc **56**, the absorption spectrum in toluene is composed of a Soret and a Q-band transition at 304 and 572 nm, respectively. Accordingly, we used in fs-TAS 550 nm photoexcitation, which resulted in the prompt formation of the first singlet excited state (^{1*}**56**). Here, the most notable features are maxima at 430 and 786 nm as well as minima at 517, 573 and 632 nm. On a timescale of 1.9 ns the triplet excited state of SubPc emerges and replaces the strongly fluorescent singlet excited state, for which a quantum yield of 0.17 was determined. The

presence of the correspondingly formed triplet excited state is corroborated by maxima at 450 and 615 nm as well as minima at 530 nm and 570 nm.

All of the aforementioned absorption and fluorescence features are in Zn(II)Pc **57** red-shifted relative to Zn(II)Por **54** and F_{12}SubPc **56**. For example, the Soret and Q-band transitions are discernible in toluene at 356 as well as 680 and 705 nm, respectively. The fluorescence maximizes with a quantum yield of 0.10 at 710 nm. For Zn(II)Pc **57**, 676 nm photoexcitation was selected for the fs-TAS measurements and the directly formed singlet excited state (^{1*}**57**) reveals maxima at 455, 635, 660, 760 and 822 nm and minima at 615, 647, 680, 710, and 796 nm. An intersystem crossing of 1.2 ns affords a prominent maximum at 492 nm, accompanied by maxima at 600, 632, and 660 nm as well as minima at 620, 648, and 708 nm. The latter are assigned to the long-lived triplet excited state (^{3*}**57**).

***Studies on dyads*.** Next, the Zn(II)Por-Zn(II)Pc **63** and Zn(II)Pc-SubPc **59** dyads were probed.

The absorption spectrum of Zn(II)Por-Zn(II)Pc dyad **63** in toluene is best described as the linear superimposition of the absorption spectra of the individual components, as in THF. On one hand, the Zn(II)Por Soret and Q-band transitions evolve at 451 and 572 nm, respectively and, on the other hand, those of Zn(II)Pc are seen at 710 and 331 nm. Not only that the transition energies in dyad **63** are identical to those of Zn(II)Por and Zn(II)Pc, but also the fact that the relative intensities/extinction coefficients are unchanged suggests lack of appreciable ground state interactions.

Notable are, however, the interactions in the excited state. From steady-state fluorescence measurements we derive that the Zn(II)Por fluorescence, with a quantum yield of 0.008, is strongly quenched and is subject to either an intramolecular energy or charge transfer. In addition, a low Zn(II)Pc fluorescence quantum yield of 0.015 suggests yet another deactivation process, that is, a charge transfer. Changes in solvent polarity (toluene, anisole, benzonitrile) only affect the Zn(II)Pc fluorescence quantum yields in the form of an overall lowering. To shed light onto the quenching of the Zn(II)Pc fluorescence we probed dyad **63** in fs-TAS experiments, using the polar anisole as solvent. Right after the conclusion of the laser pulse at 676 nm, the Zn(II)Pc singlet excited state with maxima at 513 and 605 nm as well as minima at 456 and 716 nm is populated. Due to a strong coupling with the ethynyl-bridged Zn(II)Por, the Zn(II)Pc singlet

excited state transforms rapidly within 11 ps into a delocalized excited state (Zn(II)Por−Zn(II)Pc)*. The latter is characterized by a stronger bleaching of the Zn(II)Por Soret band at 454 nm, a minimum at 716 nm as well as the growth of a transient at 595 nm. Hand-in-hand with the decay of the (Zn(II)Por−Zn(II)Pc)* state (101 ps) is the growth of a newly developing species with a maximum at 661 nm as well as a hypsochromically shifted ground state bleach (440 nm) of Zn(II)Por, which are attributed to the Zn(II)Por$^{\bullet+}$ radical cation.[163] Together with the simultaneously evolving transient at 470 and around 785 nm, which are assigned to the Zn(II)Pc$^{\bullet-}$ radical anion, we deduce the formation of a Zn(II)Por$^{\bullet+}$-Zn(II)Pc$^{\bullet-}$ charge-separated state.[164] On longer timescales, the Zn(II)Por$^{\bullet+}$-Zn(II)Pc$^{\bullet-}$ charge-separated state undergoes a charge shift with 182 ps to transform into TPA$^{\bullet+}$−Zn(II)Por−Zn(II)Pc$^{\bullet-}$. Evidence for the shift of the positive charge to the TPA unit comes from the decay of the Zn(II)Por's ground state bleach. The remaining transients are the Zn(II)Pc's ground state bleach at 714 nm as well as a slight maximum at 486 nm.

A change in polarity from toluene *via* anisole to benzonitrile impacts the excited state dynamics with 13, 11, and 7 ps for charge delocalization, 197, 101, and 19 ps for charge separation, 976, 182, and 63 ps for the charge shift and 10, 10, and 34 µs for charge recombination to the ground state, respectively.

When turning to Zn(II)Pc-SubPc dyad **59** in toluene, its absorption spectrum reveals Soret band transitions at 310 nm from SubPc and at 349 nm from Zn(II)Pc as well as Q-band transitions at 573 nm from SubPc and at 676/706 nm, accompanied by shoulders at 612/645 nm from Zn(II)Pc. Notably, these values are identical to the values determined for the individual components. In dyad **59**, the relative intensities/extinction coefficients are also in sound agreement with those of Zn(II)Pc and SubPc.

From steady-state fuorescence measurements, we derive that the SubPc fluorescence is strongly quenched and that its fluorescence quantum yield is 0.014. Evidence for an intramolecular energy transfer came from Zn(II)Pc fluorescence quantum yields as high as 0.22 while exciting SubPc. On the other hand, the Zn(II)Pc fluorescence quantum yields in toluene (0.10 compared to 0.30 of pure Zn(II)Pc) prompt, however, to an additional deactivation pathway. An increase in solvent polarity has no impact on the SubPc fluorescence quantum yields, but lowers the Zn(II)Pc fluorescence quantum yields. Due to the overall weak SubPc absorptions in dyad **59**, the focus of fs-TAS was only placed on excitation of Zn(II)Pc and on probing the latter pathway. To this end, 676 nm photoexcitation of **59** is associated with the Zn(II)Pc singlet excited state formation. It reveals maxima at 465, 598, 633, 659, 761, 826, and 983 nm and

minima at 617, 646, 681 and 706 nm, which are formed promptly. In toluene, the Zn(II)Pc singlet excited state undergoes fast (10 ps) vibrational relaxation, probably due to the presence of the free-rotating 3,5-bis(trifluoromethyl)phenyl substituents, followed by slow intersystem crossing (ISC) within 1.7 ns to populate the Zn(II)Pc triplet excited state. Turning towards more polar solvents, namely anisole and benzonitrile, instead of the slow ISC, a fast decay dominates the photoexcited state reactivity. In this context, it is important to mention that the one-electron oxidized Zn(II)Pc (broad transient around 840 nm), on one hand, and the one-electron reduced SubPc (bleaching at 578 nm, maximum at 504 nm), on the other hand, could be identified, respectively. In dyad **59**, formation of the Zn(II)Pc$^{\bullet+}$-SubPc$^{\bullet-}$ and Zn(II)Pc$^{\bullet-}$-SubPc$^{\bullet+}$ charge-separated states from photoexcited Zn(II)Pc are exergonic by about 0.3 eV and endergonic by about 0.7 eV, respectively. When comparing different solvent polarities, charge separation and charge recombination were determined as 478 ps / 2.5 ns, and 56/ 424 ps for anisole and benzonitrile solutions, respectively. The final product of this sequence is in all solvents the Zn(II)Pc triplet excited state.

***Studies on triad*.** In the final step, we performed ground- and excited state investigations with triad **65**.

The absorption spectrum in toluene features like those seen for dyad **63** and **59**, the Soret and Q-band transitions of Zn(II)Por, Zn(II)Pc, and SubPc. Analyses of the Q-band transitions at 710 and 573 nm, which are identical to those of SubPc, and Zn(II)Pc, respectively, confirm the absence of electronic interactions between the individual components.

We first conducted fs-TAS experiments with 676 nm photoexcitation to photoexcite Zn(II)Pc quantitatively in anisole solution of the triad.[i]

Initially, the Zn(II)Pc singlet excited state is formed with its characteristic maxima at 507, 602, and 983 nm and minima at 457 and 720 nm. It is rather short-lived and its decay (7.8 ps) is, similarly to what we have observed in the case of dyad **63**, synchronous with the formation of the delocalized state (Zn(II)Por−Zn(II)Pc)*, characterized by an intensified bleaching at 456 nm and the growth of the transient at 600 nm. The subsequent hypsochromic shift of the ground state bleach from 456 to 444 nm as well as the growth of the transient at 668 nm within 67 ps are attributed to the formation of the Zn(II)Por$^{\bullet+}$ radical cation, whereas the

[i] Please note that laser excitation was only conducted in anisole and benzonitrile due to the aforementioned lack of any charge separation in dyad **63** in toluene.

prominent maxima at 592 and 808 nm are indicative of the Zn(II)Pc$^{\bullet-}$ radical anion, which implies the formation of a Zn(II)Por$^{\bullet+}$-Zn(II)Pc$^{\bullet-}$-SubPc charge-separated state. The latter is followed by a charge shift (83 ps) from Zn(II)Pc to SubPc under population of the Zn(II)Por$^{\bullet+}$-Zn(II)Pc-SubPc$^{\bullet-}$ charge-separated state. Corroboration comes from the prominence of the SubPc's ground state bleach at 578 nm as well as the sharp maximum at 507 nm, which are both indicators of the SubPc$^{\bullet-}$ radical anion. Now, while SubPc$^{\bullet-}$ is persistent, Zn(II)Por$^{\bullet+}$ is found to decay, as evidenced by the regression of the ground state bleach of the Zn(II)Por at 450 nm. Importantly, its decay (1.4 ns) relates kinetically to the growth of TPA$^{\bullet+}$ under formation of TPA$^{\bullet+}$−Zn(II)Por−Zn(II)Pc$^{\bullet-}$. The latter is followed by a 4.3 ns charge recombination. In benzonitrile, charge delocalization is 4.4 ps, charge separation 30 ps, charge shift to SubPc 31 ps, charge shift from TPA to Zn(II)Por 313 ps, and charge recombination 11.2 ns. The final product of this sequence is in both solvents the Zn(II)Pc triplet excited state (46/40 µs), which is the lowest in energy among the three components, characterized by a Zn(II)Pc ground state bleach at 714 nm as well as a slight maximum at 486 nm.

2.3.3.2 Zn(II)Por-Zn(II)Pc-graphene ensembles

Synthesis and characterization

The second class of multicomponent systems was prepared by an unsymmetric functionalization of Pc **12** with the same Zn(II)Pors as donor components, and a pyrene moiety in the opposite isoindole, which can lead to stable Por–Pc–graphene ensembles by liquid-phase graphene exfoliation assisted by the pyrene moiety.

To develop this task, we planned first to functionalize the central Pc with the commercially availabe pyrene derivative, and introduce the elaborated Zn(II)Por unit in the last step. Scheme 2.16 shows the first approach towards the preparation of a Pc-pyrene ensemble (i.e., **67**) through the functionalization of one isoindole of Pc **12** with 4-(hydroxymethyl) phenyl boronic acid by Suzuki – Miyaura coupling, and a subsequent esterification of the benzyl alcohol with 1-pyrenebutyric acid under Steglich conditions.[165]

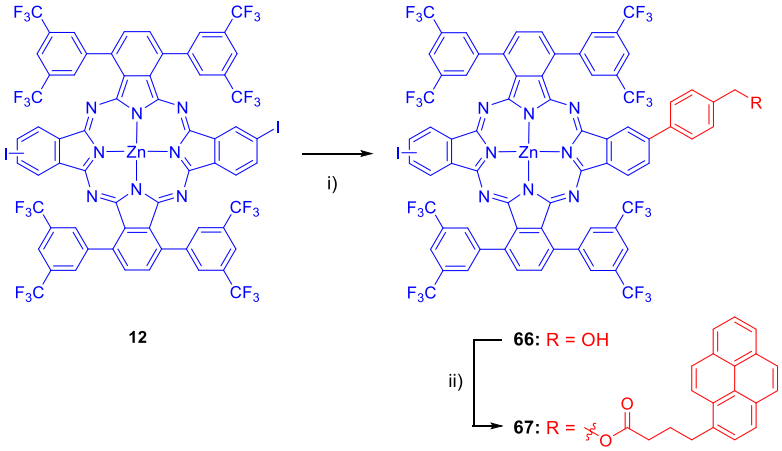

Scheme 2.16. Synthesis of Pc **66** and **67**. Conditions: i) 4-(hydroxymethyl) phenyl boronic acid, $Pd(PPh_3)_4$, K_2CO_3, DMF, 90°C, 42%; ii) 1-pyrenebutyric acid, DCC, DMAP, THF, r.t., 18%.

Unexpectedly, the following Sonogashira coupling between **67** and the deprotected Zn(II)-Pors **60** or **62** afforded a mixture of compounds, none of which corresponded to the expected triad. It seems that the presence of the pyrene somehow changes the rectivity of the system. After this result, we changed our synthetic strategy (Scheme 2.17), performing first the synthesis of Por-Pc dyads **68** and **69**. The idea was to use Pc **66**, having only one iodine atom susceptible to react with the correponding ethynyl Por, thus avoiding undesired losses of the

elaborated Por molecules. The reaction between Pc **66** and deprotected ethynyl Pors **60** and **62** was carried out under copper-free Sonogashira conditions. Unfortunatly, **69** was obtained in very low yield, and the main compound of this reaction was a Por-Por dyad as a result of a homocouplig process, despite the copper-free conditions. The low amount of **69** obtained in several reactions made us discard this dyad for further functionalization and studies. For this reason, we decided to focus our efforts on dyad **68**, which was obtained in an acceptable 47% yield and could be subsequently subjected to an esterification of the terminal benzyl alcohol moiety with 1-pyrenebutyric acid to afford the final triad **70** (Scheme 2.17).

The structure of triad **70** was unequivocally confirmed by HR-MALDI-TOF mass spectrometry, UV−vis, IR and NMR.

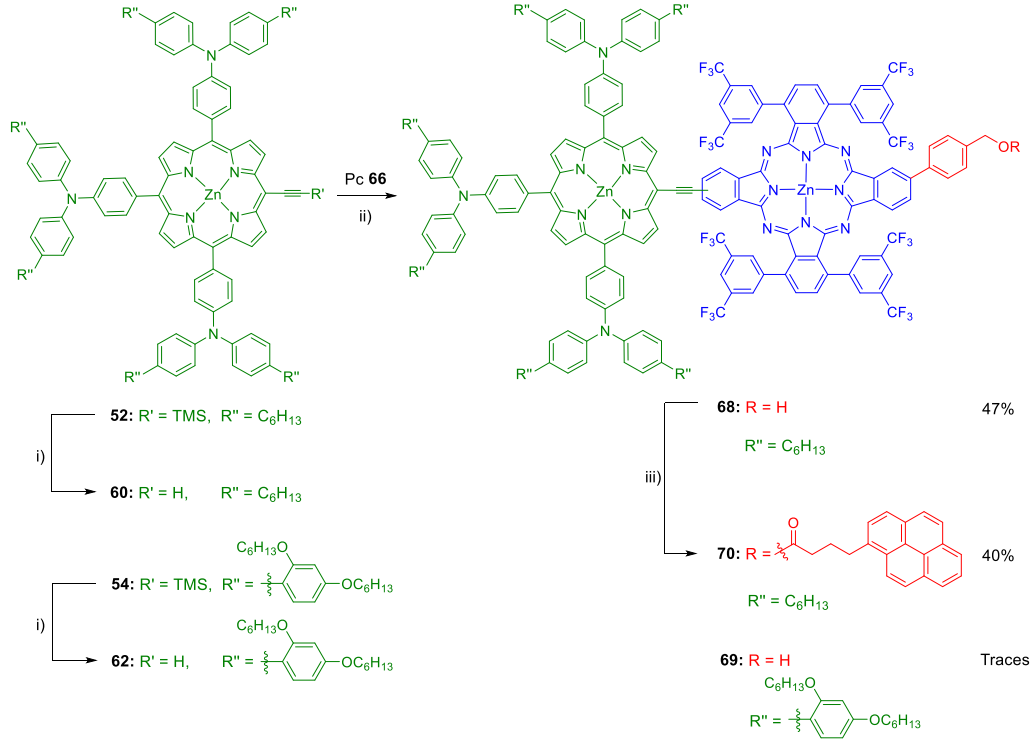

Scheme 2.17. Synthesis of Por-Pc-pyrene triad **70**. Conditions: i) TBAF, THF, 0°C; ii) Pc **66**, $Pd_2(dba)_3$, $AsPh_3$, THF/NEt_3 (2:1), 60°C; iii) 1-pyrenebutyric acid, DCC, DMAP, THF, r.t..

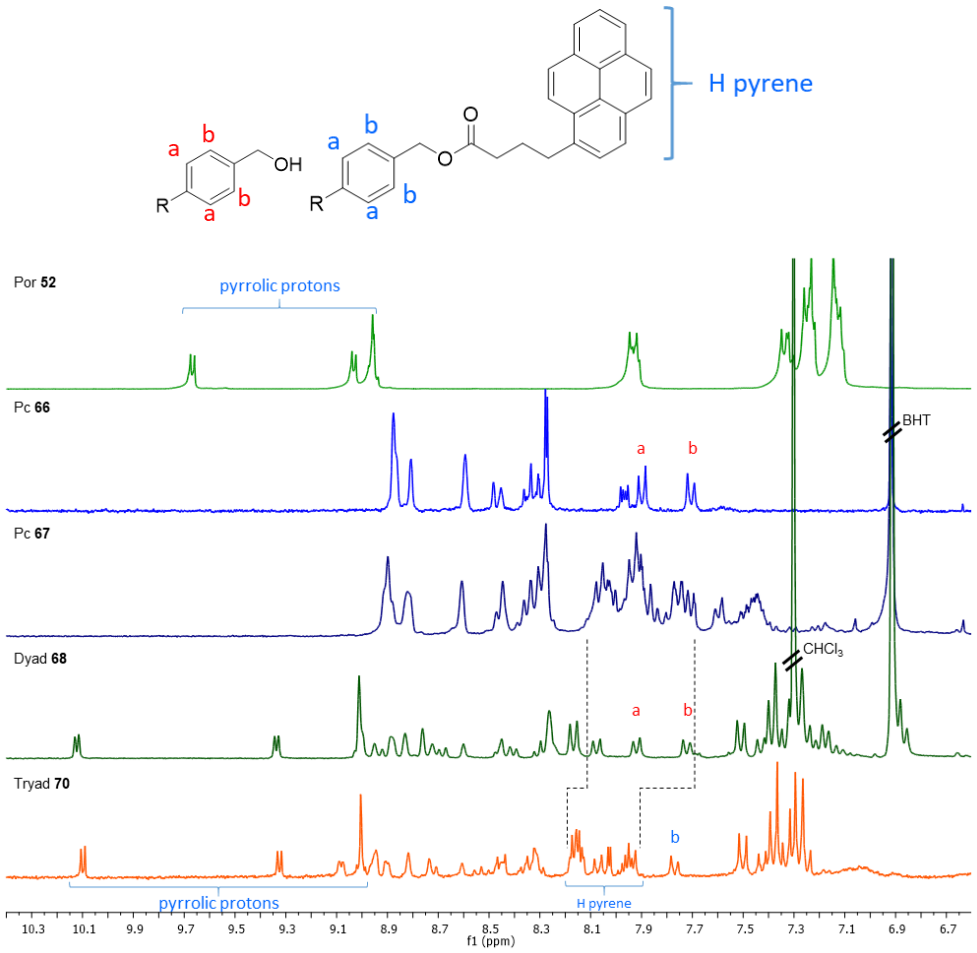

Figure 2.39. Comparison of ^{1}H-NMR spectra of **52** in $CDCl_3$, **66**, **67**, **68** and **70** in THF-d_8. Lines are drawn to guide the eye to the changes in chemical shifts of protons of pyrene functionalization.

Figure 2.39 compares the ^{1}H-NMR spectra of the individual Por and Pc components, **52** and **66** respectively, Pc-pyrene **67**, Por-Pc dyad **68** and Por-Pc-pyrene ensemble **70**. Also in this case, despite the complexity of these systems, it is possible to distinguish protons of the different components. More importantly, it is possible to discriminate the protons of the pyrene funcionalization in **67** and **70** (Figure 2.39).

As in the case of triad **65**, comparing the UV-vis spectra of the individual components with that of **70**, it is possible to appreciate the combination of typical bands of each single component in the final system **70** (Figures 2.40, 2.41 and 2.42). Pc **66** and **67** are first compared. These compounds differ just in the

presence of the pyrene group and, in fact, their UV−vis spectra show the same split Q band, while differing in the region between 250 and 350 nm, where the sharp absorptions of pyrene appear (Figure 2.40). Similarly, the UV-vis spectrum of dyad **65** shows the B- and Q-bands typical of Por **52** and Pc **66** respectively (Figure 2.41), but, noteworthy, dyad **68** exhibits a non-split, broadened Q-band because of the electronic communication with the donor Por. Finally, dyad **68** and triad **70** are compared in Figure 2.42. As expected, the UV-vis spectra of these compounds differ in the region between 250 and 350 nm, due to the characteristic bands of pyrene, and share identical shape in the rest of the spectra.

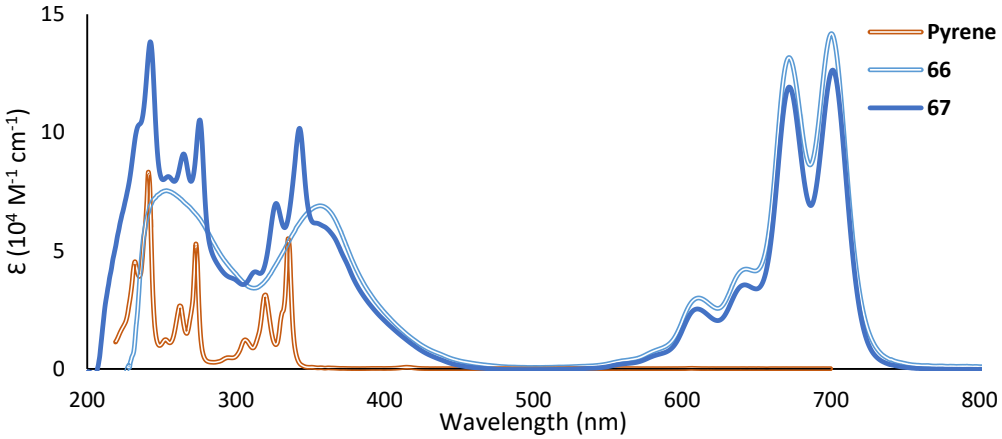

Figure 2.40. Comparison of UV-vis spectra of Pcs **66** and **67** in THF, and pyrene in cyclohexane.

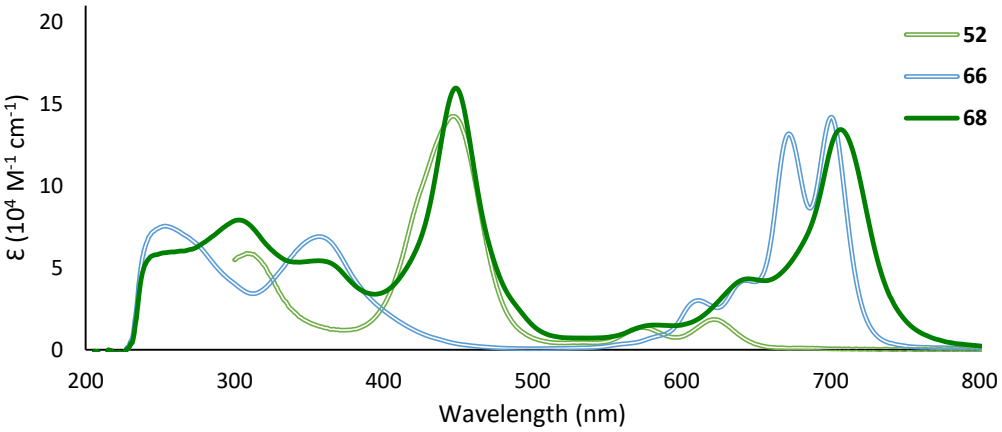

Figure 2.41. Comparison of UV-vis spectra of Por **52**, Pc **66** and Por-Pc dyad **68** in THF.

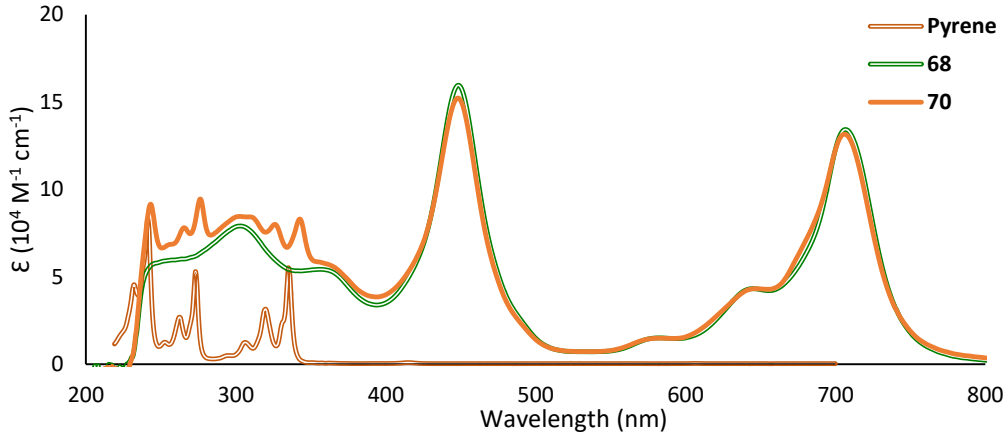

Figure 2.42. Comparison of UV-vis spectra of Por-Pc dyad **68** and Por-Pc-pyrene triad **70** in THF, and pyrene in cyclohexane.

Electrochemical studies

We performed electrochemical studies using cyclic voltammetry and square wave measurements to determine the redox potentials and the corresponding HOMO-LUMO energy values of the Zn(II)Por and the Zn(II)Pc components, in order to evaluate if, after excitation of any of the chromophores, cascade – like charge transfer processes could take place from the Zn(II)Por to the graphene sheet. Table 2.5 compiles the redox values registered for reference compounds **52** and **66**. Unfortunately, no well-defined cyclic voltammogram could be obtained for triad **70**. Together with the respective oxidation/reduction potentials, table 2.5 summarizes also the HOMO/LUMO values *vs.* vacuum of the single components, obtained using the approximation of Equation 2.3.[139] In this case, the optical ($E_{0\text{-}0}$) bandgap was used to obtain the LUMO value of **52** due to the difficulty to obtain an accurate value of its $E_{red}^{1/2}$.

Table 2.5. First oxidation and reduction potentials, optical bandgap and HOMO/LUMO levels for Por **52** and Pc **66**.

	$E_{ox}^{1/2}$ [V *vs* Fc/Fc$^+$]	$E_{red}^{1/2}$ [V *vs* Fc/Fc$^+$]	$E_{0\text{-}0}$ [eV]	HOMO [eV]	LUMO [eV]
52	0.25 [a]	-	1.97	- 5.4 [d]	- 3.4 [c]
66	0.47 [b]	-1.21 [b]	-	- 5.6 [c]	- 3.9 [c]

[a] Quasi-reversible. [b] Reversible. [c] Calculated using Equation 2.3. [d] Calculated using $E_{0\text{-}0}$.

From the previous data, it can be concluded that the HOMO of the triad **70** is centered in the Por component, while the LUMO is mostly located in the Pc acceptor, as otherwise expected. A schematic representation of the HOMO/LUMO energy values of the single components is depicted in Figure 2.43. From this HOMO/LUMO distribution, it seems plausible that, after excitation of any of the components of the triad, photoinduced, cascade – like charge transfer processes could take place from the Por component to the graphene sheet. Also in this case, the central Pc is capable to perform the anticipated dual role of accepting energy/electrons from the Por unit and transferring electrons to the acceptor graphene.

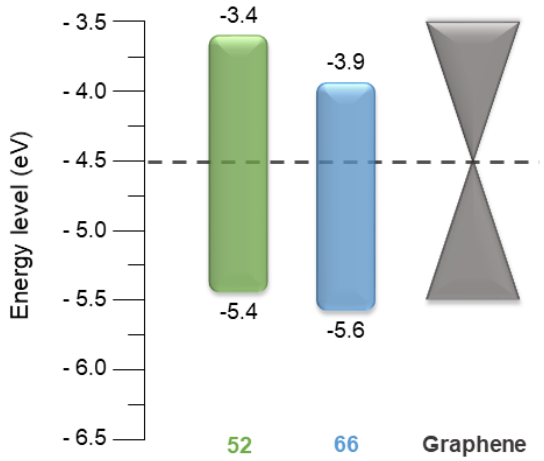

Figure 2.43. Schematic energy-levels diagram of Por **52**, Pc **66** and graphene.

Preliminary exfoliation experiments. Nanohybrid formation.

The preparation of the desired hybrid systems, that are **67**/graphene and **70**/graphene, was carried out by exfoliation of graphite *via* ultrasonic treatment in the presence of Pc-pyrene **67** or Por-Pc-pyrene **70** in THF. An efficient procedure consisted in adding graphite to a 1 x 10^{-5} M solution of either **67** or **70** in THF and ultrasonicating the mixtures for 40 minutes. The resulting dispersions were then centrifuged for 15 min at 500 rpm. Then, the supernatant was extracted and used for further enrichment cycles, that is, the addition of graphite, ultrasonication and centrifugation under the same conditions. The stability of all the dispersions was carefully tested by steady-state absorption spectroscopy before and after ultrasonication to monitor and identify any resulting spectral changes.

Regarding nanohybrid **67**/graphene, our enrichment approach led to new absorption features in the spectra of the THF dispersions recorded in steady-state absorption spectroscopic measurements (Figure 2.44). On one hand, graphene that is present within the dispersions contributes to the overall increase in optical density, especially in the blue region of the spectra. On the other hand, a new band absorption around 470 nm, and a slight blue-shift of the Zn(II)Pc Q bands is a preliminary result which demonstrates the interaction of **67** with the basal plane of graphene.

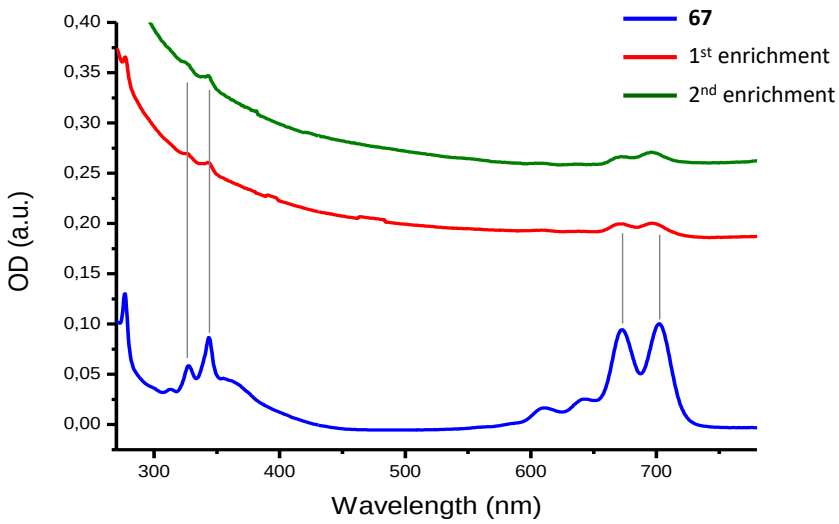

Figure 2.44. Absorption spectra of **67**/graphene in THF following the 1st and 2nd exfoliation/enrichment steps.

Relating to the **70**/graphene nanohybrid, a parallel study was performed using simple absorption spectroscopic measurements. In this case, the enrichment approach led to a similar behaviour than the **67**/graphene nanohybrid, namely the increase in optical density of graphene in the blue region of the spectra, a new band absorption around 470 nm, and a slight blue-shift of the Zn(II)Pc Q band (Figure 2.45).

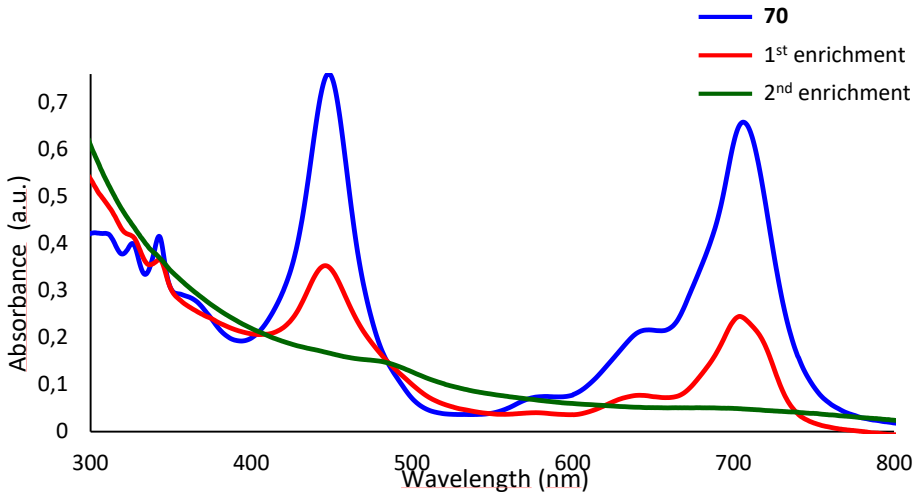

Figure 2.45. Absorption spectra of **70**/nanographene in THF following the 1st and 2nd exfoliation/enrichment steps.

This preliminary study can be considered an initial proof of the interaction of **67** with the basal plane of graphene. In addition to steady-state absorption spectroscopy, Raman measurements, AFM and TEM images are under process in the laboratory of Prof. Dirk Guldi at the Friederich-Alexander University in Erlangen, Germany, in order to complete the study of both **67**/graphene and **70**/graphene nanohybrids.

2.4 Summary and conclusions

In this chapter, the synthesis and characterization of novel linear donor–π–acceptor systems based on Pcs have been presented, taking advantage of the availability of **ABAB** Pcs with crosswise reactive groups that permit further chemical transformations.

Initially, the preparation, study and application of a battery of Pcs with a linear push-pull substitution pattern as potential photosensitizers for DSSCs have been reported. The aim here is to optimize the photosensitization efficiency, which is governed by the electronic distribution, and photo-injection abilities of the different Pcs.

This family of Pcs was obtained by unsymmetric functionalization of the **ABAB**, crosswise-functionalized Pc **12** with different electron – donor and electron – acceptor/anchoring groups. The well-known bis(4-hexylphenyl)amine and the 4-ethynyl-*N,N*-dimethylaniline were chosen as donor groups; on the other hand, a carboxylic acid was selected as anchoring group to the TiO_2 for all dyes, which is separated from the Pc core by either a triple bond or a ethynyl-BTD moiety as spacers. Functionalization of **12** was carried out using Pd-catalyzed methodologies (Shonogashira, Buchwald-Hartwig) to introduce the amino-type electron-donor groups and the carboxy-type anchoring moieties. Therefore, compounds **30**, **39** and **45** were achieved.

The electronic features of these derivatives have been studied using cyclic voltammetry and square wave measurements, together with DFT and TDDFT calculations. In general, it was observed that the direct linkage of the diphenylamino group has a strong impact on the HOMO of the Pc macrocycle. In fact, the oxidation potential of compounds **39** and **45** are 120 and 160 mV lower than that of **30**, respectively. On the other hand, incorporation of the BTD unit between the Pc core and the COOH group in **45** has a reduced influence on the electronic properties of the Pc (Figure 2.46). DFT and TDDFT calculations showed that, in all three dyes, the HOMO has extended delocalization towards the donor moiety. However, the LUMO has a slight delocalization onto the acceptor group for Pcs **30** and **39** and is rather centered in the Pc core for **45**. (Figure 2.46). These results may explain, in part, the low efficiency values found in the respective DSSCs prepared with these three push-pull phthalocyanines, namely, 1.92%, 2.43% and 1.09% for **30**, **39** and **45** respectively. The preparation of the cells and the efficiency assessment have been performed in the group of Prof. Gräzel in École Polytechnique Fédérale de Lausanne (EPFL), Switzerland.

From these results we can conclude that the linear push-pull arrangement does not improve the efficiency achieved by the Pc benchmarks, like the so-called **TT40**, which has the typical **A_3B** distribution of three donor groups and anchoring moiety. Although the presence of the 3,6-trifluoromethylphenyl substituents is necessary for the synthesis of Pcs with a linear arrangement of the donor/acceptor groups, their strong electron-withdrawing nature probably limits the photoinduced electron injection in the semiconducting material.

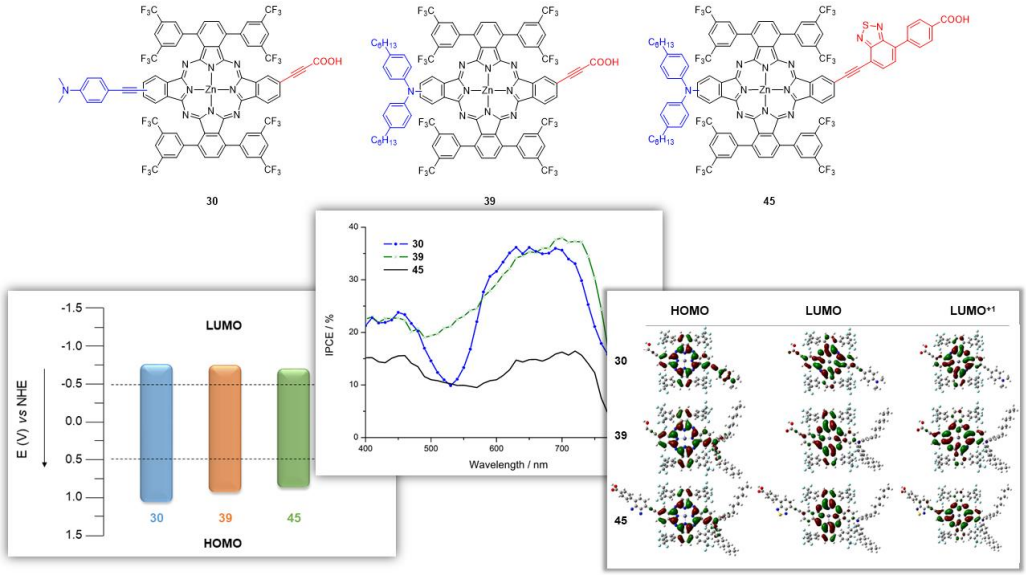

Figure 2.46. Graphical abstract of the results obtained in section *2.3.1* and *2.3.2*.

In the second part of this chapter, the preparation, and structural and photophysical characterization of new linear donor-π-acceptor multicomponent systems containing Pc units as central cores of the arrangement have been reported. The synthesis of these assemblies was carried out by an asymmetric functionalization of the **ABAB** Pc **12** with different redox-active units, performing respectively as donors or acceptors with regard to the central Pc core.

Firstly, we have succesfully prepared Zn(II)Por-Zn(II)Pc-SubPc triad **65**, bearing a Zn(II)Por and a SubPc as final donor and acceptor elements, respectively. The preparation of the triad was accomplished through an appropriate sequence of Pd-catalyzed coupling reactions over Pc **12**. Importantly, SubPc holds twelve F atoms to reduce the energy of its LUMO, and the Zn(II)Por is functionalized with TPA substituents in the *meso*-positions to increase its HOMO. With such a functionalization, an adequate energy level alignment of the Por, Pc and SubPc

components was achieved, facilitating a sequential, cascade-type charge separation. In fact, after photoexcitation of the central Pc component, the formation of Zn(II)Por$^{\bullet+}$-Zn(II)Pc$^{\bullet-}$-SubPc charge-separated state was observed, followed by a charge shift from Zn(II)Pc to SubPc under population of the Zn(II)Por$^{\bullet+}$-Zn(II)Pc-SubPc$^{\bullet-}$ charge-separated state. (Figure 2.47).

In addition, we have successfully prepared a second triad bearing an analogue tris(TPA)-Zn(II)Por as donor component, and a pyrene moiety in the opposite isoindole. Also this system was obtained through asymmetric functionalization of **12** using Pd-catalyzed methodologies and a subsequent esterification under Steglich conditions. Taking advantage of the presence of the pyrene moiety, triad **70** and dyad **67** can be exploited for the exfoliation of graphite, obtaining hybrid systems, that are **67**/nanographene and **70**/nanographene *via* ultrasonic treatment. Preliminary studies of stability of all the dispersions was tested by steady-state absorption spectroscopy before and after ultrasonication to monitor and identify any resulting spectral changes. In addition to steady-state absorption spectroscopy, Raman measurements, AFM and TEM images are under process in the laboratory of Prof. Dirk Guldi at the Friederich-Alexander University in Erlangen, Germany, in order to complete the study of both nanohybrids **67**/nanographene and **70**/nanographene, and obtain a photoinduced charge-separated state.

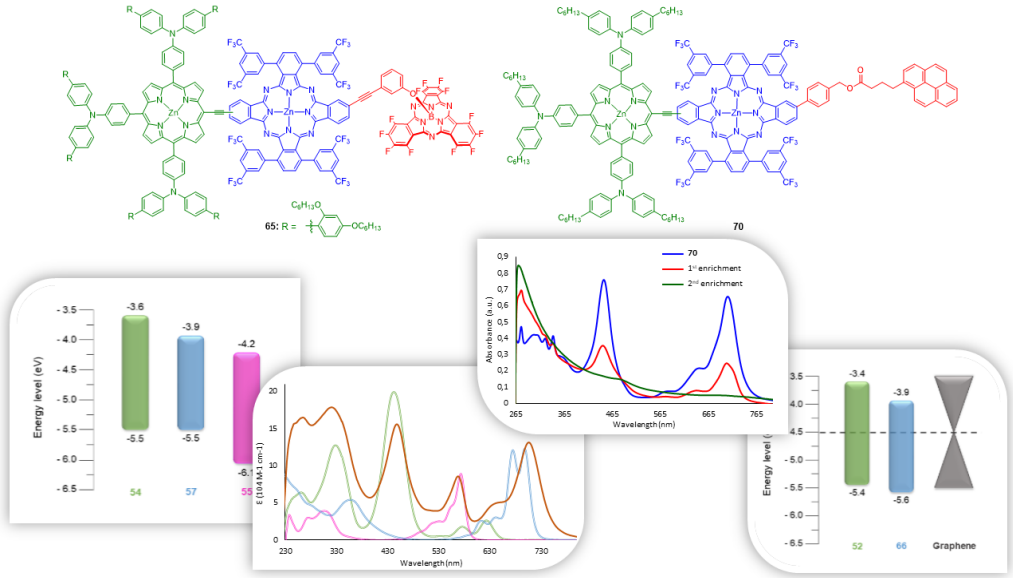

Figure 2.47. Graphical abstract of the results obtained in section *2.3.3*.

2.5 Experimental section

In this *Experimental section*, the preparation and characterization of the compounds has been organized following the order as they appear in the text.

2.5.1 Specific Methods in Chapter 2

Cyclic Voltammetry (CV) and Square Wave Voltammetry (SWV): Electrochemical measurements were performed on an Autolab PGStat 30 equipment using a three electrode configuration system. The measurements were carried out using freshly distilled THF solutions containing 0.1 M tetrabutylammonium hexafluorophosphate ($TBAPF_6$) and a concentration of approximately 10^{-4} M of the corresponding compound. A glassy carbon electrode (3 mm diameter) was used as the working electrode, and a platinum wire and an $Ag/AgNO_3$ (in CH_3CN) electrode were employed as the counter and the reference electrodes, respectively. Ferrocene (Fc) was used as an internal reference and all the potentials were given relative to the Fc/Fc+ couple. Scan rate was 100 mV s^{-1} unless otherwise specified.

Theoretical Calculation: DFT and TDDFT calculations have been performed using the Gaussian 09 Revision B.01 package.[166] The ground state geometries have been optimized using the popular B3LYP exchange-correlation functional[167] with the 6-31G(d) basis set and a LANL2DZ pseudopotential[168] for the Zn atom. All optimized geometries have been confirmed by computation of the harmonic vibrational frequencies at the same level of theory (B3LYP/6-31G(d)/LANL2DZ). The vertical electronic transitions have been computed using the wB97xD functional[169] with the 6-31G(d) basis set for all atoms, the first 15 excited singlet states have been calculated for the Pcs. In all calculations the solvent effect has been taken into account using a Self-Consistent Reaction Field (SCRF) with the CPCM method as implemented in Gaussian09.[170]

Femtosecond and nanosecond transient absorption spectroscopy: pump probe experiments were performed in Friederich-Alexander University in Erlangen, with an amplified Ti:Sapphire CPA-2110 fs laser system (Clark MXR: output 775 nm, 1 kHz, 150 fs pulse width) using transient absorption pump/probe detection systems (Helios and Eos, Ultrafast Systems). The 530 and 656 nm excitation wavelengths were generated with a noncolinear optical parametric amplifier (NOPA, Clark MXR). Fluorescence lifetimes were determined by the time correlated single photon counting technique using a FluoroLog3 emission spectrometer (Horiba JobinYvon) equipped with an R3809U-58 MCP (Hamamatsu) and a 405LH laser diode (Horiba JobinYvon) exciting at 403 nm

(675 ps fwhm) as well as a 650L laser diode (Horiba JobinYvon) exciting at 647 nm (<200 ps fwhm).

Optical characterization. Steady-state absorption spectra were recorded with a Perkin-Elmer Lambda 35. Steady-state emission spectra were recorded with a Fluoromax-3-spectrometer from HORIBA Jobin Yvon. All samples were measured in a fused quartz glass cuvette with a diameter of 10 mm.

Materials. Graphite flakes (+100 mesh (≥75% min) were purchased from Aldrich. All other reagents were purchased from commercial suppliers and used without further purification.

2.5.2 Device preparation and photovoltaic characterization

Photoanode preparation: A transparent fluorine-doped tin oxide conducting glass (NSG10) was cleaned using ethanol and water followed by an ultrasonic cleaning in Deconnex^{TM} solution for 30 min. The electrodes were then washed with water and ethanol. To remove the organics, a further thermal treatment was done at 500 °C for 30 min. The clean FTO glass were treated twice with $TiCl_4$ (40 mM, 30 min, 75 °C). Two different TiO_2 pastes (transparent layer and scattering layer) were screen printed on to the $TiCl_4$ pretreated electrode and followed a series sintering step as described elsewhere in the literature.[171] A 9 µm thickness for the transparent layer (20 nm particles with a pore diameter of 32 nm) and another 5 µm for the scattering layer (400 nm particles) were estimated. The photoanodes were further treated with $TiCl_4$ following the steps described above.

Device fabrication: The TiO_2 electrodes were dried at 500°C for 30 min prior to the sensitization in the dye solution. The dye solutions were composed of 0.1 mM of Pc in THF. After 14–18h of dipping, the electrodes were washed with EtOH to remove the loosely bounded dye molecules. The counter electrodes were made by drop casting of isopropanolic solution of H_2PtCl_6 (5 mM) onto a pre-cleaned FTO glass (TEC7, Solaronix, Switzerland) and the electrodes were fired at 410 °C for 30 min. The sensitized photoanode and counter electrode were melt sealed using a 25 µm polymeric spacer (Surlyn^{TM}, Dupont, USA). The electrolyte in acetonitrile was then injected by the vacuum backfilling process through a hole drilled at the side of the counter electrode. The cell fabrication was completed by melt sealing the hole with a glass and soldering the metal solder to make contacts.

Photovoltaic characterization: A 450W xenon lamp (Oriel, USA) was used as a light source. The spectral output of the lamp was filtered using a Schott K113 Tempax sunlight filter (Präzisions Glas & Optik GmbH, Germany) to reduce the mismatch between the simulated and actual solar spectrum to less than 2%. The current-voltage characteristics of the cell were recorded with a Keithley model 2400 digital source meter (Keithley, USA). The photoactive area of 0.159 cm] was defined by a black metal mask. The values reported are for the best devices obtained in each configuration. Four-to-five cells were made for each condition.

Dye-loading measurements: For dye-loading measurements, the TiO_2 electrodes consisted of a 9 µm thick TiO_2 active layer (no scattering layer). The sensitisation of the photoanodes was done following the same procedure described above for the preparation of the device (dye-uptake solution 0.1 mM

of Pc in THF and dipping time 14–18h). The amounts of dye-loading for Pcs **27**, **36** and **42** were then determined from the desorption of the dye molecules by immersion of the sensitized films in a 0.1 M basic solution of tetrabutylammonium hydroxide in DMF and the calibrated absorption spectra of each dye.

2.5.3 Synthesis of novel donor-π-acceptor substituted Pcs for DSSCs

*1,4,15,18-Tetrakis(3,5-bis(trifluoromethyl)phenyl)-9-(3'-hydroxypropyn-1-yl)-23[24]-iodo zinc (II) phthalocyanine (**27**)*

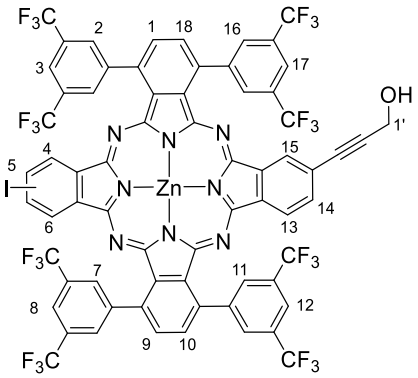

To a solution of **12** (0.036 mmol, 60 mg) in freshly distilled THF (3 mL) were added Et_3N (1 mL), $Pd(PPh_3)_4$ (5% mol, 2 mg) and CuI (10% mol, 0.7 mg). The mixture was deoxygenated by bubbling argon through it for 20 min. Propargylic alcohol (0.036 mmol, 2.1 µL) was subsequently added and the mixture was stirred at 50ºC for 4 h. Then, solvents were evaporated and the crude mixture was dissolved in CH_2Cl_2 and washed with water. The combined organic layers were dried over $MgSO_4$ and concentrated in vacuo. Purification by column chromatography on silica gel (heptane / THF 4:1) gives the desired product as a blue solid. Yield: 48 mg, 83%

^{1}H-NMR (300 MHz, THF-d_8), δ (ppm): 8.84 (s, 4H; H-2, H-7), 8.77 (2 x s, 4H; H-11, H-16), 8.64 (s, 2H; H-3, H-8), 8.57 (s, 2H; H-12, H-17), 8.53 (d, *J* = 9.1 Hz, 1H; H-6), 8.32 – 8.25 (m, 6H; H-1, H-9, H-10, H-18, H-5, H-14), 8.25 – 8.18 (m, 1H; H-15), 8.08 – 7.93 (m, 2H; H-4, H-13), 4.62 (d, *J* = 5.9 Hz, 2H; H-1'), 4.50 (d, *J* = 5.7 Hz, 1H; OH).

HR-MS (MALDI) m/z Calcd for $[C_{67}H_{25}F_{24}IN_8OZn]$: 1604.0104; Found: 1604.0137.

UV-Vis (THF), λmax (log ε): 695 (4.92), 677 (4.93), 616 (4.28) 356 (4.57) nm.

IR (KBr) ν^{-1} (cm^{-1}): 3641, 3385, 2953, 2926, 2858, 1649, 1380, 1272, 1137, 894, 840, 745, 705.

Mp > 250°C.

*1,4,15,18 - Tetrakis(3,5-bis(trifluoromethyl)phenyl) – 9 - (3'-hydroxypropyn–1-yl) - 23 [24] - ((4-(dimethylamino)phenyl)ethynyl) zinc (II) phthalocyanine (**28**)*

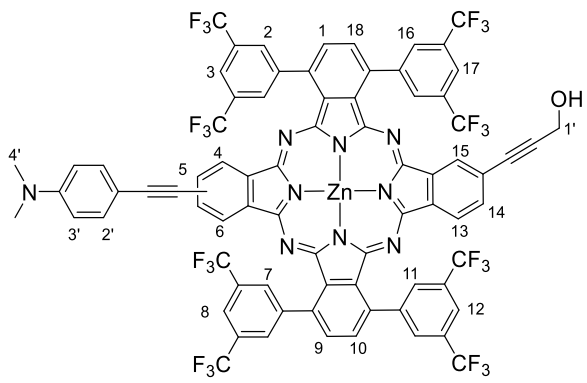

To a solution of **27** (0.03 mmol, 48 mg) in freshly distilled THF (3 mL) were added Et_3N (1 mL), $Pd(PPh_3)_4$ (5% mol, 1.7 mg) and CuI (12% mol, 0.7 mg) and 4-ethynyl-*N,N*-dimethylaniline (0.045 mmol, 6.5 mg). The mixture was deoxygenated by bubbling argon through it for 20 min. After that the mixture was stirred at 50ºC for 18 h. Then, solvents were evaporated and the crude mixture was dissolved in CH_2Cl_2 and washed with water. The combined organic layers were dried over MgSO4 and concentrated in vacuo. Purification by column chromatography on silica gel (heptane / THF 10:1, then 5:1 and 3:1) gives the desired product as a green solid. Yield: 43 mg, 88%.

^{1}H-NMR (300 MHz, THF-d_8), δ (ppm): 8.80 (m, 8H; H-2, H-7, H-11, H-16), 8.64 (s, 2H; H-3, H-8), 8.58 (s, 2H; H-12, H-17), 8.32 (s, 1H; H-6), 8.26 (m, 4H; H-1, H-9, H-10, H-18), 8.22 (m, 3H; H-13, H-14, H-15), 8.01 (d, *J* = 7.8 Hz, 1H; H-5), 7.96 (d, *J* = 7.8 Hz, 1H; H-4) 7.62 (d, *J* = 8.9 Hz, 2H; H-2'), 6.91 (d, *J* = 8.9 Hz, 2H; H-3'), 4.61 (d, *J* = 6.3 Hz, 2H; H-1'), 4.51 (t, *J* = 6.3 Hz, 1H; OH), 3.09 (s, 6H; H-4').

HR-MS (MALDI) m/z Calcd for [$C_{77}H_{35}F_{24}N_9OZn$]: 1621.1873; Found: 1621.1883.

UV-Vis (THF), λmax (log ε): 700 (5.11), 687 (5.15), 623 (4.50) 354 (4.81) nm.

IR (KBr) ν^{-1} (cm^{-1}): 3641, 3371, 2953, 1603, 1374, 1279, 1131, 901, 803, 753, 712.

Mp > 250°C.

*1,4,15,18 - Tetrakis(3,5-bis(trifluoromethyl)phenyl) - 9 - (carboxyethynyl)- 23 [24] - ((4-(dimethylamino)phenyl)ethynyl) zinc (II) phthalocyanine (**30**)*

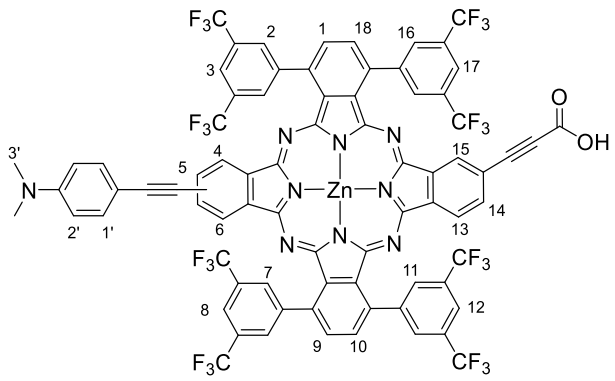

To a stirred solution of periodinane 1-hydroxy-1,2-benziodoxole-3(1H)-one-1-oxide (IBX) (0.117 mmol, 33 mg) in DMSO (2 mL) was added at once a solution of **28** (0.026 mmol, 43 mg) in THF / DMSO 1:1 (2 mL). The mixture was left stirring at 30ºC for 4h (TLC). After the complete oxidation of alcohol group to aldehyde one, *N*-hydroxysuccinimide (1.17 mmol, 134 mg) was added at once and the mixture was left stirring at 40ºC for 22 h. Then the mixture was washed with water and NH_4Cl. The combined organic layers were dried over $MgSO_4$ and concentrated in vacuo. Trituration with heptane gives the desired product as a green solid. Yield: 38 mg, 90%.

^{1}H-NMR (300 MHz, THF-d_8), δ (ppm): 10.80 (s, 1H; COOH), 8.84 (s, 8H; H-2, H-7, H-11, H-16), 8.75 (s, 1H; H-15), 8.65 (s, 1H; H-14), 8.59 (s, 4H; H-3, H-8, H-12, H-17), 8.28 (m, 4H; H-1, H-9, H-10, H-18), 8.19 (d, *J* = 7.9 Hz, 2H; H-13), 7.62 (s, 2H; H-5), 7.52 (s, 2H; H-4), 7.26 (d, *J* = 8.7 Hz, 2H; H-1'), 6.89 (d, *J* = 8.7 Hz, 2H; H-2'), 2.95 (s, 6H; H-3').

HR-MS (MALDI) m/z Calcd for [$C_{77}H_{33}F_{24}N_9O_2Zn$]: 1635.1665; Found: 1635.1638.

UV-Vis (THF), λmax (log ε): 691 (4.58), 623 (3.89), 354 (4.23) nm.

IR (KBr) ν^{-1} (cm^{-1}): 3302, 2932, 1721, 1642, 1615, 1383, 1272, 1137, 678, 610.

Mp > 250°C.

*Bis(4-hexylphenyl)amine (**31**)*[134]

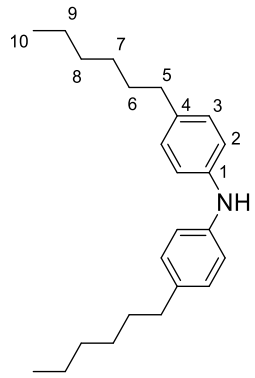

4-Hexylaniline (2.16 mmol, 382 mg), 4-hexyloxybromobenzene (2.38 mmol, 574 mg), $Pd_2(dba)_3$ (0.0216 mmol, 19.7 mg), NaO^tBu (3.67 mmol, 353 mg) were placed in a Schlenk tube. Several vacuum – Argon cycles have been made for 30 minutes. After that freshly distilled and deoxygenated by bubbling argon (30 minutes) toluene (30 mL) and $^tBu_3P$ (0.065 mmol, 15.5 μl) were added and the mixture was stirred at reflux for 18 hours. Then, solvents were evaporated and the crude mixture was dissolved in CH_2Cl_2 and washed with water and brine. The combined organic layers were dried over $MgSO_4$ and concentrated in vacuo. Purification by column chromatography on silica gel (heptane/CH_2Cl_2 6:1 and then 2:1) gives the desired product. Yield: 626 mg, 86%.

^{1}H-NMR (300 MHz, $CHCl_3$), δ (ppm): 7.06 (d, J = 8.1 Hz, 4H; H-2), 6.97 (d, J = 8.4 Hz, 4H; H-3), 5.53 (s, br, 1H; NH) 2.54 (m, 4H; H-5), 1.54 (m, 4H; H-6), 1.29 (m, 12H; H-7, H-8, H-9), 0.85 (m, 6H; H-10).

^{13}C-NMR (75 MHz, $CHCl_3$), δ (ppm): 141.4 (C-1), 135.5 (C-4), 129.3 (C-3), 117.9 (C-2), 35.4, 31.9, 31.8, 29.1, 22.8, 14.2 (C-10).

*1,4,15,18-Tetrakis(3,5-bis(trifluoromethyl)phenyl)-9–(N,N-bis(4'-hexylphenyl)amine)-23[24]-iodo zinc (II) phthalocyanine (**33**)*

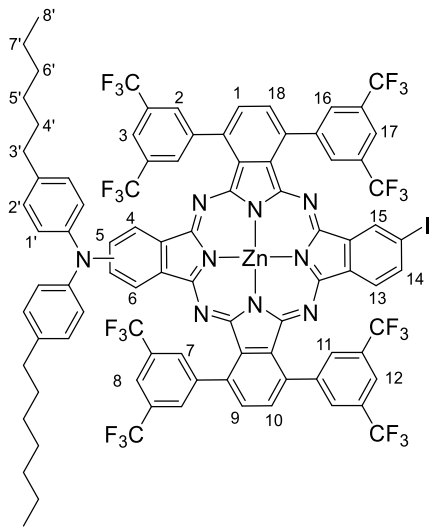

12 (0.06 mmol, 100 mg), bis(4-hexylphenyl)amine **31** (0.063 mmol, 21 mg), $Pd_2(dba)_3$ (0.006 mmol, 5.5 mg), and ^tBuONa (0.12 mmol, 12 mg) were placed in a Schlenk tube. Several vacuum – Argon cycles have been made for 30 minutes. After that freshly distilled and deoxygenated by bubbling argon (30 minutes) toluene (2 mL) and $^tBu_3P$ (0.006 mmol, 1.5 μl) were added and the mixture was stirred at reflux for 20 minutes. Then, solvents were evaporated and the crude mixture was purified by column chromatography on silica gel using toluene as eluent. The second fraction to elute containing a mixture of the desired product **33** and the mono de-iodinate **35**, preceded by compound **34** and followed by compound **36**. A blue solid was obtained, which was washed with acetonitrile / water (5:1). Yield: 30 mg, 33%.

^{1}H-NMR (300 MHz, THF-d_8), δ (ppm): 8.81 (m, 8H; H-2, H-7; H-11; H-16), 8.74 (2 x s, 2H; H-3, H-8), 8.70 (s, 2H; H-12, H-17), 8.61 (s, 1H; H-6), 8.56 (s, 1H; H-4), 8.29 – 8.16 (m, 5H; H-1, H-9, H-10, H-18, H-5), 8.06 (m, 3H; H-13, H-14, H-15), 7.19 (d, *J* = 8.4 Hz, 4H; H-1'), 7.12 (d, *J* = 8.4 Hz, 4H; H-2'), 2.69 (t, J = 7.6 Hz, 4H; H-3'), 1.60 – 1.55 (m, 16H; H-4', H-5', H-6', H-7'), 0.97 – 0.92 (m, 12H; H-8').

HR-MS (MALDI) m/z Calcd for [$C_{88}H_{56}F_{24}IN_9Zn$]: 1885.2612; Found: 1885.2606.

UV-Vis (THF), λmax (log ε): 702 (4.93), 632 (4.41), 356 (4.72), 246 (4.79) nm.

IR (KBr) ν^{-1} (cm^{-1}): 2924, 2860, 1607, 1511, 1279, 1180, 1140, 897, 826, 710.

Mp > 250°C.

*1,4,15,18-Tetrakis(3,5-bis(trifluoromethyl)phenyl)-9–(N,N-bis(4'-hexylphenyl)amine)-23[24]-(3''-hydroxypropyn-1-yl) zinc (II) phthalocyanine (**37**)*

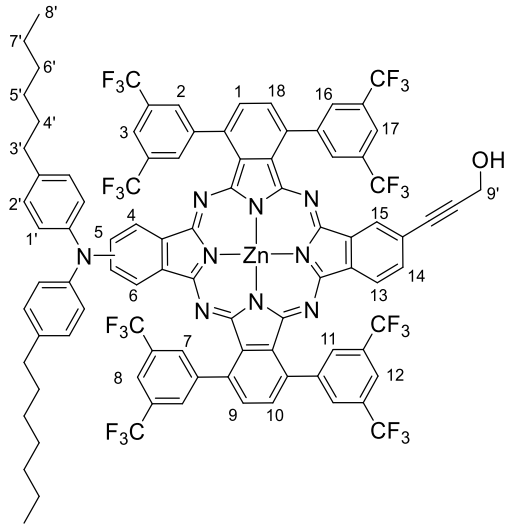

To a solution of **33** (0.016 mmol, 30 mg) in freshly distilled THF (3 mL) were added Et_3N (1 mL), $Pd(PPh_3)_4$ (6% mol, 1 mg*) and CuI (10% mol, 0.3 mg*). The mixture was deoxygenated by bubbling argon through it for 20 min. Propargyl alcohol (0.032 mmol, 2 µL*) was subsequently added and the mixture was stirred at 50ºC for 4 h. Then, solvents were evaporated and the crude mixture was dissolved in CH_2Cl_2 and washed with water. The combined organic layers were dried over $MgSO_4$ and concentrated in vacuo and the crude mixture was purified by column chromatography on silica gel using heptane/ THF (4:1) as eluent. The second fraction to elute containing the desired product preceded by the deiodinated starting product. The unreacted compound **35** was triturated with acetonitrile/water (5:1) in order to obtain a blue solid (9.3 mg, 0.0053 mmol). From the second chromatographic fraction a blue solid was obtained, which was washed with methanol / water (5:1) obtaining 15 mg of desired product. Considering the unreacted quantity, the effective yield is 75%.

^{1}H-NMR (300 MHz, THF-d_8), δ (ppm): 8.82 (2 x s, 8H; H-2, H-7, H-11, H-16), 8.75 (2 x s, 2H; H-3, H-8), 8.70 (s, 2H; H-12, H-17), 8.63 (s, 1H; H-6), 8.57 (s, 1H; H-4), 8.51 (s, 1H; H-5), 8.24 (m, 4H; H-1, H-9, H-10, H-18), 8.21 – 8.17 (m, 2H; H-13, H-15), 8.11 (d, *J* = 8.5 Hz, 1H; H-14), 7.20 (d, *J* = 8.7 Hz, 4H; H-1'), 7.13 (d, *J* = 8.7 Hz, 4H; H-2'), 4.61 (d, *J* = 5.7 Hz, 2H; H-9'), 4.54 (m, 1H; OH), 2.69 (m, 8H; H-3', H-4'), 0.95 (m, 12H; H-8').

HR-MS (MALDI) m/z Calcd for [$C_{91}H_{59}F_{24}N_9OZn$]: 1813.3751; Found: 1813.3756.

UV-Vis (THF), λmax (log ε): 701 (4.97), 633 (4.44), 359 (4.73), 248 (4.79) nm.

IR (KBr) ν^{-1} (cm^{-1}): 3402, 2957, 2930, 2862, 1609, 1457, 1376, 1277, 1179, 1139, 1058, 896, 687.

Mp > 250°C.

*Considering the quantity of unreacted starting material, it should be noted that the real percentages of catalysts are 8.7% for $Pd(PPh_3)_4$, 14.5% for CuI, and propargyl alcohol was added with an excess of 2.9 eq.

*1,4,15,18-Tetrakis(3,5-bis(trifluoromethyl)phenyl)-9–(N,N-bis(4'-hexylphenyl)amine)-23[24]- (formylethynyl) zinc (II) phthalocyanine (**38**)*

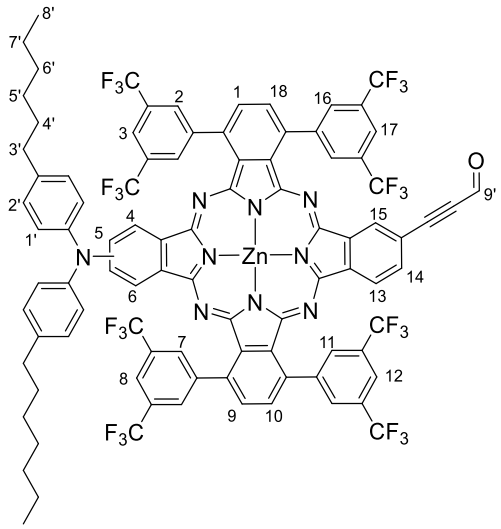

To a stirred solution of periodinane 1-hydroxy-1,2-benziodoxole-3(1H)-one-1-oxide (IBX) (0.037 mmol, 10.5 mg) in DMSO (2 mL) was added at once **37** (0.0083 mmol, 15 mg). The mixture was left stirring at room temperature for 5h (TLC). It was then poured into brine and extracted with CH_2Cl_2. The organic layers were washed with $NaHCO_3$ and brine, dried over $MgSO_4$ and concentrated. Purification by column chromatography (Heptane / THF 4:1) gives the desired product as a blue solid tritured by acetonitrile/water (5:1). Yield: 11 mg, 77%.

^{1}H-NMR (300 MHz, THF-d_8), δ (ppm): 9.66 (s, 2H; H-9'), 8.82 (m, 8H; H-2, H-7, H-11, H-16), 8.76 (2 x s, 2H; H-3, H-8), 8.69 (m, 2H; H-12, H-17), 8.59 (m, 1H; H-6), 8.52 (s, 1H; H-4), 8.43 (m, 1H; H-5), 8.28 – 8.24 (m, 4H; H-1, H-9, H-10, H-18), 8.23 – 8.20 (m, 2H; H-13, H-15), 8.12 (s, 1H; H-14), 7.21 (d, *J* = 8.4 Hz, 4H; H-1'), 7.13 (d, *J* = 8.4 Hz, 4H; H-2'), 2.70 (m, 8H; H-3', H-4'), 0.91 (m, 12H; H-8').

HR-MS (MALDI) m/z Calcd for [$C_{91}H_{57}F_{24}N_9OZn$]: 1811.3594; Found: 1811.3589.

UV-Vis (THF), λmax (log ε): 710 (4.93), 640 (4.37), 358 (4.62), 282 (4.62), 246 (4.74) nm.

Mp > 250°C.

*1,4,15,18-Tetrakis(3,5-bis(trifluoromethyl)phenyl)-9–(N,N-bis(4'-hexylphenyl)amine)-23[24]- (carboxyethynyl) zinc (II) phthalocyanine (**39**)*

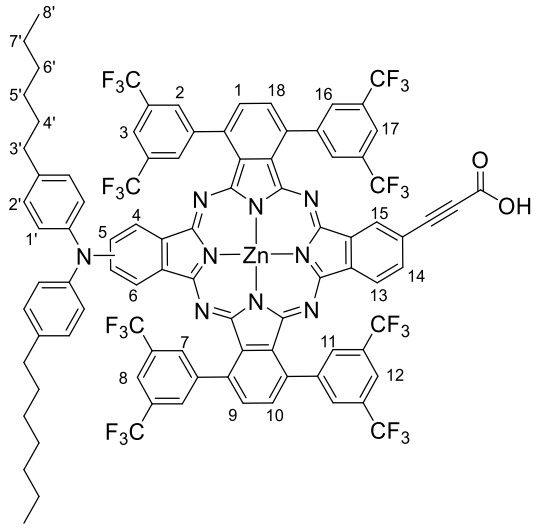

To a vigorously stirred solution of **38** (0.0061 mmol, 11 mg) in THF (3 mL) at 0ºC, sulfamic acid (0.0092 mmol, 0.89 mg) in Milli-Q-grade deionized H_2O (0.5 mL) was added, followed by $NaClO_2$ (0.0092 mmol, 0.83 mg) in Milli-Q-grade deionized H_2O (0.5 mL) in few portions. The solution was brought to room temperature and left stirring until the starting material was consumed. The crude was then poured into water and extract several times with CH_2Cl_2, washed with NH_4Cl and dried with Na_2SO_4. Purification by bio-beads column chromatography gives the desired product that was washed with heptane. Yield: 6.5 mg, 58%.

^{1}H-NMR (300 MHz, THF-d_8), δ (ppm): 8.8 (2 x s, 8H; H-2, H-7, H-11, H-16), 8.7 (m, 4H; H-3, H-8, H-12, H-17), 8.6 (s, 1H; H-6), 8.5 (s, 1H; H-4), 8.4 (m, 1H; H-5), 8.34 – 8.16 (m, 4H; H-1, H-9, H-10, H-18), 7.9 (m, 2H; H-13, H-15), 7.6 (d, J = 8.1 Hz, 1H; H-14), 7.2 (d, J = 8.4 Hz, 4H; H-1'), 7.1 (d, J = 8.4 Hz, 4H; H-2'), 2.7 (m, 8H; H-3', H-4'), 0.9 (m, 12H; H-8').

HR-MS (MALDI) m/z Calcd for [$C_{91}H_{57}F_{24}N_9O_2Zn$]: 1827.3542; Found: 1827.3538.

UV-Vis (THF), λmax (log ε): 704 (4.48), 638 (3.92), 358 (4.22), 266 (4.40) nm.

IR (KBr) ν^{-1} (cm^{-1}): 3379, 2922, 2853, 1730, 1632, 1275, 1086, 734, 680, 612.

Mp > 250°C.

*Methyl-4-(tri-tert-butylstannyl)benzoate (**40**)*[172]

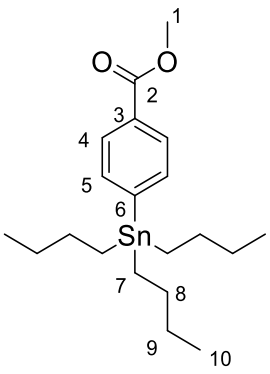

Methyl-4-iodobenzoate (1.15 mmol, 300 mg) and $Pd(PPh_3)_4$ (0.06 mmol, 70 mg) were placed in a Schlenk tube. Several were made for 30 minutes. After that freshly distilled and deoxygenated by bubbling argon (30 minutes) toluene (12 mL) and hexa-*n*-butylditin, (2.29 mmol, 1.15 mL) were added and the mixture was stirred at reflux for 5 hours under Ar atmosphere. Then the solvent was evaporated and the crude mixture was purificated by short column chromatography on silica gel using heptane as eluent in order to obtain the desired product as a yellow/white liquid. Yield: 358 mg, 73%.

^{1}H-NMR (300 MHz, $CHCl_3$), δ (ppm): 7.9 (d, 2H, *J* = 8.1Hz; H-4), 7.5 (d, 2H, *J* = 8.1Hz; H-5), 3.9 (s, 3H; H-1), 1.57 – 1.48 (m, 6H; H-7), 1.40 – 1.26 (m, 6H; H-8), 1.11 – 1.05 (m, 6H; H-9), 0.95 – 0.86 (m, 9H; H-10).

^{13}C-NMR (75 MHz, $CHCl_3$), δ (ppm): 167.79 (C-2), 149.88 (C-5), 136.60 (C-6), 129.75 (C-4), 128.55 (C-3), 51.92 (C-1), 28.92, 27.19, 13.47, 9.47.

*Methyl-4-(7-bromobenzo[c][1,2,5]thiadiazol-4-yl)benzoate (**41**)*[56]

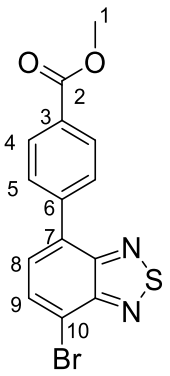

40 (359 mg, 0.84 mmol), 4,7-bromo-2,1,3-benzothiadiazole (164 mg, 0.56 mmol), CsF (170 mg, 1.12 mmol), $PdCl_2$ (5 mg, 0.028 mmol), CuI (5 mg, 0.028 mmol) were placed in a Schlenk tube. Several vacuum – Argon cycles were made for 30 minutes. After that freshly distilled and deoxygenated by bubbling argon (30 minutes) DMF (4 mL) and ^{t}Bu$_3$P (20 μL, 0.084 mmol) were added and the mixture was stirred at 45ºC under Ar atmosphere until the starting material was consumed (TLC Heptane/ AcOEt 4:1). The reaction mixture was diluted with AcOEt (50 mL) and washed with water (3 × 50 mL), dried (Na_2SO_4) and concentrated in vacuo and the crude mixture was purificated by column chromatography on silica gel using heptane / AcOEt (5:1) as eluent to afford the desired product as a yellow solid. Yield: 50 mg, 17%.

^{1}H-NMR (300 MHz, $CHCl_3$), δ (ppm): 8.2 (d, 2H, *J* = 8.4 Hz; H-4), 8.00 – 7.95 (m, 2H; H-5), 7.7 (s, 1H; H-9), 7.6 (s, 1H; H-8) 4.0 (s, 3H; H-1).

^{13}C-NMR (75 MHz, $CHCl_3$), δ (ppm): 166.7, 153.9, 152.8, 140.9, 132.8, 132.2, 129.9, 129.1, 128.7, 127.2, 114.2, 52.3.

UV-Vis (THF) λmax (log ε): 363 (3.85), 313 (4.07), 302 (4.14), 275 (4.31), 242 (3.91) nm.

HR-MS (APPI - FTMS) m/z Calcd for [$C_{14}H_9BrN_2O_2S$]: 347.9568; Found: 347.9562.

*Methyl-4-(7-((trimethylsilyl)ethynyl)benzo[c][1,2,5]thiadiazol-4-yl)benzoate (**42**)*

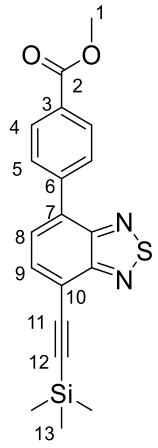

41 (0.14 mmol, 50 mg), $Pd(PPh_3)_2Cl_2$ (5% mol, 5 mg) and CuI (10% mol, 2.6 mg) were placed in a 25 mL round-bottom flask and Ar atmosphere was made for 30 minutes. Freshly distilled THF (3 mL) and Et_3N (1 mL) were added after freeze-pump-thaw cycles. Ethynyltrimethylsilane (0.21 mmol, 30 μL) was subsequently added and the mixture was stirred at 60ºC until the starting material was consumed (TLC heptane/THF 5:1). Then, solvents were evaporated and the crude mixture was dissolved in CH_2Cl_2 and washed with water. The combined organic layers were dried over $MgSO_4$ and concentrated in vacuo. Purification by column chromatography on silica gel (heptane/THF 8:1) gives the desired product as a yellow solid. Yield: 10 mg, 20%.

^{1}H-NMR (300 MHz, $CHCl_3$), δ (ppm): 8.19 (d, 2H, *J* = 8.4 Hz; H-4), 8.03 (d, 2H, *J* = 8.7 Hz; H-5), 7.87 (d, 1H, *J* = 7.2 Hz; H-9), 7.72 (d, 1H, *J* = 7.5 Hz; H-8) 3.97 (s, 3H; H-1), 0.35 (s, 9H; H-12).

^{13}C-NMR (75 MHz, $CHCl_3$), δ (ppm): 175.0, 155.4, 141.4, 133.8, 130.0, 129.4, 128.1, 115.2, 111.7, 100.3, 87.2, 85.9, 52.4, 0.1.

UV-Vis (THF) λmax (log ε): 380 (4.07), 321 (3.99), 285 (4.33), 242 (3.88) nm.

HR-MS (APPI - FTMS) m/z Calcd for [$C_{19}H_{18}N_2O_2SSi$]: 366.0858; Found: 366.0851.

*1,4,15,18-Tetrakis(3,5-bis(trifluoromethyl)phenyl)-9–(N,N-bis(4'-hexylphenyl)amine)-23[24]- (methyl 4''-(7''-ethynylbenzo[c][1'',2'',5'']thiadiazol-4''-yl)benzoate) zinc (II) phthalocyanine (**44**)*

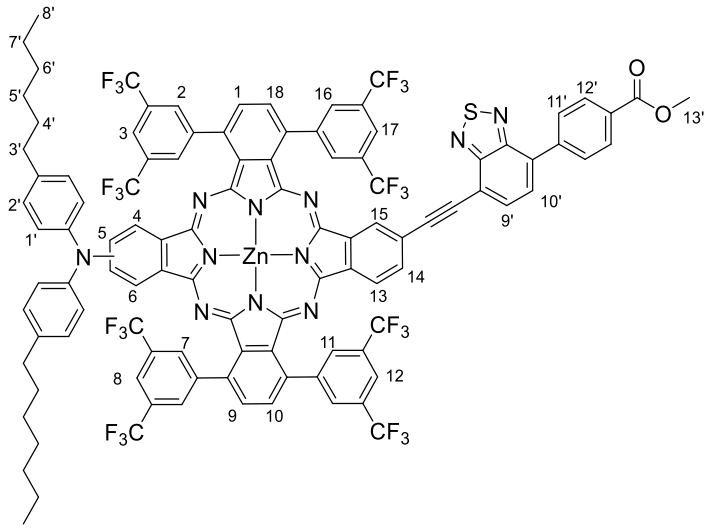

To a stirred solution of **42** (0.0137 mmol, 5 mg) in dry THF (2 mL) at 0ºC a solution of TBAF in THF (1 M, 0.055 mmol, 55 μL) was added. The solution was brought to room temperature and left stirring until the starting material was consumed (30 minutes, TLC). The crude was then poured into water and extract several times with CH_2Cl_2 and dried with Na_2SO_4. Then the de-protected product **43** without other further purification was dissolved in freshly distilled and deoxygenated by bubbling argon for 20 min THF (3 mL) and Et_3N (1 mL). $Pd(PPh_3)_4$ (5% mol, 0.46 mg[#]) and CuI (10% mol, 0.15 mg[#]) and **33** (0.008 mmol, 15 mg) were added and the mixture was stirred for 18 h at 50ºC. Then, solvents were evaporated and the crude mixture was dissolved in CH_2Cl_2 and washed with water. The combined organic layers were dried over $MgSO_4$ and concentrated in vacuo and the crude mixture was purified by column chromatography on silica gel using heptane/THF (4:1) as eluent. The second fraction to elute containing the desired product preceded by the deiodinated starting product. The unreacted compound was triturated with acetonitrile/water (5:1) in order to obtain a blue solid (1.9 mg, 0.0011 mmol). From the second chromatographic fraction a green solid was obtained, which was washed with heptane obtaining 9 mg of desired product. Considering the unreacted quantity, the effective yield is 64%.

^{1}H-NMR (300 MHz, THF-d_8), δ (ppm): 8.83 (s, 16H; H-2, H-7, H-11, H-16), 8.71 (m, 4H; H-3, H-8), 8.63 – 8.58 (m, 4H; H-12, H-17), 8.51 (m, 4H; H-6, H-4), 8.32 (m, 4H; H-5, H-14), 8.24 – 8.20 (m, 12H; H-1, H-9, H-10, H-13, H-15, H-18), 8.11 (d, *J* = 8.2 Hz, 4H; H-12'), 7.91 (s, 2H; H-9'), 7.81 (d, *J* = 8.2 Hz, 4H; H-11'), 7.66 – 7.52 (m, 2H; H-10'), 7.20 (d, J = 8.7 Hz, 8H; H-1'), 7.14 (d, J = 8.7 Hz, 8H; H-

2'), 3.95 (s, 3H; H-13'), 3.88 (s, 3H; H-13'), 2.70 (m, 8H; H-3', H-4'), 0.94 (m, 12H; H-8').

HR-MS (MALDI) m/z Calcd for [$C_{104}H_{65}F_{24}N_{11}O_2SZn$]: 2051.3952; Found: 2051.3946.

UV-Vis (THF), λmax (log ε): 706 (4.94), 637 (4.40), 447 (4.04), 363 (4.69), 285 (4.73), 262 (4.75) nm.

IR (KBr) ν^{-1} (cm^{-1}): 3639, 2959, 2918, 2864, 1711, 1590, 1441, 1256, 1094, 807, 701, 626.

Mp > 250°C.

[#]Considering the quantity of unreacted starting material, it should be noted that the real percentages of catalysts are 6% for $Pd(PPh_3)_4$, 11.8% for CuI, and propargyl alcohol was added with an excess of 2 eq.

*1,4,15,18-Tetrakis(3,5-bis(trifluoromethyl)phenyl)-9–(N,N-bis(4'-hexylphenyl)amine)-23[24]-(4''-(7''-ethynylbenzo[c][1'',2'',5'']thiadiazol-4''-yl)benzoic acid) zinc (II) phthalocyanine (**45**)*

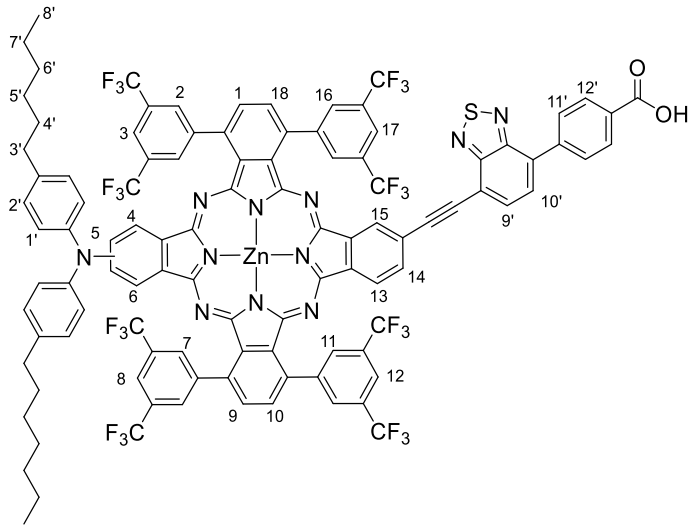

44 (9 mg, 0.0044 mmol) was dissolved in THF (3 mL), MeOH (2 mL) and a solution of NaOH (20 % w/w in water, 0.8 mL) was added. The solution was heated at 40°C for 1 hour upon which TLC indicated complete hydrolysis of the ester. The reaction mixture was diluted with CH_2Cl_2 (10 mL) washed with water (10 mL), HCl (1M, 12 mL), water (10 mL), the organics dried (Na_2SO_4) and evaporated. The product was purified by bio-beads column chromatography on silica gel and triturated with heptane to afford a green solid. Yield: 5 mg, 62%.

^{1}H-NMR (300 MHz, THF-d_8), δ (ppm): 8.81 (s, 16H; H-2, H-7, H-11, H-16), 8.70 (s, 4H; H-3, H-8), 8,65 (s, 4H; H-12, H-17), 8.60 (m, 4H; H-6, H-4), 8.51 (m, 4H; H-5, H-14), 8.24 – 8.10 (m, 12H; H-1, H-9, H-10, H-13, H-15, H-18), 8.12 (m, 4H; H-12'), 8.02 (s, 2H; H-9'), 7.79 (d, *J* = 8.4Hz, 4H; H-11'), 7.71 – 7.62 (m, 2H; H-10'), 7.20 (d, *J* = 8.7 Hz, 8H; H-1'), 7.14 (d, *J* = 8.7 Hz, 8H; H-2'), 2.68 (m, 8H; H-3', H-4'), 1.00 – 0.81 (m, 12H; H-8').

HR-MS (MALDI) m/z Calcd for [$C_{103}H_{63}F_{24}N_{11}O_2SZn$]: 2037.3795; Found: 2037.3790.

UV-Vis (THF), λmax (log ε): 708 (4.71), 641 (4.16), 448 (3.92), 363 (4.44), 281 (4.55), 246 (4.59) nm.

IR (KBr) ν^{-1} (cm^{-1}): 3308, 2957, 2930, 2862, 1723, 1655, 1601, 1430, 1275, 1088, 805, 616.

Mp > 250°C.

2.5.4 Synthesis of novel donor-π-acceptor multicomponent systems based on Pcs

*4-(Bis(4-hexylphenyl)amino)benzaldehyde (**46**)* [173]

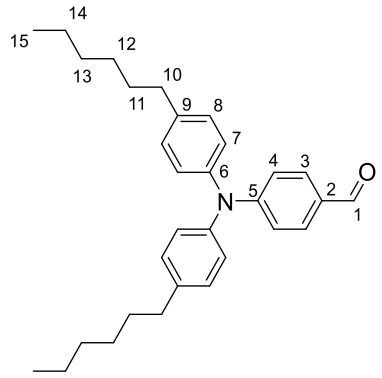

A mixure of **31** (6.67 g, 19.76 mmol), 4-bromobenzaldehyde (4.5 g, 23.3 mmol), K_3PO_4 (8.6 g, 40.6 mmol) in dry dioxane (120 ml) was deoxygenated by bubbling argon through it for 20 min. $Pd_2(dba)_3$ (147 mg, 0.16 mmol), X-Phos (295 mg, 0.62 mmol) were subsequently added and the mixture was stirred at 80ºC overnight. Then, the solvent was evaporated and the crude mixture was dissolved in $CHCl_3$ and filtrated over $MgSO_4$. Purification by column chromatography on silica gel (heptane/$CHCl_3$ 3:1 and then 1:1) gives the desired product as a yellow oil. Yield: 3.53 g, 40%.

^{1}H-NMR (300 MHz, $CHCl_3$), δ (ppm): 9.78 (s, 1H; H-1), 7.65 (d, *J* = 8.7 Hz, 2H; H-4), 7.16 (d, *J* = 8.3 Hz, 4H; H-7), 7.09 (d, *J* = 8.4 Hz, 4H; H-8), 6.96 (d, *J* = 8.6 Hz, 2H; H-3), 2.66 (m, 4H; H-10), 1.63 (m, 4H; H-11), 1.34 (m, 12H; H-12, H-13, H-14), 0.91 (m, 6H; H-15).

*1-Bromo-2,4-bis(hexyloxy)benzene (**47**)* [174]

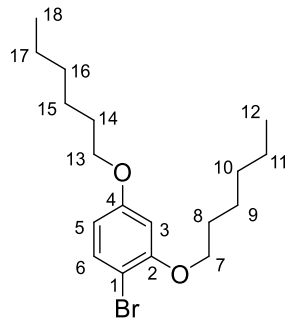

4-Bromoresorcinol (1 g, 5.3 mmol), 1-bromohexane (4 mL, 28.6 mmol) and K_2CO_3 (5.9 g, 43.46 mmol) in 7 mL of DMF were stirred at 90 °C for 4 h under argon. After cooling to room temperature, the mixture was poured into 100 mL water and extracted with CH_2Cl_2. The combined organic layers were dried over $MgSO_4$ and concentrated in vacuo. Purification by column chromatography (Heptane/CH_2Cl_2 2:1) gives the desired product as a colourless oil. Yield: 1.41 g, 74%.

^{1}H-NMR (300 MHz, $CHCl_3$), δ (ppm): 7.37 (d, *J* = 8.7 Hz, 1H; H-6), 6.46 (d, J = 2.7 Hz, 1H; H-3), 6.37 (dd, *J* = 8.7, 2.7 Hz, 1H; H-5), 3.98 (t, *J* = 6.5 Hz, 2H; H-7), 3.92 (t, *J* = 6.6 Hz, 2H; H-13), 1.90 – 1.70 (m, 4H; H-8, H-14), 1.58 – 1.24 (m, 12H; H-9, H-10, H-11, H-15, H-16, H-17), 0.91 (t, J = 7.0 Hz, 6H; H-12, H-18).

*2-(2,4-Bis(hexyloxy)phenyl)-4,4,5,5-tetramethyl-1,3,2-dioxaborolane (**48**)* [174]

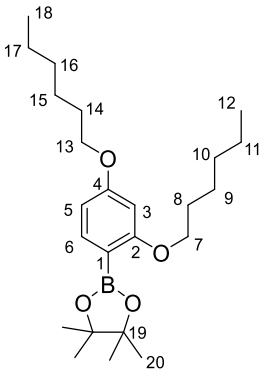

To a cold solution of **47** (1 g, 2.8 mmol) in 40 mL THF at -78 °C was added ^{n}BuLi (1.25 ml from a 2.5 M solution in hexane) under argon. The mixture was stirred for 1 h at the same temperature and then isopropyl pinacol borate (0.62ml, 3.1 mmol) was added dropwise, the resulting mixture was allowed to warm to room temperature and stirred overnight. The reaction was quenched by adding 20 mL saturated NH_4Cl aqueous solution, the resulting mixture was poured into 100 mL water, and the solution was extracted several times with ethyl acetate. The combined organic phase was dried over $MgSO_4$. After removing the solvent under reduced pressure, the residue was purified by column chromatography on silica gel (heptane/CH_2Cl_2 2:1) to obtain the desired compound as a colorless oil. Yield 486 mg, 43%.

^{1}H-NMR (300 MHz, $CHCl_3$), δ (ppm): 7.57 (d, *J* = 8.1 Hz, 1H; H-6), 6.42 (dd, *J* = 8.1, 2.1 Hz, 1H; H-5), 6.38 (d, *J* = 2.1 Hz, 1H; H-3), 3.94 (m, 4H; H-7, H-13), 1.95 (m, 4H; H-8, H-14), 1.76 (m, 8H; H-9, H-10), 1.61 (m, 8H; H-15, H-16), 1.32 (s, 12H; H-20), 0.90 (m, 6H; H-12, H-18).

*Bis(2',4'-dihexoxybiphenyl-4-yl) amine (**49**)*[175]

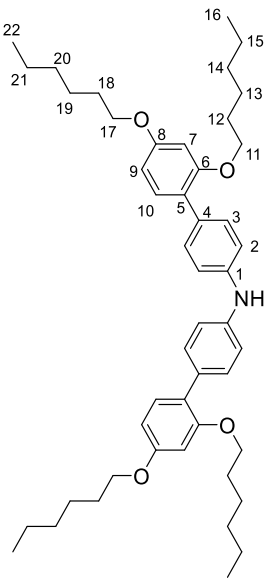

48 (1.5 g, 3.71 mmol), 4,4'-dibromodiphenylamine (550 mg, 1.7 mmol), K_2CO_3, (7 ml from a 2 M aqueous solution) and $Pd(PPh_3)_4$ (40 mg, 0.34 mmol) in 20 mL of deoxygenated toluene were refluxed under argon overnight.

Upon cooling, 50 mL water was added, and the solution was extracted several times by CH_2Cl_2. The combined organic layers were washed with brine, dried over $MgSO_4$, and then concentrated in vacuo. Purification by column chromatography on silica gel (heptane/CH_2Cl_2 4:1 and then 1:1) gives the desired product as a colourless oil. Yield: 516 mg, 42%.

^{1}H-NMR (300 MHz, $CHCl_3$), δ (ppm): 7.45 (d, *J* = 8.6 Hz, 4H; H-3), 7.24 (d, *J* = 8.6 Hz, 2H; H-10), 7.11 (d, *J* = 8.6

Hz, 4H; H-2), 6.55 (m, 4H; H-7, H-9), 5.77 (s, 1H; NH), 3.96 (m, 8H; H-11, H-17), 1.86 – 1.67 (m, 8H; H-12, H-18), 1.58 – 1.21 (m, 24H; H-13, H-14, H-15, H-19, H-20, H-21,), 0.91 (dt, *J* = 7.2, 6.3 Hz, 12H; H-16, H-22).

*4-(Bis(2',4'-bis(hexyloxy)-[1,1'-biphenyl]-4-yl) amino) benzaldehyde (**50**)*[176]

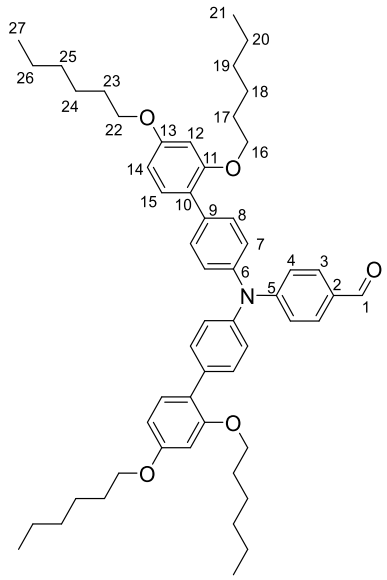

A mixure of **49** (1.6 g, 2.2 mmol), 4-bromobenzaldehyde (492 mg, 2.6 mmol), K_3PO_4 (934 g, 4.4 mmol) in dry dioxane (10 ml) was deoxygenated by bubbling argon through it for 20 min. $Pd_2(dba)_3$ (15 mg, 0.016 mmol), X-Phos (32 mg, 0.067 mmol) were subsequently added and the mixture was stirred at 80ºC overnight. Then, the solvent was evaporated and the crude mixture was dissolved in $CHCl_3$ and filtrated over $MgSO_4$. Purification by column chromatography on silica gel (heptane/CH_2Cl_2 3:1 and then 1:2) gives the desired product as a yellow oil. Yield: 3.53 g, 40%.

^{1}H-NMR (300 MHz, $CHCl_3$), δ (ppm): 9.81 (s, 1H; H-1), 7.69 (d, *J* = 9 Hz, 2H; H-4), 7.52 (d, *J* = 8.6 Hz, 4H; H-8), 7.26 (m, 2H; H-15), 7.20 (d, *J* = 8.6 Hz, 4H; H-7), 7.12 (d, *J* = 9 Hz, 2H; H-3), 6.55 (m, 4H; H-12, H-14), 3.98 (m, 8H; H-16, H-22), 1.86 – 1.68 (m, 8H; H-17, H-23), 1.33 (m, 24H; H-18, H-19, H-20; H-24, H-25, H-26), 0.95 – 0.81 (m, 12H; H-21, H-27).

*5,10,15-Tris(4'-(bis(4''-hexylphenyl)amino)phenyl)-20-(trimethylsilyl)porphyrin (**51**)*

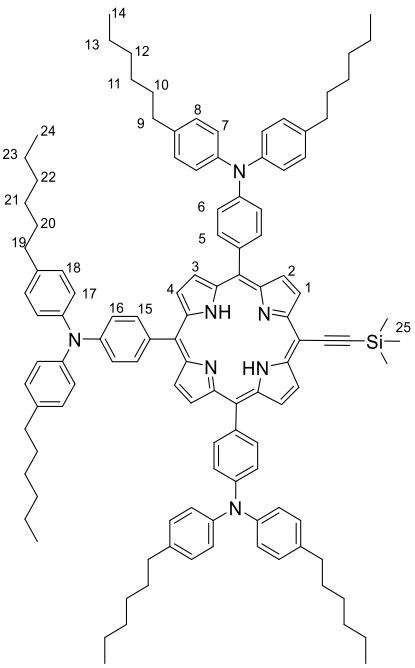

A mixture of **46** (2 g, 4.54 mmol), 3-(trimethylsilyl)-2-propynal (0.22 mL, 1.51 mmol) freshly distilled pirrol (0.42 mL, 6.05 mmol), BF_3OEt_2 (0.25 mL, 2.04 mmol), EtOH (4.4 mL) in 60 ml of $CHCl_3$ was stirred at r.t. for two hours. After that, DDQ (1.03 g, 4.55 mmol) was added, and the mixture was left stirring at r.t. for one further hour. Finally, addition of Et_3N (1 mL) and filtration through silica gave a crude mixture, which was purified by column chromatography on silica gel (heptane/toluene 3:1) and washed with MeOH to give the desired product. Yield: 181 mg, 7%.

^{1}H-NMR (300 MHz, $CHCl_3$), δ (ppm): 9.67 (d, *J* = 4.8 Hz, 2H; H-1), 9.05 (d, *J* = 4.8 Hz, 2H; H-2), 8.97 – 8.91 (m, 4H; H-3, H-4), 8.07 – 7.98 (m, 6H; H-5, H-15), 7.42 (m, 6H; H-6, H-16), 7.34 (m, 12H; H-8, H-18), 7.26 (m, 12H; H-7, H-17), 2.66 (t, *J* = 7.7 Hz, 12H; H-9, H-19), 1.68 (m, 12H; H-10, H-20), 1.40 (m, 36H; H-11, H-12. H-13, H-21, H-22, H-23), 0.99 – 0.85 (m, 18H; H-14, H-24), 0.64 (s, 9H; H-25), -2.28 (s, 2H; NH).

^{13}C-NMR (75 MHz, $CHCl_3$), δ (ppm): 148.22, 145.63, 138.31, 135.69, 134.67, 129.55, 125.24, 122.59, 121.32, 120.45, 120.29, 107.54, 101.65, 98.57, 77.16, 35.66, 31.95, 31.69, 29.86, 29.29, 22.81, 14.28, 0.54.

HR-MS (MALDI) m/z Calcd for [$C_{115}H_{133}N_7Si$]: 1640.0386; Found: 1640.0424.

UV-Vis (THF), λmax (log ε): 674 (4.06), 585 (4.43), 542 (4.14), 426 (5.20), 305 (4.89) nm.

*5,10,15-Tris(4'-(bis(4''-hexylphenyl)amino)phenyl)-20-(trimethylsilyl)porphyrinatozinc(II) (**52**)*

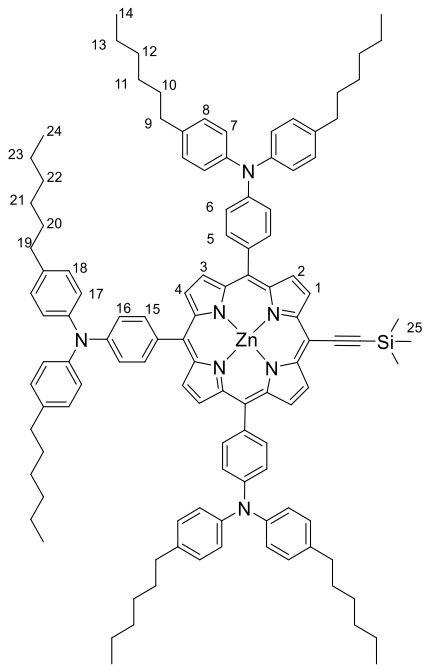

$Zn(OAc)_2$ (147 mg, 0.8 mmol) was added to a solution of **51** (132 mg, 0.08 mmol) in CH_2Cl_2 (36 mL) and MeOH (12 mL). The mixture was stirred at r.t. for 30 minutes, after which the solvents were evaporated under vacuo and the residue was extracted with CH_2Cl_2 and washed with MeOH to give compound **52** as a dark green solid. Yield: 134 mg, 98%.

^{1}H-NMR (300 MHz, $CHCl_3$), δ (ppm): 9.67 (d, *J* = 4.7 Hz, 2H; H-1), 9.03 (d, *J* = 4.7 Hz, 2H; H-2), 8.96 (m, 4H; H-3, H-4), 8.06 – 7.87 (m, 6H; H-5, H-15), 7.33 (m, 6H; H-6, H-16), 7.26 (m, 12H; H-8, H-18), 7.20 – 7.06 (m, 12H; H-7, H-17), 2.56 (t, *J* = 7.6 Hz, 12H; H-9, H-19), 1.60 (m, 12H; H-10, H-20), 1.28 (m, 36H; H-11, H-12, H-13, H-21, H-22, H-23), 0.83 (m, 18H; H-14, H-24), 0.55 (s, 9H; H-25).

^{13}C-NMR (75 MHz, $CHCl_3$), δ (ppm): 152.69, 151.02, 150.32, 150.23, 148.00, 145.72, 138.17, 135.63, 135.49, 133.13, 132.43, 131.96, 130.97, 129.53, 125.15, 123.38, 122.22, 120.50, 120.40, 108.01, 101.17, 99.42, 77.16, 35.66, 31.95, 31.70, 29.30, 22.81, 14.28, 0.60.

HR-MS (MALDI) m/z Calcd for [$C_{115}H_{131}N_7SiZn$]: 1701.9521; Found: 1701.9551.

UV-Vis (THF), λmax (log ε): 622 (4.27), 572 (4.13), 446 (5.15), 309 (4.77) nm.

*5, 10, 15 – Tris(bis(2',4'-bis(hexyloxy)-[1,1'- biphenyl]-4-yl)amino)phenyl–20-(trimethylsilyl) porphyrin (**53**)*

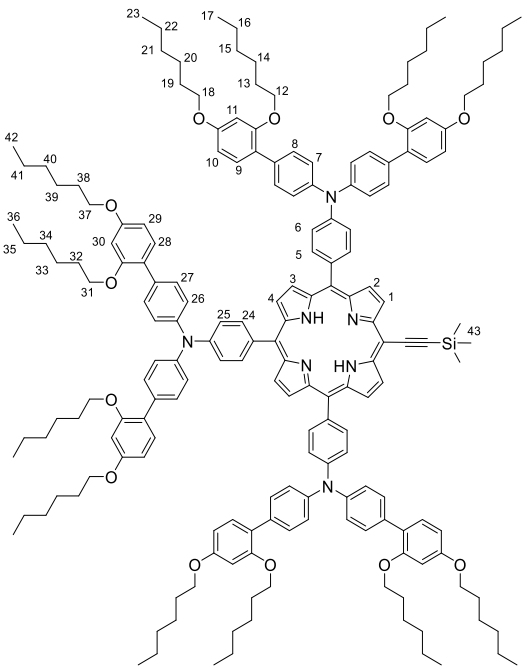

A mixture of **50** (1.34 g, 1.58 mmol), 3-(trimethylsilyl)-2-propynal (0.78 μL, 0.53 mmol) freshly distilled pirrol (0.15 mL, 2.11 mmol), BF_3OEt_2 (88 μL, 0.71 mmol), EtOH (1.5 mL) in 211 ml of $CHCl_3$ was stirred at r.t. for two hours. After that, DDQ (360 g, 1.59 mmol) was added, and the mixture was left stirring at r.t. for one further hour. Finally, addition of Et_3N (0.35 mL) and filtration through silica gave a crude mixture, which was purified by column chromatography (heptane/toluene 1:3) and washed with MeOH to give the desired product. Yield: 114 mg, 8%.

^{1}H-NMR (300 MHz, $CHCl_3$), δ (ppm): 9.61 (d, *J* = 4.8 Hz, 2H; H-1), 9.00 (d, *J* = 4.8 Hz, 2H; H-2), 8.91 (s, 4H; H-3, H-4), 8.01 (m, 6H; H-5, H-24), 7.57 – 7.45 (m, 18H; H-9, H-10, H-11, H-28, H-29, H-30), 7.39 (m, 12H; H-8, H-27), 7.26 (m, 6H; H-6, H-25), 6.50 (m, 12H; H-7, H-26), 3.93 (t, *J* = 6.5 Hz, 24H; H-12, H-18, H-31, H-37), 1.81 – 1.65 (m, 24H; H-13, H-19, H-32, H-38), 1.43 – 1.37 (m, 24H; H-14, H-20, H-33, H-39), 1.32 – 1.24 (m, 48H; H-15, H-16, H-21, H-22, H-34, H-35, H-40, H-41), 0.91 – 0.72 (m, 36H; H-17, H-23, H-36, H-42), 0.56 (s, 9H; H-43), -2.34 (s, 2H; NH).

^{13}C-NMR (75 MHz, $CHCl_3$), δ (ppm): 159.77, 157.23, 147.90, 146.10, 135.72, 135.63, 135.32, 133.63, 131.08, 130.60, 124.44, 123.29, 121.45, 121.27, 105.57, 100.84, 77.16, 68.64, 68.30, 31.78, 31.63, 29.85, 29.50, 29.28, 25.94, 22.78, 22.75, 14.20, 0.52.

HR-MS (MALDI) m/z Calcd for [$C_{187}H_{229}N_7O_{12}Si$]: 2792.7288; Found: 2792.7348.

UV-Vis (THF), λmax (log ε): 673 (4.18), 586 (4.50), 538 (4.28), 425 (5.38), 332 (5.17) nm.

*5, 10, 15 – Tris(bis (2',4'-bis(hexyloxy) [1,1'-biphenyl]-4-yl) amino) phenyl) – 20 - (trimethylsilyl) porphyrinato zinc(II) (**54**)*

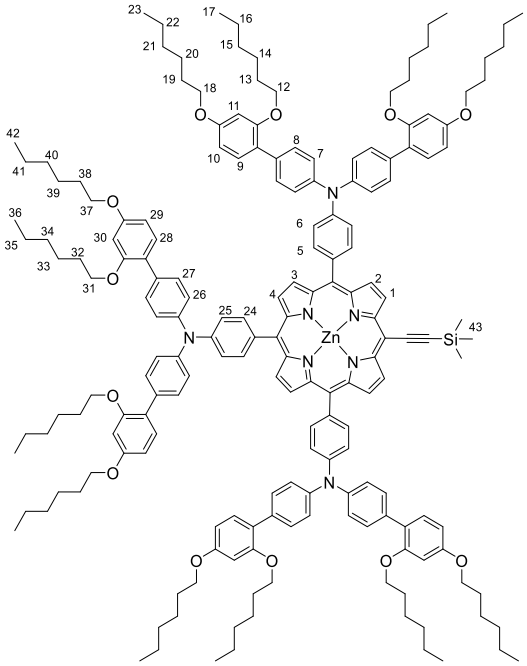

$Zn(OAc)_2$ (49 mg, 0.27 mmol) was added to a solution of **53** (70 mg, 0.025 mmol) in CH_2Cl_2 (12 mL) and MeOH (4 mL). The mixture was stirred at r.t. for 30 minutes, after which the solvents were evaporated under vacuo and the residue was extracted with CH_2Cl_2 and washed with MeOH to give compound **54** as a dark green solid. Yield: 69 mg, 96%.

^{1}H-NMR (300 MHz, $CHCl_3$), δ (ppm): 9.78 (d, *J* = 4.7 Hz, 2H; H-1), 9.16 (d, *J* = 4.7 Hz, 2H; H-2), 9.08 (m, 4H; H-3, H-4), 8.16 – 8.01 (m, 6H; H-5, H-24), 7.68 – 7.52 (m, 18H; H-9, H-10, H-11, H-28, H-29, H-30), 7.46 (m, 12H; H-8, H-27), 7.34 (m 6H; H-6, H-25), 6.58 (m, 12H; H-7, H-26), 4.01 (t, *J* = 5.6 Hz, 24H; H-12, H-18, H-31, H-37), 1.80 (m, 24H; H-13, H-19, H-32, H-38), 1.52 – 1.47 (m, 24H; H-14, H-20, H-33, H-39), 1.38 – 1.31 (m, 48H; H-15, H-16, H-21, H-22, H-34, H-35, H-40, H-41), 0.95 – 0.85 (m, 36H; H-17, H-23, H-36, H-42), 0.62 (s, 9H; H-43).

HR-MS (MALDI) m/z Calcd for $[C_{187}H_{227}N_7O_{12}SiZn]$: 2854.6423; Found: 2854.6451.

UV-Vis (THF), λmax (log ε): 622 (4.43), 576 (4.27), 441 (5.31), 327 (5.12) nm.

*Chloro-1,2,3,4,8,9,10,11,15,16,17,18-dodecafluorosubphthalocyaninateboron(III) (**55**)*[177,178]

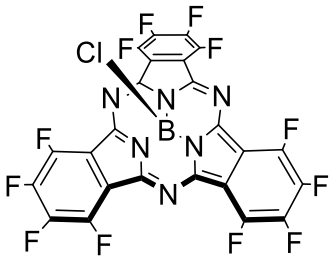

BCl_3 (10 mL of a 1M solution in *p*-xylene) was added dropwise to a solid mixture of tetrafluorophthalonitrile (0.01 mol, 2 g) under argon and magnetic stirring. The reaction mixture was refluxed for 30 minutes and after cooling down to room temperature was flushed with argon. The resulting dark-purple slurry was then evaporated under vacuo. The residue was purified by column chromatography on silica gel using heptane/AcOEt (3:1) as eluent and washed with heptane to afford the desired compound as a purple powder. Yield: 570 mg, 53%.

HR-MS (MALDI) m/z Calcd for [$C_{24}F_{12}N_6BCl$]: 645.9774; Found: 645.9792.

*(3-Ethynylphenoxy)-1,2,3,4,8,9,10,11,15,16,17,18-dodecafluorosubphthalocyaninateboron (III) (**56**)*

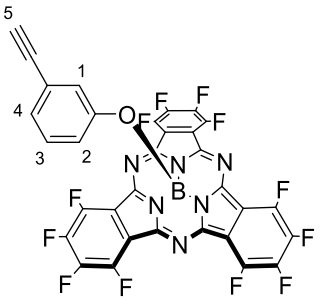

A mixture of 3-ethynylphenol (0.154 mmol, 17 μL), **55** (0.077 mmol, 50 mg) and DIPEA (0.154 mmol, 27 μL) in toluene (5 mL) was refluxed for 8 h. upon cooling, the solvent was evaporated under vacuo and the residue was purified by column chromatography on silica gel (heptane/toluene 1:1) to give the desired compound as a purple powder. Yield: 21 mg, 38%.

^{1}H-NMR (300 MHz, $CHCl_3$), δ (ppm): 6.83 (dt, J_1 = 9 Hz, J_2 = 1.2 Hz, 1H; H-4), 6.75 (t, J = 9 Hz, 1H; H-3), 5.56 (s, 1H; H-1), 5.28-5.24 (m, 1H; H-2), 2.91 (s, 1H; H-5).

HR-MS (MALDI) m/z Calcd for [$C_{32}H_5F_{12}N_6BO$]: 728.0426; Found: 728.0418.

Mp > 250°C.

*1,4,15,18-Tetrakis (3,5 - bis (trifluoromethyl) phenyl) -9 - (ethynyl - 3' - phenol) – 23 [24] - iodo zinc (II) phthalocyanine (**57**)*

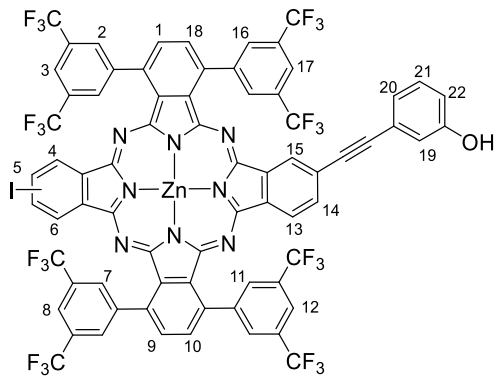

To a solution of **12** (0.06 mmol, 100 mg) in freshly distilled THF (3.5 mL) were added Et_3N (1.5 mL), $Pd(PPh_3)_4$ (10% mol, 7 mg) and CuI (10% mol, 1.1 mg). The mixture was deoxygenated by bubbling argon through it for 20 min. 3-ethynylphenol (0.06 mmol, 6 µL) was subsequently added and the mixture was stirred at 58ºC for 40 minutes. Then, solvents were evaporated and the crude mixture was dissolved in CH_2Cl_2 and washed with water. The combined organic layers were dried over $MgSO_4$ and concentrated in vacuo. Purification by column chromatography on silica gel (heptane/THF 4:1) gives the desired product as a blue solid, which was washed with heptane. Yield: 30 mg, 30%

^{1}H-NMR (300 MHz, THF-d_8), δ (ppm): 8.88-8.84 (m, 8H; H-2, H-7, H-11, H-16), 8.62 (s, 4H; H-3, H-8, H-12, H-17), 8.36-8.25 (m, 8H; H-1, H-4, H-5, H-6, H-9, H-10, H-13, H-18), 8.12-8.07 (m, 1H; H-15), 8.00-7.97 (m, 1H; H-14), 7.38-7.27 (m, 3H; H-20, H-21, H-22), 7.22 (s, 1H; H-19).

MS (MALDI) m/z: 1666.0 [M^+].

UV-Vis (THF), λmax (log ε): 699 (5.03), 674 (5.02), 640 (4.42), 614 (4.35), 356 (4.67), 215 (5.02) nm.

Mp > 250°C.

*Zn(II)Pc-SubPc dyad **59***

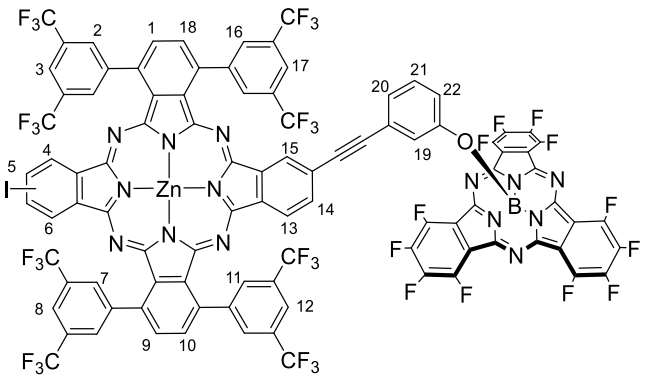

In a 25-mL round-bottomed flask, equipped with a magnetic stirrer, **55** (0.017 mmol, 11 mg) and AgOTf (0.02 mmol, 6 mg) were placed. Dry toluene (1.5 mL) was added and the mixture was stirred at 60°C under argon atmosphere until the **55** is consumed (easily monitored by TLC heptane/THF 3:1). Once the intermediate triflate-SubPc **58** is generated, a solution of **57** (0.017 mmol, 26 mg) and freshly distilled DIPEA (0.023 mmol, 3 μL) in dry toluene (2 mL) was added. The mixture was stirred at reflux for 5 hours. The solvent was removed by evaporation under reduced pressure and the product was directly purified by chromatography on silica gel using toluene as eluent. The second fraction of the column is the desired compound, which was washed with MeOH/H_2O (10:1) to afford **59** as a dark violet solid. Yield: 6 mg, 15%.

^{1}H-NMR (300 MHz, THF-d_8), δ (ppm): 8.85 (m, 6H; H-2, H-7, H-3, H-8), 8.80 (s, 2H; H-12, H-17), 8.59 (s, 4H; H-11, H-16), 8.14 (s, 1H; H-6), 8.31-8.25 (m, 6H; H-1, H-4, H-5, H-9, H-10, H-18), 8.21-8.17 (m, 1H; H-13), 7.97-7.93 (m, 2H; H-14, H-15), 7.14 (d, *J* = 7.8 Hz, 1H; H-20), 7.00 (t, *J* = 7.8 Hz, 1H; H-21), 5.99 (s, 1H; H-19), 5.53 (d, J = 8.7 Hz, 1H; H-22).

MS (MALDI) m/z: 2276.0 [M^+].

UV-Vis (THF), λmax (log ε): 696 (5.02), 675 (5.05), 640 (4.41), 615 (4.38), 567 (4.81), 512 (4.28) 353 (4.70) nm.

Mp > 250°C.

*Zn(II)Por-Zn(II)Pc dyad **61***

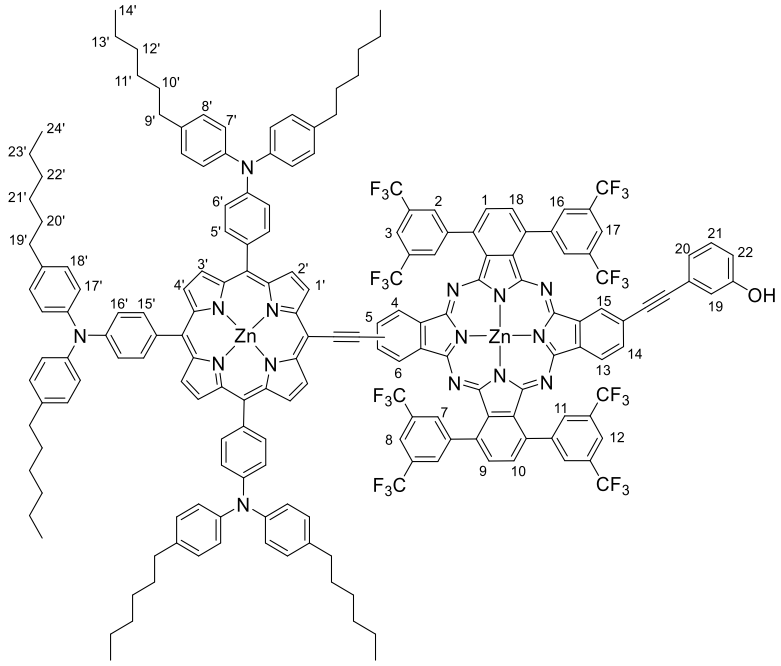

TBAF (0.047 mmol, 47 μL of a 1M solution in THF) was added to a solution of **52** (0.012 mmol, 20 mg) in THF (5 mL) at 0°C and under argon. The reaction mixture was stirred at r.t. for 30 minutes. Once the deprotected Por **60** is generated, and the starting **52** totally consumed (easily monitored by TLC heptane/toluene 1:1), the reaction mixture was poured into water and extract several times with CH_2Cl_2 and dried with $MgSO_4$. Then, the solvent was evaporated and **60** was used for the next reaction without any further purification. To a solution of **57** (0.012 mmol, 20 mg) in freshly distilled THF (2 mL) were added Et_3N (1 mL), $Pd_2(dba)_3$ (10% mol, 1 mg), $AsPh_3$ (0.012 mmol, 4 mg) and the freshly deprotected Por **60** (0.012 mmol). The mixture was deoxygenated by bubbling argon through it for 20 min. The mixture was stirred at 55ºC for 16 h. Then, solvents were evaporated and the crude mixture was dissolved in CH_2Cl_2 and washed with water. The combined organic layers were dried over $MgSO_4$ and concentrated in vacuo. Purification by column chromatography on silica gel (heptane / THF 4:1) gives the desired product as a dark green solid, which was washed with acetonitrile. Yield: 29 mg, 77%.

^{1}H-NMR (300 MHz, THF-d_8), δ (ppm): 10.10 (d, *J* = 4.5 Hz, 2H; H-1'), 9.32 (d, *J* = 4.5 Hz, 2H; H-2'), 9.10 (d, *J* = 3.9 Hz, 4H), 9.00 (s, 4H; H-3', H-4'), 8.96 (m, 10H), 8.91-8.83 (m, 12H), 8.75 (s, 2H), 8.71 (d, *J* = 6 Hz, 2H), 8.63 (m, 6H), 8.50 (dd, J_1 = 6 Hz, J_2 = 2.1 Hz, 4H), 8.3-8.29 (m, 10H) 8.16 (d, *J* = 8.7 Hz, 2H), 8.06 (d, J = 8.7 Hz, 2H), 7.71-7.67 (m, 8H), 1.29 (m, 36H; H-11', H-12', H-13', H-21', H-22', H-23'), 0.89 (m, 18H; H-14', H-24').

HR-MS (MALDI) m/z Calcd for [$C_{184}H_{149}F_{24}N_{15}OZn_2$]: 3168.0264; Found: 3168.0294.

UV-Vis (THF), λmax (log ε): 709 (5.00), 643 (4.51), 578 (4.04), 449 (5.09), 310 (5.02), 212 (5.17) nm.

Mp > 250°C.

*Zn(II)Por-Zn(II)Pc dyad **63***

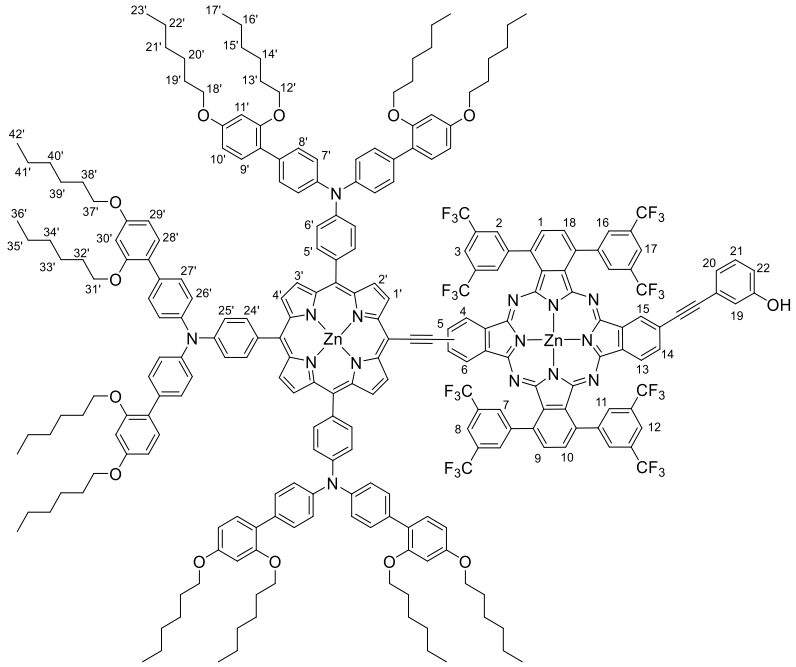

TBAF (0.036 mmol, 36 μL of a 1M solution in THF) was added to a solution of **54** (0.009 mmol, 26 mg) in THF (5 mL) at 0°C and under argon. The reaction mixture was stirred at r.t. for 45 minutes. Once the deprotected Por **62** is generated, and the starting **54** totally consumed (easily monitored by TLC heptane/toluene 1:2), the reaction mixture was poured into water and extract several times with CH_2Cl_2 and dried with $MgSO_4$. Then, the solvent was evaporated and **62** was used for the next reaction without any further purification. To a solution of **57** (0.009 mmol, 15 mg) in freshly distilled THF (3 mL) were added Et_3N (1.5 mL), $Pd_2(dba)_3$ (20% mol, 1.6 mg), $AsPh_3$ (0.009 mmol, 3 mg) and the recently deprotected Por **62** (0.009 mmol). The mixture was deoxygenated by bubbling argon through it for 20 min. The mixture was stirred at 50ºC for 20 h. Then, solvents were evaporated and the crude mixture was dissolved in CH_2Cl_2 and washed with water. The combined organic layers were dried over $MgSO_4$ and concentrated in vacuo. Purification by

column chromatography on silica gel (heptane/THF 3:1) gives the desired product as a dark green solid, which was washed with acetonitrile. Yield: 32 mg, 82%.

^{1}H-NMR (300 MHz, THF-d_8), δ (ppm): 10.13 (d, *J* = 4.5 Hz, 2H; H-1'), 9.38 (d, *J* = 4.5 Hz, 2H; H-2'), 9.08 (s, 4H; H-3', H-4'), 8.98-8.95 (m, 6H), 8.87 (s, 4H), 8.74 (s, 2H), 8.66 (s, 1H), 8.63 (s, 2H), 8.33-8.28 (m, 6H), 8.24 (d, *J* = 8.6 Hz, 4H), 8.16 (d, *J* = 8.3 Hz, 2H), 8.10 (d, *J* = 7.8 Hz, 1H), 7.70 – 7.57 (m, 20H), 7.54-7.46 (m, 12H), 7.37-7.30 (m, 10H), 6.67 – 6.56 (m, 12H), 4.03 (q, *J* = 6.3 Hz, 24H; H-12', H-18', H-31', H-37'), 2.47 (m, 12H), 1.87 – 1.77 (m, 24H), 1.53 (m, 24H), 0.92 (dt, *J* = 14.1, 5.7 Hz, 36H; H-17', H-23', H-36', H-42').

HR-MS (MALDI) m/z Calcd for [$C_{256}H_{245}F_{24}N_{15}O_{13}Zn_2$]: 4322.7210; Found: 4322.7315.

UV-Vis (THF), λmax (log ε): 708 (5.00), 642 (4.52), 581 (4.06), 448 (5.06), 330 (5.01), 256 (4.90) nm.

Mp > 250°C.

*Zn(II)Por-Zn(II)Pc-SubPc Triad **64***

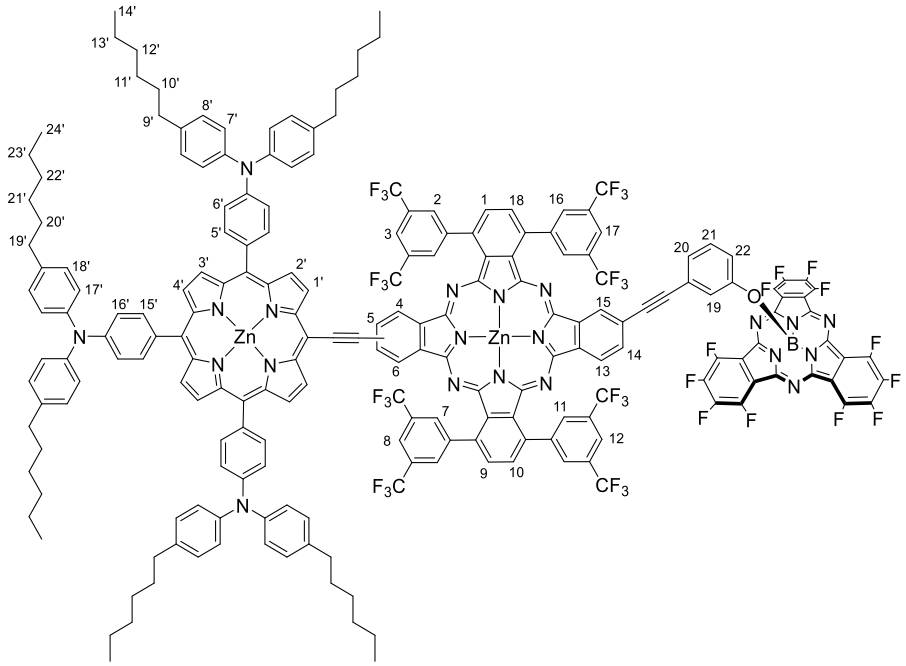

In a 25-mL round-bottomed flask, equipped with a magnetic stirrer, **55** (0.018 mmol, 12 mg) and AgOTf (0.0225 mmol, 6 mg) were placed. Dry toluene (1.5 mL) was added and the mixture was stirred at 50°C under argon atmosphere until the **55** is consumed (easily monitored by TLC heptane/THF 3:1). Once the intermediate triflate-SubPc **58** is generated, a solution of **61** (0.009 mmol, 29 mg) and freshly distilled DIPEA (0.023 mmol, 4 μL) in dry toluene (2 mL) was added. The mixture was stirred at 100°C for 12 hours. The solvent was removed by evaporation under reduced pressure and the product was directly purified by chromatography on silica gel using toluene as eluent. Then the solvent was evaporated under vacuo to afford the desired triad as a dark brown solid. Yield ≈ 0.1 mg, < 1%. *

HR-MS (MALDI) m/z Calcd for [$C_{184}H_{149}F_{24}N_{15}OZn_2$]: 3778.0296; Found: 3778.0297.

* The characterization of this compound could not be performed optimally due to the low amount of compound available, which was not enough to obtain a well-defined ^{1}H-NMR spectrum.

*Zn(II)Por-Zn(II)Pc-SubPc triad **65***

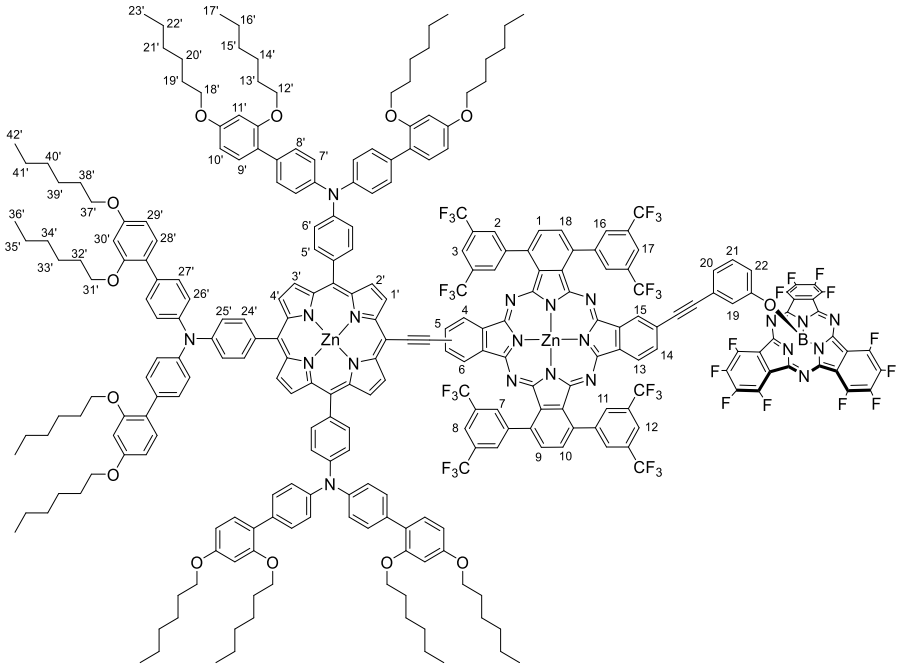

In a 25-mL round-bottomed flask, equipped with a magnetic stirrer, **55** (0.035 mmol, 23 mg) and AgOTf (0.0455 mmol, 12 mg) were placed. Dry toluene (2 mL) was added and the mixture was stirred at 50°C under argon atmosphere until the **55** is consumed (easily monitored by TLC heptane/THF 3:1). Once the intermediate triflate-SubPc **58** is generated, a solution of **63** (0.007 mmol, 32 mg) and freshly distilled DIPEA (0.0455 mmol, 8 μL) in dry toluene (2 mL) was added. The mixture was stirred at 100°C for 12 hours. The solvent was removed by evaporation under reduced pressure and the product was directly purified by chromatography on silica gel using toluene as eluent. Then the solvent was evaporated under vacuo to afford the desired triad as a dark brown solid. Yield: 2 mg, 6%.

^{1}H-NMR (300 MHz, THF-d_8), δ (ppm): 10.11 (d, *J* = 4.5 Hz, 2H; H-1'), 9.37 (d, *J* = 4.5 Hz, 2H; H-2'), 9.06 (s, 4H; H-3', H-4'), 8.95 (m, 6H), 8.87-8.80 (m, 4H), 8.72 (s, 2H), 8.61 (s, 2H), 8.39 (s, 2H), 8.32 (m, 4H), 8.23 (d, *J* = 8.3 Hz, 6H), 8.14 (d, *J* = 8.6 Hz, 3H), 8.03 – 7.95 (m, 3H), 7.66-7-56 (m, 20H), 7.52-7-44 (m, 12H), 7.40 – 7.26 (m, 10H), 7.16 (d, *J* = 7.2 Hz, 1H), 7.03 (m, 1H), 6.64 – 6.58 (m, 12H), 6.01 (s, 1H), 5.56 – 5.52 (m, 1H), 4.02 (m, 24H; H-12', H-18', H-31', H-37'), 1.51

(m, 24H; H-13', H-14', H-19', H-20', H-32', H-33', H-38', H-39'), 1.45 – 1.32 (m, 72H), 0.91 (m, 36H; H-17', H-23', H-36', H-42').

HR-MS (MALDI) m/z Calcd for [$C_{280}H_{244}BF_{36}N_{21}O_{13}Zn_2$]: 4931.7222; Found: 4931.7156.

UV-Vis (THF), λmax (log ε): 705 (5.10), 639 (4.68), 568 (4.95), 447 (5.18), 319 (5.24), 261 (5.22) nm.

Mp > 250°C.

*1,4,15,18-Tetrakis (3,5 - bis (trifluoromethyl) phenyl) - 9 - (4'-hydroxymethylphenyl) – 23 [24] - iodo zinc (II) phthalocyanine (**66**)*

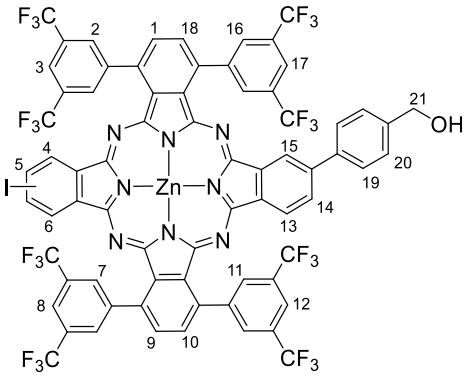

In a 25-mL round-bottomed flask, equipped with a magnetic stirrer, **12** (0.048 mmol, 80 mg), 4-(hydroxymethyl) phenylboronic acid (0.071 mmol, 11 mg), $Pd(PPh_3)_4$ (10% mol, 5 mg) and K_2CO_3 (0.284 mmol, 39 mg) were placed. Freshly distilled DMF (10 mL), which was previously deoxigenated by several freeze pump thaw cycles, was added and the mixture was stirred at 90°C under argon atmosphere overnight. Upon cooling, the solvent was evaporated and the crude mixture was dissolved in $CHCl_3$ and washed twice with NaOH (2 M solution) and twice with water. The organic phase was dried over $MgSO_4$ and concentrated in vacuo. Purification by column chromatography on silica gel (heptane / THF 2:1) gives the desired product as a blue solid, which was washed with MeOH/H_2O (5:1). Yield: 33 mg, 42%

^{1}H-NMR (300 MHz, THF-d_8), δ (ppm): 8.88 (m, 6H; H-2, H-3, H-7, H-8), 8.81 (s, 2H; H-12, H-17), 8.59 (s, 4H; H-11, H-16), 8.47 (m, 2H), 8.33 (m, 2H), 8.27 (m, 4H; H-1, H-9, H-10, H-18), 7.97 (m, 2H), 7.90 (d, *J* = 8.1 Hz, 2H; H-20), 7.71 (d, *J* = 8.1 Hz, 2H; H-19), 4.82 (d, *J* = 5.9 Hz, 2H; H-21), 4.40 (t, *J* = 5.9 Hz, 1H; OH).

MS (MALDI) m/z:1656.0 [M^+].

UV-Vis (THF), λmax (log ε): 700 (5.16), 672 (5.13), 642 (4.63), 610 (4.48), 356 (4.85), 248 (4.93) nm.

Mp > 250°C.

*1,4,15,18-Tetrakis (3,5 - bis (trifluoromethyl) phenyl) - 9 - (p-(4'-pyrenbutyryloxy-methyl)phenyl) – 23 [24] - iodo zinc (II) phthalocyanine (**67**)*

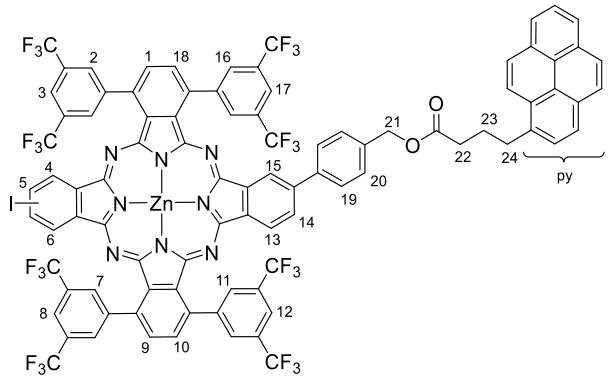

A mixture of 1-pyrenebutyric acid (0.143 mmol, 41 mg), DCC (0.143 mmol, 29.5 mg) and DMAP (0.143 mmol, 17.5 mg) was stirred in dry THF (10 ml) at 0°C for 30 min. Then, a solution of **66** (0.036 mmol, 59 mg) in dry THF (5 ml) was added dropwise. The mixture was stirred for 1 h at 0°C and for 36 h at room temperature. The resulting reaction crude was filtered through a glass frit and the filtrate was then evaporated. The crude was dissolved in $CHCl_3$ and washed with water, dried over Na_2SO_4 and concentrated in vacuo. Purification by column chromatography on silica gel (heptane / THF 2:1) gives the desired product as a blue solid, which was washed with MeOH/H_2O (5:1). Yield: 18.5 mg, 18%.

^{1}H-NMR (300 MHz, THF-d_8), δ (ppm): 8.90 (m, 6H; H-2, H-3, H-7, H-8), 8.82 (s, 4H; H-11, H-16), 8.61 (s, 2H; H-12, H-17), 8.46 (m, 2H), 8.36 – 8.28 (m, 8H; H-1, H-9, H-10, H-18), 8.14 – 7.99 (m, 4H; H-py), 7.96 – 7.88 (m, 5H; H-py), 7.73 (dd, J_1 = 15.6, J_2 = 8.1 Hz, 2H; H-20), 7.60 (d, J = 8.1 Hz, 2H; H-19), 5.38 (s, 2H; H-21), 3.50 – 3.25 (m, 2H; H-22), 2.61 (m, 4H; H-23, H-24).

MS (MALDI) m/z : 1926.1 [M^+].

UV-Vis (THF), λmax (log ε): 701 (4.8), 672 (4.77), 642 (4.25), 611 (4.1), 343 (4.7), 327 (4.54) 276 (4.73), 264 (4.67), 242 (4.85) nm.

Mp > 250°C.

*Zn(II)Por-Zn(II)Pc Dyad **68***

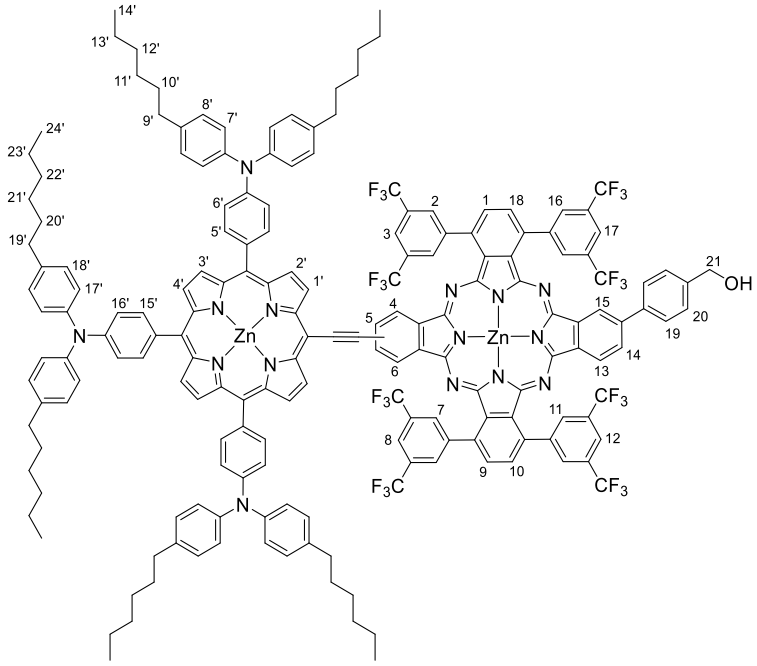

TBAF (0.024 mmol, 24 μL of a 1M solution in THF) was added to a solution of **52** (0.0059 mmol, 10 mg) in THF (2 mL) at 0°C and under argon. The reaction mixture was stirred at r.t. for 30 minutes. Once the deprotected Por **60** is generated, and the starting **52** totally consumed (easily monitored by TLC heptane/toluene 1:1), the reaction mixture was poured into water and extract several times with CH_2Cl_2 and dried with $MgSO_4$. Then, the solvent was evaporated and **60** was used for the next reaction without any further purification. To a solution of **66** (0.0054 mmol, 10 mg) in freshly distilled THF (2 mL) were added Et_3N (1 mL), $Pd_2(dba)_3$ (20% mol, 1 mg), $AsPh_3$ (0.0054 mmol, 2 mg) and the recently deprotected Por **60** (0.0059 mmol). The mixture was deoxygenated by bubbling argon through it for 20 min. The mixture was stirred at 50ºC for 18 h. Then, solvents were evaporated and the crude mixture was dissolved in CH_2Cl_2 and washed with water. The combined organic layers were dried over $MgSO_4$ and concentrated in vacuo. Purification by column chromatography on silica gel (heptane / THF 3:1) gives the desired product as a dark green solid, which was tritured with MeOH/H_2O (5:1). Yield: 8 mg, 47%.

^{1}H-NMR (300 MHz, THF-d_8), δ (ppm): 10.12 (d, *J* = 4.6 Hz, 2H; H-1'), 9.34 (d, *J* = 4.5 Hz, 2H; H-2'), 9.01 (s, 8H), 8.93 (2 x s, 2H), 8.89 (s, 3H), 8.83 (s, 3H), 8.76 (s, 2H), 8.72 (s, 2H), 8.68 (d, *J* = 7.9 Hz, 1H), 8.60 (s, 1H), 8.49 – 8.36 (m, 4H), 8.17 (d, *J* = 8.4 Hz, 4H; H-5'), 8.08 (d, *J* = 8.4 Hz, 2H), 7.92 (d, *J* = 8.1 Hz, 2H; H-20), 7.72 (d, *J* = 8.1 Hz, 2H; H-19), 7.51 (d, *J* = 8.4 Hz, 4H; H-6'), 7.44 – 7.34 (m, 16H), 7.30 (m, 10H), 4.83 (s, 2H; H-21), 4.19 (m, 1H; OH), 2.68 (m, 12H; H-

9', H-19'), 2.45 (m, 48H; H-10', H-11', H-12', H-13', H-20', H-21', H-22', H-23'), 0.93 (m, 18H; H-14', H-24').

HR-MS (MALDI) m/z Calcd for [$C_{183}H_{151}F_{24}N_{15}OZn_2$]: 3158.0420; Found: 3158.0257.

UV-Vis (THF), λmax (log ε): 705 (5.10), 642 (4.61), 448 (5.17), 363 (4.70), 301 (4.87) nm.

Mp > 250°C.

*Zn(II)Por-Zn(II)Pc-Pyrene Triad **69***

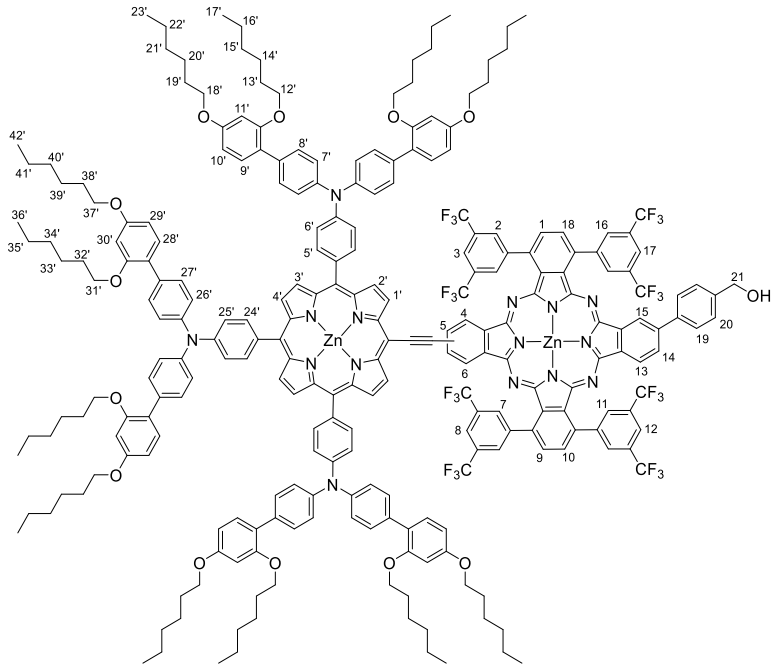

TBAF (0.039 mmol, 39 μL of a 1M solution in THF) was added to a solution of **54** (0.0098 mmol, 28 mg) in THF (5 mL) at 0°C and under argon. The reaction mixture was stirred at r.t. for 45 minutes. Once the deprotected Por **62** is generated, and the starting **54** totally consumed (easily monitored by TLC heptane/toluene 1:2), the reaction mixture was poured into water and extract several times with CH_2Cl_2 and dried with $MgSO_4$. Then, the solvent was evaporated and **62** was used for the next reaction without any further purification. To a solution of **66** (0.0135 mmol, 22 mg) in freshly distilled THF (3 mL) were added Et_3N (1.5 mL), $Pd_2(dba)_3$ (20% mol, 2 mg), $AsPh_3$ (0.0098 mmol, 3 mg) and the recently deprotected Por **62** (0.0098 mmol). The mixture was deoxygenated by bubbling argon through it for 20 min. The mixture was stirred at 50ºC for 20 h. Then, solvents were evaporated and the crude mixture was dissolved in CH_2Cl_2 and washed with water. The combined organic layers were

dried over $MgSO_4$ and concentrated in vacuo. Purification by column chromatography on silica gel (heptane / THF 3:1) gives the desired product as a dark green solid, which was washed with acetonitrile. Yield ≈ 0.5 mg, < 1%. *

MS (MALDI) m/z: 4310.7 [M^+].

* The characterization of this compound could not be performed optimally due to the low amount of compound available, which was not enough to obtain a well-defined ^{1}H-NMR spectrum.

Zn(II)Por-Zn(II)Pc-Pyrene Triad ***70***

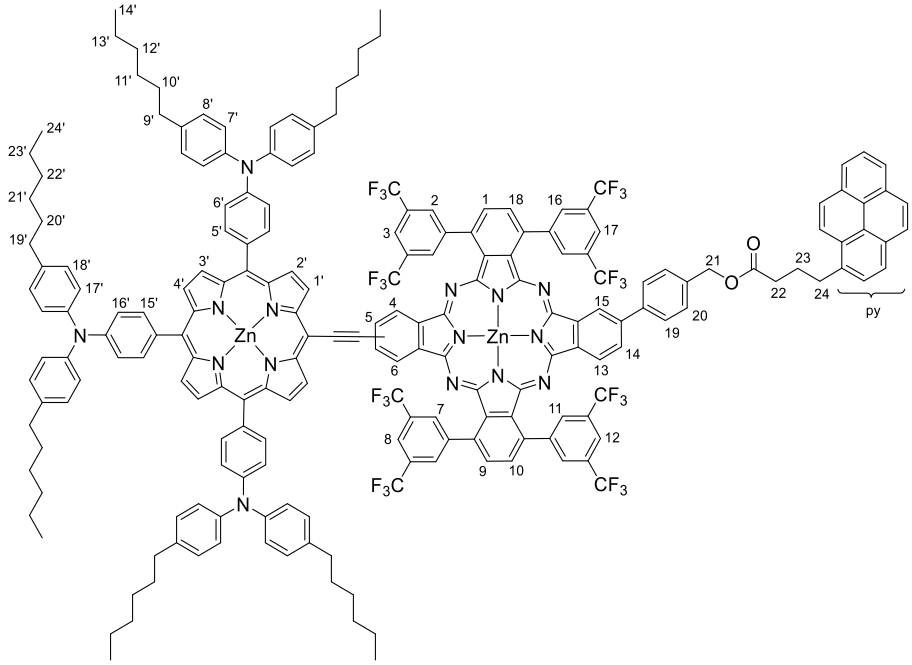

A mixture of 1-pyrenebutyric acid (0.0037 mmol, 1 mg), DCC (0.0037 mmol, 0.7 mg) and DMAP (0.0037 mmol, 0.5 mg) was stirred in dry THF (3 ml) at 0°C for 30 min. Then, a solution of **68** (0.0025 mmol, 8 mg) in dry THF (2 ml) was added dropwise. The mixture was stirred for 1 h at 0°C and for 36 h at room temperature. The resulting reaction crude was filtered through a glass frit and the filtrate was then evaporated. The crude was dissolved in $CHCl_3$ and washed with water, dried over Na_2SO_4 and concentrated in vacuo. Purification by column chromatography (Heptane / THF 3:1) gives the desired product, which was further purified by size exclusion (Bio-Beads) column chromatography in CH_2Cl_2 and triturated with MeOH/H_2O (10:1) to afford a dark green solid. Yield: 3 mg, 40%.

^{1}H-NMR (300 MHz, THF-d_8), δ (ppm): 10.10 (d, *J* = 4.6 Hz, 2H; H-1'), 9.32 (d, *J* = 4.6 Hz, 2H; H-2'), 9.09 (s, 4H; H-3', H-4'), 9.01 (s, 6H), 8.94 (s, 4H), 8.91 (s, 2H), 8.82 (s, 2H), 8.74 (s, 2H), 8.71 (s, 2H), 8.61 (s, 2H), 8.53 (m, 2H), 8.47 – 8.44 (m, 4H), 8.37 – 8.31 (m, 6H), 8.18 – 8.13 (m, 4H; H-py), 8.07 (d, *J* = 8.5 Hz, 2H; H-20), 8.03 (m, 2H), 8.00 – 7.90 (m, 5H; H-py), 7.77 (d, *J* = 8.1 Hz, 2H; H-19), 7.50 (d, *J* = 8.4 Hz, 4H; H-6'), 7.46 – 7.22 (m, 20H), 5.40 (s, 2H; H-21), 2.67 (m, 14H), 1.00 – 0.79 (m, 18H; H-14', H-24').

HR-MS (MALDI) m/z Calcd for [$C_{203}H_{165}F_{24}N_{15}O_2Zn_2$]: 3428.1465; Found: 3428.1544.

UV-Vis (THF), λmax (log ε): 706 (5.11), 645 (4.62), 448 (5.16), 342 (4.9), 325 (4.88), 303 (4.91), 276 (4.95), 243 (4.93) nm.

Mp > 250°C.

2.6 References

(1) *BP Statistical Review of World Energy*; 2016.

(2) Samseth, J.; Banford, A.; Batandjieva-Metcalf, B.; Cantone, M. C.; Lietava, P.; Peimani, H.; Szilagyi, A. *UNEP Year Book - Closing and Decommissioning Nuclear Power Reactors*; 2012.

(3) Smil, V. *Oil: A Beginner's Guide*; Beginner's Guides; Oneworld Publications, 2008.

(4) Vennestrøm, P. N. R.; Osmundsen, C. M.; Christensen, C. H.; Taarning, E. Beyond Petrochemicals: The Renewable Chemicals Industry. *Angew. Chemie Int. Ed.* **2011**, *50* (45), 10502–10509.

(5) Joyce, M. Nonpetroleum share of transportation energy at highest level since 1954 https://www.eia.gov/todayinenergy/detail.php?id=21272.

(6) Balzani, V.; Armaroli, N. *Energy for a Sustainable World: From the Oil Age to a Sun-Powered Future*; Wiley, 2010.

(7) Heede, R. Tracing Anthropogenic Carbon Dioxide and Methane Emissions to Fossil Fuel and Cement Producers, 1854--2010. *Clim. Change* **2014**, *122* (1), 229–241.

(8) Starr, D. The Carbon Accountant. *Science (80-.).* **2016**, *353* (6302), 858 LP-861.

(9) Malakoff, D. The Gas Surge. *Science (80-.).* **2014**, *344* (6191), 1464 LP-1467.

(10) Adgate, J. L.; Goldstein, B. D.; McKenzie, L. M. Potential Public Health Hazards, Exposures and Health Effects from Unconventional Natural Gas Development. *Environ. Sci. Technol.* **2014**, *48* (15), 8307–8320.

(11) Vengosh, A.; Jackson, R. B.; Warner, N.; Darrah, T. H.; Kondash, A. A Critical Review of the Risks to Water Resources from Unconventional Shale Gas Development and Hydraulic Fracturing in the United States. *Environ. Sci. Technol.* **2014**, *48* (15), 8334–8348.

(12) Caulton, D. R.; Shepson, P. B.; Santoro, R. L.; Sparks, J. P.; Howarth, R. W.; Ingraffea, A. R.; Cambaliza, M. O. L.; Sweeney, C.; Karion, A.; Davis, K. J.; et al. Toward a Better Understanding and Quantification of Methane Emissions from Shale Gas Development. *Proc. Natl. Acad. Sci.* **2014**, *111* (17), 6237–6242.

(13) Keranen, K. M.; Weingarten, M.; Abers, G. A.; Bekins, B. A.; Ge, S. Sharp Increase in Central Oklahoma Seismicity since 2008 Induced by Massive Wastewater Injection. *Science (80-.).* **2014**, *345* (6195), 448 LP-451.

(14) Weingarten, M.; Ge, S.; Godt, J. W.; Bekins, B. A.; Rubinstein, J. L. High-Rate Injection Is Associated with the Increase in U.S. Mid-Continent Seismicity. *Science (80-.).* **2015**, *348* (6241), 1336 LP-1340.

(15) Hughes, J. D. Energy: A Reality Check on the Shale Revolution. *Nature* **2013**, *494* (7437), 307–308.

(16) REN 21—Renewable Energy Policy Network for the 21 st Century. *Renewables 2016 Global Status Report*; 2016.

(17) Mathews, J. *Greening of Capitalism: How Asia Is Driving the Next Great Transformation*; Stanford University Press, 2014.

(18) Smil, V. *Energy Transitions: History, Requirements, Prospects*; Praeger, 2010.
(19) Armaroli, N.; Balzani, V. The Future of Energy Supply: Challenges and Opportunities. *Angew. Chemie Int. Ed.* **2007**, *46* (1–2), 52–66.
(20) Schiermeier, Q.; Tollefson, J.; Scully, T.; Witze, A.; Morton, O. Energy Alternatives: Electricity without Carbon. *Nature* **2008**, *454*, 816–823.
(21) Armaroli, N.; Balzani, V. Solar Electricity and Solar Fuels: Status and Perspectives in the Context of the Energy Transition. *Chem. – A Eur. J.* **2016**, *22* (1), 32–57.
(22) Richter, C.; Lincot, D.; Gueymard, C. A. *Solar Energy*; Solar Energy; Springer New York, 2012.
(23) Norton, B. *Harnessing Solar Heat*; Lecture Notes in Energy; Springer Netherlands, 2016.
(24) Chapin, D. M.; Fuller, C. S.; Pearson, G. L. A New Silicon P-n Junction Photocell for Converting Solar Radiation into Electrical Power. *J. Appl. Phys.* **1954**, *25* (5), 676–677.
(25) Nelson, C. A.; Monahan, N. R.; Zhu, X.-Y. Exceeding the Shockley-Queisser Limit in Solar Energy Conversion. *Energy Environ. Sci.* **2013**, *6* (12), 3508–3519.
(26) Peter, L. M. Towards Sustainable Photovoltaics: The Search for New Materials. *Philos. Trans. R. Soc. London A Math. Phys. Eng. Sci.* **2011**, *369* (1942), 1840–1856.
(27) International Energy Agency. *Technology Roadmap—Solar Photovoltaic Energy*; 2014.
(28) Mathews, J. A.; Tan, H. Economics: Manufacture Renewables to Build Energy Security. *Nature* **2014**, *513*, 166–168.
(29) Fthenakis, V. M. End-of-Life Management and Recycling of PV Modules. *Energy Policy* **2000**, *28* (14), 1051–1058.
(30) International Energy Agency-Photovoltaic Power Systems Programme and International Renewable Energy Agency. *End-of-Life Management Solar Photovolatic Panels*; 2016.
(31) Green, M. A. *Third Generation Photovoltaics: Advanced Solar Energy Conversion*; Physics and astronomy online library; Springer, 2003.
(32) Mazzio, K. A.; Luscombe, C. K. The Future of Organic Photovoltaics. *Chem. Soc. Rev.* **2015**, *44* (1), 78–90.
(33) Kearns, D.; Calvin, M. Photovoltaic Effect and Photoconductivity in Laminated Organic Systems. *J. Chem. Phys.* **1958**, *29* (4), 950–951.
(34) Tang, C. W. Two-layer Organic Photovoltaic Cell. *Appl. Phys. Lett.* **1986**, *48* (2), 183–185.
(35) Yu, G.; Gao, J.; Hummelen, J. C.; Wudl, F.; Heeger, A. J. Polymer Photovoltaic Cells: Enhanced Efficiencies via a Network of Internal Donor-Acceptor Heterojunctions. *Science (80-.).* **1995**, *270* (5243), 1789–1791.
(36) Hiramoto, M.; Fujiwara, H.; Yokoyama, M. Three-layered Organic Solar Cell with a Photoactive Interlayer of Codeposited Pigments. *Appl. Phys. Lett.* **1991**, *58* (10), 1062–1064.

(37) Halls, J. J. M.; Walsh, C. A.; Greenham, N. C.; Marseglia, E. A.; Friend, R. H.; Moratti, S. C.; Holmes, A. B. Efficient Photodiodes from Interpenetrating Polymer Networks. *Nature* **1995**, *376* (6540), 498–500.
(38) Roncali, J. Molecular Bulk Heterojunctions: An Emerging Approach to Organic Solar Cells. *Acc. Chem. Res.* **2009**, *42*, 1719–1730.
(39) Kim, J. Y.; Lee, K.; Coates, N. E.; Moses, D.; Nguyen, T.-Q.; Dante, M.; Heeger, A. J. Efficient Tandem Polymer Solar Cells Fabricated by All-Solution Processing. *Science (80-.).* **2007**, *317* (5835), 222–225.
(40) Riede, M.; Uhrich, C.; Widmer, J.; Timmreck, R.; Wynands, D.; Schwartz, G.; Gnehr, W.-M.; Hildebrandt, D.; Weiss, A.; Hwang, J.; et al. Efficient Organic Tandem Solar Cells Based on Small Molecules. *Adv. Funct. Mater.* **2011**, *21* (16), 3019–3028.
(41) Ameri, T.; Li, N.; Brabec, C. J. Highly Efficient Organic Tandem Solar Cells: A Follow up Review. *Energy Environ. Sci.* **2013**, *6* (8), 2390–2413.
(42) Adebanjo, O.; Vaagensmith, B.; Qiao, Q. Double Junction Polymer Solar Cells. *J. Mater. Chem. A* **2014**, *2* (27), 10331–10349.
(43) Peet, J.; Heeger, A. J.; Bazan, G. C. "Plastic" Solar Cells: Self-Assembly of Bulk Heterojunction Nanomaterials by Spontaneous Phase Separation. *Acc. Chem. Res.* **2009**, *42* (11), 1700–1708.
(44) Dennler, G.; Scharber, M. C.; Brabec, C. J. Polymer-Fullerene Bulk-Heterojunction Solar Cells. *Adv. Mater.* **2009**, *21*, 1323–1338.
(45) Gendron, D.; Leclerc, M. New Conjugated Polymers for Plastic Solar Cells. *Energy Environ. Sci.* **2011**, *4* (4), 1225–1237.
(46) Lin, Y.; Li, Y.; Zhan, X. Small Molecule Semiconductors for High-Efficiency Organic Photovoltaics. *Chem. Soc. Rev.* **2012**, *41* (11), 4245–4272.
(47) Mishra, A.; Bäuerle, P. Small Molecule Organic Semiconductors on the Move: Promises for Future Solar Energy Technology. *Angew. Chemie Int. Ed.* **2012**, *51* (9), 2020–2067.
(48) Li, S.; Ye, L.; Zhao, W.; Zhang, S.; Mukherjee, S.; Ade, H.; Hou, J. Energy-Level Modulation of Small-Molecule Electron Acceptors to Achieve over 12% Efficiency in Polymer Solar Cells. *Adv. Mater.* **2016**, *28* (42), 9423–9429.
(49) Heliatek. Heliatek sets new Organic Photovoltaic world record efficiency of 13.2% http://www.heliatek.com/en/press/press-releases/details/heliatek-sets-new-organic-photovoltaic-world-record-efficiency-of-13-2.
(50) Mori, S.; Oh-oka, H.; Nakao, H.; Gotanda, T.; Nakano, Y.; Jung, H.; Iida, A.; Hayase, R.; Shida, N.; Saito, M.; et al. Organic Photovoltaic Module Development with Inverted Device Structure. *MRS Proc. 1737*.
(51) Green, M. A.; Hishikawa, Y.; Dunlop, E. D.; Levi, D. H.; Hohl-Ebinger, J.; Ho-Baillie, A. W. Y. Solar Cell Efficiency Tables (Version 51). *Prog. Photovoltaics Res. Appl.* **2018**, *26* (1), 3–12.
(52) Hagfeldt, A.; Boschloo, G.; Sun, L.; Kloo, L.; Pettersson, H. Dye-Sensitized Solar Cells. *Chem. Rev.* **2010**, *110* (11), 6595–6663.
(53) Nazeeruddin, M. K.; Baranoff, E.; Grätzel, M. Dye-Sensitized Solar Cells:

A Brief Overview. *Sol. Energy* **2011**, *85* (6), 1172–1178.
(54) O'Regan, B.; Gratzel, M. A Low-Cost, High-Efficiency Solar Cell Based on Dye-Sensitized Colloidal TiO2 Films. *Nature* **1991**, *353*, 737–740.
(55) Jung, H. S.; Lee, J.-K. Dye Sensitized Solar Cells for Economically Viable Photovoltaic Systems. *J. Phys. Chem. Lett.* **2013**, *4* (10), 1682–1693.
(56) Mathew, S.; Yella, A.; Gao, P.; Humphry-Baker, R.; CurchodBasile, F. E.; Ashari-Astani, N.; Tavernelli, I.; Rothlisberger, U.; NazeeruddinMd, K.; Grätzel, M. Dye-Sensitized Solar Cells with 13% Efficiency Achieved through the Molecular Engineering of Porphyrin Sensitizers. *Nat Chem* **2014**, *6*, 242–247.
(57) Odobel, F.; Pellegrin, Y.; Gibson, E. A.; Hagfeldt, A.; Smeigh, A. L.; Hammarström, L. Recent Advances and Future Directions to Optimize the Performances of P-Type Dye-Sensitized Solar Cells. *Coord. Chem. Rev.* **2012**, *256* (21–22), 2414–2423.
(58) Perera, I. R.; Daeneke, T.; Makuta, S.; Yu, Z.; Tachibana, Y.; Mishra, A.; Bäuerle, P.; Ohlin, C. A.; Bach, U.; Spiccia, L. Application of the Tris(acetylacetonato)iron(III)/(II) Redox Couple in P-Type Dye-Sensitized Solar Cells. *Angew. Chemie Int. Ed.* **2015**, *54* (12), 3758–3762.
(59) Docampo, P.; Guldin, S.; Leijtens, T.; Noel, N. K.; Steiner, U.; Snaith, H. J. Lessons Learned: From Dye-Sensitized Solar Cells to All-Solid-State Hybrid Devices. *Adv. Mater.* **2014**, *26* (24), 4013–4030.
(60) Fakharuddin, A.; Jose, R.; Brown, T. M.; Fabregat-Santiago, F.; Bisquert, J. A Perspective on the Production of Dye-Sensitized Solar Modules. *Energy Environ. Sci.* **2014**, *7* (12), 3952–3981.
(61) Sharifi, N.; Tajabadi, F.; Taghavinia, N. Recent Developments in Dye-Sensitized Solar Cells. *ChemPhysChem* **2014**, *15*, 3902–3927.
(62) Wu, J.; Lan, Z.; Lin, J.; Huang, M.; Huang, Y.; Fan, L.; Luo, G. Electrolytes in Dye-Sensitized Solar Cells. *Chem. Rev.* **2015**, *115*, 2136–2173.
(63) Haque, S. A.; Palomares, E.; Cho, B. M.; Green, A. N. M.; Hirata, N.; Klug, D. R.; Durrant, J. R. Charge Separation versus Recombination in Dye-Sensitized Nanocrystalline Solar Cells: The Minimization of Kinetic Redundancy. *J. Am. Chem. Soc.* **2005**, *127*, 3456–3462.
(64) Hardin, B. E.; Snaith, H. J.; McGehee, M. D. The Renaissance of Dye-Sensitized Solar Cells. *Nat Phot.* **2012**, *6* (3), 162–169.
(65) Chen, C.-Y.; Wang, M.; Li, J.-Y.; Pootrakulchote, N.; Alibabaei, L.; Ngoc-le, C.; Decoppet, J.-D.; Tsai, J.-H.; Grätzel, C.; Wu, C.-G.; et al. Highly Efficient Light-Harvesting Ruthenium Sensitizer for Thin-Film Dye-Sensitized Solar Cells. *ACS Nano* **2009**, *3*, 3103–3109.
(66) Yin, J.-F.; Velayudham, M.; Bhattacharya, D.; Lin, H.-C.; Lu, K.-L. Structure Optimization of Ruthenium Photosensitizers for Efficient Dye-Sensitized Solar Cells – A Goal toward a "bright" Future. *Coord. Chem. Rev.* **2012**, *256* (23), 3008–3035.
(67) Clifford, J. N.; Planells, M.; Palomares, E. Advances in High Efficiency Dye Sensitized Solar Cells Based on Ru(ii) Free Sensitizers and a Liquid Redox Electrolyte. *J. Mater. Chem.* **2012**, *22* (46), 24195–24201.

(68) Kanaparthi, R. K.; Kandhadi, J.; Giribabu, L. Metal-Free Organic Dyes for Dye-Sensitized Solar Cells: Recent Advances. *Tetrahedron* **2012**, *68* (40), 8383–8393.
(69) Li, L.-L.; Diau, E. W.-G. Porphyrin-Sensitized Solar Cells. *Chem. Soc. Rev.* **2013**, *42* (1), 291–304.
(70) Imahori, H.; Umeyama, T.; Ito, S. Large π-Aromatic Molecules as Potential Sensitizers for Highly Efficient Dye-Sensitized Solar Cells. *Acc. Chem. Res.* **2009**, *42*, 1809–1818.
(71) Lee, M. M.; Teuscher, J.; Miyasaka, T.; Murakami, T. N.; Snaith, H. J. Efficient Hybrid Solar Cells Based on Meso-Superstructured Organometal Halide Perovskites. *Science (80-.).* **2012**, *338* (6107), 643 LP-647.
(72) Kim, H.-S.; Lee, C.-R.; Im, J.-H.; Lee, K.-B.; Moehl, T.; Marchioro, A.; Moon, S.-J.; Humphry-Baker, R.; Yum, J.-H.; Moser, J. E.; et al. Lead Iodide Perovskite Sensitized All-Solid-State Submicron Thin Film Mesoscopic Solar Cell with Efficiency Exceeding 9%. *Sci. Rep.* **2012**, *2*, 591.
(73) Sum, T. C.; Mathews, N. Advancements in Perovskite Solar Cells: Photophysics behind the Photovoltaics. *Energy Environ. Sci.* **2014**, *7* (8), 2518–2534.
(74) Snaith, H. J. Perovskites: The Emergence of a New Era for Low-Cost, High-Efficiency Solar Cells. *J. Phys. Chem. Lett.* **2013**, *4* (21), 3623–3630.
(75) Gao, P.; Gratzel, M.; Nazeeruddin, M. K. Organohalide Lead Perovskites for Photovoltaic Applications. *Energy Environ. Sci.* **2014**, *7* (8), 2448–2463.
(76) Kojima, A.; Teshima, K.; Shirai, Y.; Miyasaka, T. Organometal Halide Perovskites as Visible-Light Sensitizers for Photovoltaic Cells. *J. Am. Chem. Soc.* **2009**, *131* (17), 6050–6051.
(77) Im, J.-H.; Lee, C.-R.; Lee, J.-W.; Park, S.-W.; Park, N.-G. 6.5% Efficient Perovskite Quantum-Dot-Sensitized Solar Cell. *Nanoscale* **2011**, *3* (10), 4088–4093.
(78) Yang, W. S.; Park, B.-W.; Jung, E. H.; Jeon, N. J.; Kim, Y. C.; Lee, D. U.; Shin, S. S.; Seo, J.; Kim, E. K.; Noh, J. H.; et al. Iodide Management in Formamidinium-Lead-Halide Ased Perovskite Layers for Efficient Solar Cells. *Science (80-.).* **2017**, *356*, 1376–1379.
(79) Shi, D.; Adinolfi, V.; Comin, R.; Yuan, M.; Alarousu, E.; Buin, A.; Chen, Y.; Hoogland, S.; Rothenberger, A.; Katsiev, K.; et al. Low Trap-State Density and Long Carrier Diffusion in Organolead Trihalide Perovskite Single Crystals. *Science (80-.).* **2015**, *347* (6221), 519 LP-522.
(80) Boix, P. P.; Agarwala, S.; Koh, T. M.; Mathews, N.; Mhaisalkar, S. G. Perovskite Solar Cells: Beyond Methylammonium Lead Iodide. *J. Phys. Chem. Lett.* **2015**, *6* (5), 898–907.
(81) Gratzel, M. The Light and Shade of Perovskite Solar Cells. *Nat Mater* **2014**, *13* (9), 838–842.
(82) Hailegnaw, B.; Kirmayer, S.; Edri, E.; Hodes, G.; Cahen, D. Rain on Methylammonium Lead Iodide Based Perovskites: Possible

Environmental Effects of Perovskite Solar Cells. *J. Phys. Chem. Lett.* **2015**, *6* (9), 1543–1547.

(83) Ladomenou, K.; Kitsopoulos, T. N.; Sharma, G. D.; Coutsolelos, A. G. The Importance of Various Anchoring Groups Attached on Porphyrins as Potential Dyes for DSSC Applications. *RSC Adv.* **2014**, *4* (41), 21379–21404.

(84) Kay, A.; Graetzel, M. Artificial Photosynthesis. 1. Photosensitization of Titania Solar Cells with Chlorophyll Derivatives and Related Natural Porphyrins. *J. Phys. Chem.* **1993**, *97* (23), 6272–6277.

(85) Martinez-Diaz, M. V.; de la Torre, G.; Torres, T. Lighting Porphyrins and Phthalocyanines for Molecular Photovoltaics. *Chem. Commun.* **2010**, *46*, 7090–7108.

(86) Urbani, M.; Grätzel, M.; Nazeeruddin, M. K.; Torres, T. Meso-Substituted Porphyrins for Dye-Sensitized Solar Cells. *Chem. Rev.* **2014**, *114*, 12330–12396.

(87) Bessho, T.; Zakeeruddin, S. M.; Yeh, C.-Y.; Diau, E. W.-G.; Grätzel, M. Highly Efficient Mesoscopic Dye-Sensitized Solar Cells Based on Donor–Acceptor-Substituted Porphyrins. *Angew. Chemie Int. Ed.* **2010**, *49* (37), 6646–6649.

(88) Yella, A.; Lee, H.-W.; Tsao, H. N.; Yi, C.; Chandiran, A. K.; Nazeeruddin, M. K.; Diau, E. W.-G.; Yeh, C.-Y.; Zakeeruddin, S. M.; Grätzel, M. Porphyrin-Sensitized Solar Cells with Cobalt (II/III)–Based Redox Electrolyte Exceed 12 Percent Efficiency. *Science (80-.).* **2011**, *334*, 629–634.

(89) de la Torre, G.; Claessens, C. G.; Torres, T. Phthalocyanines: Old Dyes, New Materials. Putting Color in Nanotechnology. *Chem. Commun.* **2007**, 2000–2015.

(90) Claessens, C. G.; Hahn, U.; Torres, T. Phthalocyanines: From Outstanding Electronic Properties to Emerging Applications. *Chem. Rec.* **2008**, *8*, 75–97.

(91) Martínez-Díaz, M. V.; Ince, M.; Torres, T. Phthalocyanines: Colorful Macroheterocyclic Sensitizers for Dye-Sensitized Solar Cells. *Monatshefte f{ü}r Chemie - Chem. Mon.* **2011**, *142* (7), 699–707.

(92) Ragoussi, M.-E.; Ince, M.; Torres, T. Recent Advances in Phthalocyanine-Based Sensitizers for Dye-Sensitized Solar Cells. *European J. Org. Chem.* **2013**, *2013*, 6475–6489.

(93) Reddy, P. Y.; Giribabu, L.; Lyness, C.; Snaith, H. J.; Vijaykumar, C.; Chandrasekharam, M.; Lakshmikantam, M.; Yum, J.-H.; Kalyanasundaram, K.; Grätzel, M.; et al. Efficient Sensitization of Nanocrystalline TiO2 Films by a Near-IR-Absorbing Unsymmetrical Zinc Phthalocyanine. *Angew. Chemie Int. Ed.* **2007**, *46* (3), 373–376.

(94) Cid, J.-J.; Yum, J.-H.; Jang, S.-R.; Nazeeruddin, M. K.; Martínez-Ferrero, E.; Palomares, E.; Ko, J.; Grätzel, M.; Torres, T. Molecular Cosensitization for Efficient Panchromatic Dye-Sensitized Solar Cells. *Angew. Chemie Int. Ed.* **2007**, *46*, 8358–8362.

(95) Morandeira, A.; Lopez-Duarte, I.; O'Regan, B.; Martinez-Diaz, M. V.; Forneli, A.; Palomares, E.; Torres, T.; Durrant, J. R. Ru(II)-Phthalocyanine Sensitized Solar Cells: The Influence of Co-Adsorbents upon Interfacial Electron Transfer Kinetics. *J. Mater. Chem.* **2009**, *19*, 5016–5026.
(96) Yum, J.-H.; Jang, S.; Humphry-Baker, R.; Grätzel, M.; Cid, J.-J.; Torres, T.; Nazeeruddin, M. K. Effect of Coadsorbent on the Photovoltaic Performance of Zinc Pthalocyanine-Sensitized Solar Cells. *Langmuir* **2008**, *24* (10), 5636–5640.
(97) Mori, S.; Nagata, M.; Nakahata, Y.; Yasuta, K.; Goto, R.; Kimura, M.; Taya, M. Enhancement of Incident Photon-to-Current Conversion Efficiency for Phthalocyanine-Sensitized Solar Cells by 3D Molecular Structuralization. *J. Am. Chem. Soc.* **2010**, *132* (12), 4054–4055.
(98) O'Regan, B. C.; López-Duarte, I.; Martínez-Díaz, M. V.; Forneli, A.; Albero, J.; Morandeira, A.; Palomares, E.; Torres, T.; Durrant, J. R. Catalysis of Recombination and Its Limitation on Open Circuit Voltage for Dye Sensitized Photovoltaic Cells Using Phthalocyanine Dyes. *J. Am. Chem. Soc.* **2008**, *130*, 2906–2907.
(99) Kimura, M.; Nomoto, H.; Masaki, N.; Mori, S. Dye Molecules for Simple Co-Sensitization Process: Fabrication of Mixed-Dye-Sensitized Solar Cells. *Angew. Chemie Int. Ed.* **2012**, *51*, 4371–4374.
(100) Ikeuchi, T.; Nomoto, H.; Masaki, N.; Griffith, M. J.; Mori, S.; Kimura, M. Molecular Engineering of Zinc Phthalocyanine Sensitizers for Efficient Dye-Sensitized Solar Cells. *Chem. Commun.* **2014**, *50*, 1941–1943.
(101) Ragoussi, M.-E.; Cid, J.-J.; Yum, J.-H.; de la Torre, G.; Di Censo, D.; Grätzel, M.; Nazeeruddin, M. K.; Torres, T. Carboxyethynyl Anchoring Ligands: A Means to Improving the Efficiency of Phthalocyanine-Sensitized Solar Cells. *Angew. Chemie Int. Ed.* **2012**, *51*, 4375–4378.
(102) Alberts, B.; Johnson, A.; Lewis, J.; Morgan, D.; Raff, M.; Roberts, K.; Walter, P. *Molecular Biology of the Cell*; 500 Tips; Garland Science, 2014.
(103) Helms, V. *Principles of Computational Cell Biology*; Wiley, 2008.
(104) Paddon-Row, M. N. Covalently Linked Systems Based on Organic Components. In *Electron Transfer in Chemistry*; Wiley-VCH Verlag GmbH, 2008; pp 178–271.
(105) Gust, D. Very Small Arrays. *Nature* **1997**, *386* (6620), 21–22.
(106) Fox, M. A. PHOTOINDUCED ELECTRON TRANSFER. *Photochem. Photobiol.* **1990**, *52* (3), 617–627.
(107) Fox, M. A.; Chanon, M. *Photoinduced Electron Transfer: Photoinduced Electron Transfer Reactions, Organic Substrates*; Photoinduced Electron Transfer; Elsevier, 1988.
(108) Speiser, S. Photophysics and Mechanisms of Intramolecular Electronic Energy Transfer in Bichromophoric Molecular Systems: Solution and Supersonic Jet Studies. *Chem. Rev.* **1996**, *96* (6), 1953–1976.
(109) Balzani, V. *Electron Transfer in Chemistry*; Electron Transfer in Chemistry; Wiley-VCH Verlag GmbH, 2001.
(110) Poddutoori, P. K.; Bregles, L. P.; Lim, G. N.; Boland, P.; Kerr, R. G.;

D'Souza, F. Modulation of Energy Transfer into Sequential Electron Transfer upon Axial Coordination of Tetrathiafulvalene in an Aluminum(III) Porphyrin–Free-Base Porphyrin Dyad. *Inorg. Chem.* **2015**, *54* (17), 8482–8494.

(111) Fathalla, M.; Barnes, J. C.; Young, R. M.; Hartlieb, K. J.; Dyar, S. M.; Eaton, S. W.; Sarjeant, A. A.; Co, D. T.; Wasielewski, M. R.; Stoddart, J. F. Photoinduced Electron Transfer within a Zinc Porphyrin–Cyclobis(paraquat-P-Phenylene) Donor–Acceptor Dyad. *Chem. – A Eur. J.* **2014**, *20* (45), 14690–14697.

(112) Konev, A. S.; Khlebnikov, A. F.; Prolubnikov, P. I.; Mereshchenko, A. S.; Povolotskiy, A. V; Levin, O. V; Hirsch, A. Synthesis of New Porphyrin–Fullerene Dyads Capable of Forming Charge-Separated States on a Microsecond Lifetime Scale. *Chem. – A Eur. J.* **2015**, *21* (3), 1237–1250.

(113) Guldi, D. M.; Rahman, G. M. A.; Sgobba, V.; Ehli, C. Multifunctional Molecular Carbon Materials-from Fullerenes to Carbon Nanotubes. *Chem. Soc. Rev.* **2006**, *35* (5), 471–487.

(114) Webb, L. E.; Fleischer, E. B. The Structure of Porphine1. *J. Am. Chem. Soc.* **1965**, *87* (3), 667–669.

(115) Ivanov, A. S.; Boldyrev, A. I. Deciphering Aromaticity in Porphyrinoids via Adaptive Natural Density Partitioning. *Org. Biomol. Chem.* **2014**, *12* (32), 6145–6150.

(116) Lash, T. D. Origin of Aromatic Character in Porphyrinoid Systems. *J. Porphyr. Phthalocyanines* **2011**, *15* (11n12), 1093–1115.

(117) D'Souza, F.; Ito, O. Supramolecular Donor-Acceptor Hybrids of Porphyrins/phthalocyanines with Fullerenes/carbon Nanotubes: Electron Transfer, Sensing, Switching, and Catalytic Applications. *Chem. Commun.* **2009**, No. 33, 4913–4928.

(118) Bottari, G.; de la Torre, G.; Guldi, D.; Torres, T. Phthalocyanine-Porphyrin Heteroarrays. In *Multiporphyrin Arrays*; Pan Stanford Publishing, 2012; pp 149–216.

(119) Lo, P.-C.; Leng, X.; Ng, D. K. P. Hetero-Arrays of Porphyrins and Phthalocyanines. *Coord. Chem. Rev.* **2007**, *251* (17–20), 2334–2353.

(120) Liu, J.-Y.; Lo, P.-C.; Ng, D. K. P. Phthalocyanine-Containing Supramolecular Arrays. In *Functional Phthalocyanine Molecular Materials*; Jiang, J., Ed.; Springer Berlin Heidelberg: Berlin, Heidelberg, 2010; pp 169–209.

(121) de la Torre, G.; Bottari, G.; Sekita, M.; Hausmann, A.; Guldi, D. M.; Torres, T. A Voyage into the Synthesis and Photophysics of Homo- and Heterobinuclear Ensembles of Phthalocyanines and Porphyrins. *Chem. Soc. Rev.* **2013**, *42*, 8049–8105.

(122) Ambroise, A.; Wagner, R. W.; Rao, P. D.; Riggs, J. A.; Hascoat, P.; Diers, J. R.; Seth, J.; Lammi, R. K.; Bocian, D. F.; Holten, D.; et al. Design and Synthesis of Porphyrin-Based Optoelectronic Gates. *Chem. Mater.* **2001**, *13* (3), 1023–1034.

(123) El-Khouly, M. E.; Ju, D. K.; Kay, K.-Y.; D'Souza, F.; Fukuzumi, S.

Supramolecular Tetrad of Subphthalocyanine–Triphenylamine–Zinc Porphyrin Coordinated to Fullerene as an "Antenna-Reaction-Center" Mimic: Formation of a Long-Lived Charge-Separated State in Nonpolar Solvent. *Chem. – A Eur. J.* **2010**, *16* (21), 6193–6202.

(124) Menting, R.; Lau, J. T. F.; Xu, H.; Ng, D. K. P.; Roder, B.; Ermilov, E. A. Formation and Photoinduced Processes of a Self-Assembled Subphthalocyanine-Porphyrin-Phthalocyanine Supramolecular Complex. *Chem. Commun.* **2012**, *48* (38), 4597–4599.

(125) Enes, R. F.; Cid, J.-J.; Hausmann, A.; Trukhina, O.; Gouloumis, A.; Vázquez, P.; Cavaleiro, J. A. S.; Tomé, A. C.; Guldi, D. M.; Torres, T. Synthesis and Photophysical Properties of Fullerene–Phthalocyanine–Porphyrin Triads and Pentads. *Chem. – A Eur. J.* **2012**, *18* (6), 1727–1736.

(126) García-Iglesias, M.; Peuntinger, K.; Kahnt, A.; Krausmann, J.; Vázquez, P.; González-Rodríguez, D.; Guldi, D. M.; Torres, T. Supramolecular Assembly of Multicomponent Photoactive Systems via Cooperatively Coupled Equilibria. *J. Am. Chem. Soc.* **2013**, *135* (51), 19311–19318.

(127) Gommans, H.; Aernouts, T.; Verreet, B.; Heremans, P.; Medina, A.; Claessens, C. G.; Torres, T. Perfluorinated Subphthalocyanine as a New Acceptor Material in a Small-Molecule Bilayer Organic Solar Cell. *Adv. Funct. Mater.* **2009**, *19*, 3435–3439.

(128) Iglesias, R. S.; Claessens, C. G.; Torres, T.; Herranz, M. Á.; Ferro, V. R.; García de la Vega, J. M. Subphthalocyanine-Fused Dimers and Trimers: Synthetic, Electrochemical, and Theoretical Studies. *J. Org. Chem.* **2007**, *72* (8), 2967–2977.

(129) Wijesinghe, C. A.; El-Khouly, M. E.; Zandler, M. E.; Fukuzumi, S.; D'Souza, F. A Charge-Stabilizing, Multimodular, Ferrocene–Bis(triphenylamine)–Zinc-porphyrin–Fullerene Polyad. *Chem. – A Eur. J.* **2013**, *19* (29), 9629–9638.

(130) D'Souza, F.; Gadde, S.; Islam, D.-M. S.; Wijesinghe, C. A.; Schumacher, A. L.; Zandler, M. E.; Araki, Y.; Ito, O. Multi-Triphenylamine-Substituted Porphyrin-Fullerene Conjugates as Charge Stabilizing "Antenna−Reaction Center" Mimics. *J. Phys. Chem. A* **2007**, *111* (35), 8552–8560.

(131) Lo, C.-F.; Hsu, S.-J.; Wang, C.-L.; Cheng, Y.-H.; Lu, H.-P.; Diau, E. W.-G.; Lin, C.-Y. Tuning Spectral and Electrochemical Properties of Porphyrin-Sensitized Solar Cells. *J. Phys. Chem. C* **2010**, *114*, 12018–12023.

(132) Chang, Y.-C.; Wang, C.-L.; Pan, T.-Y.; Hong, S.-H.; Lan, C.-M.; Kuo, H.-H.; Lo, C.-F.; Hsu, H.-Y.; Lin, C.-Y.; Diau, E. W.-G. A Strategy to Design Highly Efficient Porphyrin Sensitizers for Dye-Sensitized Solar Cells. *Chem. Commun.* **2011**, *47*, 8910–8912.

(133) Mazitschek, R.; Mülbaier, M.; Giannis, A. IBX-Mediated Oxidation of Primary Alcohols and Aldehydes To Form Carboxylic Acids. *Angew. Chemie Int. Ed.* **2002**, *41*, 4059–4061.

(134) Kang, S. H.; Choi, I. T.; Kang, M. S.; Eom, Y. K.; Ju, M. J.; Hong, J. Y.; Kang, H. S.; Kim, H. K. Novel D-P-A Structured Porphyrin Dyes with

Diphenylamine Derived Electron-Donating Substituents for Highly Efficient Dye-Sensitized Solar Cells. *J. Mater. Chem. A* **2013**, *1* (12), 3977–3982.

(135) Tian, H.; Ali, H.; van Lier, J. E. Synthesis of Water Soluble Trisulfonated Phthalocyanines via Palladium-Catalysed Cross Coupling Reactions. *Tetrahedron Lett.* **2000**, *41*, 8435–8438.

(136) Haumesser, J.; Pereira, A. M. V. M.; Gisselbrecht, J.-P.; Merahi, K.; Choua, S.; Weiss, J.; Cavaleiro, J. A. S.; Ruppert, R. Inexpensive and Efficient Ullmann Methodology To Prepare Donor-Substituted Porphyrins. *Org. Lett.* **2013**, *15*, 6282–6285.

(137) Yella, A.; Mai, C.-L.; Zakeeruddin, S. M.; Chang, S.-N.; Hsieh, C.-H.; Yeh, C.-Y.; Grätzel, M. Molecular Engineering of Push–Pull Porphyrin Dyes for Highly Efficient Dye-Sensitized Solar Cells: The Role of Benzene Spacers. *Angew. Chemie Int. Ed.* **2014**, *53*, 2973–2977.

(138) He, J.; Benkö, G.; Korodi, F.; Polívka, T.; Lomoth, R.; Åkermark, B.; Sun, L.; Hagfeldt, A.; Sundström, V. Modified Phthalocyanines for Efficient Near-IR Sensitization of Nanostructured TiO2 Electrode. *J. Am. Chem. Soc.* **2002**, *124* (17), 4922–4932.

(139) Cardona, C. M.; Li, W.; Kaifer, A. E.; Stockdale, D.; Bazan, G. C. Electrochemical Considerations for Determining Absolute Frontier Orbital Energy Levels of Conjugated Polymers for Solar Cell Applications. *Adv. Mater.* **2011**, *23* (20), 2367–2371.

(140) Connelly, N. G.; Geiger, W. E. Chemical Redox Agents for Organometallic Chemistry. *Chem. Rev.* **1996**, *96* (2), 877–910.

(141) Wu, S.-L.; Lu, H.-P.; Yu, H.-T.; Chuang, S.-H.; Chiu, C.-L.; Lee, C.-W.; Diau, E. W.-G.; Yeh, C.-Y. Design and Characterization of Porphyrin Sensitizers with a Push-Pull Framework for Highly Efficient Dye-Sensitized Solar Cells. *Energy Environ. Sci.* **2010**, *3* (7), 949–955.

(142) Imahori, H.; Matsubara, Y.; Iijima, H.; Umeyama, T.; Matano, Y.; Ito, S.; Niemi, M.; Tkachenko, N. V; Lemmetyinen, H. Effects of Meso-Diarylamino Group of Porphyrins as Sensitizers in Dye-Sensitized Solar Cells on Optical, Electrochemical, and Photovoltaic Properties. *J. Phys. Chem. C* **2010**, *114* (23), 10656–10665.

(143) Meyer, T.; Ogermann, D.; Pankrath, A.; Kleinermanns, K.; Müller, T. J. J. Phenothiazinyl Rhodanylidene Merocyanines for Dye-Sensitized Solar Cells. *J. Org. Chem.* **2012**, *77* (8), 3704–3715.

(144) Ragoussi, M.-E.; de la Torre, G.; Torres, T. Tuning the Electronic Properties of Porphyrin Dyes: Effects of Meso Substitution on Their Optical and Electrochemical Behaviour. *European J. Org. Chem.* **2013**, *2013* (14), 2832–2840.

(145) Paulsson, H.; Kloo, L.; Hagfeldt, A.; Boschloo, G. Electron Transport and Recombination in Dye-Sensitized Solar Cells with Ionic Liquid Electrolytes. *J. Electroanal. Chem.* **2006**, *586*, 56–61.

(146) Nakade, S.; Kanzaki, T.; Kubo, W.; Kitamura, T.; Wada, Y.; Yanagida, S. Role of Electrolytes on Charge Recombination in Dye-Sensitized TiO2 Solar Cell (1): The Case of Solar Cells Using the I-/I3- Redox Couple. *J.*

Phys. Chem. B **2005**, *109*, 3480–3487.
(147) Lee, K.-M.; Suryanarayanan, V.; Ho, K.-C.; Justin Thomas, K. R.; Lin, J. T. Effects of Co-Adsorbate and Additive on the Performance of Dye-Sensitized Solar Cells: A Photophysical Study. *Sol. Energy Mater. Sol. Cells* **2007**, *91*, 1426–1431.
(148) Kopidakis, N.; Neale, N. R.; Frank, A. J. Effect of an Adsorbent on Recombination and Band-Edge Movement in Dye-Sensitized TiO2 Solar Cells: Evidence for Surface Passivation. *J. Phys. Chem. B* **2006**, *110*, 12485–12489.
(149) Boschloo, G.; Häggman, L.; Hagfeldt, A. Quantification of the Effect of 4-Tert-Butylpyridine Addition to I-/I3- Redox Electrolytes in Dye-Sensitized Nanostructured TiO2 Solar Cells. *J. Phys. Chem. B* **2006**, *110*, 13144–13150.
(150) Stathatos, E.; Lianos, P.; Zakeeruddin, S. M.; Liska, P.; Grätzel, M. A Quasi-Solid-State Dye-Sensitized Solar Cell Based on a Sol−Gel Nanocomposite Electrolyte Containing Ionic Liquid. *Chem. Mater.* **2003**, *15*, 1825–1829.
(151) Kimura, M.; Nomoto, H.; Suzuki, H.; Ikeuchi, T.; Matsuzaki, H.; Murakami, T. N.; Furube, A.; Masaki, N.; Griffith, M. J.; Mori, S. Molecular Design Rule of Phthalocyanine Dyes for Highly Efficient Near-IR Performance in Dye-Sensitized Solar Cells. *Chem. – A Eur. J.* **2013**, *19*, 7496–7502.
(152) Haid, S.; Marszalek, M.; Mishra, A.; Wielopolski, M.; Teuscher, J.; Moser, J.-E.; Humphry-Baker, R.; Zakeeruddin, S. M.; Grätzel, M.; Bäuerle, P. Significant Improvement of Dye-Sensitized Solar Cell Performance by Small Structural Modification in π-Conjugated Donor–Acceptor Dyes. *Adv. Funct. Mater.* **2012**, *22*, 1291–1302.
(153) Lindsey, J. S.; Schreiman, I. C.; Hsu, H. C.; Kearney, P. C.; Marguerettaz, A. M. Rothemund and Adler-Longo Reactions Revisited: Synthesis of Tetraphenylporphyrins under Equilibrium Conditions. *J. Org. Chem.* **1987**, *52* (5), 827–836.
(154) Claessens, C. G.; González-Rodríguez, D.; Torres, T. Subphthalocyanines: Singular Nonplanar Aromatic CompoundsSynthesis, Reactivity, and Physical Properties. *Chem. Rev.* **2002**, *102*, 835–854.
(155) Gotfredsen, H.; Jevric, M.; Kadziola, A.; Nielsen, M. B. Acetylenic Scaffolding with Subphthalocyanines. *European J. Org. Chem.* **2016**, *2016* (1), 17–21.
(156) Guilleme, J.; González-Rodríguez, D.; Torres, T. Triflate-Subphthalocyanines: Versatile, Reactive Intermediates for Axial Functionalization at the Boron Atom. *Angew. Chemie Int. Ed.* **2011**, *50* (15), 3506–3509.
(157) Böhm, V. P. W.; Herrmann, W. A. A Copper-Free Procedure for the Palladium-Catalyzed Sonogashira Reaction of Aryl Bromides with Terminal Alkynes at Room Temperature. *European J. Org. Chem.* **2000**, *2000* (22), 3679–3681.
(158) Mery, D.; Heuze, K.; Astruc, D. A Very Efficient, Copper-Free Palladium

Catalyst for the Sonogashira Reaction with Aryl Halides. *Chem. Commun.* **2003**, No. 15, 1934–1935.
(159) Liu, B.; Zhu, W.; Wang, Y.; Wu, W.; Li, X.; Chen, B.; Long, Y.-T.; Xie, Y. Modulation of Energy Levels by Donor Groups: An Effective Approach for Optimizing the Efficiency of Zinc-Porphyrin Based Solar Cells. *J. Mater. Chem.* **2012**, *22* (15), 7434–7444.
(160) Berera, R.; van Grondelle, R.; Kennis, J. T. M. Ultrafast Transient Absorption Spectroscopy: Principles and Application to Photosynthetic Systems. *Photosynth. Res.* **2009**, *101*, 105–118.
(161) Telle, H. H.; Ureña, A. G.; Donovan, R. J. *Laser Chemistry: Spectroscopy, Dynamics and Applications*; Wiley, 2007.
(162) Maciejewski, A.; Naskrecki, R.; Lorenc, M.; Ziolek, M.; Karolczak, J.; Kubicki, J.; Matysiak, M.; Szymanski, M. Transient Absorption Experimental Set-up with Femtosecond Time Resolution. Femto- and Picosecond Study of DCM Molecule in Cyclohexane and Methanol Solution. *J. Mol. Struct.* **2000**, *555* (1), 1–13.
(163) Yzambart, G.; Zieleniewska, A.; Bauroth, S.; Clark, T.; Bryce, M. R.; Guldi, D. M. Charge-Gating Dibenzothiophene-S,S-Dioxide Bridges in Electron Donor–Bridge–Acceptor Conjugates. *J. Phys. Chem. C* **2017**, *121* (25), 13557–13569.
(164) Trukhina, O.; Rudolf, M.; Bottari, G.; Akasaka, T.; Echegoyen, L.; Torres, T.; Guldi, D. M. Bidirectional Electron Transfer Capability in Phthalocyanine–Sc3N@Ih–C80 Complexes. *J. Am. Chem. Soc.* **2015**, *137*, 12914–12922.
(165) Neises, B.; Steglich, W. Simple Method for the Esterification of Carboxylic Acids. *Angew. Chemie Int. Ed. English* **1978**, *17* (7), 522–524.
(166) Frisch, M. J.; Trucks, G. W.; Schlegel, H. B.; Scuseria, G. E.; Robb, M. A.; Cheeseman, J. R.; Scalmani, G.; Barone, V.; Mennucci, B.; Petersson, G. A.; et al. Gaussian 09, Revision B.01. *Gaussian 09, Revision B.01, Gaussian, Inc., Wallingford CT*. Wallingford CT 2009.
(167) Lynch, B. J.; Fast, P. L.; Harris, M.; Truhlar, D. G. Adiabatic Connection for Kinetics. *J. Phys. Chem. A* **2000**, *104* (21), 4811–4815.
(168) Hay, P. J.; Wadt, W. R. Ab Initio Effective Core Potentials for Molecular Calculations. Potentials for the Transition Metal Atoms Sc to Hg. *J. Chem. Phys.* **1985**, *82* (1), 270–283.
(169) Chai, J.-D.; Head-Gordon, M. Long-Range Corrected Hybrid Density Functionals with Damped Atom-Atom Dispersion Corrections. *Phys. Chem. Chem. Phys.* **2008**, *10* (44), 6615–6620.
(170) Barone, V.; Cossi, M. Quantum Calculation of Molecular Energies and Energy Gradients in Solution by a Conductor Solvent Model. *J. Phys. Chem. A* **1998**, *102* (11), 1995–2001.
(171) Ito, S.; Murakami, T. N.; Comte, P.; Liska, P.; Grätzel, C.; Nazeeruddin, M. K.; Grätzel, M. Fabrication of Thin Film Dye Sensitized Solar Cells with Solar to Electric Power Conversion Efficiency over 10%. *Thin Solid Films* **2008**, *516* (14), 4613–4619.

(172) Hylarides, M. D.; Scott Wilbur, D.; Hadley, S. W.; Fritzberg, A. R. Synthesis and Iodination of Methyl 4-Tri-N-Butylstannylbenzoate, P-(Methoxycarbonyl)phenylmercuric Chloride and P-(Methoxycarbonyl)phenylboronic Acid. *J. Organomet. Chem.* **1989**, *367*, 259–265.

(173) Urnikaite, S.; Malinauskas, T.; Bruder, I.; Send, R.; Gaidelis, V.; Sens, R.; Getautis, V. Organic Dyes with Hydrazone Moieties: A Study of Correlation between Structure and Performance in the Solid-State Dye-Sensitized Solar Cells. *J. Phys. Chem. C* **2014**, *118* (15), 7832–7843.

(174) Nok, T. H.; Chenyi, Y.; Moehl, T.; Yum, J.-H.; Zakeeruddin, S. M.; Nazeeruddin, M. K.; Grätzel, M. Cyclopentadithiophene Bridged Donor–Acceptor Dyes Achieve High Power Conversion Efficiencies in Dye-Sensitized Solar Cells Based on the Tris-Cobalt Bipyridine Redox Couple. *ChemSusChem* **2011**, *4* (5), 591–594.

(175) Yi, C.; Giordano, F.; Cevey-Ha, N.-L.; Tsao, H. N.; Zakeeruddin, S. M.; Grätzel, M. Influence of Structural Variations in Push–Pull Zinc Porphyrins on Photovoltaic Performance of Dye-Sensitized Solar Cells. *ChemSusChem* **2014**, *7* (4), 1107–1113.

(176) Gao, P.; Kim, Y. J.; Yum, J.-H.; Holcombe, T. W.; Nazeeruddin, M. K.; Gratzel, M. Facile Synthesis of a Bulky BPTPA Donor Group Suitable for Cobalt Electrolyte Based Dye Sensitized Solar Cells. *J. Mater. Chem. A* **2013**, *1* (18), 5535–5544.

(177) Claessens, C. G.; Torres, T. Synthesis, Separation, and Characterization of the Topoisomers of Fused Bicyclic Subphthalocyanine Dimers. *Angew. Chemie Int. Ed.* **2002**, *41*, 2561–2565.

(178) Claessens, C. G.; González-Rodríguez, D.; del Rey, B.; Torres, T.; Mark, G.; Schuchmann, H.-P.; von Sonntag, C.; MacDonald, J. G.; Nohr, R. S. Highly Efficient Synthesis of Chloro- and Phenoxy-Substituted Subphthalocyanines. *European J. Org. Chem.* **2003**, *2003* (14), 2547–2551.

Chapter 3 – Metallo-Organic Helicate based on Phthalocyanines: Preparation and Host-Guest studies

3.1 Supramolecular chemistry

According 1987 Nobel laureate Jean-Marie Lehn, *supramolecular chemistry may be defined as "chemistry beyond the molecule", bearing on the organized entities of higher complexity that result from the association of two or more chemical species held together by intermolecular forces.*[1]

This area of chemistry is based, in fact, upon molecular systems whose components are held together by weak and reversible intermolecular forces, such as hydrogen bonding, metal coordination, hydrophobic forces, van der Waals forces, π–π interactions and electrostatic effects. This strategy makes it possible to construct highly complex functional chemical systems, by overcoming problems arising through traditional chemistry utilizing strong covalent bonds, which typically results in low yields as the complexity of the molecule increases. For these reasons the multidisciplinary area of supramolecular chemistry has undergone extraordinary development during the last decades.[2]

The existence of intermolecular forces was first postulated by Johannes Diderik van der Waals in 1873. However, Nobel laureate Hermann Emil Fischer developed supramolecular chemistry's philosophical roots. In 1894 Fischer suggested that enzyme-substrate interactions take the form of a *lock and key*,[3] the fundamental principle of molecular recognition and host-guest chemistry. The breakthrough came in the 1960s with the discoveries of *crown ethers*, *cryptands* and *spherands* respectively by Pedersen,[4] Lehn[1] and Cram,[5] as shape- and ion-selective receptors.

Afterwards, throughout the 1980s research in the area takes a brisk pace with emerging concepts such as mechanically interlocked molecular architectures.[6,7] In the 1990s, supramolecular chemistry became even more sophisticated, with molecular machinery and highly complex self-assembled structures, the importance of which was established by the 2016 Nobel Prize for Chemistry, which was awarded to Jean-Pierre Sauvage, Sir J. Fraser Stoddart, and Ben L. Feringa in recognition of their work in this area.[8]

Other important concepts that go hand in hand with supramolecular chemistry include molecular self-assembly, molecular recognition, host-guest chemistry and dynamic covalent chemistry.

3.1.1 Molecular Self – Assembly

The molecular self – assembly is the spontaneous association of two or more molecules, through reversible intermolecular interactions and under equilibrium conditions, into larger, stable and structurally well-defined supramolecules, which have different physicochemical properties than those of precursor building blocks.

Typical systems are designed such that the self-assembly process is kinetically reversible; the individual building blocks gradually funnel towards an ensemble that represents the thermodynamic minimum of the system via numerous association and dissociation steps, thus providing a number of interesting properties such as error correction, self-healing, and high sensitivity to external stimuli.[9] By tuning various reaction parameters, the reaction equilibrium can be shifted towards the desired product. As such, self-assembly has a distinct advantage over traditional stepwise synthetic approaches when accessing large molecules.

The molecules participating in the self-assembly process contain complementary functionalities capable of driving the organization of matter over its structural features.

On the basis of the interactions used in the self-assembly process, supramolecular chemistry can be broadly classified into three main branches: (i) those that utilize H-bonding motifs in the supramolecular architectures; (ii) processes that primarily use other noncovalent interactions such as ion-ion, ion-dipole, $\pi-\pi$ stacking, cation-π, van der Waals, and hydrophobic interactions; and (iii) those that employ strong and directional metal-ligand bonds for the assembly process. However, as the scale and degree of complexity of desired molecules increase, the assembly of small molecular units into larger, discrete supramolecules becomes an increasingly daunting task. This has been due in large part to the inability to completely control the directionality of the weak forces employed in the first two classifications above. *Coordination-driven self-assembly*, which defines the third approach, affords a greater control over the rational design of two- and three-dimensional architectures.

3.1.2 Metal-Organic Self-Assembly of 3D Complexes

Metal-organic self-assembly describes the formation of species where the self-assembly process is directed by the formation of multiple dative metal-ligand bonds.[10]

This approach has been used extensively in the formation of a variety of diverse chemical assemblies, including helicates,[11] 2D grids/arrays,[12] 3D molecular containers,[13] metallopolymers,[14] and topological species such as catenanes[15] and knots.[16,17]

The widespread application of metal-organic self-assembly is indicative of its advantages over other self-assembly approaches, all of which stem from the ability to control the nature of metal-ligand interactions. The lability of a metal-ligand interaction is dependent on the metal ion employed and the nature of the ligands.[18] The energies of metal-ligand bonds (15-50 kcal/mol), which are intermediate between the energies of organic covalent bonds (*ca*. 60-120 kcal/mol) and other weak interactions (*ca*. 0.5-10 kcal/mol), help in modulating the coordination kinetics of the self-assembly process. The kinetic reversibility between complementary building blocks, reaction intermediates, and self-assembled architectures provides a way for the system to self-correct (an "incorrectly" formed bond can dissociate and re-associate "correctly"), leading to a product that is thermodynamically more stable than the starting components and any kinetically formed intermediates.[19]

Another important feature is the directional nature of metal-ligand interactions. This is a consequence of the well-defined coordination geometries adopted by different metal ions. Thus, transition metals, with their preferred coordination geometries, act as acceptor units that can logically self-assemble with various rigid or flexible donors into predictable architectures. This has led to different research groups to propose design strategies for building large metal-organic assemblies.[10,19,20] Two of the main strategies developed and adopted in recent years are the so-called *directional bonding*[10,21,22] and *symmetry interaction*[23–26] approaches. These synthetic strategies have led to a wide variety of 2D and 3D molecular architectures of different shapes and sizes, which can be modulated through the judicious choice of metals and ligands. Mechanistically speaking, these approaches rely on thermodynamic control: the global minimum of the reaction coordinate is the desired product.

3.1.2.1 Directional Bonding Approach

This methodology was developed principally by Stang and co-workers. There are two basic structural requirements for the construction of supramolecular architectures by this approach: first, the complementary precursor units (called *donor* and *acceptor*) must be structurally rigid with predefined bite angles; and second, the appropriate stoichiometric ratio of the precursors must be used.

The donor building blocks are generally organic ligands having two or more binding sites. The acceptors are metal-containing subunits that are vital in this design approach because they possess available coordination sites, which are at a fixed angle relative to one another for binding incoming ligands. The symmetry and number of binding sites within each precursor unit guide the shape of the target assembly (Figure 3.1).

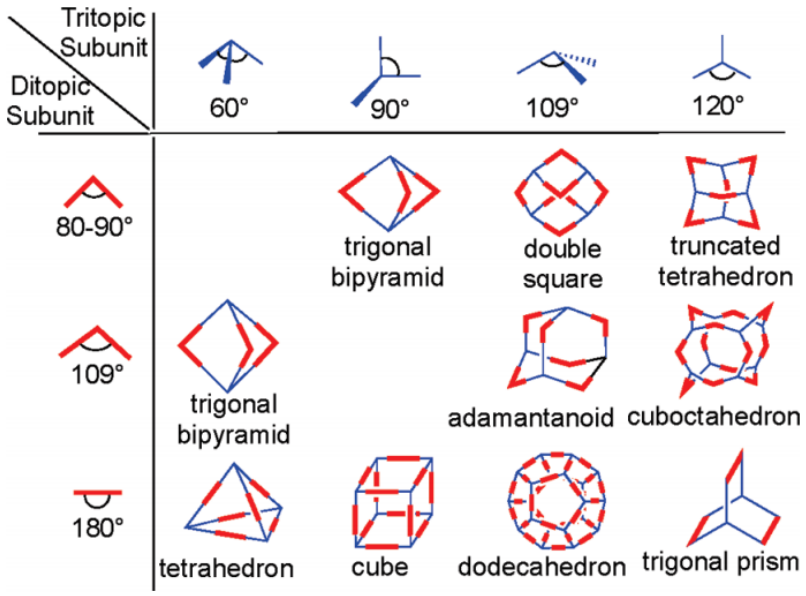

Figure 3.1. Three-dimensional architectures formed by the combination of ditopic and tritopic subunits by the directional bonding approach.

3.1.2.2 Symmetry Interaction Approach

This design strategy has been developed as a rational synthetic approach for the synthesis of high-symmetry coordination clusters using metal-ligand bonds. It is based on the geometric relationship between the chelating ligands and the metals used. The strong binding affinity and coordination mode of chelating ligands, along with the inherent symmetry of the coordination sites available on

the naked metal center, act as the driving force for the assembly process. In general, multibranched chelating ligands with rigid backbones are used in conjunction with transition metals or main group metals. The orientation of the multiple binding sites that are rigidly fixed is critical to the selectivity of a particular molecular geometry and helps to avoid the formation of oligomers and polymers.

Raymond and co-workers have defined the requisites of this design principle in terms of the geometric relationship between the ligand and the metal component using symmetry considerations.[24] A *coordinate vector* represents the interaction between a ligand and metal. For chelating ligands, the plane orthogonal to the major symmetry axis of a metal complex is the *chelate plane* (Figure 3.2), which in the case of bidentate chelators holds all chelate vectors.[25] Thus, depending on the orientation of the chelate planes, the construction of high-symmetrical coordination clusters can be realized. Furthermore, the proper organization of the multiple binding sites with respect to one another is of paramount importance.

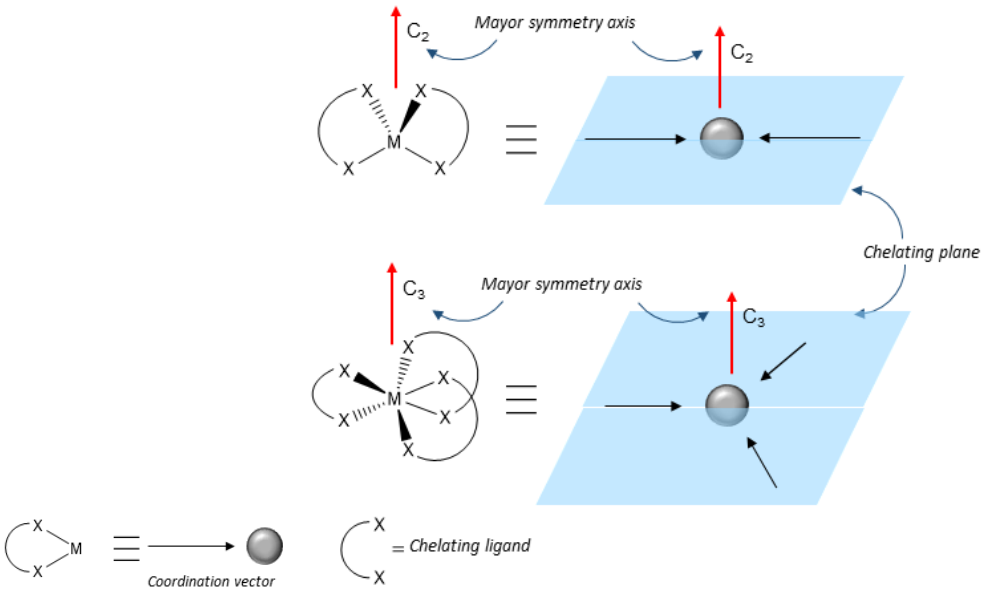

Figure 3.2. Coordinate vector, chelating plane and mayor symmetry axis for the symmetry interaction method.

For example, to design a M_2L_3 triple helicate having an idealized D_{3h} symmetry, it must be ensured that both the C_2 and C_3 axes are orthogonal and are pre-programmed into the chelating ligand and the metal center. Since the two pseudo-octahedral metal centers share the same C_3 axis, the two chelating planes must be parallel to achieve the triple helicate (Figure 3.3).

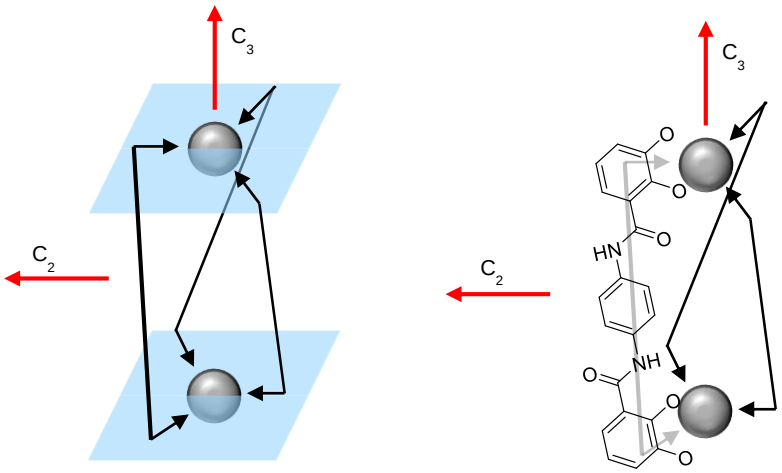

Figure 3.3. Design of a D_3-symmetrical triple helicate.

A similar approach can be applied for the rational design of tetrahedral clusters. In a M_4L_6 tetrahedron, the four metal atoms occupy the vertices and the six ligands are disposed on the edges of the tetrahedron. This requires that the C_2 axes of the tetrahedron lie within the chelate plane at each of the metal centers. Furthermore, the chelate vectors within the ligand must maintain an angle of 70.6° (Figure 3.4).[26]

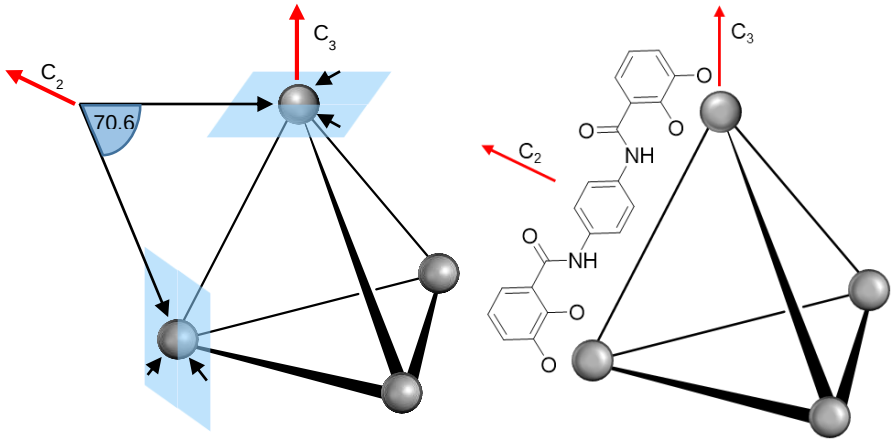

Figure 3.4. Design of an M_4L_6 tetrahedron.

3.1.2.3 The Subcomponent Self-Assembly Approach

The *subcomponent self-assembly* can be considered as a subset of metalloorganic self-assembly.[27–29] This technique involves the assembly of building blocks by the formation of coordinative (N → metal) and covalent (N=C)[30,31] bonds during a single overall process.[32]

The first example of this approach was reported by Melson *et al* as a way to prepare dynamic covalent macrocycles about a central Ni^{II} ion.[33] Similar approaches were later adopted by other other researchers to prepare a wealth of structures, including macrocycles,[34,35] helicates,[36,37] rotaxanes,[38,39] catenanes,[39,40] grids,[41,42] and a Borromean link.[43]

An important proof-of-concept of this method was reported by J. Nitschke in 2004, who formed a stable pyridylimine-based mononuclear $Cu^{I}L_2$ complex in water by subcomponent self-assembly (Scheme 3.1).[44] Imine formation is a dynamic process that occurs through the condensation of an aldehyde and an amine, thus imine formation is disfavoured in water. Moreover, Cu^{I} disproportionates to Cu^{0} metal and Cu^{II} in aqueous media. However, when both Cu^{I} and pyridylimine subcomponents are present in solution, the imine condensation is driven by the chelating product coordinating to the Cu^{I} centre, while the metal ion is also stabilized by the formation of dative metal-ligand bonds. Thus, the components of the reaction are mutually stabilized.

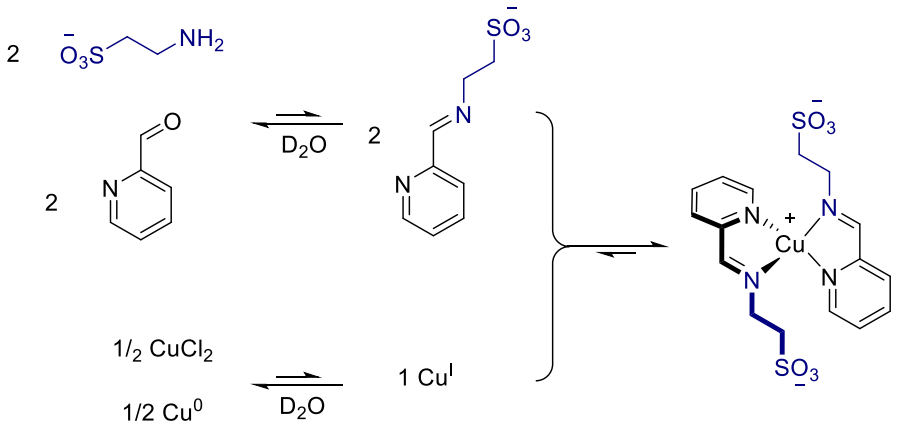

Scheme 3.1. The mutual stabilization of imine ligands and Cu^{I} ions in aqueous solution.

3.1.3 Coordination Cages and Host-Guest interactions

Following the previous strategy, a wide variety of metallo-supramolecular structures have been reported, which have been defined in some cases as capsules, cages or molecular containers.[30,45] Some of these metal-organic ensembles, in fact, can act as a receptor (*host*), since they hold well-enclosed cavities, which are able to accommodate a smaller molecule (*guest*) through complexation events, obtaining a so-called *host-guest complex*.

There are several factors to take into account for the design of the host molecule in order to obtain a highly stable host-guest adduct, since supramolecular interactions are weak. When two or more binding sites on a receptor cooperate to bind to a guest the phenomenon is known as *cooperativity*. Additionally, it is essential a size and shape complementarity between the binding sites of the interacting species, which is known as *preorganization*. Finally, it is very important to consider that the interactions between a host and its guest are not isolated as a result of external influences. In fact, in real systems, guests are competing with surrounding solvent molecules. For binding to occur, many interactions between the receptor and solvent molecules must be broken, which has both enthalpic and entropic consequences. The ultimate goals in the design of supramolecular receptors is the achievement of *selectivity* and *reversibility*. *Selectivity* is the preferential encapsulation of a guest over another. In the design of host molecules, the binding sites need to be tuned in order to target a specific guest. With regard to *reversibility*, it is understood as the possibility to liberate the sequestered guest. The process of guest exchange in supramolecular systems can occur via the total or partial dissociation of the receptor, or by diffusion through the gate apertures, or even through a simply replacement of the non-covalently bound molecule from the interior of a larger host structure by a new preferential guest. [46–48]

3.1.3.1 Applications of Coordination Cages

The development of three dimensional coordination architectures has drawn the attention of many researchers due to the multiple potential applications that these structures can offer. Their isolated cavities create a unique environment and geometric constraint which can be selectively functionalized, and thus provide different interactions with a molecule from those of the bulk solution. The wide range of applications that 3D coordination capsules confer, can be classified in four main categories:

- *Biomedical applications.* The use of coordination capsules for biological and medical applications is a developing field of research. Many research groups have become interested in the design of drug carriers.[49,50] In these systems, a biologically active compound is confined within a capsule, in order to protect it from the environment. Then the encapsulated molecule is carried to a specific location in the organism, where it can be liberated upon application of an external stimulus. For example, Lippard *et al*. reported on an innovative application of a tetrahedral metallo-supramolecular cage as nanocontainer of a cis-platinum prodrug able to exhibit high cellular uptake.[51] More recently, Mascareñas *et al*. presented a novel approach to control the cell uptake of oligoarginine cell-penetrating peptides based on the formation of a host−guest supramolecular complex involving an anion recognition process. The strategy relies on the encapsulation of a negatively charged pyranine attached to the N-terminus of a peptide containing an octaarginine cell-penetrating peptide (Figure 3.5).[52] Interestingly, the covalent cage used as host was synthetized by reduction of the corresponding metallo–organic precursor.[53]

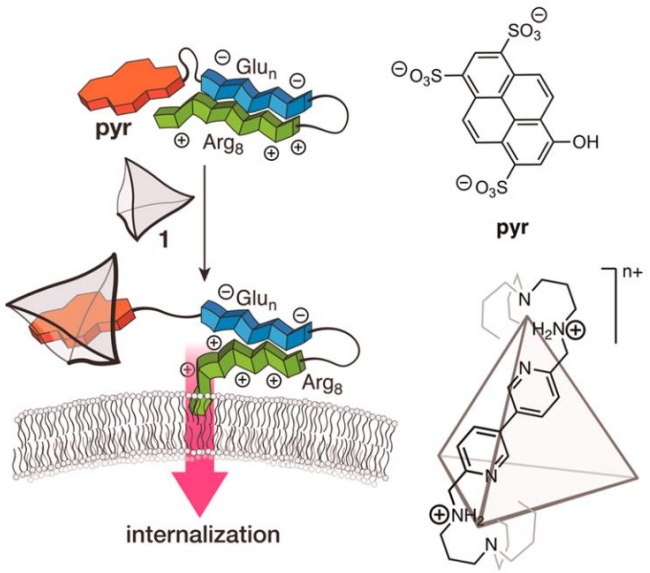

Figure 3.5. Concept of the cell-penetrating peptides strategy and structures of pyranine (pyr), and the covalent host cage.[52]

Last but not least in the field of biomedical applications, it was demonstrated that metal-organic architectures can be taken up by tumor cells and exhibit antitumor activity.[54]

- *Molecular sensors.* Several research groups have developed nanocapsules which can be used as molecular sensors.[55,56] The host-guest interaction can be measured by a chemical or physical change on the receptor that in some cases can be easily observed. For instance, Stang *et al*. reported trigonal-prismatic cages based on 1,3,5-tris(4-pyridyl ethenyl)benzene ligands and dinuclear ruthenium arene metallo-linkers.[57] The fluorescence emission of these electron-rich capsules was quenched upon addition of electron deficient nitroaromatic substrates. Another very interesting example comes from the Duanand co-workers's work (Figure 3.6).[58] They prepared an emissive M_4L_4 molecular tetrahedral cage wherein four cerium(IV) ions act as the vertices, and four tridentate *N*′,*N*″,*N*‴-nitrilo-tris-4,4′,4″-(2-hydroxybenzylidene)-benzohydrazid ligands define the faces. The encapsulation of a molecule of 2-phenyl-4,4,5,5-tetra-methylimidazolineyloxyl-3-oxide (PTIO) completely quenches its emission. Remarkably, the addition of 0.45 mM NO to the host−guest system containing 15 μM of the cage and 0.3 mM PTIO again turns on the fluorescence emission with a 12-fold increase of intensity compared to the free cage. This is because the oxidation of NO to NO_2 via PTIO eliminates the fluorescence quencher and results in an ON−OFF−ON fluorescence signalling.

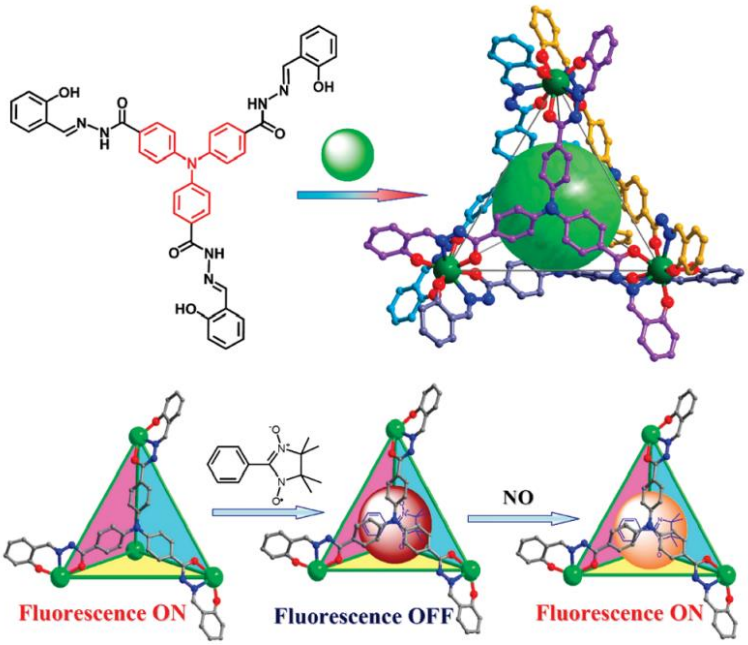

Figure 3.6. Structure of the tetrahedral structure reported by Duan *et al*. and the sequence of fluorescent variation of the it upon the addition of PTIO and NO.[58]

- *Catalysis.* Supramolecular cages can influence a chemical reaction just by providing an isolated cavity of particular size and shape. The inclusion of two molecules within such a small volume leads to a high concentration of the guests and, consequently, to an increased likelihood of reaction between them.[59,60]
  Fujita et al. demonstrated, very recently, that $M_{12}L_{24}$ molecular capsules can serve as catalyst carriers for enabling continuous chemical transformations.[61] This architecture is a palladium metal complex quantitatively self-assembled from 12 Pd(II) ions (M) and 24 bent, ditopic ligands (L) (Figure 3.7).

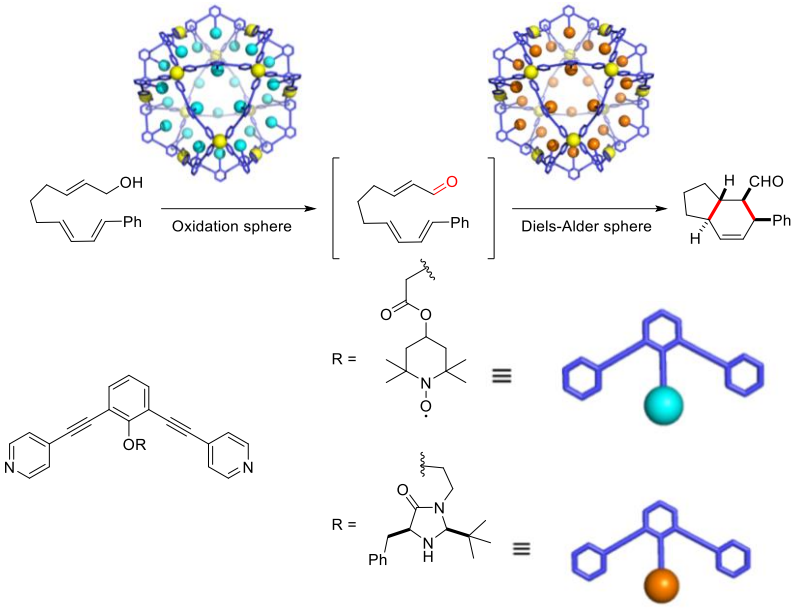

Figure 3.7. Cascade reaction catalysed by two $M_{12}L_{24}$ capsules.[61]

They reported a stereocontrolled cascade reaction using two sphere-like capsules, whose voids are decorated with two different catalysts: TEMPO for an oxidation reaction and MacMillan's catalyst for Diels−Alder chemistry. Without an appropriate carrier, the Diels-Alder catalyst is promptly oxidized by TEMPO, rendering each incompatible with the other. By encapsulating each of them separately within the cavity of an $M_{12}L_{24}$-type molecular capsule, the cascade reaction proceeded smoothly. Capsule-like receptors are also able to modify the reactivity of the molecules they are hosting. In fact, there are coordination cages able to

stabilize highly reactive chemical species or unstable reaction intermediates,[62–64] as well as to suppress undesired reaction pathways.[65]

- *Storage applications.* As said previously, organometallic containers can be designed in order to encapsulate selectively a target molecule by host-guest interactions. Thus, depending on the size and chemical nature of the cavities, these supramolecular receptors will be able to recognize compatible substrates. An important example has been provided in 2011 by Nitschke and co-workers, which synthesized a coordination capsule able to encapsulate and store sulfur hexafluoride (SF_6), the most potent green-house gas known.[66] More recently Yoo et al. reported the synthesis of a cobalt supramolecular triple-stranded helicate-based discrete molecular cage.[67] Using other words, this organometallic structure is composed of six triple-stranded helicates interconnected by four linking cobalt species and it is an important example of a highly symmetric cage architecture resulting from the coordination-driven assembly of metallosupramolecular modules (Figure 3.8). Furthermore, this architecture shows much higher CO_2 uptake properties and selectivity compared with the separate supramolecular modules and other molecular platforms.

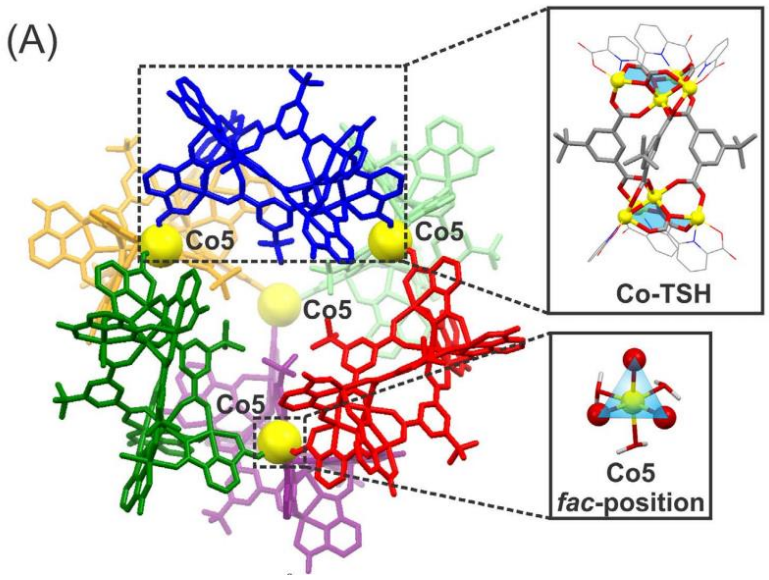

Figure 3.8. Structure of Yoo's discrete molecular cage composed of six triple-stranded helicates (= Co-TSHs portrayed in different colors) interconnected by four Co atoms (yellow balls).[67]

3.1.3.2 Fullerene recognition

Coordination cages allow the selective separation of specific molecules from mixtures of different species, taking advantage of different binding affinities. For example, different supramolecular containers can be used to separate fullerenes in a selectively way from mixtures of differently sized fullerenes.

Since their discovery in 1985,[68] fullerenes and their derivatives had shown a wide range of applications that include biomedical chemistry,[69] materials science,[70–72] and solar energy conversion.[73] However, all these applications are limited in origin by the current tedious and expensive methodologies for selective purification of fullerenes.[74,75] The use of molecular receptors for fullerene separation in solution has emerged as an attractive alternative since it allows potential selectivity, do not require specific equipment and ideal recyclable hosts can be designed. Additionally, the encapsulation promotes the solubilization and chemical modification of fullerenes.[76]

For these reasons, many host platforms containing extended π-systems have been designed because of their affinity towards the sphere-like structure of fullerenes.[77,78]

In 2013 Würthner and co-workers prepared a giant electroactive tetrahedron by the directional bonding approach. The self-assembly of octahedral Fe(II) ions and linear PDI dyes with 2,2′-bipyridine groups covalently attached at the imide positions quantitatively yields an $Fe_4(PDI)_6$ tetrahedron, which was used as a supramolecular container for fullerene C_{60}. Cyclic voltammetry of the metallosupramolecular tetrahedron suggested that this host should be suitable to support photo- and electrocatalytic processes (Figure 3.9).[79]

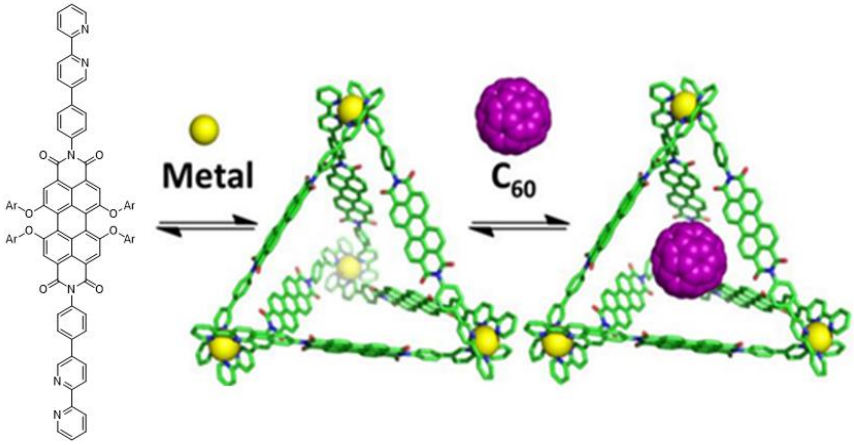

Figure 3.9. Structure of Würthner's metallosupramolecular tetrahedron and the host-guest complex obtained with fullerene C_{60}.[79]

Another extremely interesting example was reported more recently by Nitschke and co-workers.[80] They prepared a cubic $M^{II}_8L_6$ cage by self-assembly of 4-fold-symmetric porphyrins with Fe^{II} or Zn^{II}, which is able to bound C_{60}-indene or C_{60}-anthracene bisadducts selectively, whereas unfunctionalized fullerenes and monoadducts were not encapsulated. Such binding might be developed into a means of purification given the ability of such cages to open and close reversibly.

In particular, using bis-bidentate ligands and octahedral metal centers, either edge-bridged M_4L_6 tetrahedral capsules or M_2L_3 triple helicates can be formed, depending on the stoichiometry of the reactants and on the chemical structure of the ligand.[81,82] Until now, a wide variety of appropriately functionalized ditopic ligands, such as pyrene,[83] perylene bisimide,[79] and porphyrin,[84,85] have been used to build metal-organic cages endowed with an aromatic internal surface.

Figure 3.10 shows an example of what has been explained so far. The combination of a diamino(nickel(II)porphyrin) with 2-formylpyridine (2FP) and Fe^{II} yields a tetrahedral structure $Fe^{II}_4L_6$ cage with four octahedral metal iron located into the vertices and six bidentate porphyrins functionalized with imine-pyridine moieties in the opposite site of the macrocycle. Upon treatment with the fullerene C_{60} or C_{70}, this cage is transformed into a new host–guest complex incorporating three Fe^{II} centers and four porphyrin ligands, in an arrangement that is hypothesized to maximize π–interactions between the porphyrin units of the host and the fullerene guest bound within its central cavity.[84]

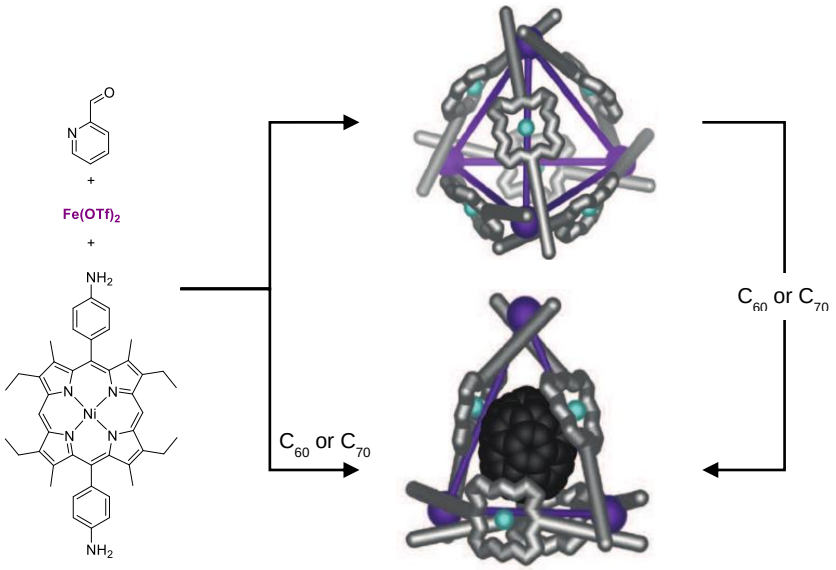

Figure 3.10. Subcomponent self-assembly of 2FP, iron (II) triflate and a dianiline porphyrin to yield a $Fe^{II}_4L_6$ tetrahedral cage.[84]

Also SubPcs have been used for the design organometallic cages capable to encapsulate fullerene within.[86,87] The curved-shape structure and the synthetic versatility of SubPcs make them ideal building blocks for the construction of functional homodimeric capsules. Figure 3.11 shows the synthesis of a M_3L_2 cage in which two SubPc units, arranged in a tail-to-tail disposition, are linked by three metal platinum or palladium ions. The resulting architecture is able to accommodate in its internal cavity different guests such as C_{60}, C_{70} and their PCBM ([6,6]-phenyl-C_{61}butyric acid methyl ester) derivatives.

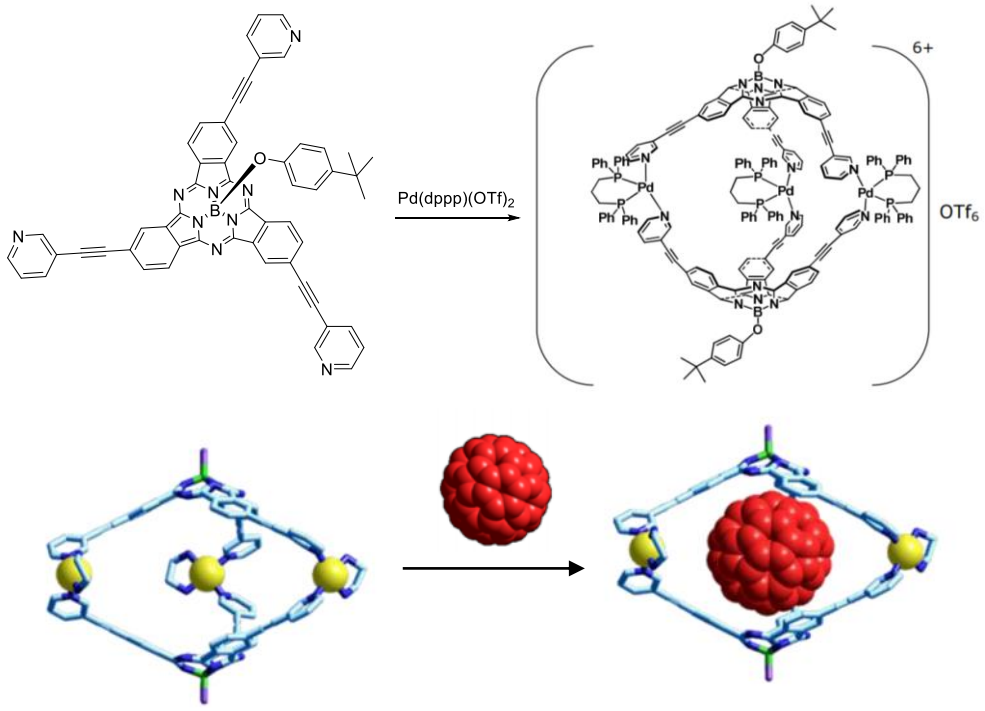

Figure 3.11. Synthesis of the M_3L_2 SubPcs cage (top) and encapsulation of fullerene C_{60} (bottom).[87]

Numerous examples of Pc's attached to fullerenes have been reported and reviewed.[88–90] Attachment can be achieved either by covalent binding via various spacer, or by non-covalent interactions, e.g., hydrogen or coordination bonding. In almost all reported cases, fullerenes are chemically modified, which results in transformation of sp^2-carbon atoms in intact fullerenes into sp^3-carbon, which cannot participate in electronic conjugation. The examples of Pcs – receptors that can bind unmodified fullerenes in solution are still relatively rare.[91–93]

3.2 Objectives

The use of Pcs as subcomponents for the self-assembly of supramolecular hosts relies on the preparation of unsymmetricaly functionalized **ABAB** derivatives holding two opposite bridging units. The synthetic difficulties of this task have precluded the use of Pcs for the preparation of polyhedral ensembles via coordinative bonds. In fact, to the best of our knowledge, there are no examples on the literature of metallo-supramolecular capsules built with Pc ligands.

In this context, the main goal of this chapter is the synthesis and characterization of novel supramolecular organometallic architectures based on Pcs exploiting the well-established *subcomponent self-assembly* strategy of Nitschke's group, that is, the reaction between ditopic amino-containing ligands with 2FP and salts of metals with octahedral coordination spheres that drive the coordination towards helicate-type or tetrahedral architectures. For this purpose, the synthesis of ditopic **ABAB** Pc ligands will be accomplished by functionalization of Pc **12** with aniline moieties (Scheme 3.2). It is worth mentioning that two regioisomers (i.e. *syn* and *anti*) can be obtained from **12** and, therefore, two Pc ligands with different coordination geometries can be separated and explored as building blocks for the assembly of metal-organic structures by reaction with 2FP and metal salts.

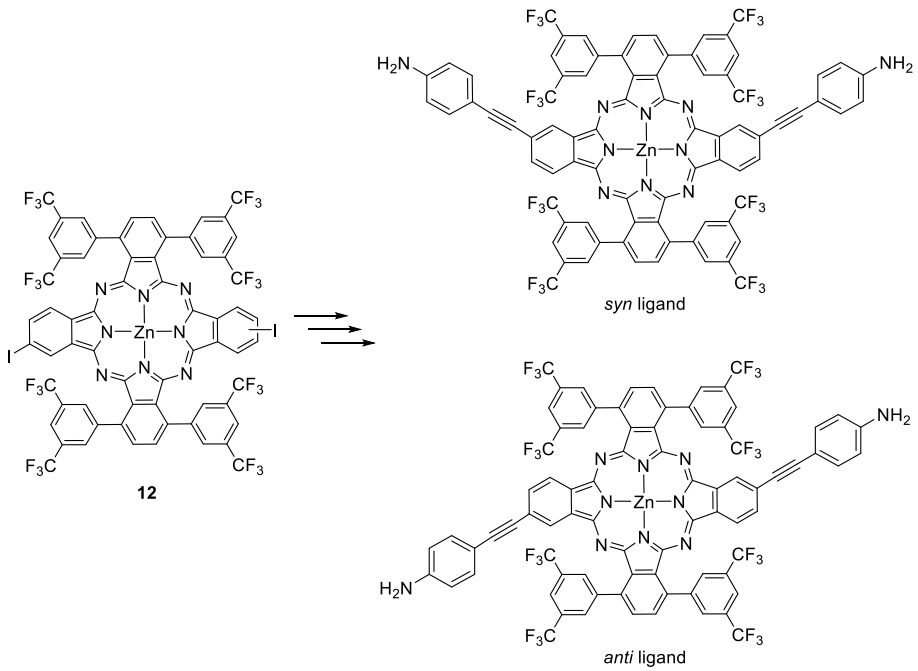

Scheme 3.2. Synthesis of targeted Pc ligands.

Assuming that distance, size and geometry of ligands are key parameters that allow to control the size and geometry of the final assemblies,[94] *syn* and *anti* regioisomers can bring about different architectures. The bent structure of the *syn* isomer can lead the self-assembly process towards helical structures, as widely observed in the literature.[82,95,96] On the other hand, the *anti* compound does not possess the linearity shown by other ditopic ligands,[94] however, a tetrahedral assembly cannot be discarded since M_4L_6 structures have been reported using planar and rigid bidentate ligands based on 2,6- substituted naphthalene, anthracene, and anthraquinone.[97]

The host-guest properties of these metallo-supramolecular assemblies will be explored using neutral guests, such as fullerenes and N-containing ligands that exploit their high affinity for the Zn(II) metal in the cavity of the Pcs to strongly bind to the assembly. Moreover, as subcomponent self-assembly generates inherently chiral structures from the spatial arrangement of the achiral pyridyl-imine ligands around the metal templates,[98,99] we aim to explore the possible *asymmetric induction* of chiral guests, which could influence the preferential formation of a diastereoisomer over the others. Furthermore, guest-exchange process and competitive experiments can be studied in order to define complexation hierarchies or a possible selectivity towards a specific guest

Supramolecular structures and corresponding host-guest complexes will be characterized by ^{1}H-NMR, ^{19}F-NMR, diffusion –ordered spectroscopy (DOSY), COSY, UV-vis fluorescence spectroscopy and ESI-MS.

The self-assembly process of aniline-functionalized Pcs will be carried out in the laboratory of Prof. Jonathan Nitschke at the Department of Chemistry of the University of Cambridge, England.

3.3 Results and discussion

3.3.1 Synthesis of Pc ligands

Pcs **73a** and **73s** (Scheme 3.4) were targeted to fabricate Pc-based metallo-supramolecular ensembles. For that purpose, it is compulsory to separate the *syn* and *anti* isomers of the Pc core at some point of the conversion of **12** into **73a**/**73s**.

Generally speaking, Pc regioisomers are very difficult to separate by chromatographic means owing to their very similar structural features. Nevertheless, examples of separation of four possible structural isomers of $\mathbf{A_4}$ Pcs have been reported using preparative thin layer chromatography and high-performance liquid chromatography (HPLC).[100,101]

In previous experiments towards the preparation of push-pull Pcs for DSSCs (see Chapter 2), we obtained Pc **71** (Scheme 3.3) as a secondary product, and observed that, in fact, the two regioisomeric components, *syn* and *anti*, could be isolated by column chromatography (Figure 3.12). This serendipitous separation allowed us to design a synthetic route towards the preparation of amino-containing Pc ligands with well-defined geometries starting from **71a** and **71s**. Therefore, we first accomplished the functionalization of the starting Zn(II)Pc **12** with 3 equivalents of propargyl alcohol under Shonogashira conditions (Scheme 3.3) to obtain a 1:1 ratio of **71a** and **71s** as the main reaction products, and performed the separation of the two isomers by column chromatography. It is important to remark that the complete separation of the **71a/71s** mixture is a tedious process that requires several purification cycles.

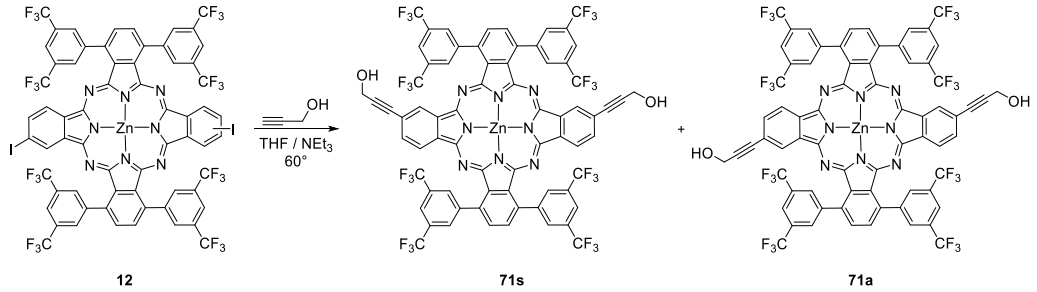

Scheme 3.3. Synthesis of regioisomers **71a/71s**. Conditions: a) propargylic alcohol (3 eq.), $Pd(PPh_3)_4$, CuI, Et_3N, THF, 16h 50°C, 38% for both *syn* and *anti* Pcs.

Figure 3.12. Separation of the fraction corresponding to Pcs **71a/71s**.

The structure of Pcs **71a** and **71s** were unequivocally confirmed by MALDI-TOF mass spectrometry, UV−vis, and NMR.

An initial identification of *anti*/*syn* regioisomers was performed by ^{1}H-NMR spectroscopy. C_{2v} *syn* isomer **71s** could be distinguised from the C_{2h} *anti* **71a**, even if they show the same number of different aromatic protons and, therefore, very similar ^{1}H-NMR spectra. In Figure 3.13, magnification of the aromatic part shows four signals for the protons of the bis(trifluoromethyl)phenyl rings (**a**/**a**' and **b**/**b**') and other four signals for the protons of the propargyl-substituted isoindoles (**d**, **e**, **f**) and the remaining Pc-centered nuclei (**c**, **c**') . The main difference arises from the presence of an AB system in **71a** for protons **c** and **c'**, which appears as a singlet at 8.28 ppm, while the C_{2v} **71s** shows two signals for protons **c** and **c'** at 8.27 and 8.29 ppm, which are clearly assigned as two singlets through a COSY correlation experiment (Figure 3.14).

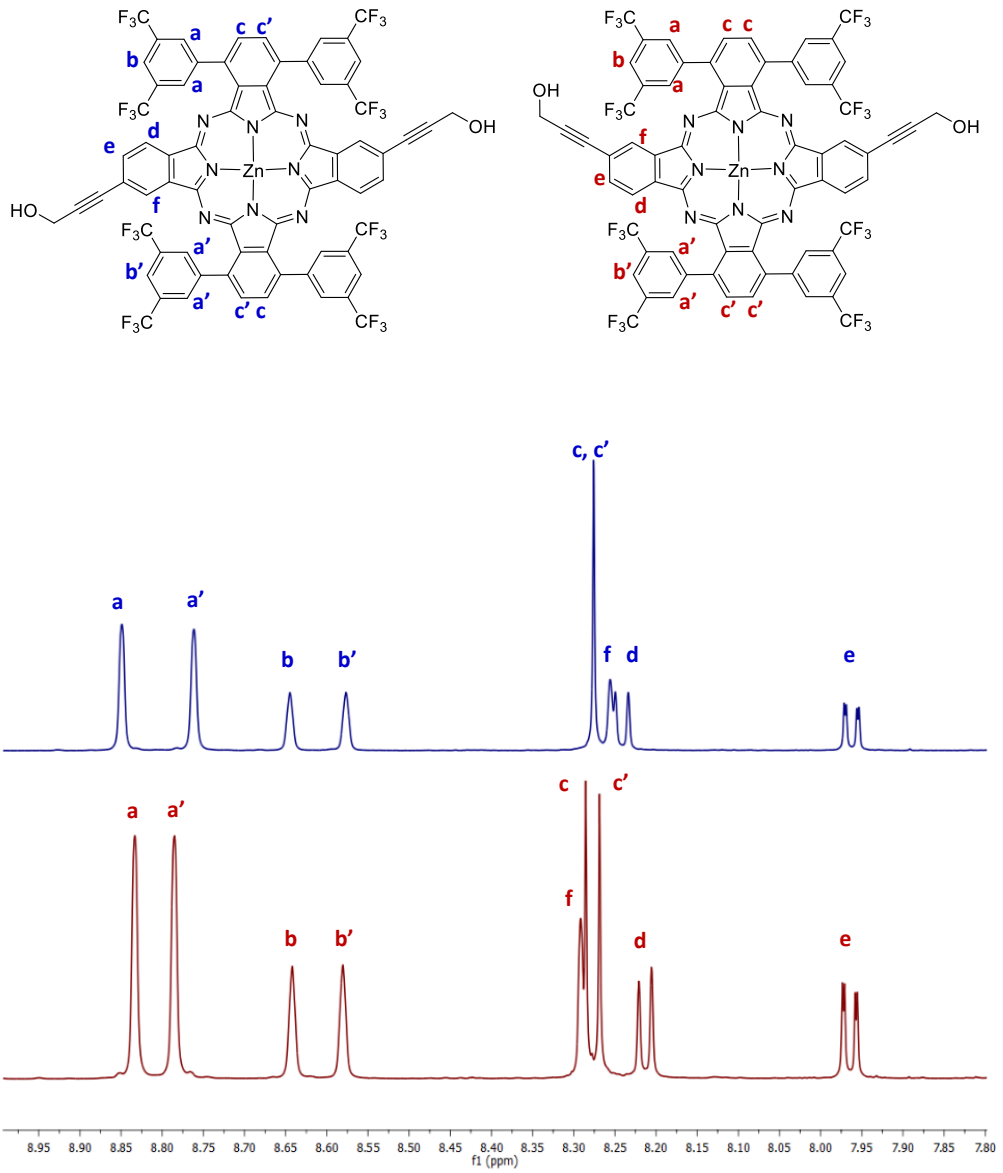

Figure 3.13. Magnification of the aromatic region of the ^{1}H-NMR spectra in THF-d_8 of **71a** (top) and **71s** (bottom).

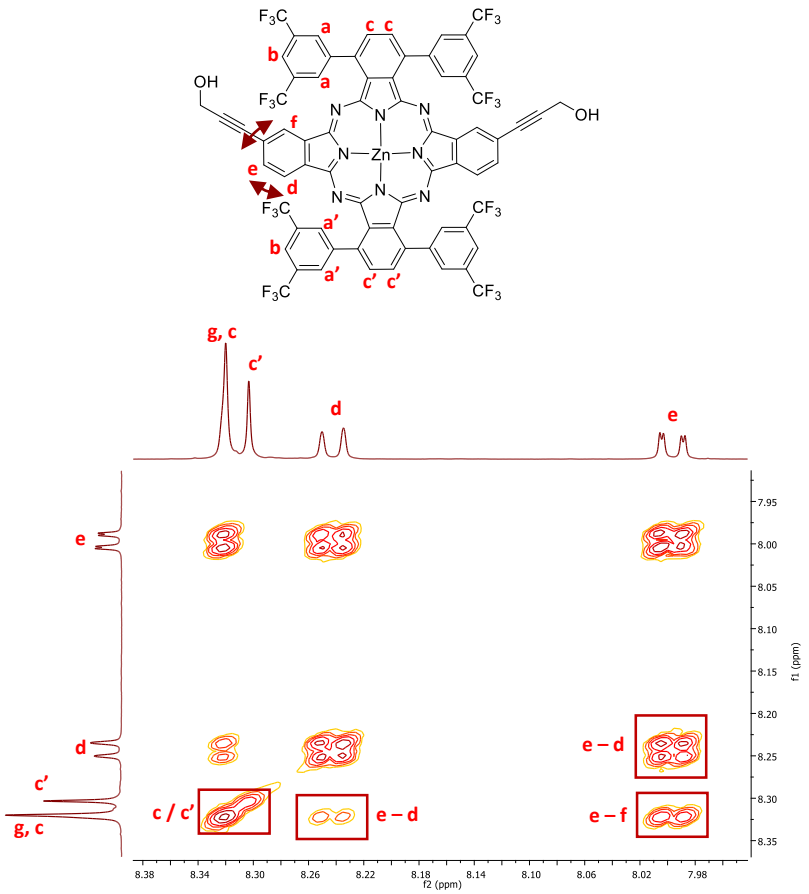

Figure 3.14. Aromatic region magnification of ^{1}H COSY NMR of **71s** in THF-d_8.

Ultimate evidence of the successful separation of the two regioisomers and assignation of their geometries arose from X-ray diffraction studies. Although single crystals from **71s** could not be grown, X-ray diffraction data of single crystals from **71a** (Figure 3.15) confirmed the initial assignation.

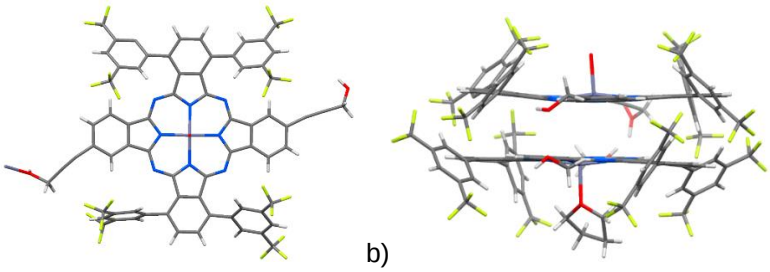

a) b)

Figure 3.15. X-ray structure of **71a**. a) Frontal view of the C_{2h} isomer **71a**, in which solvent molecules were omitted for clarity; b) Side view of a stacked dimer of **71a** with a THF molecule.

The second step towards the preparation of amino-containing Pc ligands **73a** and **73s** was a one-pot oxidation-decarboxylation of the propargyl groups in the presence of MnO_2 and KOH in diethyl ether,[102] which yielded the intermediate Pcs **72a** and **72s**. These compounds were respectively subjected to a Sonogashira reaction with *p*-iodoaniline in the presence of $Pd(PPh_3)_4$ and CuI, affording the targeted Pcs **73a** and **73s** (Scheme 3.4).

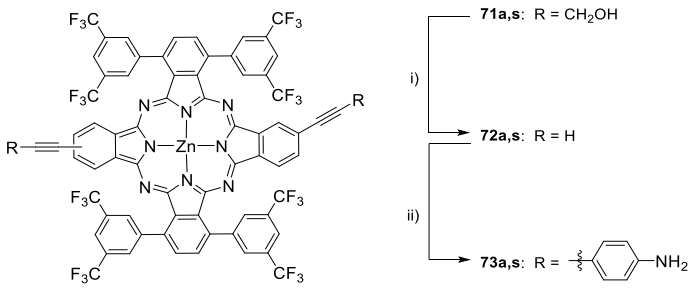

Scheme 3.4. Synthesis of Pcs **73a** and **73s**. Conditions: i) MnO_2, KOH, Et_2O, reflux, 16h 86%; ii) *p*-iodoaniline, $Pd(PPh_3)_4$, CuI, NEt_3, THF, 60°C, 3h, 83%.

Considering the problematic separation of **71a/s** isomers, we tackled an alternative synthetic route to obtain Pcs **73a/s** (Scheme 3.5), which relied on a presumable better separation of *syn* and *anti* isomers of related Pcs functionalized with hydroxyl-containing ethynyl moieties. As carbinol groups are commonly used to protect terminal alkynes, and are afterwards easily cleavable using basic conditions *via* retro-Favorskii reaction,[103] we performed the functionalization of Pc **12** with 2-methyl-3-butyn-2-ol under Shonogashira conditions to obtain a mixture of **74a/s**.

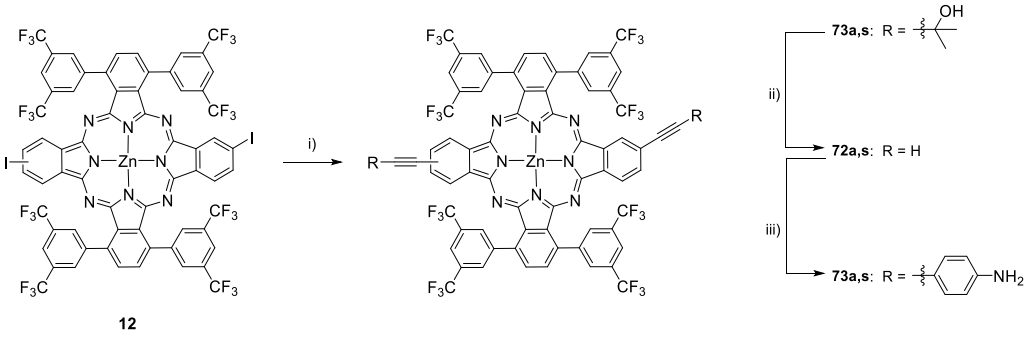

Scheme 3.5. Alternative synthetic route of Pcs **73a** and **73s**. Conditions: i) 2-methyl-3-butyn-2-ol, $Pd(PPh_3)_4$, CuI, NEt_3, THF, 60°C, 3h, 37% for the *syn* isomer and 16% for the *anti* one; ii) KOH, Toluene, reflux, 5h, 60%; iii) *p*-iodoaniline, $Pd(PPh_3)_4$, CuI, NEt_3, THF, 60°C, 3h, 83%.

Unfortunately, the separation of the regioisomers resulted even more complicated than in the previous case and in lower yield. Figure 3.16 shows a magnification of the aromatic region of the ^{1}H-NMR spectra of **74a** and **74s**, which are very similar to the spectra of Pcs **71a/s**. Also here, the main difference arises from the presence of two signals for protons **c** and **c'** in the case of the *syn* isomer, while only a singlet is present for protons **c** and **c'** in the *anti* compound. A clear contamination with **74a** is visible in the ^{1}H-NMR of Pc **74s** due to the more difficult separation of these isomers.

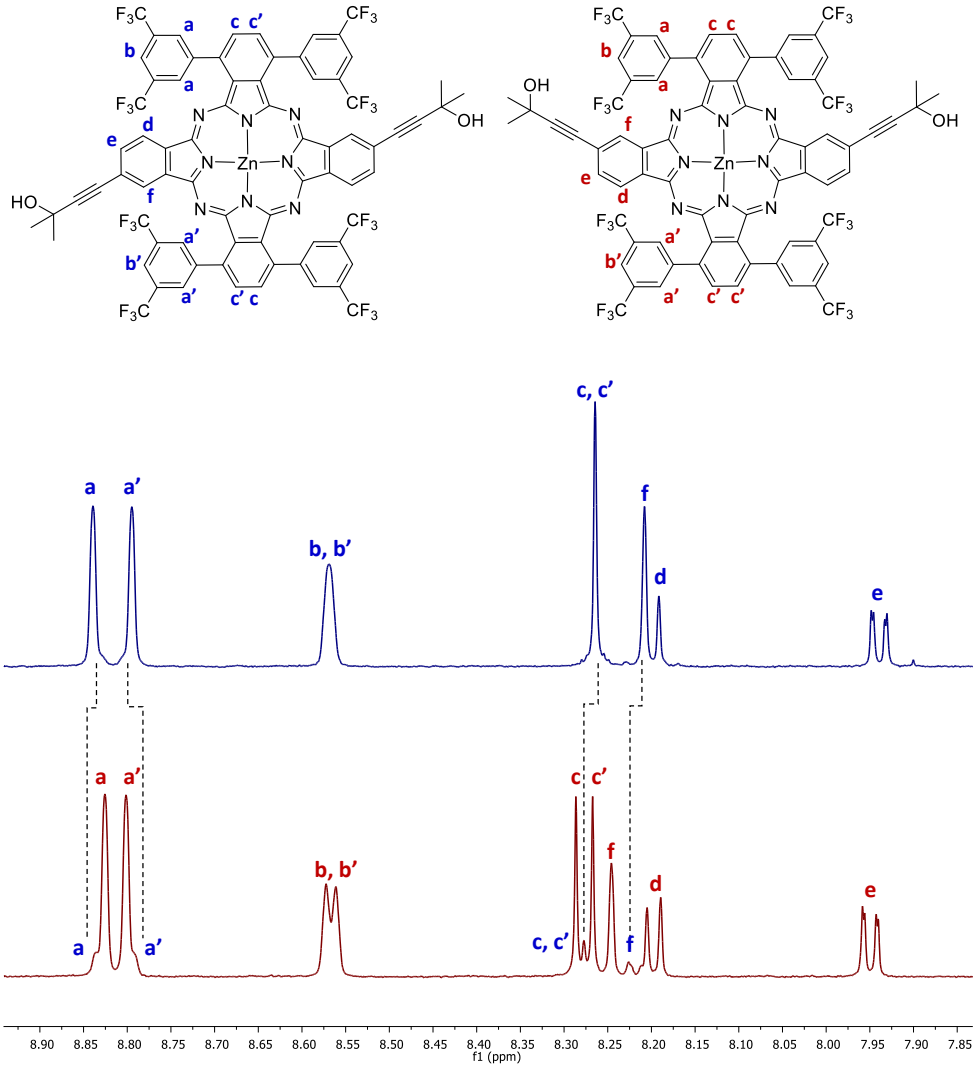

Figure 3.16. Magnification of the aromatic region of the ^{1}H-NMR spectra in THF-d_8 of **74a** (top) and **74s** (bottom). The *syn* isomer results contaminated by the *anti* one in a proportion 7:1 respectively.

3.3.2 Self-Assembly process

3.3.2.1 Syn Isomer

To explore the capability of *syn* Zn(II)Pc **73s** to form metallo-supramolecular assemblies through the reversible formation of imine-pyridine bonds and their coordination to metal centers, we set up several experiments with different metal salts under different conditions. In all the cases, we mixed the *syn* Zn(II)Pc **73s**, 2FP and iron (II) triflate in a 3:6:2 ratio, respectively, in CD_3CN at room temperature and under nitrogen atmosphere. This stoichiometry is effective for the preparation of both M_4L_6 tetrahedrons and M_2L_3 helicates, which are the plausible architectures to achieve with our Pc ligands. The self-assembly assays were performed in J-Young NMR tubes in order to monitor their evolution by ^{1}H-NMR.

Fe(OTf)$_2$. The self-assembly progress was easily followed by ^{1}H-NMR, checking the disappearance of the signal of the aldehyde of 2FP at 9.9 ppm (Figure 3.17). Initially, the starting Pc is scarcely soluble in acetonitrile, even after the addition of 2-FP; in fact, only the peaks corresponding to 2FP are observable by ^{1}H-NMR (purple spectrum in Figure 3.17). After the addition of stoichiometric amounts of iron(II) triflate with regard to the Pc, the self-assembly process begins immediately, as observed in the ^{1}H-NMR, where a new series of well-resolved peaks appears, which correspond to the protons of the Pc core that is forming the soluble, supramolecular structure. The conversion proceeds at room temperature, ending in 24 hours.

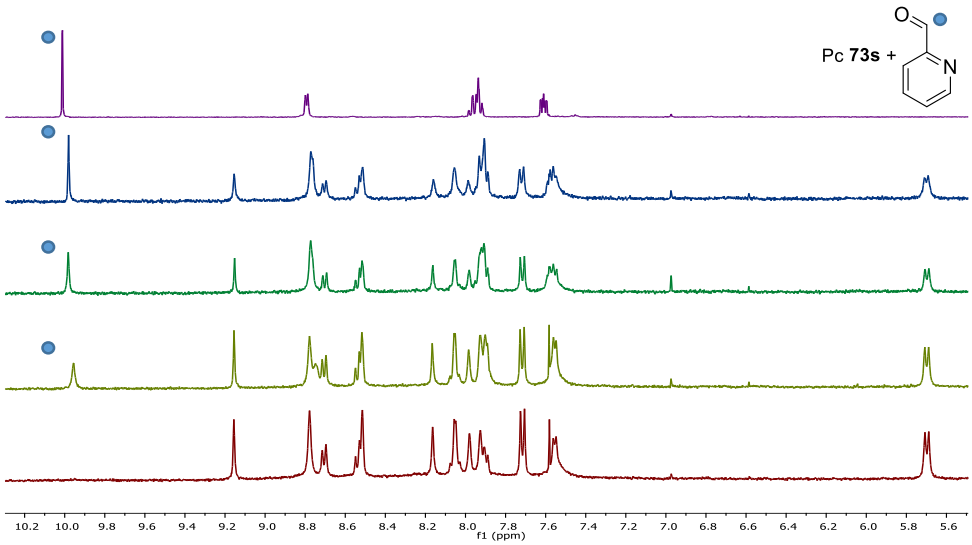

Figure 3.17. Magnification of the aromatic region of the ^{1}H-NMR spectra in CD_3CN where the evolution over 24 hours of the reaction of Pc **73s** with 2FP and $Fe(OTf)_2$ is observable.

Zn(OTf)$_2$. As in the previous case, a series of new peaks appears after the addition of stoichiometric amounts of Zn(II), but the completion of the reaction is not achieved even after heating at 50°C or at 70°C for 24 hours (Figure 3.18). In fact, it was not possible to isolate the metallo-supramolecular ensemble due to its rapid decomposition (red spectrum in the bottom in Figure 3.18).

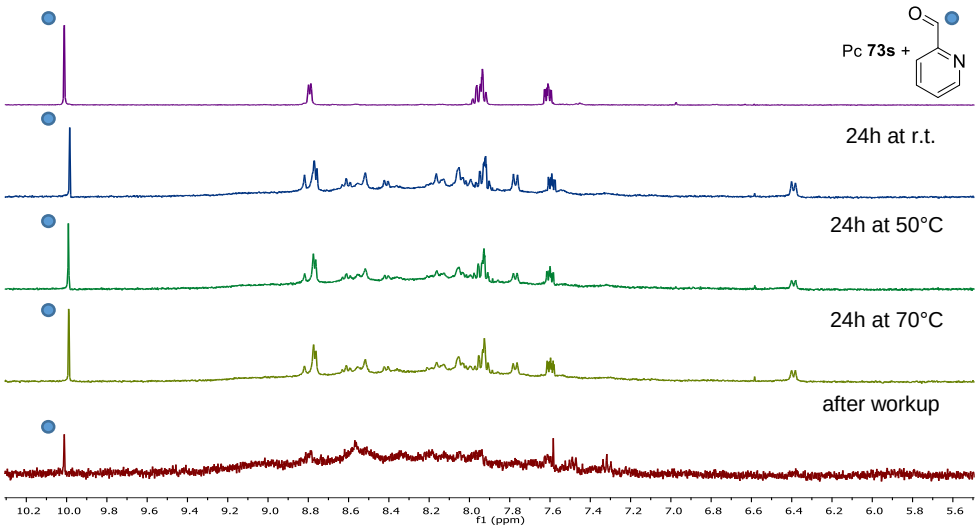

Figure 3.18. Magnification of the aromatic region of the ^{1}H-NMR spectra in CD_3CN where the evolution of the reaction of Pc **73s** with 2FP and $Zn(OTf)_2$ is observable.

Co(OTf)$_2$. Monitoring the reaction proved more complicated when using cobalt(II) triflate, due to the paramagnetic nature of the metal center. Even though, ^{1}H-NMR spectra could be registered after 24h at rt, at 50°C and at 70ºC, as shown in Figures 3.19 and 3.20. Also in this case, new peaks appear at -20, 50, 80 and 240 ppm, accompanied by others in the classic diamagnetic region.

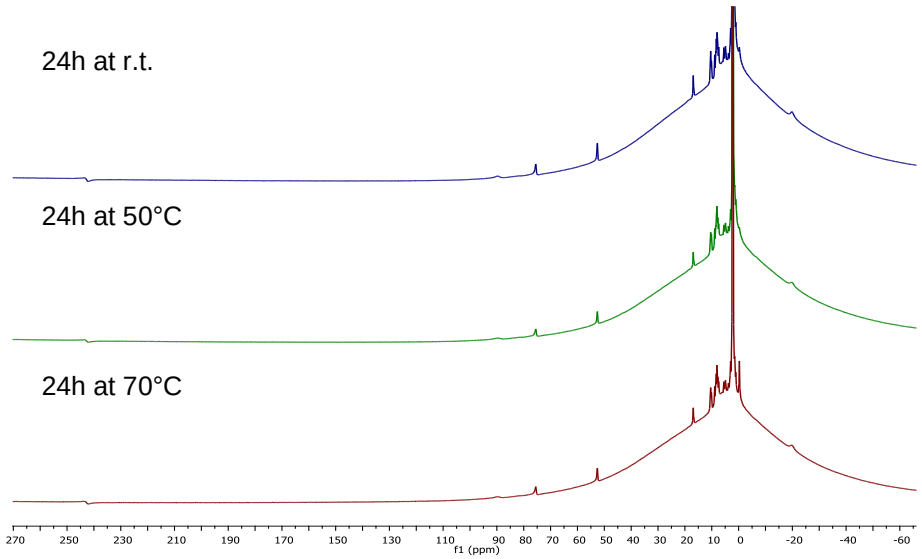

Figure 3.19. ^{1}H-NMR spectra in CD_3CN of the reaction of Pc **73s** with 2FP and $Co(OTf)_2$ at different times.

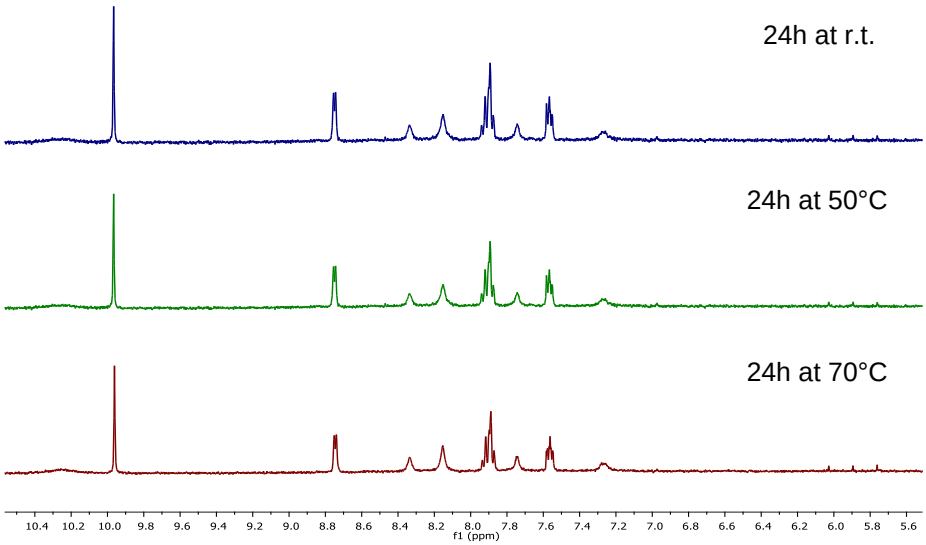

Figure 3.20. Magnification of the aromatic region of the ^{1}H-NMR spectra in CD_3CN of the reaction of Pc **73s** with 2FP and $Co(OTf)_2$ at different time.

The low stability of the complex obtained with $Zn(OTf)_2$ and the difficulties in monitoring the formation of the metallo-supramolecular complex when using of $Co(OTf)_2$, encouraged us to keep using $Fe(OTf)_2$ for the preparation of the metallo-supramolecular hosts and further complexation studies.

ESI-MS, ^{1}H-NMR, ^{19}F-NMR, diffusion – ordered spectroscopy (DOSY), COSY and UV-vis spectroscopy esperiments confirmed that the reaction of the *syn* Zn(II)Pc **73s** (3 equiv) with 2FP (6 equiv) and iron (II) triflate (2 equiv) in CD_3CN at room temperature under nitrogen atmosphere yielded the $Fe^{II}_2L_3(OTf)_4$ assembly **75** (Scheme 3.6).

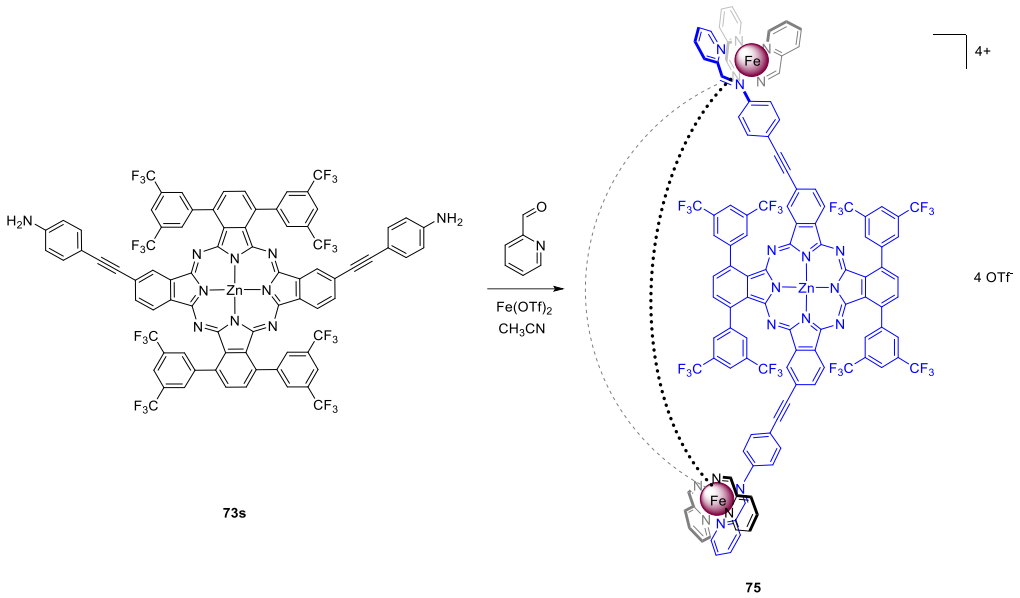

Scheme 3.6. Self-assembly of Pc **73s**, 2FP and iron (II) triflate to yield $Fe^{II}_2L_3(OTf)_4$ helical structure **75** (Fe^{II} = purple).

The electrospray ionization time-of-flight (ESI-TOF) mass spectrum of **75** is depicted in Figure 3.21, showing two of the three peaks that fit with a helical metallo-supramolecular structure. The most abundant peak was observed at *m/z* = 1403.9029, which exhibits the typical *m/z* splitting for a +4 charged species and was assigned to $[Fe^{II}_2L_3]^{4+}$ (Figure 3.22). Two less abundant peaks at *m/z* = 1921.5208, and 2956.7497 (Figure 3.23) were assigned to helicate-counterion complexes $[Fe^{II}_2L_3](OTf)^{3+}$, and $[Fe^{II}_2L_3](OTf)_2^{2+}$ respectively.

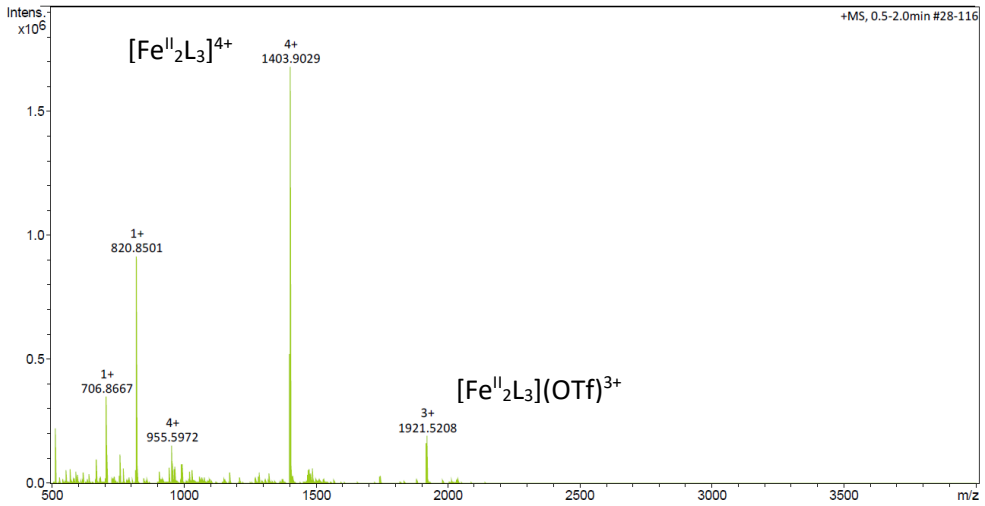

Figure 3.21. HR-ESI mass spectrum of **75**, showing two of the three characteristic peaks at *m/z* = 1403.9029 for $[Fe^{II}_2L_3]^{4+}$ and *m/z* = 1921.5208 for $[Fe^{II}_2L_3](OTf)^{3+}$.

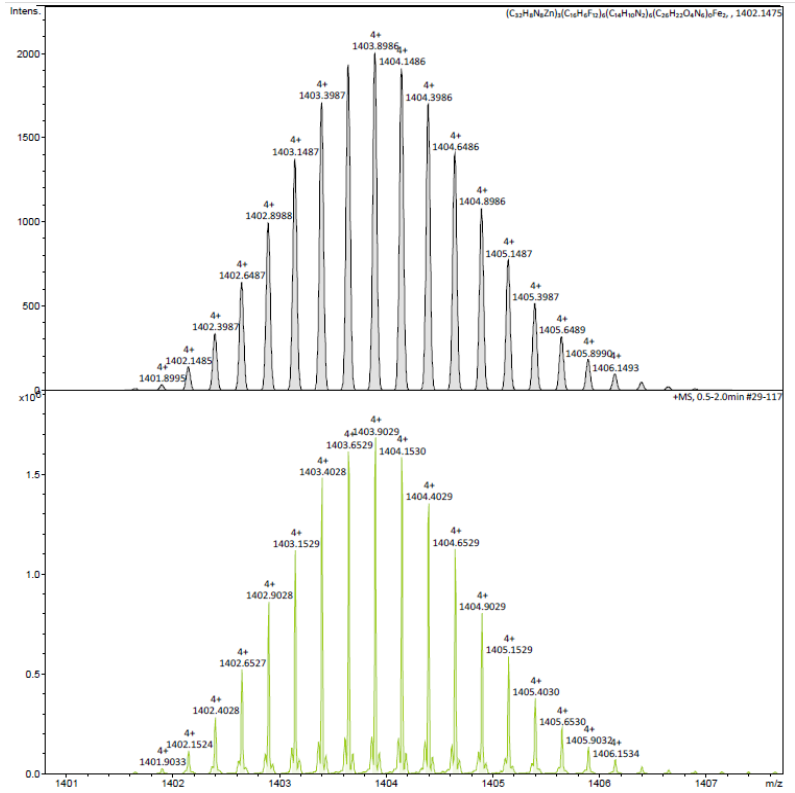

Figure 3.22. HR- ESI mass spectrum of **75**, showing the observed *z* = +4 charge for the peak at *m/z* = 1403.9029 (bottom) compared to the theoretical isotopic pattern (top).

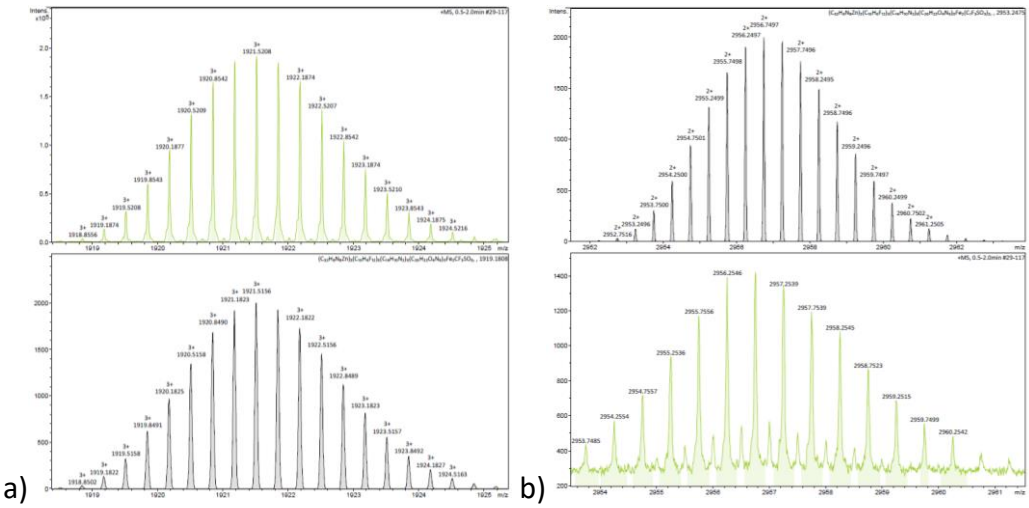

Figure 3.23. a) HR-ESI mass spectrum of **75**, showing the observed *z* = +3 charge for the peak at *m/z* = 1921.5208 (top) compared to the theoretical isotope pattern (bottom); b) HR-ESI mass spectrum of **75**, showing the observed *z* = +2 charge for the peak at *m/z* =2956.2546 (bottom) compared to the theoretical isotopic pattern (top).

The simple and well-defined ^{1}H-NMR spectrum of **75** (Figures 3.24 and 3.25) is indicative of a high symmetric structure in solution. According to the chirality at both six-coordinated iron center, dinuclear [Fe_2L_3] structures may exhibit three stereoisomeric configurations: ΔΔ, ΛΛ, and ΔΛ, which result in two possible architectures using achiral ligands: homochiral helicates (ΔΔ or ΛΛ) and achiral mesocates (ΔΛ).[11,104,105] In the last twenty years, different research groups have been attempting to control the formation of helicates versus mesocates, using cations or anions as templating agents[106–109] and proposing empirical rules.[11,110] Generally little and flexible ligands can drive to both helicate and mesocate complexes due to their ability to adopt both “pseudo-S” and “pseudo-C” conformations necessary to obtain helicates and mesocates, respectively.[106] Additionally, according to the *symmetry interaction approach*, the octahedral coordination geometry around two metal centers of opposite chirality imposes a distortion from the planarity of the ligands and forces them to be parallel to the C_3 axis (Figure 3.3).[23] For all these reasons, and for the simple and very symmetrical ^{1}H-NMR, we can assume that the rigidity of the Pc ligand and the steric demands imposed by the bulky trifluoromethylphenyl groups preclude the formation of a *meso* structure. Thus, the formation of homochiral helical ensemble occurs in a diastereoselectivity way, since the *meso* form would present a greater number of signals in the ^{1}H-NMR due to the lower symmetry of

the structure.[106] Unfortunately, all efforts to grow single crystals of **75** for X-ray diffraction to confirm this assumption were unsuccessful.

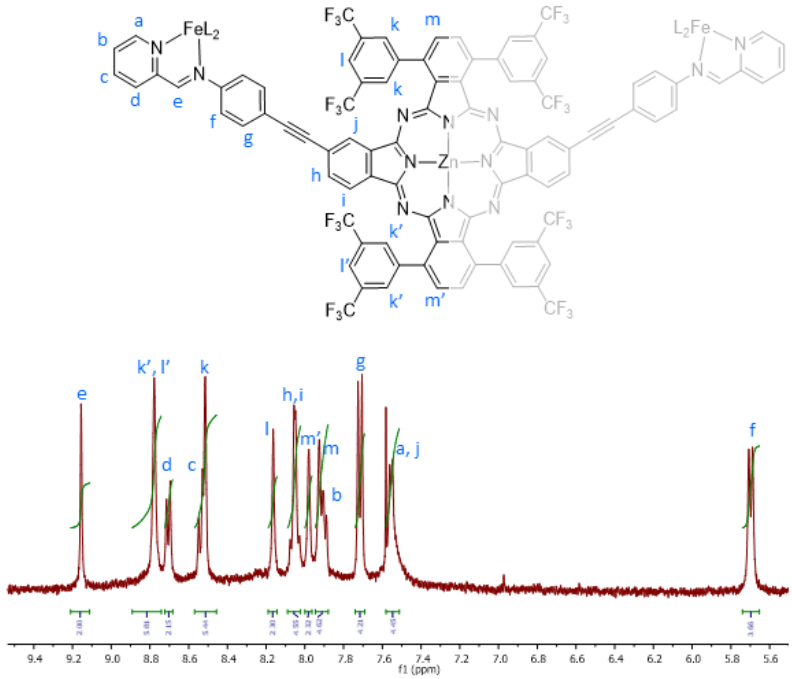

Figure 3.24. Aromatic region magnification of ^{1}H-NMR spectrum of **75** in CD_3CN.

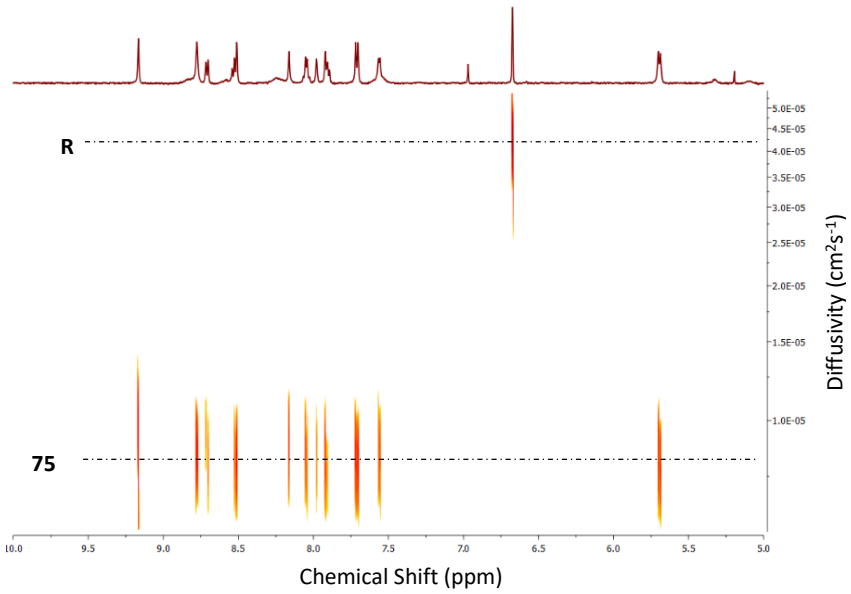

Figure 3.25. Downfield portion of ^{1}H DOSY NMR spectrum of **75** in CD_3CN.

Diffusion ordered spectroscopy (DOSY) was also carried out in the presence of mesitylene as reference compound (**R**) to calculate the hydrodynamic radius (R_h) of **75** in solution (Figure 3.25). Diffusion coefficients (D), in fact, are related to the effective radius of the molecular species through the Stokes– Einstein equation (Eq. 3.1):[111,112]

$$D = \frac{k_B T}{6\pi\eta R_h} \tag{3.1}$$

where k_B is the Boltzmann's constant, T the temperature and η is the viscosity of the solvent. For many cages and organometallic capsules which are relatively large molecules (compared to the solvent molecules) and in which the various axes are not very different, it appears that the Stokes–Einstein equation is a reasonable approximation to measure the radius of supramolecular assemblies.[113,114] It is important to note that R_h represents the hydrodynamic size, and as such, it is a measure related to the nature of the solvent in which the diffusion occurs. In fact, it represents the radius of a hypothetical hard sphere that diffuses with the same speed as the examined particle, and therefore possess some redundancy.

That said, it should be noted that the equation 3.1 is valid only for hard spheres, and for this reason a modified Stokes–Einstein equation (Eq. 3.2) should be used for molecular and supramolecular architectures with non-spherical structure. This equation considers the deviations from the hard sphere approximation and the deviation from the continuum fluid approximation of the starting equation 3.2:

$$D = \frac{k_B T}{c\pi\eta R_h f_h} \tag{3.2}$$

where f_h is the shape factor and is always greater than unity, while c is the size factor and relates to the ratio of the size of the diffusing entity to the solvent in which diffusion occurs. The shape factor f_h was computed for prolate and oblate ellipsoids,[115] for ellipsoids having three different axes[116] and for cylindrical species.[117] Nevertheless, different works in literature show that, despite the fact that many of the helicates are clearly not spherical, the differences between data calculated using the Stokes–Einstein equation (Eq. 3.1) and obtained by X-ray structures of the complexes are in the order of 10–15%,[118,119] therefore negligible.

For these reasons, we assumed that also in our case diffusion coefficients can be used to determine the size of our supramolecular structure, according to the previously reported methodologies in literature.[79,120,121] The use of an internal reference whose hydrodynamic radius is known, like mesitylene in this case (R_{ref} = 3.0 Å), allows the estimation of the aggregate size by direct D_0 comparison, using equation 3.3:[120,122]

$$R_0 = \frac{R_{ref} \times D_{ref}}{D_0} \tag{3.3}$$

The calculated diffusion coefficients and the estimated hydrodynamic radii are shown in Table 3.1.

Table 3.1. Calculated diffusion coefficients and the estimated hydrodynamic radii.

	Peak ppm	**D_0** m^2/s	**$R^{[a]}$** Å	**$R^{[b]}$** Å
Helicate **75**	9.86	3.306×10^{-12}	17.23	**15.9**
	8.81	3.645×10^{-12}	15.63	
	8.74	3.489×10^{-12}	16.33	
	8.08	3.784×10^{-12}	15.05	
	7.74	3.973×10^{-12}	14.34	
Average *R*			**15.7**	
Mesitylene	6.70			3

[a] Calculated using mesitylene as an internal reference. [b] Calculated from computed models.

An average experimental radius of 15.7 Å was determined for **75**, which is consistent with the value of 15.9 Å derived from the model shown in in Figure 3.26 and 3.27.

In this model the helical structure of **75** is approximated to a prolate spheroid described by two semi-axes, *a* and *b* (Figure 3.27a). The semi-axis *b* is the distance from center to pole along the symmetry axis, and is estimated as the average half-distance between two opposite pyridines among the six iron-coordinating ligands (Figure 3.27b). On the other hand, the semi-axis *a* is the equatorial radius of the spheroid, and can be estimated as the radius of the circumscribed circle of the triangle obtained combining Pc-centered opposite and extreme hydrogen atoms of the three Pcs forming the helicate (Figure 3.27c). Using this modelling, values of 14.3 Å and 17.5 Å were calculated for semi-axes *a* and *b* respectively. The average measure of these two values (i.e., 15.9 Å) can be used as approximation of hydrodynamic radius for **75**.

Moreover, the fact that the same diffusion coefficient is observed for all resonance peaks is an additional evidence of the formation of only one structure.

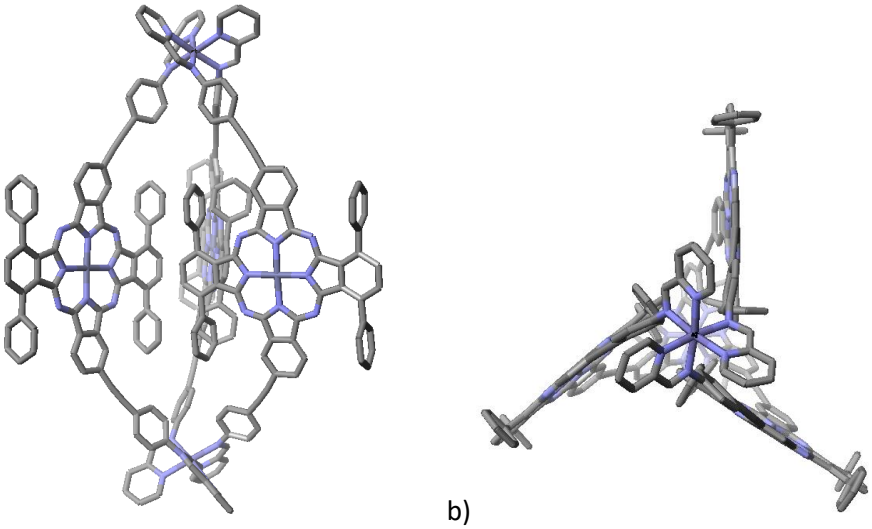

a) b)

Figure 3.26. a) side view and b) top view of an energy-minimized structure of **75**, with all Fe(pyridylimine)$_3$ vertices in the Λ conformation. Hydrogen atoms and trifluoromethyl groups are omitted for clarity (C = grey, N = blue, Fe = purple, Zn = dark grey).

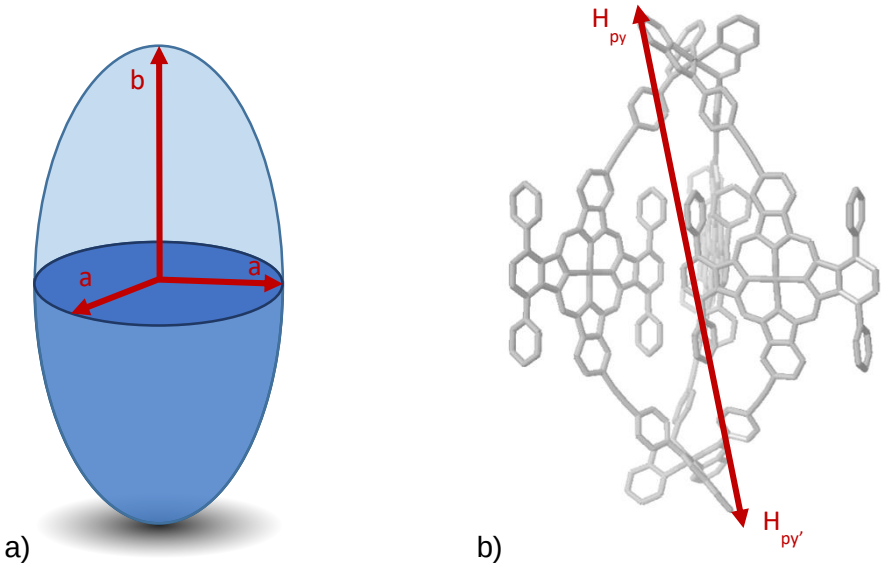

a) b)

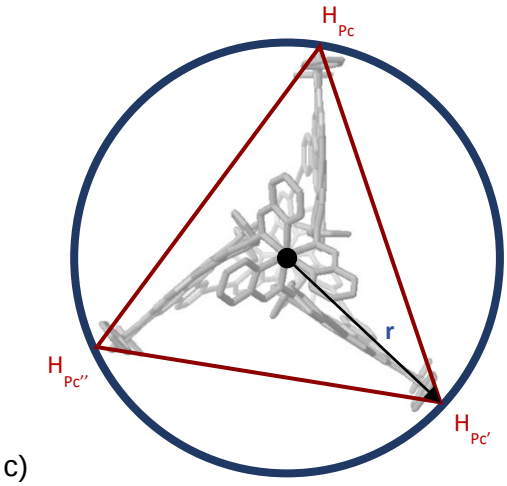

Figure 3.27. Schematic representation of a) a prolate spheroid described by the semi-axes *a* and *b*; b) the distance between two opposite pyridines; c) the radius of the circumscribed circle of the triangle obtained combining Pc-centered opposite and extreme hydrogen atoms.

The geometry of **75** was optimized by a semiempirical calculation (PM3) starting from the Λ–Λ diastereomer using the Scigress software suite.[123] The energy-minimized structure (Figure 3.26) exhibits a metal-metal distance of 27.4 Å between Fe^{II} centres, and an average separation of 13 Å between Zn metals of Pc cores. The energy-minimized model highlights the arched nature of the Pc ligand, with a 127.5° average bend (measured as the N_{imine}-Zn-N_{imine} angle). The energy-minimized model highlights an arching of the Pc ligand in the ensemble, which seems to indicate that the Pcs in the helicate may bend to accommodate large guests. Please notice that the bent structure of the Pc units increases the effective size of the internal cavity, which was estimated to be ca. 705 $Å^3$ by using VOIDOO (Figure 3.28). To the best of our knowledge, this is the largest helicate reported to date of the M_2L_3 class.

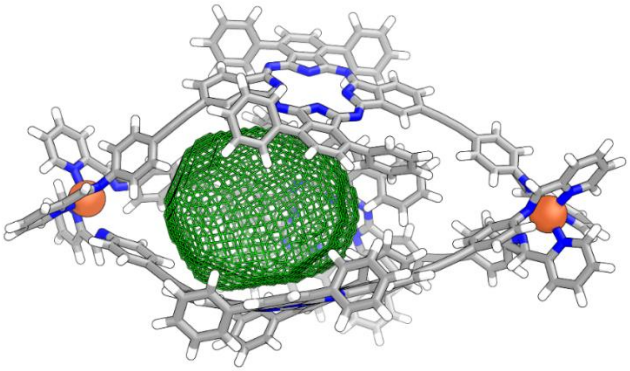

Figure 3.28. Representation of the internal cavity volume (705.228 $Å^3$ ± 1.182) calculated with VOIDOO.

The UV-vis and fluorescence spectra of **75** versus the starting Pc **73s** are depicted in Figure 3.29. A small hypsochromic and hyperchromic shift of the maximum wavelength (λmax) of the Q band is observed from **73s** (695 nm) to **75** (690 nm) in the UV-vis spectra. On the other hand, the fluorescence spectra show a clear quenched emission of **75** compared with the starting Pc one due to the presence of two octacoordinated ions in the vertices of the structure.

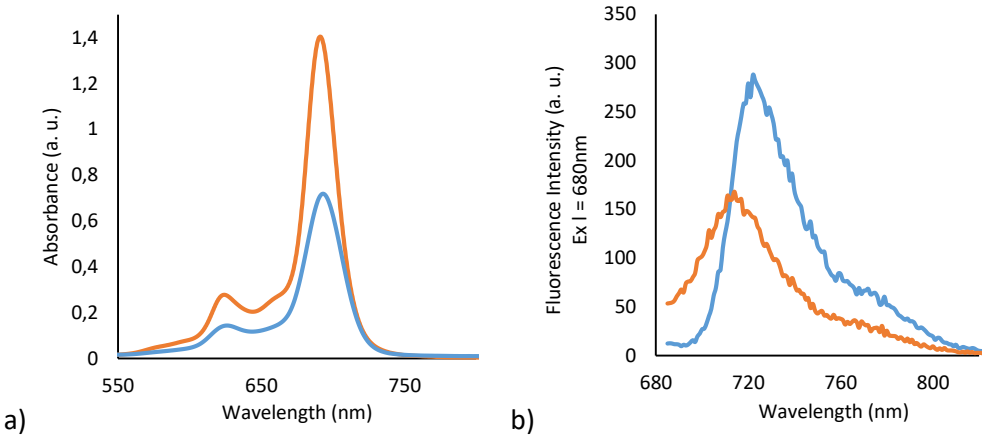

Figure 3.29. a) UV-vis spectra of Pc **73s** (blue line, 5 μm) in THF and **75** (orange line, 10 μm) in CH_3CN. b) Fluorescence spectra of Pc **73s** (blue line, 30μM) in $CHCl_3/CH_3CN$ (1:20) and **75** (orange line, 10μM) in CH_3CN.

3.3.2.2 Anti Isomer

The self-assembly reactions of *anti* Zn(II)Pc **73a** with 2FP and metal salts were performed in J-Young NMR tubes and in CD_3CN as solvent in order to monitor their evolution by ^{1}H-NMR. As in the case of the *syn* isomer, different metal salts were tested. In all the cases, we mixed the *anti* Zn(II)Pc **73a**, 2FP and iron (II) triflate in a 3:6:2 ratio, respectively, in CD_3CN at room temperature and under nitrogen atmosphere.

Fe(OTf)$_2$. Oppositely to the experiments with **73s**, it was impossible to follow the self-assembly progress using iron (II) triflate as source of metal ions. In this case, only the signals corresponding to the starting 2FP are visible, even after 24 hours at r.t., at 50°C or at 70° (Figure 3.30). Furthermore, variable temperature (VT) NMR spectra were carried out, and the range of ppm was increased in order to detect possible paramagnetic signals, but all efforts were fruitless.

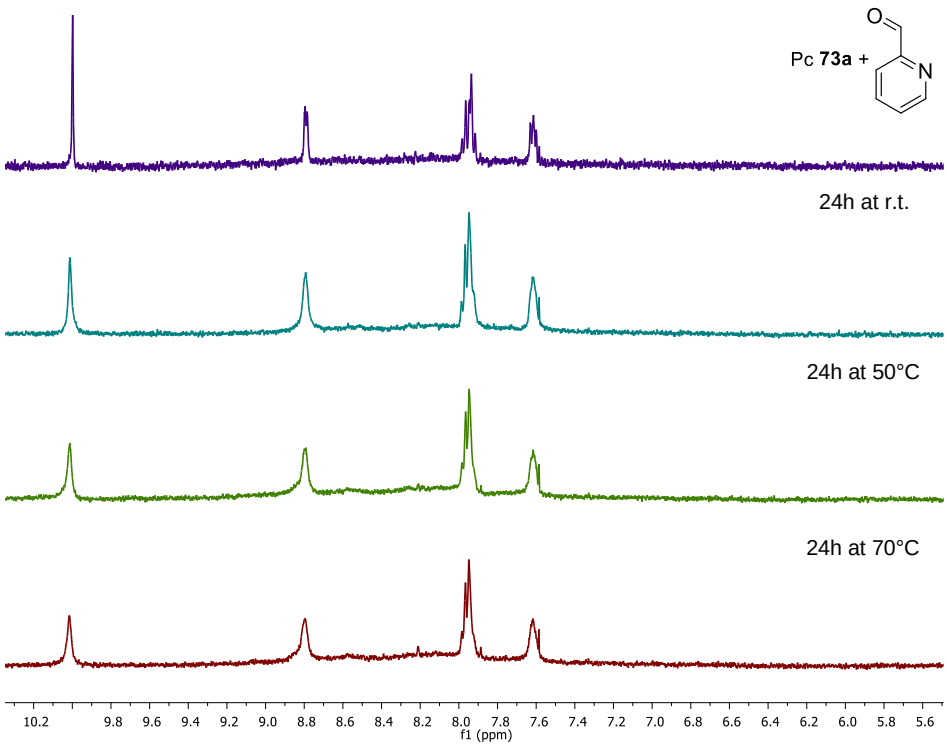

Figure 3.30. Magnification of the aromatic region of the ^{1}H-NMR spectra in CD_3CN of the reaction of Pc **73a** with 2FP and $Fe(OTf)_2$ at different time.

Co(OTf)$_2$. Also in the case of cobalt triflate, no evolution was detectable by ^{1}H-NMR, obtaining the same results shown previously. In fact, only the signals corresponding to the starting 2FP are observable in the ^{1}H-NMR spectra of the reaction of Pc **73a** with 2FP and Co(OTf)$_2$ in different experimental conditions.

Zn(OTf)$_2$. Unlike the experiments with cobalt and iron salts, it was possible to observe a significant evolution by ^{1}H-NMR upon the addition of zinc(II) triflate as source of metal ions. As shown in Figure 3.31, a series of new peaks appears, especially in the imine-region (i.e., 9.0 – 9.4 ppm), although the completion of the reaction is not achieved even after heating at 50°C or at 70°C for 24 hours. Unfortunately, no well-defined metallorganic structures were detected by ESI-MS.

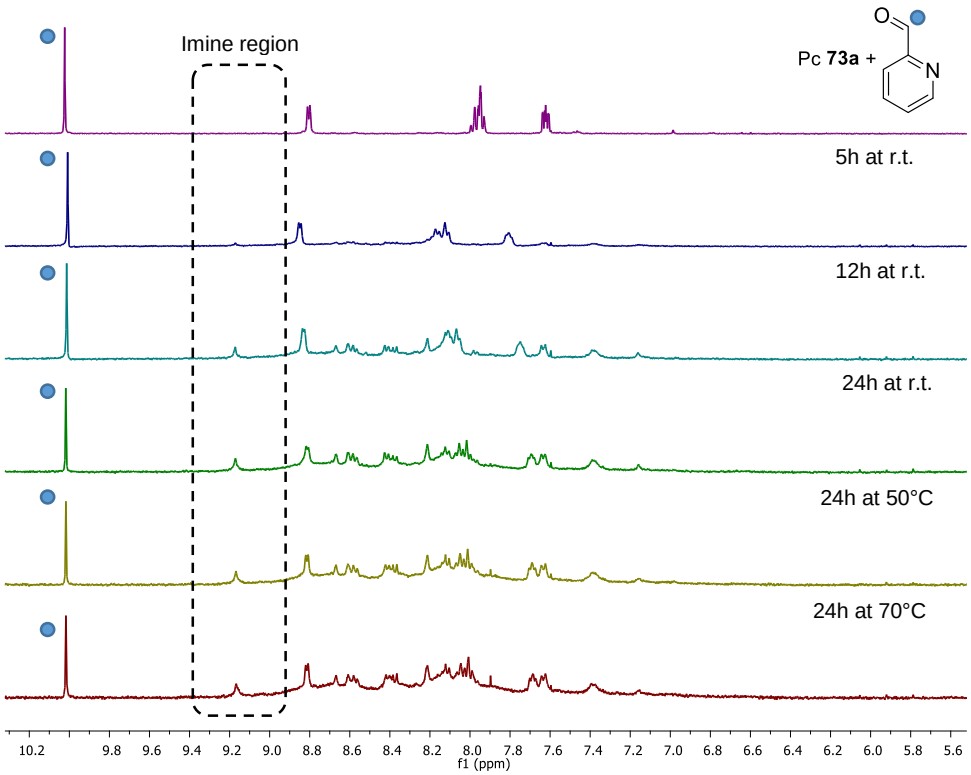

Figure 3.31. Magnification of the aromatic region of the ^{1}H-NMR spectra in CD_3CN where the evolution of the reaction of Pc **73a** with 2FP and Zn(OTf)$_2$ is observable.

All these negative results led us to conclude that the self-assembly process of Pc **73a** with 2FP and metal salts generates a *constitutional dynamic library (CDL)*, which has no natural thermodynamic preferences of the equilibrating system. A CDL is the ensemble of molecular or supramolecular objects in dynamic equilibrium obtained when more assemblies are accessible and reversible interactions are working, generally established using the *subcomponent self-assembly approach*.[20,25,124–126] Such equilibrium is based on the continuous change of its constituents through dissociation and recombination of the different components. In this case, this CDL has no natural thermodynamic minimum, for this reason the major goal is to achieve control of these library.

Several examples regarding the formation of well-defined architecture from CDLs by application of physical stimuli or chemical effectors leading to adaptive systems can be found in literature.[127,128] For this purpose, Nitschke et al. used the ability to bind guest molecules to pilot towards well-defined structures.[129] In this system, the combination of p-toluidine, 6,6'-diformyl-3,3'-bipyridine and Co^{II} salt did not yield a single chemical species, but an intractable library of different complexes in solution. However, the addition of appropriate anions templates the selective formation of Co_4L_6 tetrahedral or prismatic species, indicating that the size and shape of the anion present in the system could affect the assembly obtained.

Inspired by this and many other examples,[82,130,131] we tried to pilot our CDL towards the formation of well-defined architectures, employing different kind of guests. Only the CDL obtained using $Zn(OTf)_2$ was taken into account since it was the only one observable by ^{1}H-NMR and MS techniques.

Experiments involved a variety of anionic guests, namely molybdenum-based polyoxometalates $Mo_6O_{19}^{2-}$ and $Mo_7O_{24}^{6-}$ and the boron cluster $B_{12}F_{12}^{2-}$, which could act as templates, binding via electrostatic interactions as in the Nitschke's work described above. Neutral guests were also employed, such as fullerenes C_{60}, C_{70} and N-containing ligands, which could interact *via* $\pi-\pi$ stacking or *via* coordination bonding to the Zn(II) present into the Pc cores.

However, no reassuring variations were observed by ^{1}H-NMR. Even ESI-MS detected no peaks corresponding to any well-defined structure, making it clear that is not possible to pilot this CDL.

3.3.3 Host-Guest Experiments

The host-guest properties of **75** were studied using ESI-MS, ^{1}H-NMR, ^{19}F-NMR and UV-vis spectroscopy. The experiments involved a variety of neutral guests that could interact with the host via $\pi-\pi$ stacking or by coordination bonding to the Zn(II) present into the Pc cores. Also the host-guest experiments were performed in J-Young NMR tubes and in CD_3CN as solvent in order to monitor their evolution by ^{1}H-NMR.

3.3.3.1 N-containing ligands

We decided to employ N-containing ligands such as quinuclidine and methylimidazole, as possible neutral guests to exploit coordination bonding to the Zn(II) present into the Pc cores. Unfortunately, quinuclidine and methylimidazole caused the splitting of our cage due to their coordination to iron centers.

To overcome this problem, we envisioned the preparation of multidentate ligands capable to simultaneously bind to two or three Zn(II) metal centers, thus favouring encapsulation over the single coordination bond to Fe(II) as a result of a cooperative-like effect. First,a chiral tritopic ligand was prepared in order to form a 1:1 complex with helicate **75**. The aim was to search a possible induction of chirality in the host-guest complex. According to the chirality at both hexacoordinated iron centers, our homochiral structure exhibits two enantiomers with ΔΔ and ΛΛ configurations. Supramolecular chirality can be transferred during or after the formation of the self-assembled architecture using chiral guests, achieving in this way an optical resolution.[132,133]

For that purpose, we have designed the chiral benzene-1,3,5-tricarboxamide (BTA) derivative **81**, which was synthetized as shown in scheme 3.7. Starting from (*S*)-alanine, the carboxylic group was firstly reduced using $LiAlH_4$ to obtain the corresponding aminopropanol compound. Then, the amino moiety was protected with a Boc group and the alcohol converted in tosylate, which rendered a nucleophilic substitution with imidazole in the presence of NaH. Boc-deprotection and following reaction with 1,3,5-benzenetricarbonyl trichloride led to the desired chiral tritopic BTA derivative **81**.

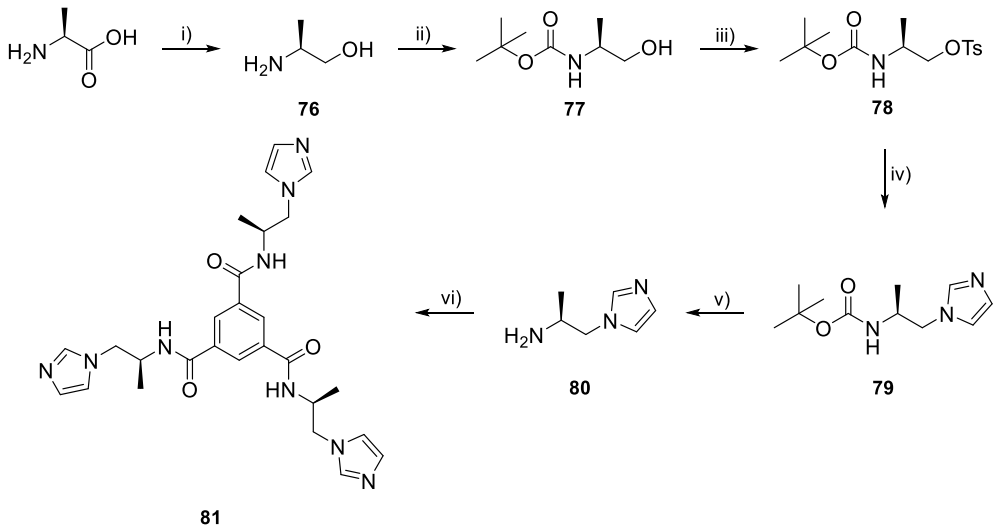

Scheme 3.7. Synthesis of **81**, conditions: i) $LiAlH_4$, THF, 0 ◦C to reflux, 90%; ii) NEt_3, Boc_2O, MeOH, r.t., 20h, 72%; iii) NEt_3, TsCl, CH_2Cl_2, r.t., 3h, 56%; iv) Imidazole, NaH, DMF, r.t., 20h, 12%; v) TFA, CH_2Cl_2, r.t., 16h, 69%; vi) 1,3,5-benzenetricarbonyl trichloride, NEt_3, $CHCl_3$, reflux, 24h, 60%.

The host-guest properties of helicate **75** towards this imidazole-functionalized BTA were first analyzed by UV-vis and fluorescence spectrophotometry techniques. Unfortunately, no measurable spectral changes occur in the UV-vis absorption and emission titrations of helicate with BTA ligand **81**, implying that no host-guest complexes are formed in this case. ESI-MS spectra support this thesis, detecting separately the peaks corresponding to the empty helicate and the BTA ligand.

Afterwards, aiming at the preparation of complexes with potential photoinduced electronic interaction between the guest and the Pc components of the host, we have designed an electron acceptor naphthalenediimide (NDI) (**82** in Scheme 3.8) functionalized with two 3-(1H-imidazole-1-yl)propyl) moieties at the nitrogen atoms. Also, an electron donor triphenylamine (TPA) tritopic ligand (**83** in Scheme 3.9), functionalized with three 3-(1H-imidazole-1-yl)propenyl) moieties has been prepared. Both target ligands have been designed for their synthetic simplicity and their affinity with helicate **75**, which was predicted by an initial geometrical optimization by model modelling calculation (MM3) using the Scigress software suite.

The synthesis of ligand **82** was carried out starting from 1,4,5,8-naphthalene tetracarboxylic anhydride, which was reacted with a small excess of 3-aminopropylimidazole (2.2 eq.) in DMF solution at 140°C, according to a previously reported procedure.[134,135]

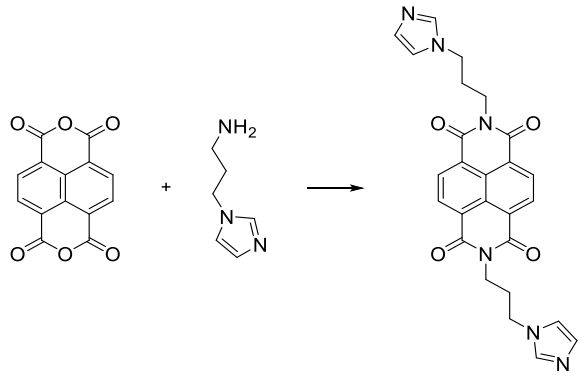

Scheme 3.8. Synthesis of ligand **82**, conditions: DMF, 140°C, 24h, 65%.

In the case of the TPA ligand **83**, a triple palladium-catalyzed Heck reaction was carried out over the commercially available tris(4-bromophenyl) amine with 1-allylimidazole under MW irradiation. The mono-, di- and tris- imidazole functionalized compounds were then separated by column chromatography. The selective formation of **83** with *all-trans* configuration was confirmed by ^{1}H-NMR.

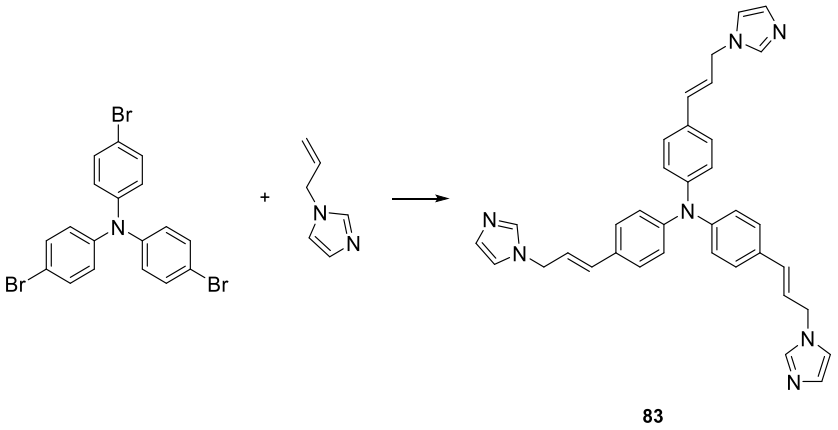

Scheme 3.9. Synthesis of ligand **83**, conditions: $Pd(OAc)_2$, $^{t}Bu_3P$, N,N-dicyclohexylmethylamine, 1,4-dioxane, 30min., 130°C under MW, 11%.

The complexing ability of helicate **75** towards different imidazole-functionalized ligands was first analyzed by UV-vis absorption and fluorescence spectrophotometry techniques. The procedure used for UV-vis and fluorescence titrations was the same reported in literature for similar host-guest complexation process:[136] a 2 mL solution of the helicate host (10 μM) in CH_3CN was titrated with a concentrated solution of guest. The total change in concentration of the host was less than 10% over the course of the titration, and the error involved was assumed to be negligible. Upon each addition, the solution was manually stirred for 1 min before acquiring the spectrum, which allowed equilibrium to be reached between the host and guest. Moreover, the host-guest equivalent ratio goes from 1:0 to 1:4 throughout the titration.

Initially, ditopic NDI ligand **82** was studied. Addition of the guest caused a bathochromic shift and decrease of intensity of the Q band of the helicate in the absorption spectra, with the formation of a clear isosbestic point at 705 nm. At the same time, a strong quenching of the emission band in fluorescence spectra was observed throughout the titration. In all cases, Job's plot experiments confirmed the formation of 1:1 complexes with maxima at 0.5 mole fraction (Figure 3.32).

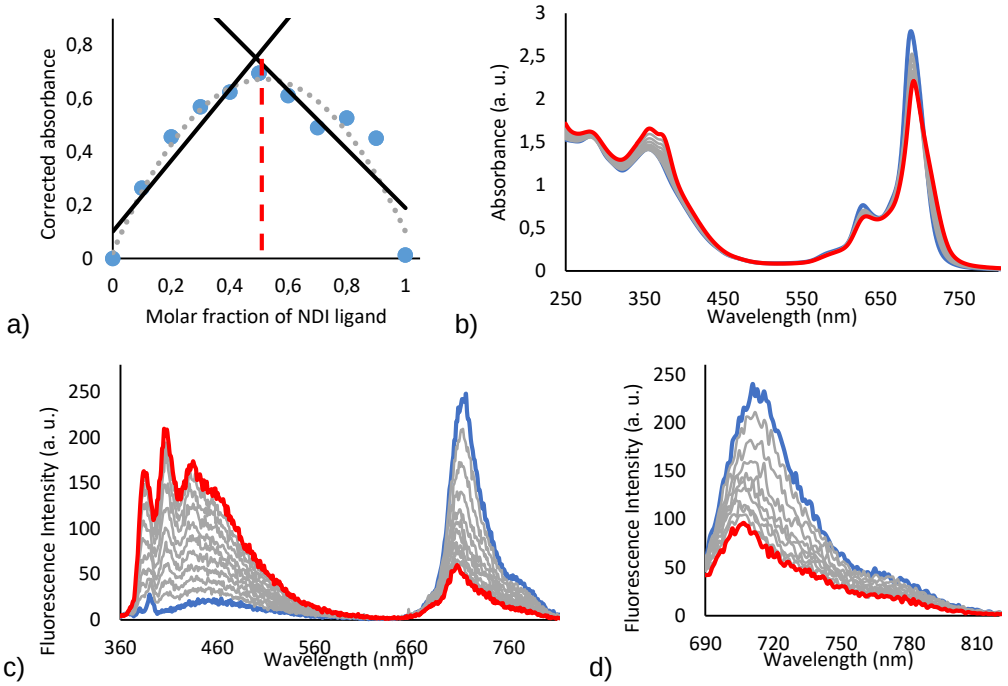

Figure 3.32. a) Job's plot diagram of the complex [**82** ⊂ **75**]$^{4+}$ (monitored at 692 nm), centered at 0.5 (1:1 stoichiometry); b) UV-vis titration and c) emission titration (λ_{exc} = 350 nm), d) (λ_{exc} = 680 nm) of helicate **75** (10 μM) with **82** from 0 (blue lines) to 4 equiv, red lines in CH_3CN:$CHCl_3$ (20:1) at 25 °C.

Interestingly, fluorescence tritrations reveal that photoactivated interactions between the Pc and the imidazolyl-NDI take place in the host-guest complex. This quenching may be related to a photoinduced charge transfer from the photoexcited Pc to the electron acceptor NDI. Please note that the LUMO level of NDI lies at -4,1 , while LUMO of Pc is at -3,9 as extracted from CV experiments using Fc/Fc+ as external reference.

Non-linear curve fitting of the spectroscopic changes in absorption and fluorescence titrations allowed determining the association constants values (K_{abs} and K_{em}, respectively) for complex [**82** ⊂ **75**]$^{4+}$ using ReactLab^{TM} EQUILIBRIA software. In this way, logarithms of association constants $logK_{abs}$ and $logK_{em}$ were respectively estimated as 5.36 ± 0.018 and 5.17 ± 0.018.

The formation of the complex with the NDI ligand can be also monitored by ^{1}H-NMR spectroscopy thanks to an upfield shift of some Pc centered protons (i.e., b in Figure 3.40 and 3.41).

Mass spectrometry corroborated the formation of 1:1 complex with ditopic ligand **82**. In fact, HR-ESI-MS detected a peak at *m/z* = 1522.6972, that shows the typical *m/z* splitting for a +4 charged species and which correspond to [**82** ⊂ **75**]$^{4+}$. It is reasonable, therefore, to conceive the formation of a 1:1 complex in which a molecule of ditopic NDI ligand binds the helical host by two simultaneous coordination bonds with two metallic Zn(II) located into Pc cores.

On the other hand, and to our surprise, no measurable spectral changes occurred in the UV-vis absorption and emission titrations of the helicate with TPA ligand **83**, implying that no host-guest complexes are formed in this case. ESI-MS spectra support this thesis, detecting separately the peaks corresponding to the empty helicate and the TPA ligand.

Further data that support the inclusion of the NDI into the cavity of the helicate were obtained from temperature dependent ^{1}H-NMR experiments, which give information about spin-crossover (SCO) processes that take place in octahedral Fe(II) complexes as a function of the temperature. Importantly, SCO can be also induced by the inclusion of a guest in the case of Fe(II)-based organometallic cages.

Spin crossover (SCO) is a phenomenon in which the electronic configuration of transition metal centers changes from high spin to low spin or *vice versa*, in response to external stimuli[137,138] such as thermal,[139] pressure,[140,141] light,[142] and magnetic ones.[143] Because of potential applications to sensors and digital memory, spin crossover materials have attracted considerable interests in chemistry and materials fields for many years.[144,145] Typically, spin crossover is observed for octahedral Fe(II), Fe(III), Co(II) complexes and rarely for other metal complexes.[137]

SCO in supramolecular structures has been explored in molecular frameworks,[146,147] polymeric materials,[148,149] discrete multinuclear complexes,[144] and, more recently, in organometallic cages.[150–153] These latter self-assembled architectures, especially those based on Fe(II) ions show a great potential in molecular switch field, since offering a bistability between two magnetically distinguishable states: the diamagnetic low-spin and the paramagnetic high-spin state.

Several methods have been used to detect the SCO phenomena in metal complexes, such as X-ray crystallography,[57] Fe Mössbauer technique and UV-vis spectroscopy. Recently, it has been shown how ^{1}H-NMR technique can be a useful tool to investigate SCO phenomena in organometallic cages, especially for the Fe(II) ones.[154] In fact, the Fe(II) SCO typically involves a change in iron–ligand distances due to changes in electronic structure.[155,156] In the case of proton-bearing organic ligands coordinating to Fe centers, the sensitivity of ^{1}H chemical shifts to the distance of individual protons from the metallic nucleus makes this spectroscopic technique well-suited for the evaluation of small structural differences that take place in the structure, for example the variation that might occur following complexation of a suitable guest.

The first example of transition from a diamagnetic state to a paramagnetic state (and *vice versa*) by host-guest complexation was reported in 2009 by Ono *et al*., who reported the change of the spin state of a Ni(II) containing guest upon encapsulation.[150] Subsequently, Nitschke *et al*. demonstrated how the encapsulation of different solvent molecules by tetrahedral Fe(II) cages affects their SCO properties, studying this phenomenon by ^{1}H-NMR technique.[154]

In this context, we studied the SCO properties of helicate **75**. From a first analysis at 298K, the ^{1}H-NMR spectrum of **75** in CD_3CN solution is consistent with a diamagnetic structure, with signals ranging from δ = 5.6 to 9.2 ppm. Variable temperature (VT) ^{1}H-NMR of the sample showed a strong downfield shift for the protons of the complex closer to the metal centers (i.e., He and Hd in Figure 3.33) when the temperature was increased beyond 308 K. In contrast, cooling the sample below 298 K led to an upfield shift of these same resonances. The imine peak showed the largest increase due to its proximity to the metal center. This shift, from δ = 9.00 ppm at 228 K to δ = 10.13 ppm at 343 K, was consistent with an increase in the high-spin population of Fe(II) ions. This analysis indicated a total diamagnetism of helicate **75** below 240 K and a rise of its partial paramagnetism beyond the same temperature (Figure 3.33).

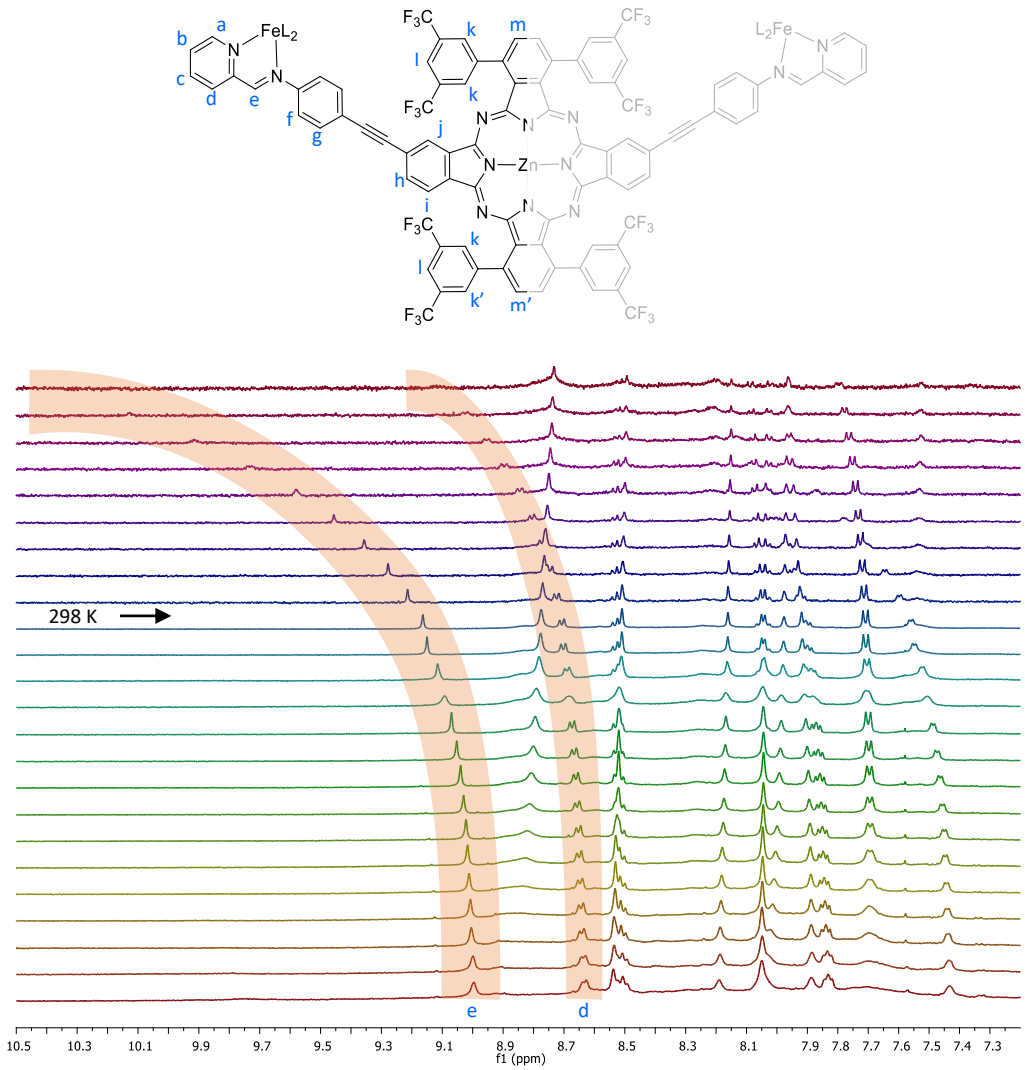

Figure 3.33. Stacked plot of ^{1}H NMR spectra for **75** in CD_3CN acquired at temperatures from 228 (bottom) to 343 K (top) in 5 K steps. Lines are drawn to guide the eye to the changes in chemical shifts of protons He and Hd.

The *ideal solution model*[157] is a rather simple and commonly used model to analyze the spin transition of individual SCO-centres in solutions that has also been applied for the analysis of oligonuclear complexes.[153,158,159]

According to the Gütlich's methodology, the thermodynamics of the SCO for helicate **75** was analyzed using a non-linear curve fitting algorithm implemented in Origin to fit the chemical shift of the imine resonance observed at different temperatures following equation (3.4).

$$\delta = \delta_{LS} + \frac{C}{T + Te^{\Delta G/RT}} \qquad \text{Eq. 3.4}$$

where δ is the imine chemical shift (ppm) observed at temperature T (K), δ_{LS} is the chemical shift of this proton in the low-spin state, *C* is a constant related to the molar susceptibility of the high-spin species, and ΔG is the free energy of spin transition. Equation 3.4 assumes a Boltzmann distribution between low-spin and high-spin states, where higher temperatures favor the latter.[157] It has been successfully used to investigate the thermodynamics of temperature-triggered SCO events across a variety of systems, metal ions and organometallic cages.[151,153,154,157,160,161]

The same analysis was performed on the complex [**82** ⊂ **75**], in order to investigate a possible guest-induced variation of the SCO behavior. Table 3.2 lists and compares the results within the experimental error obtained for **75** and [**82** ⊂ **75**]. These values are comparable to those found in previous self-assembles studies.[151,154] ΔH and ΔS resulted both positive in both cases due to the more loosely bound nature (longer, weaker Fe-N bonds) of the complex in the high-spin state than in the low-spin state. Despite the value of ΔH_{SCO} is significantly larger in presence of the NDI guest, the simultaneous entropic increase leads to a decrease in the total ΔG_{SCO}, which stabilize the high-spin state in the host-guest system.

In Figure 3.34 the fitting of ^{1}H-NMR data of empty helicate is depicted as representative example.

Table 3.2. The thermodynamic parameters of the SCO behavior

Parameters	**Helicate 75**		**Complex [82 ⊂ 75]**	
δ	9		9	
C	59688	±576	49567	±604
ΔH_{SCO} (Jmol^{-1})	42074	±520	51940	±490
ΔS_{SCO} (JK^{-1}mol^{-1})	74.39	±1.5	121.1	±1.4
ΔG_{SCO} [a] (Jmol^{-1})	19903		15837	
R^2	0.9989		0.9996	

[a] calculated at 298 K as $\Delta G=\Delta H-T\Delta S$

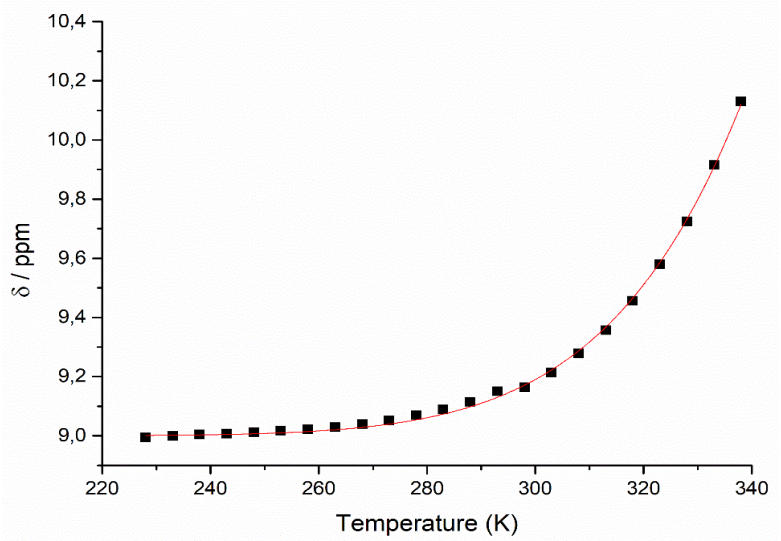

Figure 3.34. Experimental (squares) and calculated (curve obtained from Eq. 3.4) ^{1}H-NMR chemical shifts of the imine resonance for **75** as a function of temperature.

In order to confirm the stabilization of the high-spin state as a result of the host-guest interactions, it is possible to calculate the spin-state population at each temperature from the thermodynamic parameters. The transition between low-spin (LS) and high-spin (HS) state for iron(II) centers is described by an equilibrium with the corresponding constant (K_{eq} in Eq. 3.6 and Eq. 3.7):

$$LS \rightleftarrows HS \qquad \text{Eq. 3.5}$$

$$K_{eq} = \frac{[HS]}{[LS]} \qquad \text{Eq.3.6}$$

$$K_{eq} = e^{-\frac{\Delta G}{RT}} \qquad \text{Eq.3.7}$$

where [LS] and [HS] are the concentration of the low-spin and high-spin iron(II) centers respectively. Equation 3.7 allows us to calculate the equilibrium constant of the spin transition process at any given temperature from the ΔG values obtained from ΔH and ΔS parameters. The fraction of low-spin (X_{LS}) and high-spin (X_{HS}) of the total spin population for the Fe(II) centers can be defined with the following equations:

$$\mathrm{X}_{LS} = \frac{[LS]}{[HS]+[LS]} \qquad \text{Eq. 3.8}$$

$$\mathrm{X}_{HS} = \frac{[HS]}{[HS]+[LS]} \qquad \text{Eq. 3.9}$$

Taking into account the mass balance, the relationship between the low-spin (X_{LS}) and high-spin (X_{HS}) fractions can be expressed by equation 3.10:

$$X_{LS} + X_{HS} = 1 \qquad \text{Eq. 3.10}$$

Combining now equations 3.6 – 3.10, it is possible to obtain the LS and the HS populations at any given temperature from the following equations:

$$X_{LS} = \frac{1}{1+e^{-\frac{\Delta G}{RT}}} \qquad \text{Eq. 3.11}$$

$$X_{HS} = 1 - \frac{1}{1+e^{-\frac{\Delta G}{RT}}} \qquad \text{Eq. 3.12}$$

Using the above equations, the spin state populations were calculated in the presence and in the absence of NDI ligand, and represented in the Figure 3.35. This additional study confirms that the formation of the host-guest complex [**82** ⊂ **75**] affects the SCO behaviour of helicate **75**, favouring a partial stabilization of the high-spin state and thus increasing its paramagnetism. SCO is associated with substantial structural changes,[162,163] brought about by an increase in length of Fe-N bonds by about 20 pm (10%) in going from the low-spin to the high-spin state.[164,165] We infer that the presence of the guest resulted in subtle geometric influences upon the helical structure that led to major stabilization of the high-spin state.

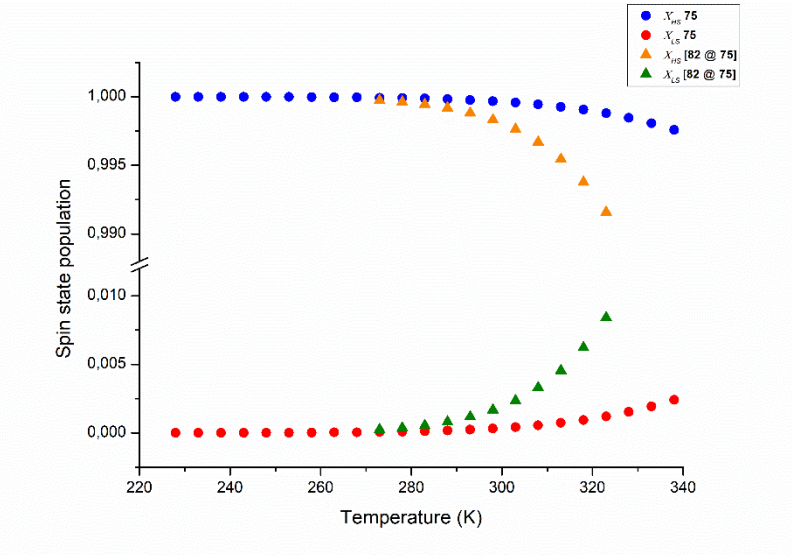

Figure 3.35. Low-spin and high-spin state fractions (X_{LS} and X_{HS}, respectively) for the Fe^{II} centers in **75** (●) and its host–guest complex with **82** (▲) plotted as a function of temperature.

3.3.3.2 Fullerene derivatives

The large aromatic internal surface of helicate **75** makes it very attractive for the complexation of aromatic species such as fullerenes. The use of molecular receptors for fullerene complexation in solution is very appealing, since it allows for a simple access to supramolecular ensembles with remarkable redox properties. Taking into account the well-established electron donor role of the Pc chromophores in covalent and supramolecular ensembles with fullerenes,[88,166] the complexation of C_{60} and C_{70} by **75** may lead to host – to – guest charge transfer complexes.

Therefore, different experiments were performed to determine the ability of **75** to bind different fullerene species. The encapsulation reactions were carried out in J-Young NMR tubes, heating the mixture of **75** in CD_3CN with an excess of the selected fullerene at 70°C for 16 hours, according to literature procedures.[83,84,167]

Upon addition of C_{60} and C_{70} over CD_3CN solutions of the preformed helicate, spectroscopical evidences of the conversion of **75** into a host–guest complex were found. It is worth mentioning that the encapsulation of fullerenes allows their solubilization in acetonitrile – otherwise extremely insoluble – so that the fullerene excess can be easily removed by filtration from the reaction mixture. The ^{1}H-NMR spectra showed, in both cases, small downfield shifts for the imine protons of **75** in the presence of the guest (Figure 3.36).

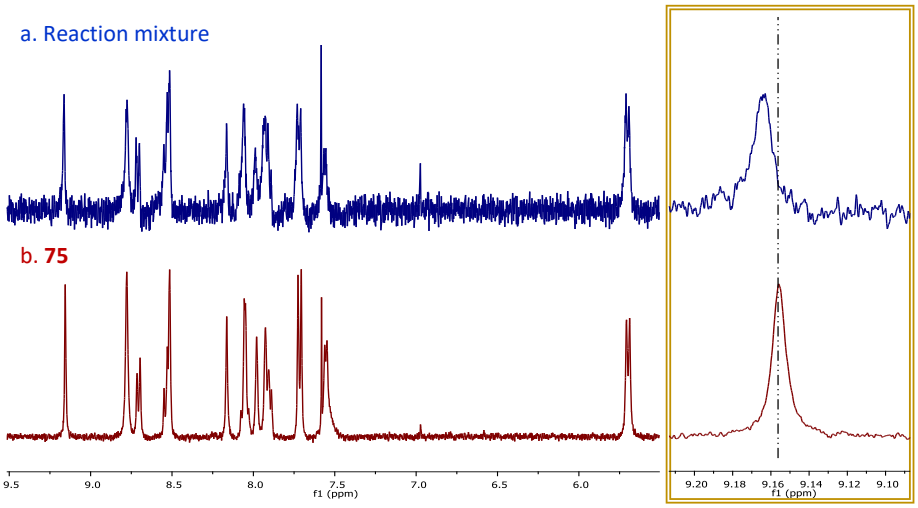

Figure 3.36. Comparison of the ^{1}H-NMR spectra for the reaction mixture containing [$C_{70} \subset$ **75**] (a-top) and empty **75** (b-bottom). **Left:** aromatic region where host peaks are located; **right:** expansion of the imine peak region showing the different chemical shifts for each species.

In UV-vis experiments a small bathochromic shift of the maximum wavelength (λmax) of the Pc Q band is observed from the free helicate **75** (690 nm) to the $[C_{60} \subset \mathbf{75}]^{4+}$ and $[C_{70} \subset \mathbf{75}]^{4+}$ complexes (695 nm) (Figure 3.37, UV-vis of the complex with C_{70} as representative example). Also, mass spectrometry experiments corroborated the formation of host-guest complexes, showing peaks at m/z = 1582.3343 and 1612.1438 for $[C_{60} \subset \mathbf{75}]^{4+}$ and $[C_{70} \subset \mathbf{75}]^{4+}$, respectively. These peaks present the typical m/z splitting for +4 charged species. Unfortunately, the presence of free host **75** was detected in both cases. Considering that the complexation kinetics with the fullerene species might be low, we subjected the samples to longer incubation times. However, after 48 hours the helicate **75** started to decompose.

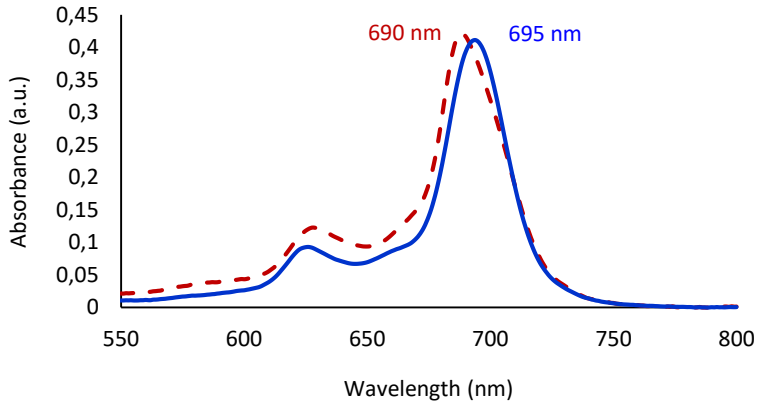

Figure 3.37. UV-vis spectra in CH_3CN. Comparison of the Q-bands for the reaction mixture containing $[C_{70} \subset \mathbf{75}]$ (solid line) and empty **75** (dashed line).

As the estimated internal volume of **75** is *ca*. 705 $Å^3$, and the volumes of C_{60} and C_{70} are 589,2 and 685,9 $Å^3$, respectively, the filling of **75** by the fullerene species largely exceeds the empirical 55% rule of Rebek.[168] Nevertheless, it should be taken into account that some fullerene complexes have shown much larger occupancies.[85,169] Moreover, the flexibility of the cage may allow it to adapt its cavity size as a function of the guest. Even though, the weak binding with the fullerene species exhibited by helicate **75** is indicative of a poor size/shape match.

Yet, competitive experiments were performed in order to study a possible selectivity of **75** towards one of the fullerene species, either C_{60} or C_{70}. Initially, an equimolar amount of C_{60} and C_{70} was mixed in a solution of the empty helicate in the experimental conditions for fullerene-complexation. Considering that imine protons suffer the same downfield shift in presence of C_{60} or C_{70}, we are not able to discriminate an eventual selectivity by ^{1}H-NMR. On the other hand, in HR-ESI-

MS experiments, and to our surprise, we were able to observe the preferential formation of 1:1 complex with C_{70}, while no encapsulated C_{60} was detected. A further experiment was carried out to confirm this selectivity, using a 2:1 ratio of C_{60} and C_{70}, respectively. Also in this case, the exclusive formation of $[C_{70} \subset \mathbf{75}]^{4+}$ complex was observed. This observation confirms the adaptability of helicate **75**, and it is indicative of the larger stability of the $[C_{70} \subset \mathbf{75}]$ complex.

The association constant (K_{ass}) or binding constant is the parameter which measures the thermodynamic stability of a host-guest adduct (Eq. 3.13). A high value of the association constant corresponds to a high relative equilibrium concentration of the bound over the free substrate, and consequently a more stable host-guest adduct. Generally, binding constants can be measured by any experimental technique that can give information about the host-guest concentration (*[H·G]*) as a function of concentration of host (*[H]*) or guest (*[G]*). Among all the methodologies available for the determination of the K_{ass}, NMR, UV-vis and fluorescence titrations are the most widely used.

$$Host + Guest \rightleftarrows Host \cdot Guest \qquad K_{ass} = \frac{[H \cdot G]}{[H] \times [G]} \qquad (3.13)$$

However, in this case the solubility of fullerenes is a limiting parameter. Mass spectrometry provides a tool to overcome this obstacle. ESI-MS(/MS) has been used as a method which allows the fast, unambiguous and sensitive simultaneous detection, and relative stability approximation of supramolecular assemblies in mixtures. In spite of the obvious fundamental differences between solution and gas phase, ESI-MS(/MS) experiments in the case of self-assembled cages have been shown to produce very similar results to single binding experiments monitored by NMR titrations, obtaining the same order of gas phase stability and solution stability.[170,171]

ESI-MS/MS stability experiments were carried out on 1:1 complexes of $[C_{60} \subset \mathbf{75}]^{4+}$ and $[C_{70} \subset \mathbf{75}]^{4+}$. In these experiments, the positively-tetracharged ion peaks were separated by their masses and accelerated into the collision cell of the mass spectrometer. In a series of experiments, the collision energy was varied and the relative amounts of intact complex compared at different energies. Initially, these data were collected at different temperatures to establish the best experimental conditions. Based on the MS/MS data, dissociation curves of the complexes were calculated and are represented in Figure 3.38. The CE_{50} values shown in Table 3.3 represent collision energies necessary for 50% complex dissociation and therefore describe the relative order of their stabilities.

Table 3.3. Stability of the $[C_{60} \subset \mathbf{75}]^{4+}$ and $[C_{70} \subset \mathbf{75}]^{4+}$ complexes as determined by ESI-MS/MS experiments.

Entry	Complex	Temperature	*CE_{50} (eV)*
1	$[C_{60} \subset \mathbf{75}]^{4+}$	50°C	4.6
2	$[C_{60} \subset \mathbf{75}]^{4+}$	100°C	6.8
3	$[C_{60} \subset \mathbf{75}]^{4+}$	200°C	13.7
4	$[C_{70} \subset \mathbf{75}]^{4+}$	50°C	4.8
5	$[C_{70} \subset \mathbf{75}]^{4+}$	100°C	8.0
6	$[C_{70} \subset \mathbf{75}]^{4+}$	200°C	29.4

As shown in Figure 3.38 and according the CE_{50} values, the stability of both complexes increases at higher temperatures, which can be explained by the lower possibilities of hydrolysis of the organometallic helicate. In fact, solvent molecules like water totally disappear at higher temperature, stabilizing the supramolecular assembly. More importantly, comparing CE_{50} values at the same temperature for both 1:1 complexes, $[C_{70} \subset \mathbf{75}]^{4+}$ proved more stable, this fact explaining the helicate selectivity towards fullerene C_{70}.

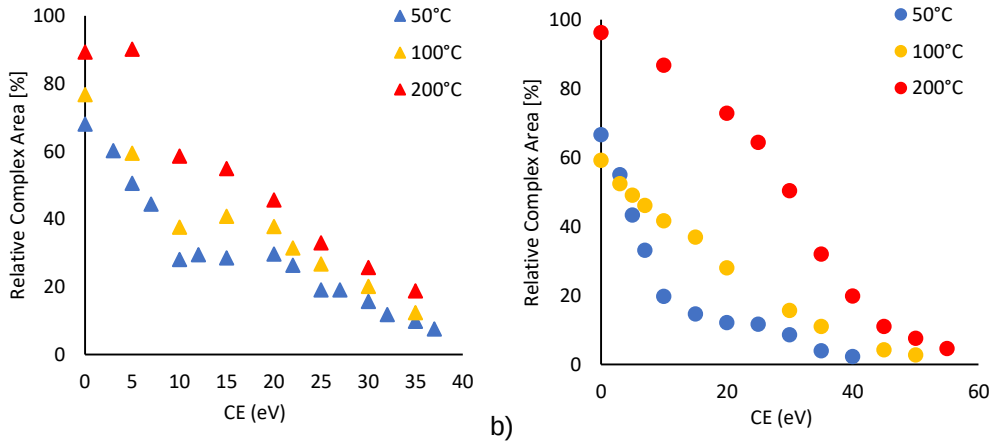

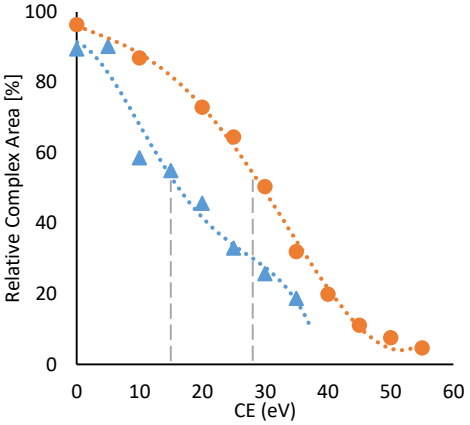

c)

Figure 3.38. Overview of all collision-induced dissociation curves of the [C60 ⊂ **75**]$^{4+}$ and [C_{70} ⊂ **75**]$^{4+}$ complexes. $Relative\ Complex\ Area = \left(A_{complex}/A_{total}\right) \times 100$, that is the pure non-fragmented complex at a specific collision energy; a) dissociation curves of [C_{60} ⊂ **75**]$^{4+}$ at different temperatures; b) dissociation curves of [C_{70} ⊂ **75**]$^{4+}$ at different temperatures; c) comparison of dissociation curves of [C_{60} ⊂ **75**]$^{4+}$ (▲) and [C_{70} ⊂ **75**]$^{4+}$ (●) at 200°C.

3.3.3.3 Guest-exchange

The control of the binding/release process of guest molecules by a host structure is of great interest for several applications, as already discussed extensively in Section 3.1.3 of this chapter. For this purpose, and learning from many natural systems, scientists have designed and constructed supramolecular assemblies, particularly metal-ligand cage complexes, that can capture and release guest molecules.[172,173]

The process of guest exchange in supramolecular systems is simply the replacement of a non-covalently bound molecule from the interior of a larger host structure by a new guest, which forms a more stable host-guest complex.

It reasonable thinking that coordination bonds between imidazole moieties and Zn(II) metals present into the Pc cores could be a driving force that lead to the preferred formation of the 1:1 complex [**82** ⊂ **75**]$^{4+}$ with respect to any of the 1:1 complexes of **75** with fullerenes. This encouraged us to use **82** as a chemical stimulus to drive the release of fullerenes guests in a controlled way.

As seen above, helicate **75** shows a strong selectivity towards the encapsulation of fullerene C_{70} from a mixture of C_{60} and C_{70}, which was explained by the higher stability of the [C_{70} ⊂ **75**]$^{4+}$ complex. For this reason, it was the target of choice for the guest-exchange experiments, which were followed by ^{1}H-NMR and ESI-MS techniques.

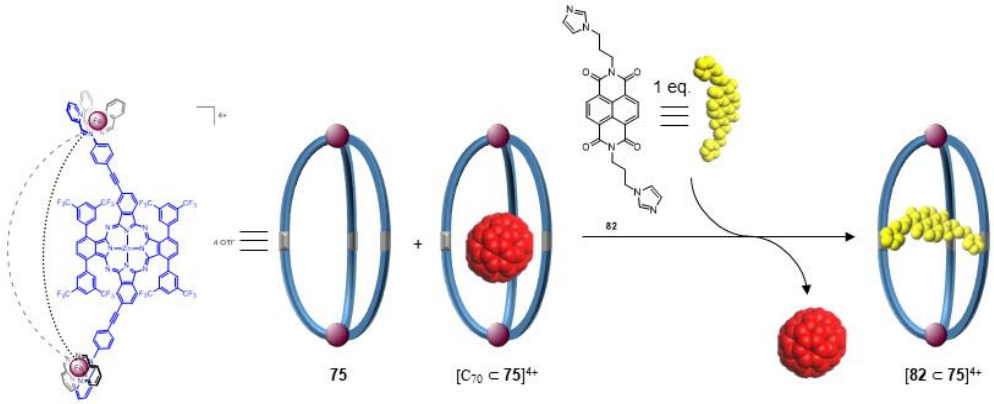

Figure 3.39. Schematic representation of guest-displacement process.

As shown in Figure 3.39, the addition of a stoichiometric amount of NDI ligand **82** (1 eq) to a C_{70} – saturated, acetonitrile solution of **75**, resulted in a complete and immediate displacement of C_{70} in favor of **82**; in fact [**82** ⊂ **75**]$^{4+}$ was the only product observed by ^{1}H-NMR spectroscopy and ESI-MS. On the other hand, no guest substitution was observed when excess C_{70} was added to a solution of [**82** ⊂ **75**]$^{4+}$ after 12h at 70°C.

^{1}H-NMR spectroscopy allowed us to discriminate easily the two complexes. While the encapsulation of fullerene was accompanied by the typical downfield shift for the imine protons of **75** (i.e., c in Figure 3.40 and 3.41), the formation of the complex with the NDI ligand led to an upfield shift of some Pc centered protons without any shifting for the imine ones (i.e., b in Figure 3.40 and 3.41).

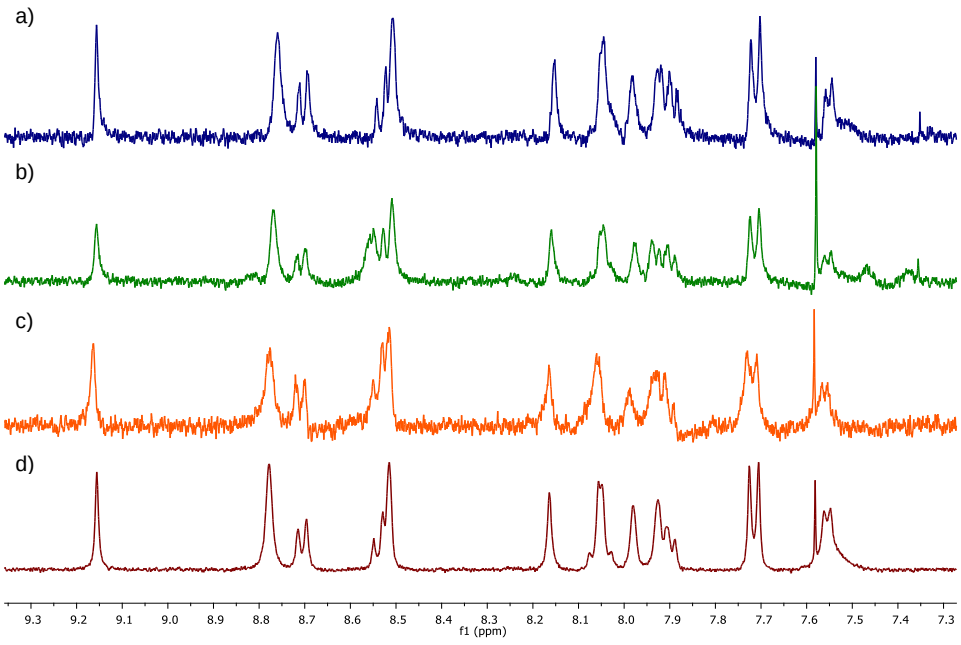

Figure 3.40. Comparison of the aromatic region of ^{1}H-NMR spectra in CD_3CN for: a) the reaction mixture of guest-exchange experiment, b) [**82** ⊂ **75**], c) [C_{70} ⊂ **75**], and d) empty **75**.

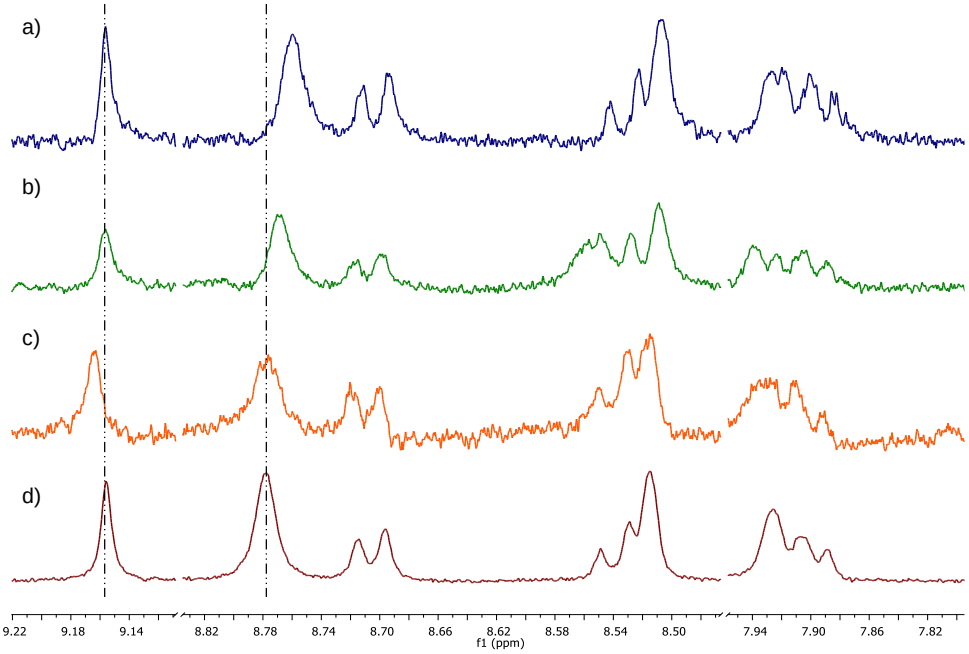

Figure 3.41. Expansion of the aromatic region of ^{1}H-NMR spectra in CD_3CN for: a) the reaction mixture of guest-exchange experiment, b) [**82** ⊂ **75**], c) [C_{70} ⊂ **75**], and d) empty **75**.

3.4 Summary and conclusions

In this chapter, the synthesis and characterization of a novel supramolecular M_2L_3 architecture based on Pc ligands, and the study of its host-guest properties have been expounded.

Initially, the separation of *syn* and *anti* isomers was compulsory in order to achieve **ABAB** Pcs with well-defined geometries that can be used as ligands for building metallo-supramolecular complexes. Separation of the positional isomers could be reached owing to an appropriate functionalization of the starting ZnPc **12** with propargyl alcohol or with 2-methyl-3-butyn-2-ol under Shonogashira conditions. The resulting mixture of Pc regioisomers was separated and subsequently transformed into amino-containing Pcs **73a** and **73s** that were separately examined as ditopic ligands.

syn Zn(II)Pc **73s** was assembled into a $Fe^{II}_2L_3(OTf)_4$ helicate (**75**) under subcomponent self-assembly conditions, namely, using 2-formylpyridine and iron(II) triflate in CD_3CN at room temperature. The structure of **75** was confirmed by ESI-MS, ^{1}H-NMR, ^{19}F-NMR, diffusion – ordered spectroscopy (DOSY), COSY and UV-vis spectroscopy. However, and to our surprise, all the attempts to form metallo-supramolecular ensembles from *anti* Zn(II)Pc **73a** were fruitless, affording in all cases a complex dynamic mixture of coordination species. Many attempts were done to pilot this mixture towards the formation of well-defined assemblies, using anionic and neutral molecules that could act as template, but all in vain.

On the other hand, the $Fe^{II}_2L_3(OTf)_4$ helicate (**75**) was successfully employed to encapsulate different kind of neutral guests functionalized with imidazole rings, which are prone to coordinate to the metal Zn(II) present into the Pc cores. A series of bis- and tris-imidazolyl-functionalized NDI, tricarboxamide, and TPA derivatives were synthetized, and tested as hosts to form complexes with helicate **75**. The complexation processes were studied employing UV-vis absorption and fluorescence spectrophotometry. From all the tested guests, only the optically and electronically active NDI derivative **82** formed a stable 1:1 complex with **75**, as confirmed by a Job's Plot study and by HR-MS studies. Interestingly, fluorescence tritrations reveal that photoactivated interactions between the Pc and the imidazolyl-NDI take place in the host-guest complex. Also, variable-temperature ^{1}H-NMR experiments confirmed the formation of [**82** ⊂ **75**]$^{4+}$, since a larger stabilization of the high spin state of Fe(II) center at high temperature could be observed as a consequence of the complexation of the NDI by the Pc helicate.

The large aromatic internal surface of helicate **75** was also exploited for the complexation of C_{60} and C_{70} fullerenes. [C_{60} ⊂ **75**]$^{4+}$ and [C_{70} ⊂ **75**]$^{4+}$ complexes

were obtained and characterized by ^{1}H-NMR, UV-vis and HR-ESI-MS. Interestingly, ESI-MS/MS experiments revealed that helicate **75** shows a strong selectivity towards the encapsulation of fullerene C_{70} from a mixture of C_{60} and C_{70}, which was explained by the higher stability of the 1:1 complex [C_{70} ⊂ **75**]$^{4+}$. Figure 3.42 shows the MM energy-minimized structure of [C_{70} ⊂ **75**]^4

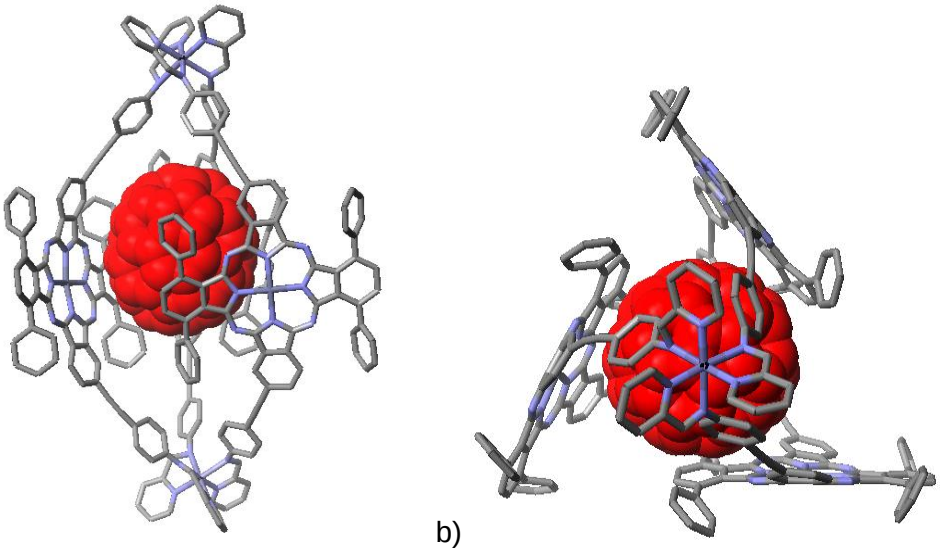

Figure 3.42. a) side view and b) top view of an energy-minimized structure of the complex [C_{70} ⊂ **75**]$^{4+}$, depicted with all Fe(pyridylimine)$_3$ vertices in the Λ conformation. Hydrogen atoms and trifluoromethyl groups are omitted for clarity (C = grey, N = blue, Fe = purple, Zn = dark grey, C_{70} = red).

Finally, the larger stability of the [**82** ⊂ **75**]$^{4+}$ complex with regard to the most stable fullerene complex, that is [C_{70} ⊂ **75**]$^{4+}$, was exploited to replace the encapsulated fullerene molecules from the internal void of the helicate in a guest-displacement process (Figure 3.43). This process can be envisioned as a practical method for the selective capture and release of fullerene derivatives from complex mixtures.

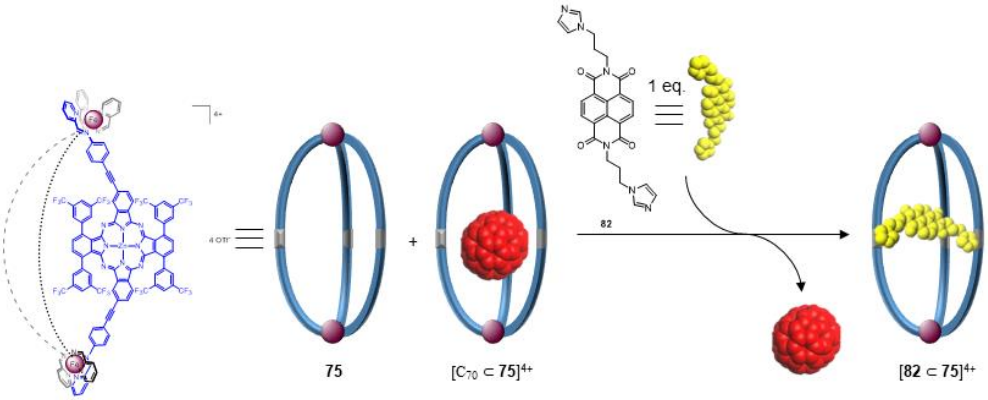

Figure 3.43. Schematic representation of guest-displacement process.

3.5 Experimental section

In this *Experimental section*, the preparation and characterization of the compounds has been organized following the order as they appear in the text.

3.5.1 Specific methods in chapter 3

X-Ray Spectroscopy: X-Ray diffraction spectra were done in SIdi with a Bruker KAPPA APEX II CCD goniometer with kappa geometry and Mo source (λ = 0.71073 Å). Data were collected at different temperatures, specified in each case, utilizing a system equipped with an Oxford Cryosystems dispositive. The distance between the sample and the detector is 3.5 cm. The data harvesting is done over 99% and the redundancy value is over 3. Data are corrected then with SADABS program. The intensities are calculated with SAINT program. Finally, the structures are resolved with SHELXS and refined with SHELXL.

3.5.2 Synthesis of ditopic Pc ligands

*1,4,15,18-Tetrakis(3,5-bis(trifluoromethyl)phenyl)-9,23[24]-bis(3'-hydroxypropyn-1-yl)- zinc (II) phthalocyanine (**71a** and **71s**)*

To a solution of Pc **12** (0.119 mmol, 200 mg) in freshly distilled THF (6 mL), NEt_3 (2 mL), $Pd(PPh_3)_4$ (10% mol, 14 mg) and CuI (10% mol, 2 mg) were added. The mixture was deoxygenated by bubbling argon through it for 20 min. Propargylic alcohol (0.357 mmol, 20.6 µL) was subsequently added and the mixture was stirred overnight at 50ºC. After evaporation of the solvents, the crude mixture was dissolved in $CHCl_3$ and washed with water. The combined organic layers were dried over $MgSO_4$ and concentrated in vacuum. Purification by column chromatography (heptane/THF 5:1) afforded the desired products as blue solids in a 1:1 ratio.

71a

The compound was washed with heptane. Yield: 70 mg, 38% yield

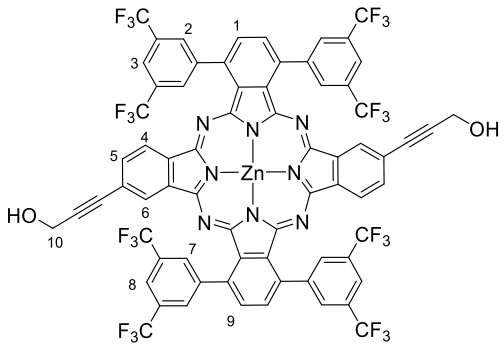

^{1}H-NMR (500 MHz, THF-d_8), δ (ppm): 8.85 (s, 4H; H-2), 8.76 (s, 4H; H-7), 8.64 (s, 2H; H-3), 8.58 (s, 2H; H-8), 8.28 (s, 4H; H-1, H-9), 8.26 (s, 2H; H-6), 8.24 (d, J = 5 Hz, 2H; H-4), 7.96 (dd, J_1 = 5 Hz, J_2 = 1 Hz, 2H, H-5), 4.62 (d, J = 5 Hz, 4H; H-10), 4.51 (t, J = 5 Hz, 2H; OH).

MS (MALDI) m/z Calcd for [$C_{70}H_{28}F_{24}N_8O_2Zn$]: 1532.1; Found: 1532.1.

UV-Vis (THF) λmax (log ε): 698 (5.05), 678 (5.06), 643 (4.40), 617 (4.40), 360 (4.71), 251 (4.70) nm.

71s

The compound was washed with heptane. Yield: 70 mg, 38% yield

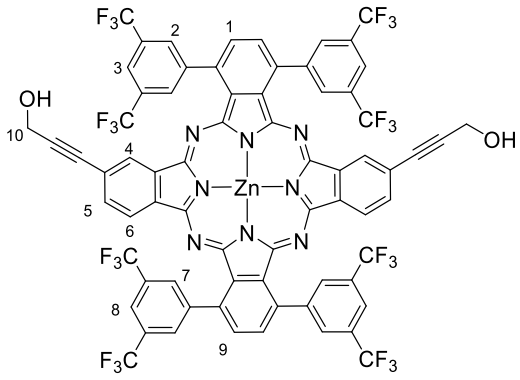

^{1}H-NMR (500 MHz, THF-d_8), δ (ppm): 8.83 (s, 4H; H-2), 8.79 (s, 4H; H-7), 8.64 (s, 2H; H-3), 8.58 (s, 2H; H-8), 8.29 (s, 2H; H-4), 8.28 (s, 2H; H-1), 8.27 (s, 2H; H-9), 8.21 (d, J = 5 Hz, 2H, H-6), 7.96 (dd, J_1 = 5 Hz, J_2 = 1.5 Hz, 2H; H-5), 4.62 (d, J = 5 Hz, 4H; H-10), 4.51 (t, J = 5, 2H; OH).

HR-MS (MALDI) m/z Calcd for [$C_{70}H_{28}F_{24}N_8O_2Zn$]: 1532.1238; Found: 1532.1279.

UV-Vis (THF) λmax (log ε): 696 (5.06), 680 (5.08), 641 (4.38), 615 (4.38), 361 (4.70), 253 (4.66) nm.

*General procedure for the synthesis of Pcs **72a** and **72s**, starting from Pcs **71a** and **71s***

To a solution of phthalocyanine **71a** or **71s** (0.0072 mmol, 11 mg) in Et_2O (2 ml), MnO_2 (0.69 mmol, 60 mg) and recently powdered KOH (0.53 mmol, 30 mg) were added. The mixture was stirred at reflux overnight (the reaction can be easily monitored by TLC with heptane/THF 3:1). Then, the solid was filtered off and washed with Et_2O. The filtrate was concentrated to dryness. Then the crude mixture was dissolved in CH_2Cl_2 and washed with water. Purification by column chromatography (heptane/THF 3:1) afforded the desired products.

*1,4,15,18-Tetrakis(3,5-bis(trifluoromethyl)phenyl)-9,24-diethynyl zinc(II) phthalocyanine (**72s**)*

The compound was isolated as a blue solid. Yield: 9 mg, 86% yield).

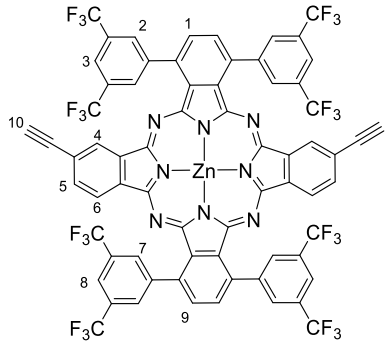

^{1}H-NMR (300 MHz, THF-d_8), δ (ppm): 8.88 (s, 4H; H-2), 8.85 (s, 4H; H-7), 8.63 (s, 2H; H-3), 8.59 (s, 2H; H-8), 8.39 (s, 2H, H-4), 8.34 (s, 2H; H-1), 8.32 (s, 2H; H-9), 8.28 (d, J = 9 Hz, 2H; H-6), 8.08 (dd, J_1 = 9 Hz, J_2 = 1.2 Hz, 2H; H-5), 4.0 (s, 2H; H-10).

HR-MS (MALDI) m/z Calcd for [$C_{68}H_{24}F_{24}N_8Zn$]: 1472.1027, Found: 1472.1058.

UV-Vis (THF) λmax (log ε): 693 (5.06), 679 (5.06), 640 (4.37), 614 (4.40), 356 (4.71), 243 (4.80), 215 (4.87) nm.

*1,4,15,18-Tetrakis(3,5-bis(trifluoromethyl)phenyl)-9,23-diethynyl zinc(II) phthalocyanine (**72a**)*

The compound was isolated as a blue solid. Yield: 9 mg, 86% yield).

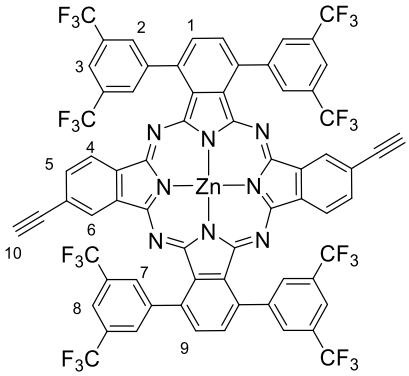

^{1}H-NMR (300 MHz, THF-d_8), δ (ppm): 8.85 (s, 4H; H-2), 8.80 (s, 4H; H-7), 8.59 (s, 2H; H-3), 8.55 (s, 2H; H-8), 8.33 (s, 2H; H-6), 8.29 (s, 4H; H-1, H-9), 8.25 (d, J = 9 Hz, 2H; H-4), 8.04 (dd, J_1 = 9 Hz, J_2 = 0.9 Hz, 2H; H-5), 3.97 (s, 2H; H-10).

MS (MALDI) m/z Calcd for [$C_{68}H_{24}F_{24}N_8Zn$]: 1472.1; Found: 1472.1

UV-Vis (THF) λmax (log ε): 694 (5.07), 678 (5.06), 642 (4.37), 615 (4.39), 354 (4.69), 245 (4.77), 214 (4.89) nm.

*General procedure for the synthesis of phthalocyanines **73a** and **73s***

Phthalocyanine **72s** or **72a** (0.03 mmol, 40 mg), 4-Iodoaniline (0.09 mmol, 20 mg), $Pd(PPh_3)_4$ (5% mol, 2 mg) and CuI (5% mol, 0.3 mg) were dissolved in freshly distilled THF (3 mL) and NEt_3 (1 mL). The mixture was stirred 3 hours at 60ºC. After evaporation of the solvents, the crude mixture was dissolved in $CHCl_3$ and washed with water. The combined organic layers were dried over $MgSO_4$ and concentrated in vacuum. Purification by column chromatography (heptane/AcOEt 1:1) and precipitation with heptane afforded the desired product.

*1,4,15,18-Tetrakis(3,5-bis(trifluoromethyl)phenyl)-9,24-bis(4,4'-dianilinethynyl) zinc(II) phthalocyanine (**73s**)*

Green solid. Yield: 41 mg, 83%.

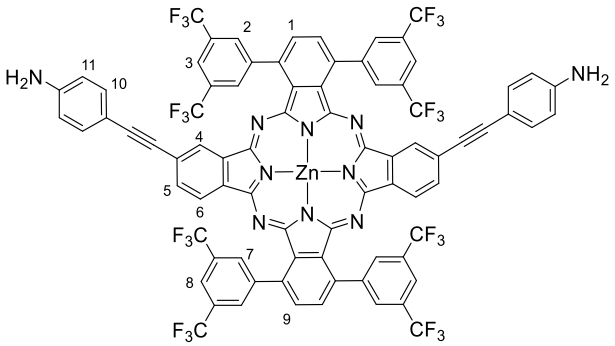

^{1}H-NMR (300 MHz, THF-d_8), δ (ppm): 8.83 (s, 8H; H-2, H-7), 8.59 (s, 4H; H-3, H-8), 8.30 (s, 2H; H-4), 8.28 (s, 2H; H-1), 8.26 (s, 2H; H-9), 8.20 (d, *J* = 9 Hz, 2H; H-6), 7.99 (dd, *J* = 9 Hz, 2H; H-5), 7.48 (d, *J* = 9 Hz, 4H; H-10), 6.71 (d, *J* = 9, 4H; H-11).

HR-MS (MALDI) m/z Calcd for [$C_{80}H_{34}F_{24}N_{10}Zn$]: 1654.1871; Found: 1654.1900.

UV-Vis (THF) λmax (log ε): 696 (5.25), 628 (4.58), 358 (4.87), 253 (4.78), 215 (4.92) nm.

*1,4,15,18-Tetrakis(3,5-bis(trifluoromethyl)phenyl)-9,23-bis(4,4'-dianilinethynyl) zinc(II) phthalocyanine (**73a**)*

Green solid. Yield: 40 mg, 83%.

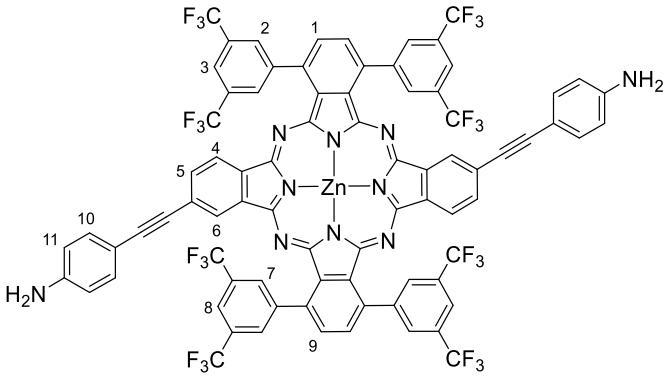

^{1}H-NMR (300 MHz, THF-d_8), δ (ppm): 8.85 (s, 4H; H-2), 8.81 (s, 4H; H-7), 8.58 (s, 4H; H-3, H-8), 8.26 (s, 6H; H-1, H-6, H-9), 8.20 (d, *J* = 9 Hz, 2H; H-4), 7.98 (dd, *J* = 9 Hz, 2H; H-5), 7.49 (d, *J* = 9 Hz, 4H; H-10), 6.72 (d, *J* = 9, 4H; H-11).

MS (MALDI) m/z Calcd. for [$C_{80}H_{34}F_{24}N_{10}Zn$]: 1654.2.; Found: 1654.2

UV-Vis (THF) λmax (log ε): 696 (5.25), 626 (4.58), 359 (4.88), 253 (4.78), 213 (4.95) nm.

*1,4,15,18-Tetrakis(3,5-bis(trifluoromethyl)phenyl)-9,23[24]-bis(3'-hydroxy-3'-methyl-butyn-1-yl)- zinc (II) phthalocyanine (**74a** and **74s**)*

To a solution of Pc **12** (0.119 mmol, 200 mg) in freshly distilled THF (6 mL), NEt_3 (2 mL), $Pd(PPh_3)_4$ (10% mol, 14 mg) and CuI (10% mol, 2 mg) were added. The mixture was deoxygenated by bubbling argon through it for 20 min. 2-methyl-3-butyn-2-ol (0.39 mmol, 38 µL) was subsequently added and the mixture was stirred 3 hours at 60ºC. After evaporation of the solvents, the crude mixture was dissolved in $CHCl_3$ and washed with water. The combined organic layers were dried over $MgSO_4$ and concentrated in vacuum. Purification by column chromatography (heptane/THF 7:1) afforded the desired products as blue solids in a 1:1 ratio.

74a

Blue solid. Yield: 30 mg, 16% yield

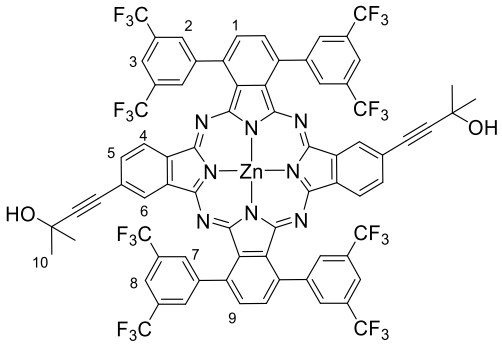

^{1}H-NMR (500 MHz, THF-d_8), δ (ppm): 8.84 (s, 4H; H-2), 8.79 (s, 4H; H-7), 8.57 (s, 4H; H-3, H-8), 8.26 (s, 4H; H-1, H-9), 8.20 (m, 4H; H-6, H-4), 7.94 (dd, J_1 = 7.5 Hz, J_2 = 1 Hz, 2H, H-5), 4.75 (s, 2H; OH), 1.77 (s, 12H; H-10).

MS (MALDI) m/z Calcd for $[C_{74}H_{36}F_{24}N_8O_2Zn]$: 1588.2; Found: 1588.2.

UV-Vis (THF) λmax (log ε): 698 (5.05), 679 (5.08), 642 (4.39), 614 (4.40), 358 (4.71), 246 (4.81) nm.

74s

Blue solid. Yield: 70 mg, 37% yield

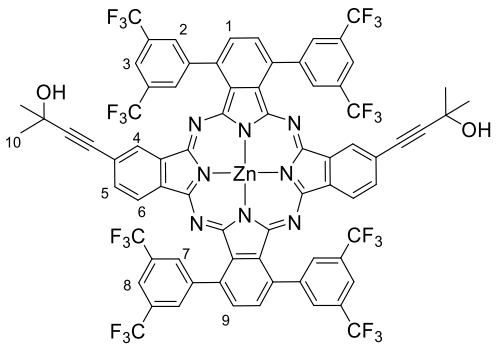

^{1}H-NMR (500 MHz, THF-d_8), δ (ppm): 8.83 (s, 4H; H-2), 8.80 (s, 4H; H-7), 8.56 (m, 4H; H-3, H-8), 8.29 (s, 2H; H-1), 8.27 (s, 2H; H-9), 8.25 (s, 2H; H-4), 8.20 (d, J = 8 Hz, 2H, H-6), 7.95 (dd, J_1 = 8 Hz, J_2 = 1 Hz, 2H; H-5), 4.70 (s, 2H; OH), 1.77 (s, 12H; H-10).

HR-MS (MALDI) m/z Calcd for [$C_{74}H_{36}F_{24}N_8O_2Zn$]: 1588.1864; Found: 1588.1889.

UV-Vis (THF) λmax (log ε): 699 (5.13), 678 (5.16), 643 (4.48), 616 (4.48), 361 (4.78), 246 (4.88) nm.

*General procedure for the synthesis of Pcs **72a** and **72s**, starting from Pcs **74a** and **74s***

To a solution of phthalocyanine **74a** or **74s** (0.013 mmol, 21 mg) in toluene (4 ml), recently powdered KOH (0.039 mmol, 2 mg) was added. The mixture was stirred at reflux for 5 hours (the reaction can be easily monitored by TLC with heptane/THF 3:1). Then, the solid was filtered off and washed with toluene. The filtrate was concentrated to dryness. Then the crude mixture was dissolved in CH_2Cl_2 and washed with water. Purification by column chromatography (heptane/THF 3:1) afforded the desired products.

3.5.3 Self-assembly and Host-Guest complexes

*Assembly of Fe_2L_3 Helicate (**75**)*

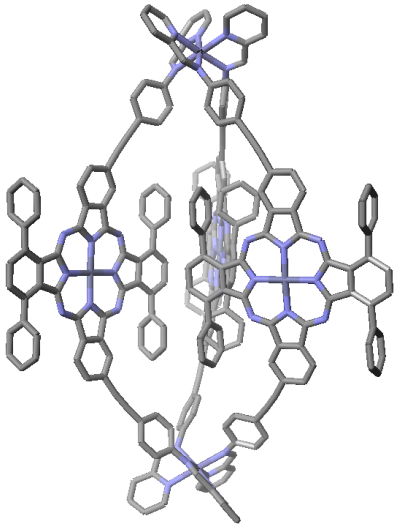

73s (2.0 mg, 1.21 µmol), $Fe(OTf)_2$ (0.3 mg, 0.81 µmol) and 2FP (24 µL of a stock solution 0.1 M in CD_3CN, 2.42 µmol) were dissolved in deuterd MeCN (0.6 mL) in a J-Young nmr tube. The solution was degassed by three evacuation/nitrogen fill cycles and, then, sonicated for 30 minutes. The resultant dark green solution was left at room teperature for 24 h. Then, the dropwise addition of Et_2O precipitates the desired product, which was collected by filtration and washed with additional Et_2O, then redissolved in MeCN (1 mL). The solution was reduced to dryness to give a green powder . Yield: 2 mg, 0.32 µmol, 80 %.

^{1}H-NMR (400 MHz, CD_3CN), δ (ppm): 9.2 (s, 2H; e), 8.8 (s, 6H; k', l'), 8.7 (d, J = 7.2 Hz, 2H; d), 8.55 – 8.51 (m 6H; c, k), 8.2 (s, 2H; l), 8.08 – 8.03 (m, 4H; h, i), 8.0 (s, 2H; m'), 7.93 – 7.89 (m, 4H; m, b), 7.7 (d, J = 8.4 Hz, 4H; g), 7.6 (d, J = 5.6 Hz, 4H; a, j), 5.7 (d, J = 7.6 Hz, 4H; f)*.

HR-MS (ESI-TOF) *m/z* Calcd. for $[C_{276}H_{120}F_{72}Fe_2N_{36}Zn_3]^{4+}$: 1402.1485; Found: 1402.1524. *m/z* Calcd. for $[C_{276}H_{120}F_{72}Fe_2N_{36}Zn_3](OTf)^{3+}$: 1919.1822; Found: 1919.1874. *m/z* Calcd. for $[C_{276}H_{120}F_{72}Fe_2N_{36}Zn_3](OTf)_2^{2+}$: 2953.7500; Found: 2953.7485.

UV-vis (CH_3CN) λmax (log ε): 690 (5.44), 628 (4.88), 356 (5.15), 285 (5.19).

* See Figure 3.24 for a clearer assignation.

*Preparation of complex [C_{60} ⊂ **75**]*

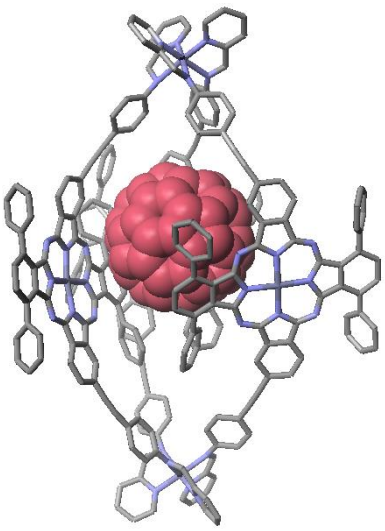

73s (2.0 mg, 1.21 µmol), $Fe(OTf)_2$ (0.3 mg, 0.81 µmol) and 2FP (24 µL of a stock solution 0.1 M in CD_3CN, 2.42 µmol) were dissolved in deuterd MeCN (0.6 mL) in a J-Young nmr tube to yield **75** as in the previous conditions. C_{60} (0.6 mg, 0.8 µmol) was added to the solution and the mixture was sonicated, followed by heating at 70˚C for 16 h. Then, the solution was filtered to remove the unreacted C_{60}.

^{1}H-NMR (400 MHz, CD_3CN), δ (ppm): 9.2 (s, 2H), 8.9 (s, 4H), 8.7 (d, J = 8 Hz, 2H), 8.55 – 8.52 (m 8H), 8.2 (s, 2H), 8.08 – 8.03 (m, 4H), 8.0 (s, 2H), 7.93 – 7.89 (m, 6H), 7.7 (d, J = 8 Hz, 4H), 7.6 (d, J = 4 Hz, 2H), 5.7 (d, J = 8 Hz, 4H).

HR-MS (ESI-TOF) *m/z* Calcd. for $[C_{336}H_{120}F_{72}Fe_2N_{36}Zn_3]^{4+}$: 1582.3989; Found: 1532.4108.

*Preparation of complex [C_{70} ⊂ **75**]*

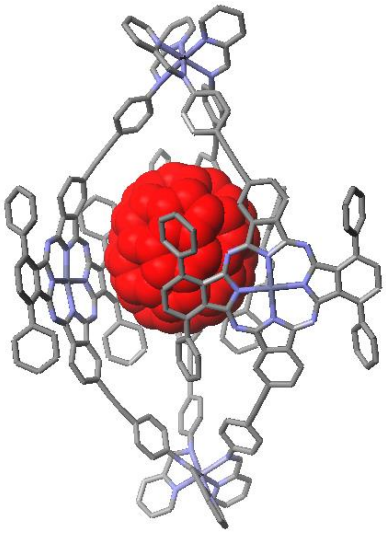

73s (2.0 mg, 1.21 µmol), $Fe(OTf)_2$ (0.3 mg, 0.81 µmol) and 2FP (24 µL of a stock solution 0.1 M in CD_3CN, 2.42 µmol) were dissolved in deuterd MeCN (0.6 mL) in a J-Young nmr tube to yield **75** as in the previous conditions. C_{70} (0.7 mg, 0.8 µmol) was added to the solution and the mixture was sonicated, followed by heating at 70˚C for 16 h. Then, the solution was filtered to remove the unreacted C_{70}.

^{1}H-NMR (400 MHz, CD_3CN), δ (ppm): 9.2 (s, 2H), 8.8 (s, 4H), 8.7 (d, J = 8 Hz, 2H), 8.55 – 8.52 (,m 8H), 8.2 (s, 2H), 8.08 – 8.03 (m, 4H), 8.0 (s, 2H), 7.93 – 7.89 (m, 6H), 7.7 (d, J = 8 Hz, 4H), 7.6 (d, J = 5 Hz, 2H), 5.7 (d, J = 8 Hz, 4H).

HR-MS (ESI-TOF) *m/z* Calcd. for $[C_{346}H_{120}F_{72}Fe_2N_{36}Zn_3]^{4+}$: 1612.1489; Found: 1612.1438.

*N,N'-bis-(3-imidazol-yl-propyl)naphthalene-diimide (**82**)*[135]

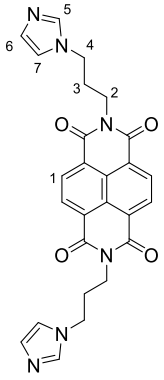

1-(3- aminopropyl) imidazole (4.10 mmol, 0.5 ml) was added to a DMF solution (5 ml) of 1,4,5,8-naphthalenetetracarboxylic dianhydride (1.86 mmol, 500 mg) in a sealed pressure tube. The mixture was stirred at 140 °C for 24 hours. The resulting mixture was allowed to cool down, poured in water/acetone (3/1; 15 mL) mixture, then in cold diethyl ether (400 ml). Vigorous stirring for 30 minutes afforded a dark precipitate. The solid was filtered off in vacuo and thoroughly washed with diethyl ether and small amounts of ethanol. Yield: 588 mg, 1.22 mmol, 65%.

^{1}H-NMR (300 MHz, $CDCl_3$), δ (ppm): 8.76 (s, 4H; H-1), 7.53 (s, 2H; H-5); 6.99 (m, 4H; H-6, H-7), 4.27 (t, *J* = 6.9 Hz, 4H; H-4), 4.11 (t, *J* = 7.8 Hz, 4H; H-2), 2.31 (q, *J* = 7.2 Hz, 4H; H-3).

MS (ESI-TOF): m/z Calcd for $[C_{26}H_{22}N_6O_4]$: 482.2; Found: 482.2.

*tris(4-((E)-3-(1H-imidazol-1-yl)prop-1-en-1-yl)phenyl)amine (**83**)*

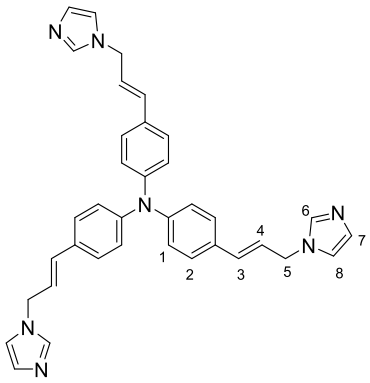

A mixture of tris(4-bromophenyl)amine (0.29 mmol, 140 mg), 1-allylimidazole (0.957 mmol, 0.1 ml), di-cyclohexyl-methylamine (1.74 mmol 0.4 ml), $Pd(OAc)_2$ (0.029 mmol, 6.5 mg) and tri-*tert*-butylphosphine (0.058 mmol, 14 μl) in dioxane (2 ml) was stirred for 30 min at 130°C in the microwave oven. The reaction mixture was extracted with EtOAc/saturated aqueous $NaHCO_3$ solution. The combined organic layers were dried over Na_2SO_4 and evaporated. The crude product was purified by chromatography column using $CHCl_3$/MeOH (from 50:1 to 20:1) as eluent. In this way, the product was obtained as a yellow oil. Yield: 18mg, 0.03 mmol, 11%.

^{1}H-NMR (300 MHz, $CDCl_3$), δ (ppm): 7.59 (s, 3H; H-6), 7.25 (d, *J* = 8.4 Hz, 6H; H-2), 7.11 (s, 3H; H-8), 7.03 (d, *J* = 8.4 Hz, 6H; H-1), 6.97 (s, 3H; H-7), 6.49 (d, *J* = 15.9 Hz, 3H; H-3), 6-24-6.13 (m, 3H; H-4), 4.71 (d, *J* = 6.3 Hz, 6H; H-5).

HR-MS (ESI-TOF) *m/z* Calcd. for [M] $[C_{36}H_{33}N_7]$: 563.2797; Found: 563.2911.

*Preparation of complex [**82** ⊂ **75**]*

73s (2.0 mg, 1.21 µmol), $Fe(OTf)_2$ (0.3 mg, 0.81 µmol) and 2FP (24 µL of a stock solution 0.1 M in CD_3CN, 2.42 µmol) were dissolved in deuterd MeCN (0.6 mL) in a J-Young nmr tube to yield **75** as in the previous conditions. Bis-imidazole NDI derivate **82** (0.32 µmol, 12 ml of a stock solution 26 mM in $CDCl_3$) was added to the solution and the mixture was sonicated. Then, the solution was filtered.

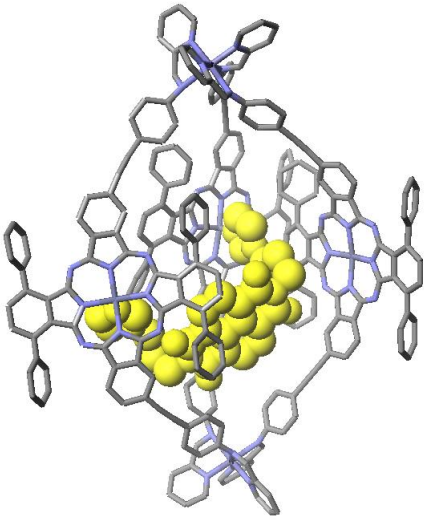

^{1}H-NMR (400 MHz, CD_3CN), δ (ppm): 9.2 (s, 2H), 8.8 (s, 4H), 8.7 (d, J = 8 Hz, 2H), 8.55 – 8.51 (m 10H), 8.2 (s, 2H), 8.08 – 8.03 (m, 4H), 8.0 (s, 2H), 7.94 – 7.89 (m, 8H), 7.7 (d, J = 8 Hz, 4H), 7.6 (d, J = 7 Hz, 2H), 7.5 (br s, 1H), 7.4 (br s 1H), 5.7 (d, J = 8 Hz, 4H), 4.2 (m., 4H), 4,0 (m., 4H), 2,3 (m., 4H).

HR-MS (ESI-TOF) *m/z* Calcd. for $[C_{302}H_{342}F_{72}Fe_2N_{42}O_4Zn_3]^{4+}$: 1522.6912; Found: 1522.6972.

*(S)-2-Aminopropan-1-ol (**76**)*[175]

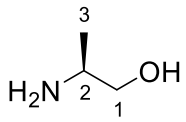

L-Alanine (1.00 g, 11.2 mmol) was added slowly to a THF solution of lithium aluminium hydride (1M, 33.7 mmol, 33.7 ml) cooled at 0°C and under argon. The reaction was heated overnight at reflux and then cooled to 0 °C. Sat. $NaHCO_3$ solution (10 ml) was added dropwise to quench the reaction. The mixture was filtered through celite, followed by removal of solvents under reduced pressure to afford the product as a pale yellow oil (757 mg, 11 mmol, 90%) which was used without further purification.

^{1}H NMR (300 MHz, $CDCl_3$), δ (ppm): 3.56 (dd, J_1 = 7.9 Hz, J_2 = 2.7 Hz, 1H; H-1), 3.24 (dd, J_1 = 7.8 Hz, J_2 = 5.7 Hz, 1H; H-1), 3.10-2.98 (m, 1H; H-2), 1.82 (br s, 3H, NH_2, OH), 1.08 (d, J = 6.4 Hz, 3H; H-3).

MS (EI): m/z Calcd for [M+H] [C_3H_9NO]: 76.1; Found: 76.1.

*(S)-2-(tert-butoxycarbonyl)aminopropan-1-ol (**77**)*[176]

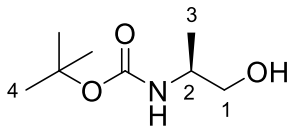

To a solution of (S)-2-aminopropan-1-ol (1.00 g, 13.3 mmol) and triethylamine (2.12 mL, 15.3 mmol) in MeOH (10 mL) at 0 °C, di-tert-butyl dicarbonate (3.2 g, 14.63 mmol) was added. After stirring at room temperature for 20 h, the solvent was evaporated. The residue was diluted with CH_2Cl_2. After washing with water, the organic phase was dried over anhydrous $MgSO_4$ and evaporated to dryness to give the product (1.67 g, 72%), which was used without further purification in the next step.

^{1}H-NMR (300 MHz, $CDCl_3$), δ (ppm): 4.71 (s, 1H; NH), 3.69-3.60 (m, 1H; H-2), 3.57-3.42 (m, 2H; H-1), 2.21 (s, 1H; OH), 1.36 (s, 9H; H-4), 1.12 (d, J = 6.4 Hz, 3H; H-3).

MS (EI): m/z Calcd for [M+H] [$C_8H_{17}NO_3$]: 176.1; Found: 176.1.

*(S)-2-(tert-Butoxycarbonylamino)propyl-4-methylbenzenesulfonate (**78**)*[177]

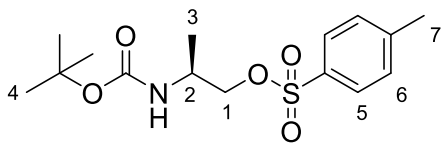

Compound **77** (1.67 g, 9.54 mmol) was dissolved in 20 mL dry CH_2Cl_2 and then it was cooled at 0 °C, followed by addition of NEt3 (2.6 ml, 18.9 mmol) and p-toluene sulfonyl chloride (2.18 g, 11.45 mmol). Then it was stirred for 3 hours at r.t. and diluted with 30 ml water. The aqueous layer was extracted with CH_2Cl_2 (2 × 50 ml) and dried over anhydrous sodium sulphate. The solvent was removed under vacuum and the crude product was then chromatographed over silica gel with the eluent heptane-AcOEt (4 : 1) to afford the title compound as a colourless oil. Yield: 1.75 g, 5.33 mmol, 56%.

^{1}H-NMR (300 MHz, $CDCl_3$), δ (ppm): 8.78 (d, *J* = 8.1 Hz, 2H; H-5), 7.34 (d, *J* = 8.1 Hz, 2H; H-6), 4.55 (br. s, 1H; NH), 3.97-3.92 (m, 1H; H-2), 2.45 (s, 3H; H-7), 1.40 (s, 9H; H-4), 1.15 (d, *J* = 6.6 Hz, 3H; H-3).

MS (EI): m/z Calcd for [M+H] [$C_{15}H_{24}NO_5S$]: 330.1; Found: 330.1.

*1-((S)-2-(tert-Butoxycarbonylamino)propyl)imidazole (**79**)*

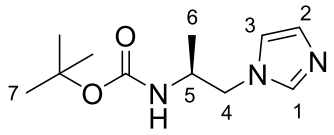

Sodium hydride (60% dispersion in mineral oil, 267 mg, 6.66 mmol) was added to a dry DMF solution (10.5 ml) of imidazole (363 mg, 5.33 mmol) and the mixture was stirred for 1 hour at r.t.. Then compound **78** was added to the solution and the reaction mixture was stirred for 20 hours at r.t.. After that, the crude was diluted with 20 ml water, the aqueous layer was extracted several times with $CHCl_3$ and dried over anhydrous sodium sulphate. The solvent was removed under vacuum to give the desired product (145 mg, 12%), which was used without further purification in the next step.

^{1}H-NMR (300 MHz, $CDCl_3$), δ (ppm): 7.43 (s, 1H; H-1), 7.05 (s, 1H; H-3), 6.90 (s, 1H; H-2), 4.48 (t, *J* = 7.5 Hz, 1H; NH), 4.03-3.91 (m, 3H; H-4, H-5), 1.43 (s, 9H; H-7), 1.10 (d, *J* = 6.9 Hz, 3H; H-6).

HR-MS (ESI-TOF): m/z Calcd for [M+H] [$C_{11}H_{20}N_3O_2$]: 226.1550; Found: 226.1542.

*1-((S)-2-aminopropyl) imidazole (**80**)*

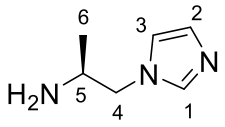

Trifluoroacetic acid (1 ml, 12.8 mmol) was added to a solution of **79** (145 mg, 0.64 mmol) in CH_2Cl_2 (6 ml) and the mixture was stirred for 16 hours at r.t.. After that, the crude was washed several times with a saturated aqueous $NaHCO_3$ solution and the organic phase was dried over anhydrous $MgSO_4$. The solvent was removed under vacuum to give the title compound (55 mg, 69%), which was used without further purification in the next step.

^{1}H-NMR (300 MHz, $CDCl_3$), δ (ppm): 8.23 (s, 1H; H-1), 7.68 (d, *J* = 8.4 Hz 1H; H-3), 7.30 (d, *J* = 8.4 Hz, 1H; H-2), 4.42 (dd, J_1 = 7.2 Hz, J_2 = 6.9 Hz, 2H; H-4), 3.91-3.85 (m, 1H; H5), 2.44 (s, 2H; NH), 1.33 (d, *J* = 7.2 Hz, 3H; H-6).

HR-MS (ESI-TOF): m/z Calcd for [M+H] [$C_6H_{12}N_3$]: 126.1031; Found: 126.1025.

*N,N',N''-Tris((S)-2-(1-imidazolyl)propyl)-1,3,5-benzenetricarboamide (**81**)*

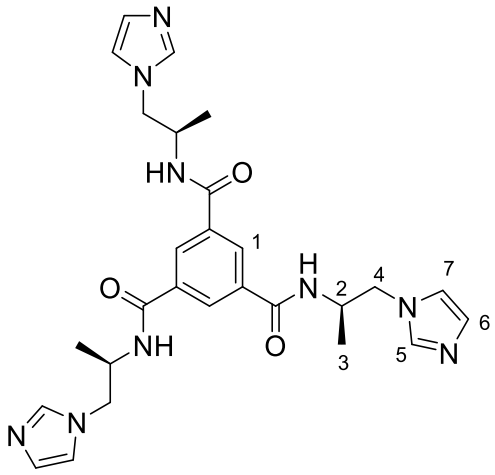

Triethylamine (0.5 mmol, 70 μl) was slowly added into a stirred mixture of **80** (0.44 mmol, 55 mg) and 1,3,5-benzenetricarbonyl trichloride (0.15 mmol, 40 mg) in chloroform (3 ml) at 60 °C, and then the reaction mixture was refluxed for 24 h. After the solution was filtered and concentrated, water was added to the solution, and the product was isolated as a viscous yellow liquid. Yield: 48 mg, 0.09 mmol, 60%.

^{1}H-NMR (300 MHz, $CHCl_3$), δ (ppm): 8.77 (s, 1H; H-1), 7.98 (s, 1H; H-5), 7.77 (s, 1H; NH), 7.65 (d, *J* = 8.4 Hz 1H; H-7), 7.18 (d, *J* = 8.4 Hz, 1H; H-6), 4.40 (m, 2H; H-4), 3.97-3.86 (m, 1H; H2), 1.25 (d, *J* = 7.2 Hz, 3H; H-6).

HR-MS (ESI-TOF): m/z Calcd for [M] [$C_{27}H_{33}N_9O_3$]: 531.2706; Found: 531.2934.

3.6 References

(1) Lehn, J.-M. Supramolecular Chemistry—Scope and Perspectives Molecules, Supermolecules, and Molecular Devices (Nobel Lecture). *Angew. Chemie Int. Ed. English* **1988**, *27* (1), 89–112.

(2) Desiraju, G. R. Chemistry beyond the Molecule. *Nature* **2001**, *412* (6845), 397–400.

(3) Fischer, E. Einfluss Der Configuration Auf Die Wirkung Der Enzyme. *Berichte der Dtsch. Chem. Gesellschaft* **1894**, *27* (3), 2985–2993.

(4) Pedersen, C. J. The Discovery of Crown Ethers (Noble Lecture). *Angew. Chemie Int. Ed. English* **1988**, *27* (8), 1021–1027.

(5) Cram, D. J. The Design of Molecular Hosts, Guests, and Their Complexes (Nobel Lecture). *Angew. Chemie Int. Ed. English* **1988**, *27* (8), 1009–1020.

(6) Bruns, C. J.; Stoddart, J. F. *The Nature of the Mechanical Bond: From Molecules to Machines*; Wiley, 2016.

(7) Stoddart, J. F. The Chemistry of the Mechanical Bond. *Chem. Soc. Rev.* **2009**, *38* (6), 1802–1820.

(8) Nobel Prizes 2016. *Angew. Chemie Int. Ed.* **2016**, *55* (45), 13925.

(9) Busseron, E.; Ruff, Y.; Moulin, E.; Giuseppone, N. Supramolecular Self-Assemblies as Functional Nanomaterials. *Nanoscale* **2013**, *5* (16), 7098–7140.

(10) Seidel, S. R.; Stang, P. J. High-Symmetry Coordination Cages via Self-Assembly. *Acc. Chem. Res.* **2002**, *35*, 972–983.

(11) Albrecht, M. “Let’s Twist Again”Double-Stranded, Triple-Stranded, and Circular Helicates. *Chem. Rev.* **2001**, *101*, 3457–3498.

(12) Baxter, P. N. W.; Khoury, R. G.; Lehn, J.-M.; Baum, G.; Fenske, D. Adaptive Self-Assembly: Environment-Induced Formation and Reversible Switching of Polynuclear Metallocyclophanes. *Chem. – A Eur. J.* **2000**, *6*, 4140–4148.

(13) Smulders, M. M. J.; Riddell, I. A.; Browne, C.; Nitschke, J. R. Building on Architectural Principles for Three-Dimensional Metallosupramolecular Construction. *Chem. Soc. Rev.* **2013**, *42*, 1728–1754.

(14) Beck, J. B.; Rowan, S. J. Multistimuli, Multiresponsive Metallo-Supramolecular Polymers. *J. Am. Chem. Soc.* **2003**, *125*, 13922–13923.

(15) Beves, J. E.; Blight, B. A.; Campbell, C. J.; Leigh, D. A.; McBurney, R. T. Strategies and Tactics for the Metal-Directed Synthesis of Rotaxanes, Knots, Catenanes, and Higher Order Links. *Angew. Chemie Int. Ed.* **2011**, *50*, 9260–9327.

(16) Forgan, R. S.; Sauvage, J.-P.; Stoddart, J. F. Chemical Topology: Complex Molecular Knots, Links, and Entanglements. *Chem. Rev.* **2011**, *111*, 5434–5464.

(17) Danon, J. J.; Krüger, A.; Leigh, D. A.; Lemonnier, J.-F.; Stephens, A. J.; Vitorica-Yrezabal, I. J.; Woltering, S. L. Braiding a Molecular Knot with Eight Crossings. *Science (80-.).* **2017**, *355* (6321), 159–162.

(18) Leigh, D. A.; Lusby, P. J.; McBurney, R. T.; Morelli, A.; Slawin, A. M. Z.; Thomson, A. R.; Walker, D. B. Getting Harder: Cobalt(III)-Template Synthesis of Catenanes and Rotaxanes. *J. Am. Chem. Soc.* **2009**, *131*, 3762–3771.

(19) Chakrabarty, R.; Mukherjee, P. S.; Stang, P. J. Supramolecular Coordination: Self-Assembly of Finite Two- and Three-Dimensional Ensembles. *Chem. Rev.* **2011**, *111*, 6810–6918.
(20) Fujita, M.; Tominaga, M.; Hori, A.; Therrien, B. Coordination Assemblies from a Pd(II)-Cornered Square Complex. *Acc. Chem. Res.* **2005**, *38*, 369–378.
(21) Northrop, B. H.; Chercka, D.; Stang, P. J. Carbon-Rich Supramolecular Metallacycles and Metallacages. *Tetrahedron* **2008**, *64* (50), 11495–11503.
(22) Leininger, S.; Olenyuk, B.; Stang, P. J. Self-Assembly of Discrete Cyclic Nanostructures Mediated by Transition Metals. *Chem. Rev.* **2000**, *100* (3), 853–908.
(23) Meyer, M.; Kersting, B.; Powers, R. E.; Raymond, K. N. Rearrangement Reactions in Dinuclear Triple Helicates1. *Inorg. Chem.* **1997**, *36* (23), 5179–5191.
(24) L. Caulder, D.; N. Raymond, K. The Rational Design of High Symmetry Coordination Clusters. *J. Chem. Soc., Dalt. Trans.* **1999**, 1185–1200.
(25) Caulder, D. L.; Raymond, K. N. Supermolecules by Design. *Acc. Chem. Res.* **1999**, *32*, 975–982.
(26) Caulder, D. L.; Brückner, C.; Powers, R. E.; König, S.; Parac, T. N.; Leary, J. A.; Raymond, K. N. Design, Formation and Properties of Tetrahedral M4L4 and M4L6 Supramolecular Clusters1. *J. Am. Chem. Soc.* **2001**, *123* (37), 8923–8938.
(27) Albrecht, M. From Molecular Diversity to Template-Directed Self-Assembly – New Trends in Metallo-Supramolecular Chemistry. *J. Incl. Phenom. Macrocycl. Chem.* **2000**, *36* (2), 127–151.
(28) Holliday, B. J.; Mirkin, C. A. Strategies for the Construction of Supramolecular Compounds through Coordination Chemistry. *Angew. Chemie Int. Ed.* **2001**, *40* (11), 2022–2043.
(29) Hosseini, M. W. Molecular Tectonics: From Simple Tectons to Complex Molecular Networks. *Acc. Chem. Res.* **2005**, *38* (4), 313–323.
(30) Belowich, M. E.; Stoddart, J. F. Dynamic Imine Chemistry. *Chem. Soc. Rev.* **2012**, *41* (6), 2003–2024.
(31) Meyer, C. D.; Joiner, C. S.; Stoddart, J. F. Template-Directed Synthesis Employing Reversible Imine Bond Formation. *Chem. Soc. Rev.* **2007**, *36* (11), 1705–1723.
(32) Nitschke, J. R. Construction, Substitution, and Sorting of Metallo-Organic Structures via Subcomponent Self-Assembly. *Acc. Chem. Res.* **2007**, *40* (2), 103–112.
(33) Melson, G. A.; Busch, D. H. Reactions of Coordinated Ligands. X. The Formation and Properties of a Tetradentate Macrocyclic Ligand by the Self-Condensation of O-Aminobenzaldehyde in the Presence of Metal Ions. *J. Am. Chem. Soc.* **1964**, *86*, 4834–4837.
(34) Schafer, L. L.; Nitschke, J. R.; Mao, S. S. H.; Liu, F.-Q.; Harder, G.; Haufe, M.; Tilley, T. D. Zirconocene-Mediated, High-Yielding Macrocyclizations of Silyl-Terminated Diynes. *Chem. – A Eur. J.* **2002**, *8* (1), 74–83.
(35) Malthus, S. J.; Wilson, R. K.; Vikas Aggarwal, A.; Cameron, S. A.; Larsen, D. S.; Brooker, S. Carbazole-Based N4-Donor Schiff Base Macrocycles:

Obtained Metal Free and as Cu(ii) and Ni(ii) Complexes. *Dalt. Trans.* **2017**, *46* (10), 3141–3149.
(36) Houjou, H.; Iwasaki, A.; Ogihara, T.; Kanesato, M.; Akabori, S.; Hiratani, K. The Architecture of Dinuclear Ni and Cu Complexes: Twisted and Parallel Forms Controlled by the Self-Assembly of Schiff Base Ligands. *New J. Chem.* **2003**, *27* (5), 886–889.
(37) Nitschke, J. R.; Schultz, D.; Bernardinelli, G.; Gérard, D. Selection Rules for Helicate Ligand Component Self-Assembly: Steric, pH, Charge, and Solvent Effects. *J. Am. Chem. Soc.* **2004**, *126* (50), 16538–16543.
(38) Xue, M.; Yang, Y.; Chi, X.; Yan, X.; Huang, F. Development of Pseudorotaxanes and Rotaxanes: From Synthesis to Stimuli-Responsive Motions to Applications. *Chem. Rev.* **2015**, *115* (15), 7398–7501.
(39) Han, X.; Liu, G.; Liu, S. H.; Yin, J. Synthesis of Rotaxanes and Catenanes Using an Imine Clipping Reaction. *Org. Biomol. Chem.* **2016**, *14* (44), 10331–10351.
(40) Gil-Ramírez, G.; Leigh, D. A.; Stephens, A. J. Catenanes: Fifty Years of Molecular Links. *Angew. Chemie Int. Ed.* **2015**, *54* (21), 6110–6150.
(41) Nitschke, J. R.; Lehn, J.-M. Self-Organization by Selection: Generation of a Metallosupramolecular Grid Architecture by Selection of Components in a Dynamic Library of Ligands. *Proc. Natl. Acad. Sci.* **2003**, *100* (21), 11970–11974.
(42) Hardy, J. G. Metallosupramolecular Grid Complexes: Towards Nanostructured Materials with High-Tech Applications. *Chem. Soc. Rev.* **2013**, *42* (19), 7881–7899.
(43) Percec, V.; Glodde, M.; Bera, T. K.; Miura, Y.; Shiyanovskaya, I.; Singer, K. D.; Balagurusamy, V. S. K.; Heiney, P. A.; Schnell, I.; Rapp, A.; et al. Self-Organization of Supramolecular Helical Dendrimers into Complex Electronic Materials. *Nature* **2002**, *417* (6905), 384–387.
(44) Nitschke, J. R. Mutual Stabilization between Imine Ligands and Copper(i) Ions in Aqueous Solution. *Angew. Chemie Int. Ed.* **2004**, *43*, 3073–3075.
(45) Zarra, S.; Wood, D. M.; Roberts, D. A.; Nitschke, J. R. Molecular Containers in Complex Chemical Systems. *Chem. Soc. Rev.* **2015**, *44*, 419–432.
(46) Lehn, J.-M. Perspectives in Supramolecular Chemistry—From Molecular Recognition towards Molecular Information Processing and Self-Organization. *Angew. Chemie Int. Ed. English* **1990**, *29* (11), 1304–1319.
(47) Huang, F.; Anslyn, E. V. Introduction: Supramolecular Chemistry. *Chem. Rev.* **2015**, *115* (15), 6999–7000.
(48) Lehn, J.-M. Supramolecular Chemistry: Where from? Where To? *Chem. Soc. Rev.* **2017**, *46* (9), 2378–2379.
(49) Therrien, B. Drug Delivery by Water-Soluble Organometallic Cages. In *Chemistry of Nanocontainers*; Albrecht, M., Hahn, E., Eds.; Springer Berlin Heidelberg: Berlin, Heidelberg, 2012; pp 35–55.
(50) Cook, T. R.; Vajpayee, V.; Lee, M. H.; Stang, P. J.; Chi, K.-W. Biomedical and Biochemical Applications of Self-Assembled Metallacycles and Metallacages. *Acc. Chem. Res.* **2013**, *46* (11), 2464–2474.
(51) Zheng, Y.-R.; Suntharalingam, K.; Johnstone, T. C.; Lippard, S. J. Encapsulation of Pt(iv) Prodrugs within a Pt(ii) Cage for Drug Delivery.

Chem. Sci. **2015**, *6* (2), 1189–1193.
(52) Rodríguez, J.; Mosquera, J.; Couceiro, J. R.; Nitschke, J. R.; Vázquez, M. E.; Mascareñas, J. L. Anion Recognition as a Supramolecular Switch of Cell Internalization. *J. Am. Chem. Soc.* **2017**, *139* (1), 55–58.
(53) Mosquera, J.; Zarra, S.; Nitschke, J. R. Aqueous Anion Receptors through Reduction of Subcomponent Self-Assembled Structures. *Angew. Chemie Int. Ed.* **2014**, *53* (6), 1556–1559.
(54) Grishagin, I. V; Pollock, J. B.; Kushal, S.; Cook, T. R.; Stang, P. J.; Olenyuk, B. Z. In Vivo Anticancer Activity of Rhomboidal Pt(II) Metallacycles. *Proc. Natl. Acad. Sci.* **2014**, *111* (52), 18448–18453.
(55) Ahmad, N.; Younus, H. A.; Chughtai, A. H.; Verpoort, F. Metal-Organic Molecular Cages: Applications of Biochemical Implications. *Chem. Soc. Rev.* **2015**, *44* (1), 9–25.
(56) Saha, M. L.; Yan, X.; Stang, P. J. Photophysical Properties of Organoplatinum(II) Compounds and Derived Self-Assembled Metallacycles and Metallacages: Fluorescence and Its Applications. *Acc. Chem. Res.* **2016**, *49* (11), 2527–2539.
(57) Wang, M.; Vajpayee, V.; Shanmugaraju, S.; Zheng, Y.-R.; Zhao, Z.; Kim, H.; Mukherjee, P. S.; Chi, K.-W.; Stang, P. J. Coordination-Driven Self-Assembly of M3L2 Trigonal Cages from Preorganized Metalloligands Incorporating Octahedral Metal Centers and Fluorescent Detection of Nitroaromatics. *Inorg. Chem.* **2011**, *50* (4), 1506–1512.
(58) Wang, J.; He, C.; Wu, P.; Wang, J.; Duan, C. An Amide-Containing Metal–Organic Tetrahedron Responding to a Spin-Trapping Reaction in a Fluorescent Enhancement Manner for Biological Imaging of NO in Living Cells. *J. Am. Chem. Soc.* **2011**, *133* (32), 12402–12405.
(59) Gangemi, C. M. A.; Pappalardo, A.; Trusso Sfrazzetto, G. Applications of Supramolecular Capsules Derived from resorcin[4]arenes{,} Calix[n]arenes and Metallo-Ligands: From Biology to Catalysis. *RSC Adv.* **2015**, *5* (64), 51919–51933.
(60) Ramamurthy, V.; Sivaguru, J. Supramolecular Photochemistry as a Potential Synthetic Tool: Photocycloaddition. *Chem. Rev.* **2016**, *116* (17), 9914–9993.
(61) Ueda, Y.; Ito, H.; Fujita, D.; Fujita, M. Permeable Self-Assembled Molecular Containers for Catalyst Isolation Enabling Two-Step Cascade Reactions. *J. Am. Chem. Soc.* **2017**, *139* (17), 6090–6093.
(62) Dong, V. M.; Fiedler, D.; Carl, B.; Bergman, R. G.; Raymond, K. N. Molecular Recognition and Stabilization of Iminium Ions in Water. *J. Am. Chem. Soc.* **2006**, *128* (45), 14464–14465.
(63) Yamashina, M.; Sei, Y.; Akita, M.; Yoshizawa, M. Safe Storage of Radical Initiators within a Polyaromatic Nanocapsule. *Nat. Commun.* **2014**, *5*, 4662.
(64) Mal, P.; Breiner, B.; Rissanen, K.; Nitschke, J. R. White Phosphorus Is Air-Stable Within a Self-Assembled Tetrahedral Capsule. *Science (80-.).* **2009**, *324*, 1697–1699.
(65) Furusawa, T.; Kawano, M.; Fujita, M. The Confined Cavity of a Coordination Cage Suppresses the Photocleavage of α-Diketones To Give Cyclization Products through Kinetically Unfavorable Pathways.

Angew. Chemie Int. Ed. **2007**, *46* (30), 5717–5719.
(66) Riddell, I. A.; Smulders, M. M. J.; Clegg, J. K.; Nitschke, J. R. Encapsulation, Storage and Controlled Release of Sulfur Hexafluoride from a Metal-Organic Capsule. *Chem. Commun.* **2011**, *47*, 457–459.
(67) Mai, H. D.; Kang, P.; Kim, J. K.; Yoo, H. A Cobalt Supramolecular Triple-Stranded Helicate-Based Discrete Molecular Cage. *Sci. Rep.* **2017**, *7*, 43448.
(68) Kroto, H. W.; Heath, J. R.; O'Brien, S. C.; Curl, R. F.; Smalley, R. E. C60: Buckminsterfullerene. *Nature* **1985**, *318*, 162–163.
(69) Biju, V. Chemical Modifications and Bioconjugate Reactions of Nanomaterials for Sensing{,} Imaging{,} Drug Delivery and Therapy. *Chem. Soc. Rev.* **2014**, *43* (3), 744–764.
(70) Prato, M. [60]Fullerene Chemistry for Materials Science Applications. *J. Mater. Chem.* **1997**, *7*, 1097–1109.
(71) Popov, A. A.; Yang, S.; Dunsch, L. Endohedral Fullerenes. *Chem. Rev.* **2013**, *113* (8), 5989–6113.
(72) Zhang, R.; Murata, M.; Aharen, T.; Wakamiya, A.; Shimoaka, T.; Hasegawa, T.; Murata, Y. Synthesis of a Distinct Water Dimer inside Fullerene C70. *Nat Chem* **2016**, *8* (5), 435–441.
(73) Dennler, G.; Scharber, M. C.; Brabec, C. J. Polymer-Fullerene Bulk-Heterojunction Solar Cells. *Adv. Mater.* **2009**, *21*, 1323–1338.
(74) Komatsu, N.; Ohe, T.; Matsushige, K. A Highly Improved Method for Purification of Fullerenes Applicable to Large-Scale Production. *Carbon N. Y.* **2004**, *42* (1), 163–167.
(75) Hirsch, A.; Brettreich, M. Parent Fullerenes. In *Fullerenes*; Wiley-VCH Verlag GmbH & Co. KGaA, 2005; pp 1–48.
(76) Canevet, D.; Pérez, E. M.; Martín, N. Wraparound Hosts for Fullerenes: Tailored Macrocycles and Cages. *Angew. Chemie Int. Ed.* **2011**, *50*, 9248–9259.
(77) Yu, C.; Jin, Y.; Zhang, W. Shape-Persistent Arylene Ethynylene Organic Hosts for Fullerenes. *Chem. Rec.* **2015**, *15* (1), 97–106.
(78) Garcia-Simon, C.; Costas, M.; Ribas, X. Metallosupramolecular Receptors for Fullerene Binding and Release. *Chem. Soc. Rev.* **2016**, *45*, 40–62.
(79) Mahata, K.; Frischmann, P. D.; Würthner, F. Giant Electroactive M4L6 Tetrahedral Host Self-Assembled with Fe(II) Vertices and Perylene Bisimide Dye Edges. *J. Am. Chem. Soc.* **2013**, *135*, 15656–15661.
(80) Brenner, W.; Ronson, T. K.; Nitschke, J. R. Separation and Selective Formation of Fullerene Adducts within an MII8L6 Cage. *J. Am. Chem. Soc.* **2017**, *139* (1), 75–78.
(81) Howson, S. E.; Bolhuis, A.; Brabec, V.; Clarkson, G. J.; Malina, J.; Rodger, A.; Scott, P. Optically Pure, Water-Stable Metallo-Helical "flexicate" Assemblies with Antibiotic Activity. *Nat Chem* **2012**, *4* (1), 31–36.
(82) Holloway, L. R.; McGarraugh, H. H.; Young, M. C.; Sontising, W.; Beran, G. J. O.; Hooley, R. J. Structural Switching in Self-Assembled Metal-Ligand Helicate Complexes via Ligand-Centered Reactions. *Chem. Sci.* **2016**, *7* (7), 4423–4427.
(83) Ronson, T. K.; League, A. B.; Gagliardi, L.; Cramer, C. J.; Nitschke, J. R. Pyrene-Edged FeII4L6 Cages Adaptively Reconfigure During Guest

Binding. *J. Am. Chem. Soc.* **2014**, *136*, 15615–15624.
(84) Wood, D. M.; Meng, W.; Ronson, T. K.; Stefankiewicz, A. R.; Sanders, J. K. M.; Nitschke, J. R. Guest-Induced Transformation of a Porphyrin-Edged FeII4L6 Capsule into a CuIFeII2L4 Fullerene Receptor. *Angew. Chemie Int. Ed.* **2015**, *54*, 3988–3992.
(85) Rizzuto, F. J.; Wood, D. M.; Ronson, T. K.; Nitschke, J. R. Tuning the Redox Properties of Fullerene Clusters within a Metal–Organic Capsule. *J. Am. Chem. Soc.* **2017**, *139* (32), 11008–11011.
(86) Claessens, C. G.; Torres, T. Inclusion of C60 Fullerene in a M3L2 Subphthalocyanine Cage. *Chem. Commun.* **2004**, No. 11, 1298–1299.
(87) Sánchez-Molina, I.; Grimm, B.; Krick Calderon, R. M.; Claessens, C. G.; Guldi, D. M.; Torres, T. Self-Assembly, Host–Guest Chemistry, and Photophysical Properties of Subphthalocyanine-Based Metallosupramolecular Capsules. *J. Am. Chem. Soc.* **2013**, *135* (28), 10503–10511.
(88) Bottari, G.; de la Torre, G.; Guldi, D. M.; Torres, T. Covalent and Noncovalent Phthalocyanine−Carbon Nanostructure Systems: Synthesis, Photoinduced Electron Transfer, and Application to Molecular Photovoltaics. *Chem. Rev.* **2010**, *110*, 6768–6816.
(89) Bottari, G.; Trukhina, O.; Ince, M.; Torres, T. Towards Artificial Photosynthesis: Supramolecular, Donor–acceptor, Porphyrin- and Phthalocyanine/carbon Nanostructure Ensembles. *Coord. Chem. Rev.* **2012**, *256*, 2453–2477.
(90) de la Torre, G.; Bottari, G.; Torres, T. Phthalocyanines and Subphthalocyanines: Perfect Partners for Fullerenes and Carbon Nanotubes in Molecular Photovoltaics. *Adv. Energy Mater.* **2016**, 1601700.
(91) Ray, A.; Chattopadhyay, S.; Bhattacharya, S. Photophysical and Theoretical Insights on Non-Covalently Linked Fullerene–zinc Phthalocyanine Complexes. *Spectrochim. Acta Part A Mol. Biomol. Spectrosc.* **2011**, *79*, 1435–1442.
(92) Ray, A.; Santhosh, K.; Chattopadhyay, S.; Samanta, A.; Bhattacharya, S. Spectroscopic and Theoretical Investigations on Effective and Selective Interaction of Fullerenes C60 and C70 with a Derivatized Zn−phthalocyanine: Stabilization of Charge-Recombined State by Side-On Approach of C70. *J. Phys. Chem. A* **2010**, *114*, 5544–5550.
(93) Nefedova, I. V; Martynov, A. G.; Averin, A. A.; Kirakosyan, G. A.; Tsivadze, A. Y.; Gorbunova, Y. G. New Octopus-like Phthalocyanines as Fullerene Receptors: Synthesis and Photophysical Investigation. *Isr. J. Chem.* **2016**, *56*, 181–187.
(94) Jansze, S. M.; Cecot, G.; Wise, M. D.; Zhurov, K. O.; Ronson, T. K.; Castilla, A. M.; Finelli, A.; Pattison, P.; Solari, E.; Scopelliti, R.; et al. Ligand Aspect Ratio as a Decisive Factor for the Self-Assembly of Coordination Cages. *J. Am. Chem. Soc.* **2016**, *138* (6), 2046–2054.
(95) Han, M.; Engelhard, D. M.; Clever, G. H. Self-Assembled Coordination Cages Based on Banana-Shaped Ligands. *Chem. Soc. Rev.* **2014**, *43* (6), 1848–1860.
(96) Young, M. C.; Johnson, A. M.; Hooley, R. J. Self-Promoted Post-Synthetic

Modification of Metal-Ligand M2L3 Mesocates. *Chem. Commun.* **2014**, *50* (11), 1378–1380.
(97) Meng, W.; Ronson, T. K.; Nitschke, J. R. Symmetry Breaking in Self-Assembled M4L6 Cage Complexes. *Proc. Natl. Acad. Sci.* **2013**, *110* (26), 10531–10535.
(98) Castilla, A. M.; Ramsay, W. J.; Nitschke, J. R. Stereochemistry in Subcomponent Self-Assembly. *Acc. Chem. Res.* **2014**, *47* (7), 2063–2073.
(99) Chen, L.-J.; Yang, H.-B.; Shionoya, M. Chiral Metallosupramolecular Architectures. *Chem. Soc. Rev.* **2017**, *46* (9), 2555–2576.
(100) Durmus, M.; Yesilot, S.; Ahsen, V. Separation and Mesogenic Properties of Tetraalkoxy-Substituted Phthalocyanine Isomers. *New J. Chem.* **2006**, *30* (5), 675–678.
(101) Görlach, B.; Dachtler, M.; Glaser, T.; Albert, K.; Hanack, M. Synthesis and Separation of Structural Isomers of 2(3),9(10),16(17),23(24)-Tetrasubstituted Phthalocyanines. *Chem. – A Eur. J.* **2001**, *7* (11), 2459–2465.
(102) Kukula, H.; Veit, S.; Godt, A. Synthesis of Monodisperse Oligo(para-Phenyleneethynylene)s Using Orthogonal Protecting Groups with Different Polarity for Terminal Acetylene Units. *European J. Org. Chem.* **1999**, *1999* (1), 277–286.
(103) Wuts, P. G. M.; Greene, T. W. Protection for the Alkyne □CH. In *Greene's Protective Groups in Organic Synthesis*; John Wiley & Sons, Inc., 2006; pp 927–933.
(104) Piguet, C.; Bernardinelli, G.; Hopfgartner, G. Helicates as Versatile Supramolecular Complexes. *Chem. Rev.* **1997**, *97* (6), 2005–2062.
(105) Knof, U.; von Zelewsky, A. Predetermined Chirality at Metal Centers. *Angew. Chemie Int. Ed.* **1999**, *38* (3), 302–322.
(106) Cui, F.; Li, S.; Jia, C.; Mathieson, J. S.; Cronin, L.; Yang, X.-J.; Wu, B. Anion-Dependent Formation of Helicates versus Mesocates of Triple-Stranded M2L3 (M = Fe2+, Cu2+) Complexes. *Inorg. Chem.* **2012**, *51* (1), 179–187.
(107) Albrecht, M.; Kotila, S. Counter-Ion Induced Self-Assembly of a Meso-Helicate Type Molecular Box. *Chem. Commun.* **1996**, No. 20, 2309–2310.
(108) Lai, S.-W.; Chan, M. C.-W.; Peng, S.-M.; Che, C.-M. Self-Assembly of Predesigned Trimetallic Macrocycles Based on Benzimidazole as Nonlinear Bridging Motifs: Crystal Structure of a Luminescent Platinum(II) Cyclic Trimer. *Angew. Chemie Int. Ed.* **1999**, *38* (5), 669–671.
(109) Albrecht, M.; Blau, O.; Fröhlich, R. "Size-Selectivity" in the Template-Directed Assembly of Dinuclear Triple-Stranded Helicates. *Proc. Natl. Acad. Sci.* **2002**, *99* (8), 4867–4872.
(110) Albrecht, M.; Kotila, S. Formation of A"meso-Helicate" by Self-Assembly of Three Bis(catecholate) Ligands and Two Titanium(IV) Ions. *Angew. Chemie Int. Ed. English* **1995**, *34* (19), 2134–2137.
(111) Einstein, A. Eine Neue Bestimmung Der Moleküldimensionen. *Ann. Phys.* **1906**, *324* (2), 289–306.
(112) Edward, J. T. Molecular Volumes and the Stokes-Einstein Equation. *J. Chem. Educ.* **1970**, *47* (4), 261.

(113) Wang, M.; Wang, K.; Wang, C.; Huang, M.; Hao, X.-Q.; Shen, M.-Z.; Shi, G.-Q.; Zhang, Z.; Song, B.; Cisneros, A.; et al. Self-Assembly of Concentric Hexagons and Hierarchical Self-Assembly of Supramolecular Metal–Organic Nanoribbons at the Solid/Liquid Interface. *J. Am. Chem. Soc.* **2016**, *138* (29), 9258–9268.
(114) Burke, M. J.; Nichol, G. S.; Lusby, P. J. Orthogonal Selection and Fixing of Coordination Self-Assembly Pathways for Robust Metallo-Organic Ensemble Construction. *J. Am. Chem. Soc.* **2016**, *138* (29), 9308–9315.
(115) Perrin, Francis. Mouvement Brownien D'un Ellipsoide (II). Rotation Libre et Dépolarisation Des Fluorescences. Translation et Diffusion de Molécules Ellipsoidales. *J. Phys. Radium* **1936**, *7* (1), 1–11.
(116) Elworthy, P. H. A Test of Perrin's Relationships for Small Molecules. *J. Chem. Soc.* **1962**, No. 0, 3718–3723.
(117) Tirado, M. M.; López Martínez, C.; de la Torre, J. G. Comparison of Theories for the Translational and Rotational Diffusion Coefficients of Rod-like Macromolecules. Application to Short DNA Fragments. *J. Chem. Phys.* **1984**, *81* (4), 2047–2052.
(118) Allouche, L.; Marquis, A.; Lehn, J.-M. Discrimination of Metallosupramolecular Architectures in Solution by Using Diffusion Ordered Spectroscopy (DOSY) Experiments: Double-Stranded Helicates of Different Lengths. *Chem. – A Eur. J.* **2006**, *12* (28), 7520–7525.
(119) Avram, L.; Cohen, Y. Diffusion NMR of Molecular Cages and Capsules. *Chem. Soc. Rev.* **2015**, *44* (2), 586–602.
(120) Cohen, Y.; Avram, L.; Frish, L. Diffusion NMR Spectroscopy in Supramolecular and Combinatorial Chemistry: An Old Parameter—New Insights. *Angew. Chemie Int. Ed.* **2005**, *44* (4), 520–554.
(121) Montoro-García, C.; Camacho-García, J.; López-Pérez, A. M.; Bilbao, N.; Romero-Pérez, S.; Mayoral, M. J.; González-Rodríguez, D. High-Fidelity Noncovalent Synthesis of Hydrogen-Bonded Macrocyclic Assemblies. *Angew. Chemie Int. Ed.* **2015**, *54* (23), 6780–6784.
(122) Timmerman, P.; Weidmann, J.-L.; Jolliffe, K. A.; Prins, L. J.; Reinhoudt, D. N.; Shinkai, S.; Frish, L.; Cohen, Y. NMR Diffusion Spectroscopy for the Characterization of Multicomponent Hydrogen-Bonded Assemblies in Solution. *J. Chem. Soc.{,} Perkin Trans. 2* **2000**, No. 10, 2077–2089.
(123) Version FJ 2.8 (EU 3.2.2).
(124) Riddell, I. A.; Hristova, Y. R.; Clegg, J. K.; Wood, C. S.; Breiner, B.; Nitschke, J. R. Five Discrete Multinuclear Metal-Organic Assemblies from One Ligand: Deciphering the Effects of Different Templates. *J. Am. Chem. Soc.* **2013**, *135* (7), 2723–2733.
(125) Stephenson, A.; Argent, S. P.; Riis-Johannessen, T.; Tidmarsh, I. S.; Ward, M. D. Structures and Dynamic Behavior of Large Polyhedral Coordination Cages: An Unusual Cage-to-Cage Interconversion. *J. Am. Chem. Soc.* **2011**, *133* (4), 858–870.
(126) Ferrer, M.; Pedrosa, A.; Rodríguez, L.; Rossell, O.; Vilaseca, M. New Insights into the Factors That Govern the Square/Triangle Equilibria of Pd(II) and Pt(II) Supramolecules. Unexpected Participation of a Mononuclear Species in the Equilibrium. *Inorg. Chem.* **2010**, *49* (20), 9438–9449.

(127) Lehn, J.-M. From Supramolecular Chemistry towards Constitutional Dynamic Chemistry and Adaptive Chemistry. *Chem. Soc. Rev.* **2007**, *36* (2), 151–160.
(128) Barboiu, M. *Constitutional Dynamic Chemistry*; Topics in Current Chemistry; Springer Berlin Heidelberg, 2012.
(129) Riddell, I. A.; Smulders, M. M. J.; Clegg, J. K.; Hristova, Y. R.; Breiner, B.; Thoburn, J. D.; Nitschke, J. R. Anion-Induced Reconstitution of a Self-Assembling System to Express a Chloride-Binding Co10L15 Pentagonal Prism. *Nat Chem* **2012**, *4*, 751–756.
(130) Rancan, M.; Dolmella, A.; Seraglia, R.; Orlandi, S.; Quici, S.; Armelao, L. A Templating Guest Sorts out a Molecular Triangle from a Dimer-Trimer Constitutional Dynamic Library. *Chem. Commun.* **2012**, *48* (25), 3115–3117.
(131) Rancan, M.; Tessarolo, J.; Zanonato, P. L.; Seraglia, R.; Quici, S.; Armelao, L. Self-Assembly of a Constitutional Dynamic Library of Cu(ii) Coordination Polygons and Reversible Sorting by Crystallization. *Dalt. Trans.* **2013**, *42* (21), 7534–7538.
(132) Kubota, R.; Tashiro, S.; Shionoya, M. Chiral Metal-Macrocycle Frameworks: Supramolecular Chirality Induction and Helicity Inversion of the Helical Macrocyclic Structures. *Chem. Sci.* **2016**, *7* (3), 2217–2221.
(133) Katoono, R.; Tanaka, Y.; Kusaka, K.; Fujiwara, K.; Suzuki, T. Dynamic Figure Eight Chirality: Multifarious Inversions of a Helical Preference Induced by Complexation. *J. Org. Chem.* **2015**, *80* (15), 7613–7625.
(134) Tansil, N. C.; Xie, H.; Xie, F.; Gao, Z. Direct Detection of DNA with an Electrocatalytic Threading Intercalator. *Anal. Chem.* **2005**, *77* (1), 126–134.
(135) Billeci, F.; D'Anna, F.; Marullo, S.; Noto, R. Self-Assembly of Fluorescent Diimidazolium Salts: Tailor Properties of the Aggregates Changing Alkyl Chain Features. *RSC Adv.* **2016**, *6* (64), 59502–59512.
(136) Rizzuto, F. J.; Wu, W.-Y.; Ronson, T. K.; Nitschke, J. R. Peripheral Templation Generates an MII6L4 Guest-Binding Capsule. *Angew. Chemie Int. Ed.* **2016**, *55* (28), 7958–7962.
(137) Gütlich, P.; Goodwin, H. A. *Spin Crossover in Transition Metal Compounds I*; Spin Crossover in Transition Metal Compounds; Springer, 2004.
(138) Sato, O.; Tao, J.; Zhang, Y.-Z. Control of Magnetic Properties through External Stimuli. *Angew. Chemie Int. Ed.* **2007**, *46* (13), 2152–2187.
(139) Real, J. A.; Gaspar, A. B.; Munoz, M. C. Thermal, Pressure and Light Switchable Spin-Crossover Materials. *Dalt. Trans.* **2005**, No. 12, 2062–2079.
(140) Fisher, D. C.; Drickamer, H. G. Effect of Pressure on the Spin State of Iron in Ferrous Phenanthroline Compounds. *J. Chem. Phys.* **1971**, *54* (11), 4825–4837.
(141) Wentzcovitch, R. M.; Justo, J. F.; Wu, Z.; da Silva, C. R. S.; Yuen, D. A.; Kohlstedt, D. Anomalous Compressibility of Ferropericlase throughout the Iron Spin Cross-Over. *Proc. Natl. Acad. Sci.* **2009**, *106* (21), 8447–8452.
(142) McGravey, J. J.; Lawthers, I. Photochemically-Induced Perturbation of the 1A [Right Left harpoons]5T Equilibrium in Fe11 Complexes by Pulsed

Laser Irradiation in the Metal-to-Ligand Charge-Transfer Absorption Band. *J. Chem. Soc.{,} Chem. Commun.* **1982**, No. 16, 906–907.
(143) Qi, Y.; Müller, E. W.; Spiering, H.; Gütlich, P. The Effect of a Magnetic Field on the High-Spin α Low-Spin Transition in [Fe(phen)2(NCS)2]. *Chem. Phys. Lett.* **1983**, *101* (4), 503–505.
(144) Halcrow, M. A. *Spin-Crossover Materials: Properties and Applications*; Wiley, 2013.
(145) Bousseksou, A.; Molnar, G.; Salmon, L.; Nicolazzi, W. Molecular Spin Crossover Phenomenon: Recent Achievements and Prospects. *Chem. Soc. Rev.* **2011**, *40* (6), 3313–3335.
(146) Bao, X.; Shepherd, H. J.; Salmon, L.; Molnár, G.; Tong, M.-L.; Bousseksou, A. The Effect of an Active Guest on the Spin Crossover Phenomenon. *Angew. Chemie Int. Ed.* **2013**, *52* (4), 1198–1202.
(147) Sciortino, N. F.; Scherl-Gruenwald, K. R.; Chastanet, G.; Halder, G. J.; Chapman, K. W.; Létard, J.-F.; Kepert, C. J. Hysteretic Three-Step Spin Crossover in a Thermo- and Photochromic 3D Pillared Hofmann-Type Metal–Organic Framework. *Angew. Chemie Int. Ed.* **2012**, *51* (40), 10154–10158.
(148) Kahn, O.; Martinez, C. J. Spin-Transition Polymers: From Molecular Materials Toward Memory Devices. *Science (80-.).* **1998**, *279* (5347), 44–48.
(149) Roubeau, O. Triazole-Based One-Dimensional Spin-Crossover Coordination Polymers. *Chem. – A Eur. J.* **2012**, *18* (48), 15230–15244.
(150) Ono, K.; Yoshizawa, M.; Akita, M.; Kato, T.; Tsunobuchi, Y.; Ohkoshi, S.; Fujita, M. Spin Crossover by Encapsulation. *J. Am. Chem. Soc.* **2009**, *131* (8), 2782–2783.
(151) Bilbeisi, R. A.; Zarra, S.; Feltham, H. L. C.; Jameson, G. N. L.; Clegg, J. K.; Brooker, S.; Nitschke, J. R. Guest Binding Subtly Influences Spin Crossover in an FeII4L4 Capsule. *Chem. – A Eur. J.* **2013**, *19* (25), 8058–8062.
(152) McConnell, A. J.; Aitchison, C. M.; Grommet, A. B.; Nitschke, J. R. Subcomponent Exchange Transforms an FeII4L4 Cage from High- to Low-Spin, Switching Guest Release in a Two-Cage System. *J. Am. Chem. Soc.* **2017**, *139* (18), 6294–6297.
(153) Struch, N.; Bannwarth, C.; Ronson, T. K.; Lorenz, Y.; Mienert, B.; Wagner, N.; Engeser, M.; Bill, E.; Puttreddy, R.; Rissanen, K.; et al. An Octanuclear Metallosupramolecular Cage Designed To Exhibit Spin-Crossover Behavior. *Angew. Chemie Int. Ed.* **2017**, *56* (18), 4930–4935.
(154) Isley III, W. C.; Zarra, S.; Carlson, R. K.; Bilbeisi, R. A.; Ronson, T. K.; Nitschke, J. R.; Gagliardi, L.; Cramer, C. J. Predicting Paramagnetic 1H NMR Chemical Shifts and State-Energy Separations in Spin-Crossover Host-Guest Systems. *Phys. Chem. Chem. Phys.* **2014**, *16* (22), 10620–10628.
(155) Wolny, J. A.; Paulsen, H.; Trautwein, A. X.; Schünemann, V. Density Functional Theory Calculations and Vibrational Spectroscopy on Iron Spin-Crossover Compounds. *Coord. Chem. Rev.* **2009**, *253* (19–20), 2423–2431.
(156) Kepenekian, M.; Robert, V.; Le Guennic, B.; De Graaf, C. Energetics of

[Fe(NCH)6]2+ via CASPT2 Calculations: A Spin-Crossover Perspective. *J. Comput. Chem.* **2009**, *30* (14), 2327–2333.
(157) Klaeui, W.; Eberspach, W.; Guetlich, P. Spin-Crossover cobalt(III) Complexes: Steric and Electronic Control of Spin State. *Inorg. Chem.* **1987**, *26* (24), 3977–3982.
(158) Ferguson, A.; Squire, M. A.; Siretanu, D.; Mitcov, D.; Mathoniere, C.; Clerac, R.; Kruger, P. E. A Face-Capped [Fe4L4]8+ Spin Crossover Tetrahedral Cage. *Chem. Commun.* **2013**, *49* (16), 1597–1599.
(159) Travieso-Puente, R.; Broekman, J. O. P.; Chang, M.-C.; Demeshko, S.; Meyer, F.; Otten, E. Spin-Crossover in a Pseudo-Tetrahedral Bis(formazanate) Iron Complex. *J. Am. Chem. Soc.* **2016**, *138* (17), 5503–5506.
(160) Smith, M. E.; Andersen, R. A. Me5C5Ni(acac): A Monomeric, Paramagnetic, 18-Electron, Spin-Equilibrium Molecule. *J. Am. Chem. Soc.* **1996**, *118* (45), 11119–11128.
(161) Askevold, B.; Khusniyarov, M. M.; Herdtweck, E.; Meyer, K.; Schneider, S. A Square-Planar Ruthenium(II) Complex with a Low-Spin Configuration. *Angew. Chemie Int. Ed.* **2010**, *49* (41), 7566–7569.
(162) König, E. Structural Changes Accompanying Continuous and Discontinuous Spin-State Transitions. In *Progress in Inorganic Chemistry*; John Wiley & Sons, Inc., 2007; pp 527–622.
(163) Gütlich, P.; Hauser, A.; Spiering, H. Thermal and Optical Switching of Iron(II) Complexes. *Angew. Chemie Int. Ed. English* **1994**, *33* (20), 2024–2054.
(164) Ruben, M.; Breuning, E.; Lehn, J.-M.; Ksenofontov, V.; Renz, F.; Gütlich, P.; Vaughan, G. B. M. Supramolecular Spintronic Devices: Spin Transitions and Magnetostructural Correlations in [Fe4IIL4]8+ [2×2]-Grid-Type Complexes. *Chem. – A Eur. J.* **2003**, *9* (18), 4422–4429.
(165) Breuning, E.; Ruben, M.; Lehn, J.-M.; Renz, F.; Garcia, Y.; Ksenofontov, V.; Gütlich, P.; Wegelius, E.; Rissanen, K. Spin Crossover in a Supramolecular Fe4II [2×2] Grid Triggered by Temperature, Pressure, and Light . *Angew. Chemie Int. Ed.* **2000**, *39* (14), 2504–2507.
(166) Bottari, G.; de la Torre, G.; Torres, T. Phthalocyanine–Nanocarbon Ensembles: From Discrete Molecular and Supramolecular Systems to Hybrid Nanomaterials. *Acc. Chem. Res.* **2015**, *48*, 900–910.
(167) Meng, W.; Breiner, B.; Rissanen, K.; Thoburn, J. D.; Clegg, J. K.; Nitschke, J. R. A Self-Assembled M8L6 Cubic Cage That Selectively Encapsulates Large Aromatic Guests. *Angew. Chemie Int. Ed.* **2011**, *50*, 3479–3483.
(168) Mecozzi, S.; Rebek Julius, J. The 55 % Solution: A Formula for Molecular Recognition in the Liquid State. *Chem. – A Eur. J.* **1998**, *4* (6), 1016–1022.
(169) Ronson, T. K.; Pilgrim, B. S.; Nitschke, J. R. Pathway-Dependent Post-Assembly Modification of an Anthracene-Edged MII4L6 Tetrahedron. *J. Am. Chem. Soc.* **2016**, *138* (33), 10417–10420.
(170) Zadmard, R.; Kraft, A.; Schrader, T.; Linne, U. Relative Binding Affinities of Molecular Capsules Investigated by ESI-Mass Spectrometry. *Chem. – A Eur. J.* **2004**, *10* (17), 4233–4239.
(171) Baytekin, B.; Baytekin, H. T.; Schalley, C. A. Mass Spectrometric Studies of Non-Covalent Compounds: Why Supramolecular Chemistry in the Gas

Phase? *Org. Biomol. Chem.* **2006**, *4* (15), 2825–2841.
(172) Qu, D.-H.; Wang, Q.-C.; Zhang, Q.-W.; Ma, X.; Tian, H. Photoresponsive Host–Guest Functional Systems. *Chem. Rev.* **2015**, *115* (15), 7543–7588.
(173) McConnell, A. J.; Wood, C. S.; Neelakandan, P. P.; Nitschke, J. R. Stimuli-Responsive Metal–Ligand Assemblies. *Chem. Rev.* **2015**, *115* (15), 7729–7793.
(174) Lee, H.; Noh, T. H.; Jung, O.-S. Construction of Hetero-Four-Layered Tripalladium(II) Cyclophanes by Transannular Π···π Interactions. *Angew. Chemie Int. Ed.* **2016**, *55* (3), 1005–1009.
(175) Feng, D.-Z.; Song, Y.-L.; Jiang, X.-H.; Chen, L.; Long, Y.-Q. Forward- and Reverse-Synthesis of Piperazinopiperidine Amide Analogs: A General Access to Structurally Diverse 4-Piperazinopiperidine-Based CCR5 Antagonists. *Org. Biomol. Chem.* **2007**, *5* (16), 2690–2697.
(176) Gobbini, M.; Armaroli, S.; Banfi, L.; Benicchio, A.; Carzana, G.; Fedrizzi, G.; Ferrari, P.; Giacalone, G.; Giubileo, M.; Marazzi, G.; et al. Novel Analogues of Istaroxime, a Potent Inhibitor of Na+,K+-ATPase: Synthesis and Structure−Activity Relationship. *J. Med. Chem.* **2008**, *51* (15), 4601–4608.
(177) Bera, S.; Panda, G. A Rapid Entry to Amino Acid Derived Diverse 3{,}4-Dihydropyrazines and dihydro[1{,}2{,}3]triazolo[1{,}5-A]pyrazines through 1{,}3-Dipolar Cycloaddition. *Org. Biomol. Chem.* **2014**, *12* (23), 3976–3985.